THE HEPATIC ADAPTIVE RESPONSE TO REPEAT ACETAMINOPHEN EXPOSURE

Thesis submitted in accordance with the requirements of the University of Liverpool for the degree of Doctor in Philosophy by

Rowena May Liddell Eakins

February 2016

DECLARATION

This thesis is the result of my own work. The material contained within this thesis has not been presented, nor is currently being presented, either wholly or in part for any other degree or qualification.

Rowena May Liddell Eakins

This research was carried out at the MRC Centre for Drug Safety Science,

Institute of Translational Medicine, University of Liverpool, UK

Contents **Page**

Abstract

The hepatic adaptive response to repeat acetaminophen exposure

The adaptive response to chemical stress arises when an injurious exposure to a drug initiates phenotypic changes in the liver. These phenotypic changes limit hepatotoxicity upon subsequent exposures, and constitute an important evolutionary safeguard to the individual's survival. The factors governing hepatic adaptation to the popular analgesic and antipyretic acetaminophen (paracetamol) represent valuable research avenues, since acetaminophen toxicity is a leading cause of emergency hospital admissions through accidental and intentional overdose. Knowledge of the broader mechanisms governing hepatic adaptation to chemical exposure are limited; and concerning acetaminophen specifically, the research focus to date has been on select proteins implicated in metabolism.

The aim of this thesis was to investigate the molecular mechanisms of adaptation to chemical stress in two preclinical models using the classical hepatotoxin acetaminophen. These models have been characterised through clinically accepted toxicological and histopathological assessments, establishing acetaminophen-induced injury in high dose acetaminophen exposure groups in both rat and mouse models. A global proteomic analysis of rat liver has given insight into the changes in abundance of a subset of proteins common to all rats throughout the duration of the repeat exposure study, demonstrating that the process of adaptation to repeat acetaminophen exposure is not mediated by a single enzyme or pathway, but rather by a dynamic shift in expression of a large number of hepatic proteins. Key observations included widespread loss of phase I, II and III drug metabolising enzymes at the peak of toxicity, indicating a phenotypic shift away from drug metabolism. Focusing on the role of cytochrome P450 2E1 (CYP2E1) as the major

bioactivator of acetaminophen revealed changes in both expression and activity of this enzyme as the timecourse progressed.

Whilst initial similarities were seen in terms of hepatocellular injury, comparison of key markers of the adaptive response in rat and mouse revealed that the regenerative response provoked in this model is incompletely conserved. The rat showed induction of Nrf2-dependent proteins implicated in redox homeostasis, as well as extensive mitotic activity, restoring both mass and function to the liver despite continued dosing. The mouse was still able to adapt despite an absence of Nrf2 activation and no significant mitosis, indicating that the mechanisms by which each organism survives is quite different.

The findings of this work have implications for research into drug development and preclinical modelling of toxicity and adaptation, since the pharmaceutical industry typically employs rats and academia uses mice; however neither is a complete analogue of the human response. Additionally, further characterisation of the influence which adaptation has on the metabolic fate of subsequent xenobiotic exposures will be of value to the drug development and clinical management pathways. Further into the future, an improved understanding of the constituents of human adaptation, and the consequences of its failure, may permit more effective management of both acute and chronic liver injury.

Rowena May Liddell Eakins
February 2016

Acknowledgements

No (wo)man is an island…

Tremendous thanks are owed to my supervisors Chris Goldring, Neil Kitteringham and Kevin Park, for the time and energy they have put into supporting my project; a debt of thanks also to the Medical Research Council and the Safe-T Consortium for funding my studentship.

Heartfelt gratitude to Neus Prats, Mariona Auli, Pepi Torres and colleagues at Almirall for their investment and ongoing interest in my humble efforts. Thank you for making me welcome in Barcelona, and being so willing to assist with all my queries despite your own substantial workloads.

Additional academic support has been provided by many, including Cliff Rowe, Roz Jenkins, Olga Vasieva, Phil Starkey Lewis, Mark Bayliss, Steve Webb, Geoff Edwards, Sophie Regan… I would have been stuck without any single one of you. Thank you.

Huge appreciation for everyone in the pharmacology labs that I've shared this journey with, and all my lovely office mates. In particular, Nicola for being a trailblazer (and Laurence for bringing up the rear!), Phil and Karthik for making me welcome upstairs, Holly and Ali for being willing huggees, Max for pep talks and help with lists, Jon and Charles for the endless entertainment, Mo for always being pleased to see me.

The marvellous Jo Walsh deserves public recognition for her relentless support and friendship, scientific guidance, patience under very trying circumstances, and spectacular baking skills. WWJD. Thanks for being an all-round good egg.

Honourable mentions to Iain, and to Paul and Jens - my Farm Urban cheerleading team. Thanks for having my back through the toughest time, and for opening my horizons. Your support means more than you know.

Extra-special thanks go to my long-suffering husband and family. Thank you for putting up with the moods, long hours, crazy workload, and general studentiness for so many years. I'll do my best to be worth the investment. Thank you for being so proud of me.

Publications

Eakins R, Walsh J, Randle L, Jenkins R, Schuppe-Koistinen I, Rowe C, Starkey Lewis P, Vasieva O, Prats N, Brillant N, Auli M, Bayliss M, Webb S, Rees J, Goldring C, Kitteringham N, Park BK (2015). **Adaptation to acetaminophen exposure elicits major changes in expression and distribution of the hepatic proteome.** *Scientific reports*, *5, 16423*.

(This paper forms the basis of chapters 2 and 3, and a copy is included at the end of the thesis.)

Godoy P, Hewitt N, Albrecht U, Andersen M, Ansari N, Bhattacharya S, Bode J, Bolleyn J, Borner C, Böttger J, Braeuning A, Budinsky R, Burkhardt B, Cameron N, Camussi G, Cho C, Choi Y, Rowls JC, Dahmen U, Damm G, Dirsch O, Donato MT, Dong J, Dooley S, Drasdo D, **Eakins R**, Ferreira K, Fonsato V, Fraczek J, Gebhardt R, Gibson A, Glanemann M, Goldring C, Gómez-Lechón M, Groothuis G, Gustavsson L, Guyot C, Hallifax D, Hammad S, Hayward A, Häussinger D, Hellerbrand C, Hewitt P, Hoehme S, Holzhütter HG, Houston JB, Hrach J, Ito K, Jaeschke H, Keitel V, Kelm J, Park BK, Kordes C, Kullak-Ublick G, LeCluyse E, Lu P, Luebke-Wheeler J, Lutz A, Maltman D, Matz-Soja M, McMullen P, Merfort I, Messner S, Meyer C, Mwinyi J, Naisbitt D, Nussler A, Olinga P, Pampaloni F, Pi J, Pluta L, Przyborski S, Ramachandran A, Rogiers V, Rowe C, Schelcher C, Schmich K, Schwarz M, Singh B, Stelzer E, Stieger B, Stöber R, Sugiyama Y, Tetta C, Thasler W, Vanhaecke T, Vinken M, Weiss T, Widera A, Woods C, Xu J, Yarborough K, Hengstler J (2013). **Recent advances in 2D and 3D in vitro systems using primary hepatocytes, alternative hepatocyte sources and non-parenchymal liver cells and their use in investigating mechanisms of hepatotoxicity, cell signaling and ADME.** *Archives of toxicology, 87 (8), pp 1315-1530*

Goldring C, Duffy P, Benvenisty N, Andrews P, Ben-David U, **Eakins R**, French N, Hanley N, Kelly L, Kitteringham N, Kurth J, Ladenheim D, Laverty H, McBlane J, Narayanan G, Patel S, Reinhardt J, Rossi A, Sharpe M, Park BK (2011). **Assessing the safety of stem cell therapeutics.** *Cell Stem Cell 8 (6) pp 618-628*

Eakins R, Brillant N, Walsh J, Schuppe-Koistinen I, Prats N, Auli M, Goldring C, Kitteringham N, Park BK. **The regenerative response in rats and mice is incompletely conserved.** *(Manuscript in preparation)*

Abstract:

Eakins R, Walsh J, Jenkins R, Rowe C, Sleckus A, Starkey Lewis P, Vasieva O, Prats N, Auli M, Schuppe-Koistinen I, Kitteringham N, Goldring C, Park BK. **Analysis of the hepatoproteome during repeat acetaminophen exposure reveals novel processes associated with the adaptation of the liver to chemical insult.** British Toxicology Society Annual Congress, 2014

Abbreviations

(-/-)	Homozygous null
(+/+)	Homozygous wild type
µl	Microlitre
µm	Micrometre
µM	Micromolar
6'-OH CZX	6-hydroxy chlorzoxazone
Å	Angstrom
ACN	Acetonitrile
ADR	Adverse drug reaction
ALR	Augmenter of liver regeneration
ALT	Alanine aminotransferase (EC 2.6.1.2)
amu	Atomic mass units
ANOVA	Analysis of variance
APAP	Paracetamol, acetaminophen
ARE	Antioxidant response element
AST	Aspartate aminotransferase (EC 2.6.1.1)
ATP	Adenosine triphosphate
BD	Bile duct
C	Centigrade
CCl_4	Carbon tetrachloride
CE	Collision energy
CL	Centrilobular
cm	Centimetre
CM	Carboxymethyl
CO	Carbon monoxide
CO_2	Carbon dioxide
CV	Central vein
CXP	Collision cell exit potential
CYP1A2	Cytochrome P450 1A2 isoform (EC 1.14.14.1)
CYP2E1	Cytochrome P450 2E1 isoform (EC 1.14.13.n7)
CYP450	Cytochrome P450
CZX	Chlorzoxazone
D	Diffuse
DAB	3', 3'-diaminobenzidine
dH_2O	Distilled water
DILI	Drug-induced liver injury
DNA	Deoxyribonucleic acid
DP	Declustering potential
EDTA	Ethylene diamine-tetracetic acid

FA	Formic acid
FDA	Food and Drug Administration
FDR	False discovery rate
FMO3	Flavin-containing monooxygenase 3 (EC 1.14.13.148)
g	Gram
GCLC	Glutamate-cysteine ligase, catalytic subunit (EC 6.3.2.2)
GS	Glutamine synthetase (EC 6.3.1.2)
GSH	Glutathione
GSSG	Oxidised glutathione
GSTP1	Glutathione-s-transferase pi (EC 2.5.1.18)
h	Hour
H&E	Haematoxylin and eosin
H_2O_2	Hydrogen peroxide
HO-1	Haemoxygenase-1 (EC 1.14.14.18)
HRP	Horseradish peroxidase
i.p.	Intraperitoneal
IAA	Iodoacetamide
ICH	International Conference on Harmonization
IHC	Immunohistochemistry
IS	Internal standard
iTRAQ	Isobaric tags for relative and absolute quantification
IU	International units
KCl	Potassium chloride
kDa	kiloDalton
Keap1	Kelch-like ECH associated protein 1
kg	Kilogram
K_m	Rate constant
L	Litre
LC	Liquid chromatography
LPC	Liver progenitor cell
M	Molar
mg	Milligram
min	Minute
miR-122	MicroRNA-122
mL	millilitre
mm	millimetre
mM	Millimolar
MMTS	Methylmethane thiosulphate
MOPS	3-morpholinopropane-1-sulfonic acid
MRM	Multiple reaction monitoring
mRNA	Messenger RNA
MRP3	Multidrug resistance-associated protein 3
MRP4	Multidrug resistance-associated protein 4
MS	Mass spectrometer/spectrometry
MS/MS	Tandem mass spectrometry

MW	Molecular weight
NADPH	Nicotinamide adenine dinucleotide phosphate
NAPQI	n-acetyl-*p*-benzoquinoneimine
nm	Nanometre
NQO1	NAD(P)H:quinine oxidoreductase 1 (EC 1.6.5.2)
Nrf2	Nuclear factor erythroid 2 related factor 2
OECD	Organisation for Economic Co-operation and Development
P	periportal
p	Probability
p.o.	*Per oralis*
PC	Principal component
PCA	Principal component analysis
PCNA	Proliferating cell nuclear antigen
PT	Portal triad
RNA	Ribonucleic acid
ROS	Reactive oxygen species
rpm	Revolutions per minute
RT	Room temperature
s	Second
SEM	Standard error of mean
TBS	Tris-buffered saline
TBS-T	Tris-buffered saline containing 0.05% Tween 20
TEAB	Triethyl ammonium bicarbonate
v/v	Volume by volume
V_{max}	Maximum rate of reaction
w/v	Weight by volume
WT	Wild type

Designation of statistical significance:

$p < 0.05$ = *

$p < 0.01$ = **

$p < 0.001$ = ***

$p < 0.0001$ = ****

Chapter 1: General Introduction

Contents

1.1. Drug-Induced Liver Injury

An adverse drug reaction (ADR) can be defined as any undesirable effect of a drug beyond its anticipated therapeutic action (Pirmohamed et al. 1998). As a major site of drug metabolism, the liver can often be affected by ADRs. The liver is considered a vital organ due to its diverse roles in maintaining homeostasis. Its functions include protein synthesis, digestion, lipid metabolism, glucose regulation, and detoxification of both endogenous and exogenous toxins. Despite the range of detoxification pathways active in the liver, it remains especially vulnerable to injury from environmental toxins or xenobiotics.

Liver injury due to prescription or non-prescription drugs is a worldwide problem. Drug induced liver injury (DILI) can occur when either a parent drug or its metabolite perturbs liver cell biochemistry, or elicits an immune response. DILI encompasses a diverse range of symptoms and may result from either acute or chronic exposure to a compound or compounds. It can loosely be categorised into hepatocellular or cholestatic injury, although it is possible to identify hallmarks of both categories in an individual patient. An individual's susceptibility to DILI is influenced by both genetic and environmental risk factors, and as such, DILI can be challenging to predict, diagnose and treat.

The main functional cell of the liver is the hepatocyte, and these cells comprise around 70% of the liver's mass. A severe toxic insult to the liver can result in widespread death of hepatocytes, and if this happens on an organ-wide scale, the outcome is fulminant hepatic failure, which necessitates urgent medical intervention. Hepatic failure carries a 60 to 80 % mortality rate in patients who do not receive a transplant (Björnsson and Olsson 2005).

When hepatocellular injury is less severe, and particularly when it is also chronic in nature, the liver can become fibrotic as scar tissue accumulates at the sites of injury. A patient may present with symptoms of hepatitis, as liver function becomes compromised by fibrosis.

Hepatitis can in turn predispose an individual to liver cancer, and both of these conditions are associated with increased morbidity and mortality (Cardin et al. 2014). Hepatocellular DILI and its potential sequelae therefore present a considerable clinical burden and public health concern.

1.1.1. DILI and drug development

DILI is a common cause of liver injury, representing around 50 % of all cases of acute liver failure (Ostapowicz et al. 2002). It therefore presents a substantial concern to the pharmaceutical industry. In excess of 600 drugs have been linked with liver toxicity (Park et al. 2005), and DILI is the most commonly cited reason for the withdrawal of drugs from the market after approval (Lee 2003). Given that the cost of developing a single drug has risen to an estimated $2.6 billion (Tufts 2014) it is imperative that potential toxicity is identified as early in the development process as possible. Similarly, robust preclinical screening will prevent the unnecessary attrition of compounds which may go on to have therapeutic value. In order to improve preclinical screening of new chemical entities, an understanding of the mechanisms underlying liver injury and the ways in which the liver can defend itself from harm are vital.

1.2. Drug Metabolism

Microanatomically, the liver is formed of hexagonal units termed lobules (Figure 1.1). These lobules are fed with blood from the digestive system via the hepatic portal vein, part of the portal triad which is located at each peripheral angle of the lobule. Blood passes along plates of hepatocytes, converging on the centre of the lobule and draining through the central vein. Hepatocytes along the portal to central axis are exposed to gradients of signalling molecules, making them phenotypically heterogeneous (Park et al. 2005; Hailfinger et al. 2006). This gives rise to a spatial pattern of gene expression called zonation (Jungermann and Katz 1989). Functional specialisation can therefore be observed across the zones.

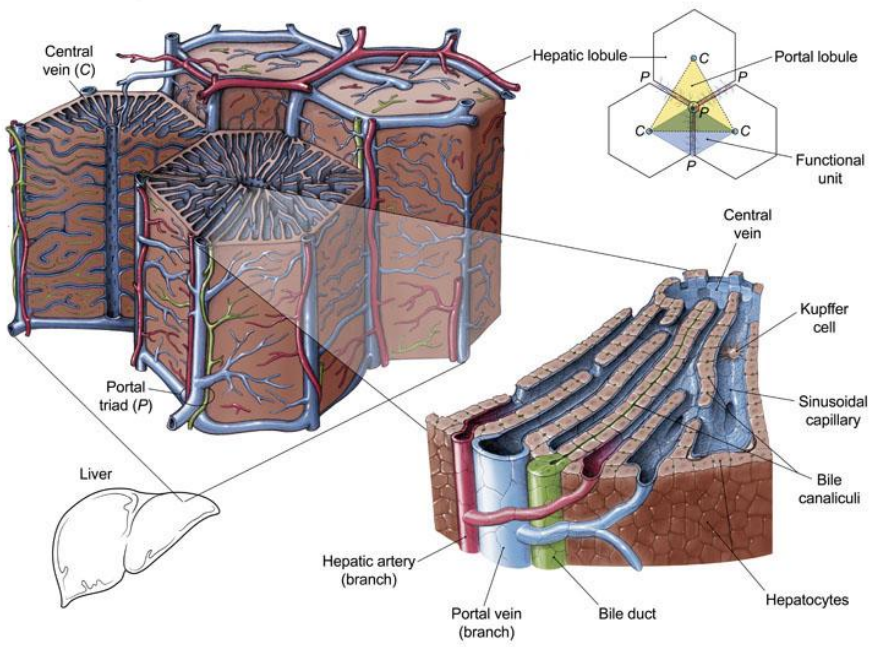

Figure 1.1: The microanatomy of the liver

Legend: The lobule is the structural unit of the liver, and is comprised primarily of hepatocytes. Plates of hepatocytes process blood from the hepatic portal vein as it passes to the centre of the lobule and exits the liver. Gradients of signalling molecules exist along the axis that runs between the portal and central veins giving rise to functional specialisation and zonation. (Killpack 2016)

Hepatocytes are particularly rich in molecules which support drug metabolism, the process by which living organisms biochemically modify xenobiotics, usually in order to facilitate their excretion. Drug metabolism is achieved through highly specialised enzymatic systems which are generally well conserved between model species. These enzymatic systems convert non-polar, lipophilic compounds into polar hydrophilic ones, reducing tissue penetration and supporting renal elimination. Effective drug metabolism therefore reduces an organism's exposure to potentially toxic xenobiotics.

Drug metabolism is categorised into distinct and usually sequential phases, which are briefly summarised below.

1.2.1. Phase I metabolism

Phase I metabolism involves the introduction into the compound of a polar or reactive group by way of oxidation, reduction or hydrolysis. The reactivity of the compound is increased, and sometimes therefore the product may be more toxic than the parent compound. Additionally, this is the means of activation of a prodrug.

The majority of phase I reactions are catalysed by the cytochrome P450 monooxygenase system, predominantly expressed in centrilobular regions (Bühler et al. 1992; Oinonen and Lindros 1998). The cytochrome P450 (CYP450) enzymes are a superfamily of related enzymes, denoted by CYP allele nomenclature (Sim and Ingelman-Sundberg 2006). The enzymes differ in structure and therefore substrate specificity, though there is much functional overlap. In the liver, CYP450 enzymes are resident in the lumen of the smooth endoplasmic reticulum, and although the pathway for CYP450-catalysed reactions can be complex, the net result is the formation of a hydroxyl group at the site of a hydrogen atom, with the by-product of a single molecule of water.

In addition to CYP450 enzymes, lesser phase I enzymes include NADPH quinone oxidoreductases, epoxide hydrolases, flavin-containing monooxygenases, cyclooxygenases, alcohol dehydrogenases, hydrolases and monoamineoxidases. All catalyse the addition of functional groups required by phase II reactions.

1.2.2. Phase II metabolism

Phase II metabolism involves conjugation reactions, which often occur sequentially after phase I, at the site of phase I modification of the compound (Hodgson 2004), in order to increase the hydrophilicity of the compound. Reactions include sulphation, glucuronidation, acetylation and glutathione conjugation.

Phase II enzymes are generally therefore transferases, adding a polar group to the compound, usually glucuronyl, sulphate, methyl or acetyl (Jancova et al. 2010). Additionally, glutathione (GSH) can conjugate drugs via its sulphydryl group. GSH conjugation is an important route of detoxification for a number of xenobiotics including epoxides, alkenes and aromatic nitro compounds (Timbrell 1999). GSH is ubiquitously present in cells, and represents a significant buffer against redox perturbation. GSH conjugation, which may occur either spontaneously or by a mechanism catalysed by glutathione s-transferase (Hodgson 2004), is a key cellular defence from electrophilic molecules. In the liver, GSH is zonally expressed, with the poorest areas found within 100 µm of the central vein (Smith et al. 1979). These perivenous hepatocytes have also been shown to be slowest to replenish GSH (Kera et al. 1988). Perivenous cells preferentially express drug metabolising enzymes (Oinonen and Lindros 1998), and these factors combine to explain these cells' peculiar susceptibility to injury.

1.2.3. Phase III metabolism

Phase III metabolism describes further structural modification of metabolites, and subsequent excretion by transmembrane transporter channels. Transporters may be ATP dependent, or independent of both ATP and sodium. Examples include P-glycoprotein, multidrug resistance protein, and organic anion transporting polypeptide (Xu et al. 2005).

1.2.4. Reactive metabolite formation and oxidative stress

In the majority of instances, the drug metabolism processes occurring in the liver very effectively detoxify compounds and permit their safe excretion. However, in some instances, these same processes result in a metabolite that is more reactive than the parent compound. This has largely been demonstrated following phase I oxidative metabolism (Park et al. 1995; Antoine et al. 2008), but can to a lesser degree occur upon phase II conjugation reactions (Kretzrommel and Boelsterli 1993; Hargus et al. 1995). The generation of reactive metabolites can result in covalent modification of cellular proteins as well as damage to nuclear and mitochondrial DNA (Hinson et al. 2010). These processes are strongly linked to GSH depletion and oxidative stress, and are exemplified by the toxicity seen in acetaminophen overdose (Josephy 2005).

Oxidative stress, therefore, arises from an imbalance between the abundance of pro-oxidant species in the cell, and the antioxidant mechanisms (such as synthesis of GSH) that exist to protect the cell from oxidative injury. Reactive oxygen species (ROS), such as free radicals, are constantly produced as a by-product of mitochondrial oxidative phosphorylation, as well as being formed by the activity of enzymes on xenobiotics (Li et al. 2015). ROS are highly unstable due to a single unpaired electron, and will remove a single electron from any molecule encountered in order to increase stability. This in turn creates a new ROS, perpetuating a chain reaction and can causing oxidative damage to proteins,

lipids and DNA. Oxidative stress has been associated with a number of disease processes including neurodegenerative conditions, cancer, and cardiovascular disease (Miller 1970; Amens 1983; Dhalla et al. 2000; Valko et al. 2007).

1.2.5. The oxidative stress response

The oxidative stress response allows an organism to manage constitutive oxidative stress on a cellular level, as well as responding swiftly to neutralise acute oxidative insult. A range of cytoprotective proteins are important for mediating the oxidative stress response, and although these proteins are expressed constitutively, their expression can also be upregulated following oxidative insult (Primiano et al. 1997), thereby helping to restore homeostasis through mechanisms such as GSH repletion and the direct detoxification of electrophiles. One of the most important mediators of this upregulation is the transcription factor nuclear factor-erythroid 2–related factor 2 (Nrf2).

1.2.5.1. The Keap1/Nrf2 pathway

The Keap1/Nrf2 pathway is a key redox sensitive cellular defence pathway (Copple et al. 2010). Keap1 (Kelch-like ECH associated protein 1) is a particularly cysteine-rich protein, and this relative overabundance of cysteine residues is thought to enable Keap1 to function as a thiol-based redox sensor (Dinkova-Kostova et al. 2002). Keap1 exists in the cytoplasm as a homodimer, and under basal conditions it sequesters Nrf2 and targets it for proteasomal degradation (Cullinan et al. 2004).

Under oxidative stress, key cysteine residues on the Keap1 homodimer become modified in specific patterns according to the structure of the reactive molecules which are disrupting redox status (Hong et al. 2005). This conformational change prevents the targeting of bound Nrf2 for degradation, so Keap1 therefore becomes saturated by incompletely bound Nrf2, and newly synthesised Nrf2 begins to accumulate in the cytoplasm. Free Nrf2

translocates into the nucleus where it interacts with the antioxidant response element (ARE), a motif within the DNA. Through this complex, Nrf2 upregulates the transcription of cytoprotective genes which facilitate restoration of redox homeostasis (Surh et al. 2008). The complex response of the cell to oxidative stress protects macromolecules from injury, and also facilitates their repair where injury occurs.

1.2.5.2. Consequences of Nrf2 activation

The 'graded Nrf2 activation' model described by Liu et al. (2013) explores the role of Nrf2 in protection from hepatotoxicants. This model used a number of different genetic systems (Figure 1.2) to demonstrate that Nrf2 plays a key role in defending the liver from several commonly encountered hepatotoxicants including acetaminophen, carbon tetrachloride and ethanol. The consequences of Nrf2 activation in this model were shown to be dose-responsive, reducing the expression of genes associated with inflammation, oxidative stress, endoplasmic reticulum stress and cell death. The protection afforded by Nrf2 activation was accompanied by induction of antioxidant genes, suppression of the inflammatory response and attenuation of oxidative stress.

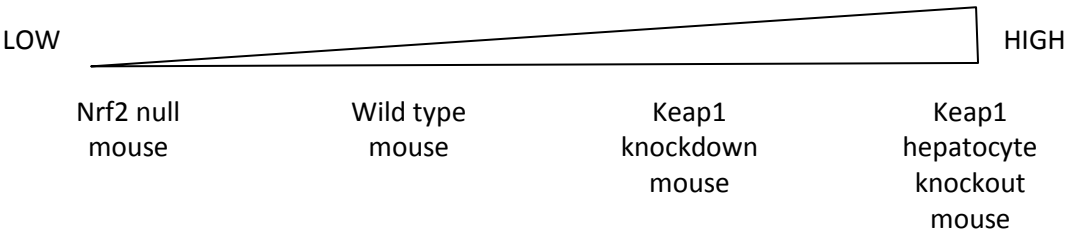

Figure 1.2: The graded Nrf2 activation model of protection from hepatotoxicants

Legend: The model presented by Liu et al. (2013) encompasses a range of possible Nrf2 activation states. Mice which do not express Nrf2 are at the lowest end of the scale and are most vulnerable to liver injury. At the highest end of the scale is a hepatocyte-specific knockout of Nrf2's repressor Keap1, mimicking maximal Nrf2 induction.

1.3. APAP as a model hepatotoxin

Acetaminophen (paracetamol, APAP) is a model hepatotoxin widely used preclinically to study liver injury because of the predictable nature of its effect. It is used clinically as an analgesic and antipyretic, and is a common cause of liver injury in man through both accidental and intentional overdose (Larson et al. 2005). APAP poisoning is the commonest cause of acute liver failure in the USA (Larson et al. 2005) and the UK (Fagan and Wannan 1996; Karvellas et al. 2010). In the UK, the annual number of deaths by poisoning through APAP alone ranged from 90 to 155 over the years of 2000 to 2008 (Hawton et al. 2011). In addition to this there are considerably more deaths involving APAP ingested alongside other toxicants (Hawton et al. 2011).

At therapeutic doses, APAP is largely excreted via urine through the phase II conjugation reactions sulphation and glucuronidation. At supratherapeutic doses (Figure 1.3), toxicity arises when APAP is extensively bioactivated by cytochrome P450 2E1 (CYP2E1), and to a lesser extent CYP1A2, CYP2A6, CYP2D6 and CYP3A4 (Patten et al. 1993; Chen et al. 1998; Dong et al. 2000). Bioactivation of APAP results in the intracellular accumulation of the highly reactive metabolite N-acetyl-*p*-benzoquinone imine (NAPQI) (Dahlin et al. 1984). NAPQI is a strongly electrophilic metabolite which can conjugate and deplete the redox buffer GSH and bind covalently to cellular macromolecules (Albano et al. 1985). When cellular defences are overwhelmed in this manner, the ensuing oxidative damage to proteins, lipids and DNA can ultimately result in cell death (Hinson et al. 2010). The evolution of toxicity can be further exacerbated by the involvement of the immune system (For a review, see Liu and Kaplowitz (2006)). Liver cell death is seen in a characteristic centrilobular distribution, reflecting the zones of the liver which are relatively rich in CYP450 and poor in GSH (Sastre et al. 1992), and therefore most vulnerable to NAPQI

accumulation. Widespread loss of liver cells can result in severe liver injury, ultimately causing organ failure and death.

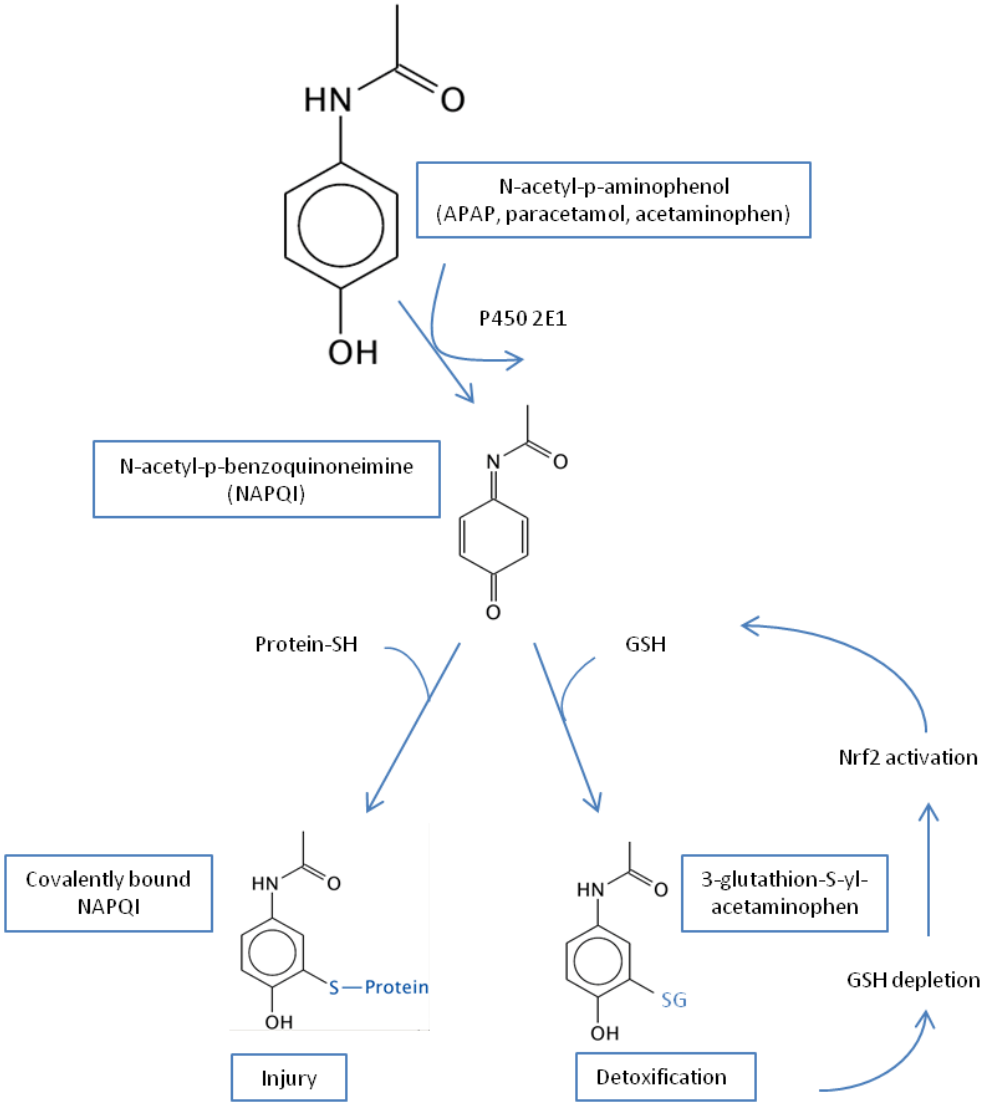

Figure 1.3: APAP metabolism at supratherapeutic doses

Legend: In APAP overdose, NAPQI is formed by direct 2 electron oxidation of APAP, which is catalysed mainly by CYP2E1. NAPQI is conjugated with glutathione to form 3-glutathion-S-yl-acetaminophen and excreted from the cell. NAPQI can also be transformed by reduction back to acetaminophen – not shown (Dahlin and Nelson 1982; Hinson et al. 1982). Both of these detoxification processes deplete glutathione by up to 80–90 % (Jollow et al. 1973; Mitchell et al. 1973a, 1973b). Loss of glutathione perturbs redox homeostasis and stimulates an oxidative stress response which is in part mediated by the transcription factor Nrf2. Nrf2 governs the expression of a large panel of cytoprotective genes, including enzymes responsible for glutathione synthesis. If formation of NAPQI outpaces restitution of glutathione, accumulating NAPQI is able to covalently bind to any sulfhydryl groups, causing cellular injury.

Compared to other organs, the liver is particularly rich in GSH, with basal levels of up to 10 mM (Lu 2009). This acts as an effective defence system to sequester electrophilic molecules thereby preventing oxidative stress. Additionally, various transcription factors including Nrf2 aid cell defence against chemical stressors by upregulating the transcription of cytoprotective genes such as haemoxygenase and glutamate-cysteine ligase (Randle et al. 2008). This is believed to play an essential role in the defence against chemical stress elicited by APAP. This response to toxicity is not unique to APAP; it is also seen with other model hepatotoxins including carbon tetrachloride (Xu et al. 2008), ethanol (Lamlé et al. 2008), bleomycin (Cho et al. 2004) and cisplatin (Liu et al. 2009). However, depletion of GSH following APAP overdose has been associated with a reduction in many oxidative stress response enzymes, including glutathione reductase, glutathione transferase, glutathione peroxidase, γ-glutamylcysteinyl synthase, catalase and superoxide dismutase (O'Brien et al. 2000; Acharya and Lau-Cam 2010). This effect may be indicative of a 'tipping point' in the process of toxicity, and further complicates the clinical picture of APAP overdose.

1.3.1. Nrf2 mediated defence against APAP toxicity

Nrf2 has been directly implicated in the *in vivo* cellular response to APAP toxicity (Goldring et al. 2004), and its involvement in defending the liver against the reactive metabolite NAPQI has been explored in the literature. NAPQI has been shown to directly activate Nrf2 (Copple et al. 2008), both by direct modification of cysteine residues on Nrf2's cytosolic repressor Keap1, and indirectly via depletion of intracellular GSH. This activation results in the increased transcription of a panel of cytoprotective genes. Within this panel, of particular pertinence to APAP toxicity are NAD(P)H quinone oxidoreductase 1 (NQO1) (Venugopal and Jaiswal 1996) , a scavenger of reactive metabolites which is also upregulated in human APAP-induced liver injury (Aleksunes et al. 2006); and the catalytic

subunit of glutamate cysteine ligase (GCLC) (Wild et al. 1999), a key step in the GSH synthesis pathway, and instrumental to patient recovery when the antidote to APAP poisoning n-acetyl cysteine is administered.

Studies using techniques such as genetic knockouts or RNA silencing have shown increased susceptibility to APAP toxicity as a consequence of inactivation or absence of Nrf2 (Itoh et al. 1997; Reisman et al. 2009b). Conversely, methods which activate Nrf2, using genetic or pharmaceutical mediators, result in protection (Okawa et al. 2006; Reisman et al. 2009a).

1.4. Liver regeneration and adaptation to hepatotoxicants

Many studies of APAP induced liver injury focus on single doses. However, a number of publications have explored the effects of the drug on liver physiology, and how the change in physiology affects the metabolism of subsequent doses (Roberts et al. 1983; Shayiq et al. 1999; Kim et al. 2009). The liver is the primary site of detoxification, and as such is particularly vulnerable to cellular damage from electrophiles and free radicals. It has therefore evolved the capacity to self-renew. It is becoming apparent that the metabolic phenotype of actively proliferating cells is altered in comparison to quiescent liver (Dalhoff et al. 2001; Aleksunes et al. 2008a). What remains unclear is the origin of cells contributing to the process of regeneration, and the metabolic profile of each cell compartment, and therefore the implications for the fate of repeat doses further to toxicity. In the quiescent liver there exists a dynamic equilibrium between cell birth and death in order to tightly regulate organ mass. Mitotic events are comparatively rare, with cellular turnover estimated to be <0.1 % (Fausto and Campbell 2003); though mature hepatocytes have an almost unlimited capacity to renew (Overturf et al. 1997).

In this context, the response the liver demonstrates to injury is not true organ regeneration; strictly it is defined as compensatory hyperplasia, and is precisely regulated by the metabolic needs of the organism (Riehle 2011). Rather than regrow an exact replica of destroyed tissue, restoration of liver mass is achieved by proliferation of cells (mitosis) and increase in the size of cells (growth) (Fujiyoshi and Ozaki 2011). Mass is restored very rapidly, as is function; however, tissue architecture is somewhat disorganised and over time becomes more structured.

Adaptation refers to the capacity of an organism to change its phenotype in response to a noxious stimulus in order to better survive in its environment. Due to the phenotypic shift

exhibited by proliferating liver, the processes of regeneration and adaptation may therefore be regarded as intimately related in the context of APAP toxicity.

1.4.1. Proposed mechanisms for liver regeneration

The processes underpinning liver regeneration are at present incompletely characterised, but tremendous research endeavours are being focused on this important subject. Although early findings have in some cases been contradictory, the currently accepted hypothesis for liver regeneration proposes that the mechanism of cellular restitution depends on the previous state of the liver. If the remaining liver has the capacity to proliferate (as seen in partial hepatectomy models) then mature hepatocytes will respond to paracrine signals inducing mitosis. If the liver's proliferative capacity is somehow compromised (for example by fibrosis, hepatitis or age) then liver progenitor cells (LPCs) are recruited. In rodents these cells are seen to originate from periportal zones, and they proliferate and differentiate in chords that extend towards centrilobular zones in order to restore mass and function. This hypothesis is presented graphically in Figure 1.4.

The partial hepatectomy model of liver regeneration presents an appropriate platform for probing alterations in phenotype as a consequence of cellular proliferation: it is well characterised, highly reproducible and is an example of 'clean' liver injury, since a lobe or lobes may be excised without extensively damaging surrounding tissues. In 1983, examination of hepatocytes isolated from rats which had undergone partial hepatectomy showed significant loss of total CYP450 alongside an increase in GSH (Roberts et al. 1983), thought to be mediating *in vitro* resistance to a panel of hepatotoxicants. Subsequent publications validated these findings at both protein and mRNA levels (Tygstrup et al. 1996; Favre et al. 1998). Alongside these data, other studies showed evidence that the regeneration-associated hepatoprotective phenotype was also detectable in models employing toxic liver injury. In rats, regeneration after partial hepatectomy provided

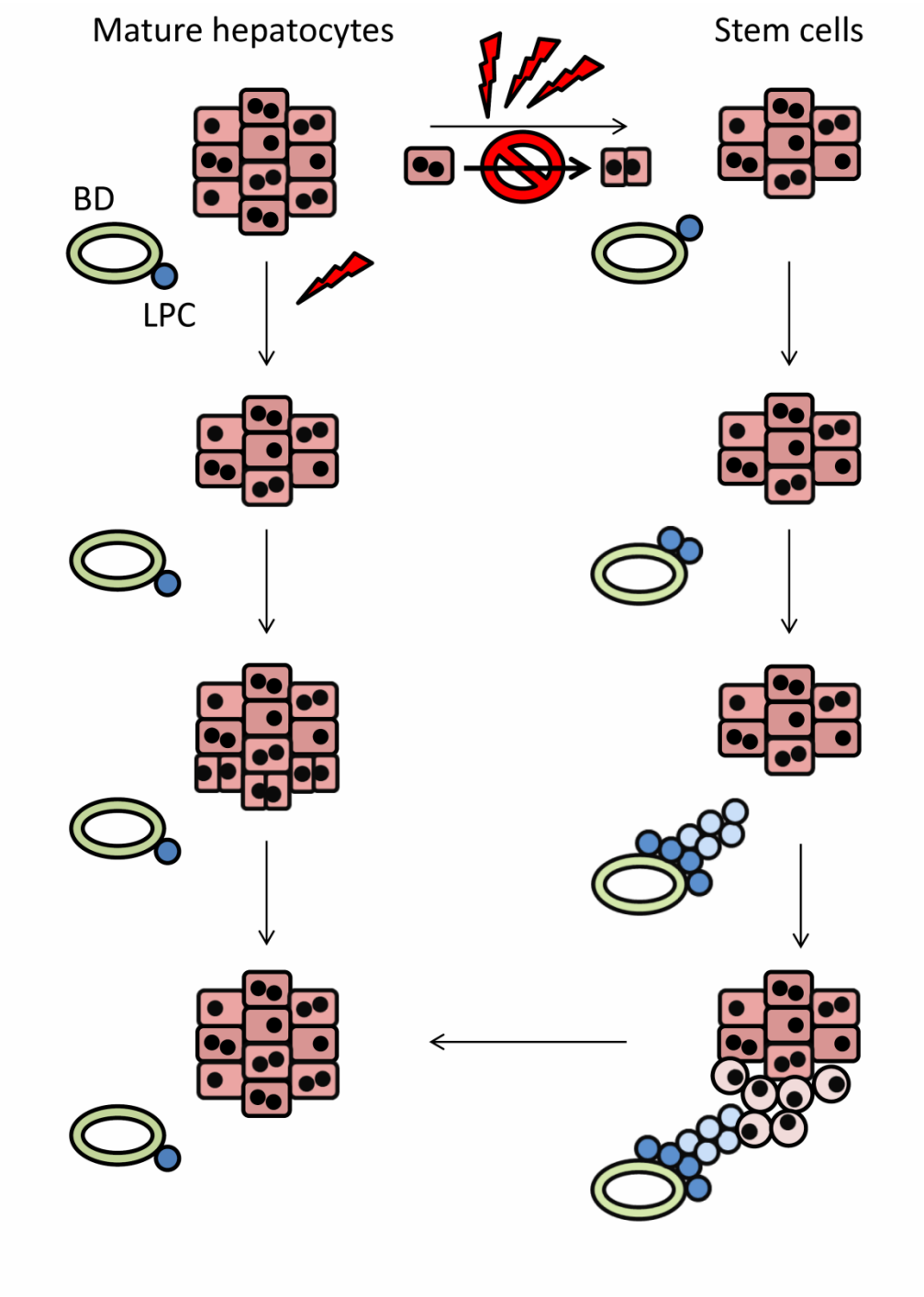

Figure 1.4: Mechanisms of liver regeneration

Legend: When injury is sustained in healthy liver, mature hepatocytes re-enter mitosis in order to restore organ mass (left side). If, however, the organ's proliferative capacity is impaired or mitosis is blocked, then liver progenitor cells (LPC) are activated (right side). LPCs proliferate and differentiate in chords extending from the bile duct (BD) towards the centrilobular region. Adapted from Dollé et al. (2010)

resistance to carbon tetrachloride induced toxicity (Zhang et al. 1999), and cell division stimulated by a low thioacetamide exposure mediated resistance to toxicity arising from a second, higher exposure (Mangipudy et al. 1995). The phenomenon has also been demonstrated in human primary hepatocytes. In human cells CYP450 activity was downregulated when cultures were treated with hepatocyte growth factor, a potent mitogen (Donato et al. 1998).

Liver regeneration is relevant to drug metabolism and adaptation to repeated toxicity, since actively regenerating liver tissue exhibits a different profile of drug metabolising enzymes compared to quiescent liver. This phenotypic shift has been demonstrated in a range of models of regeneration, including drug-induced liver injury, partial hepatectomy and even during postnatal development (Mangipudy et al. 1995; Zhang et al. 1999; Dalhoff et al. 2001; Limaye et al. 2006; Aleksunes et al. 2008a). It is clear that new cells arising from these mediators of liver injury exhibit a phenotype that exerts some kind of protection over the regenerating organ, perhaps permitting non-essential activities to be sidelined in favour of short-term preservation of critical function. The precise nature of the phenotypic shift, however, is less apparent, although the functional consequence is an enhanced resistance to drug toxicity, thereby linking regeneration to adaptation.

1.5. Adaptation and APAP

Where adaptation to a noxious substance arises from earlier exposure to the same substance, the process is termed autoprotection. Studies of APAP-induced autoprotection have implicated a number of possible candidate proteins in the process of adaptation, including CYP2E1 (Shayiq et al. 1999), the key CYP450 involved in APAP metabolism (Patten et al. 1993; Chen et al. 1998) and multidrug resistance-associated protein 4 (MRP4), a basolateral efflux transporter protein (Aleksunes et al. 2008a). However, the true breadth of the biological processes that underpin the adaptive response to chemical exposure in general, and to APAP in particular, are not known. Exploring this should begin to reveal what adaptation during drug exposure in the liver normally consists of, and therefore provide a starting point for the investigation of sources of inter-individual variability in response to drug exposure.

Pretreatment of cultured primary hepatocytes with APAP, and also incubation with growth factors, diminished CYP450 expression and prevented the bioactivation of APAP on a subsequent toxic challenge (Grunnet et al. 2003), intimating a link between regeneration and adaptation arising specifically from the action of APAP. In this study, cells treated with growth factors had higher GSH concentrations, showing that actively proliferating cells have a greater capacity to buffer oxidative stress. In rodents, although APAP toxicity is known to reduce CYP450 abundance (Shayiq et al. 1999), a subtoxic dose has the inverse effect of inducing CYP450 (Kim et al. 2009) raising questions about where on the spectrum of physiological stress (i.e. from hormesis to surmounting a toxic challenge) lies the optimum range for inciting adaptation.

In 2013, a proteomic investigation of adaptation to APAP in a mouse model was published, revealing metabolic detoxification processes were activated in mice pretreated with APAP prior to a toxic challenge (O'Connor et al. 2013). These processes were mediated by the

transcription factor Nrf2. Nrf2 has also been shown to activate the hepatotrophic factor ALR (augmenter of liver regeneration) via the ARE (Dayoub et al. 2013); and to be necessary for normal cellular proliferation to occur (Zou et al. 2015), reinforcing links between oxidative stress and hepatic regeneration, and in doing so indicating a novel survival mechanism for damaged cells.

A summary of the current understanding of APAP-induced autoprotection in rodents is shown in Figure 1.5.

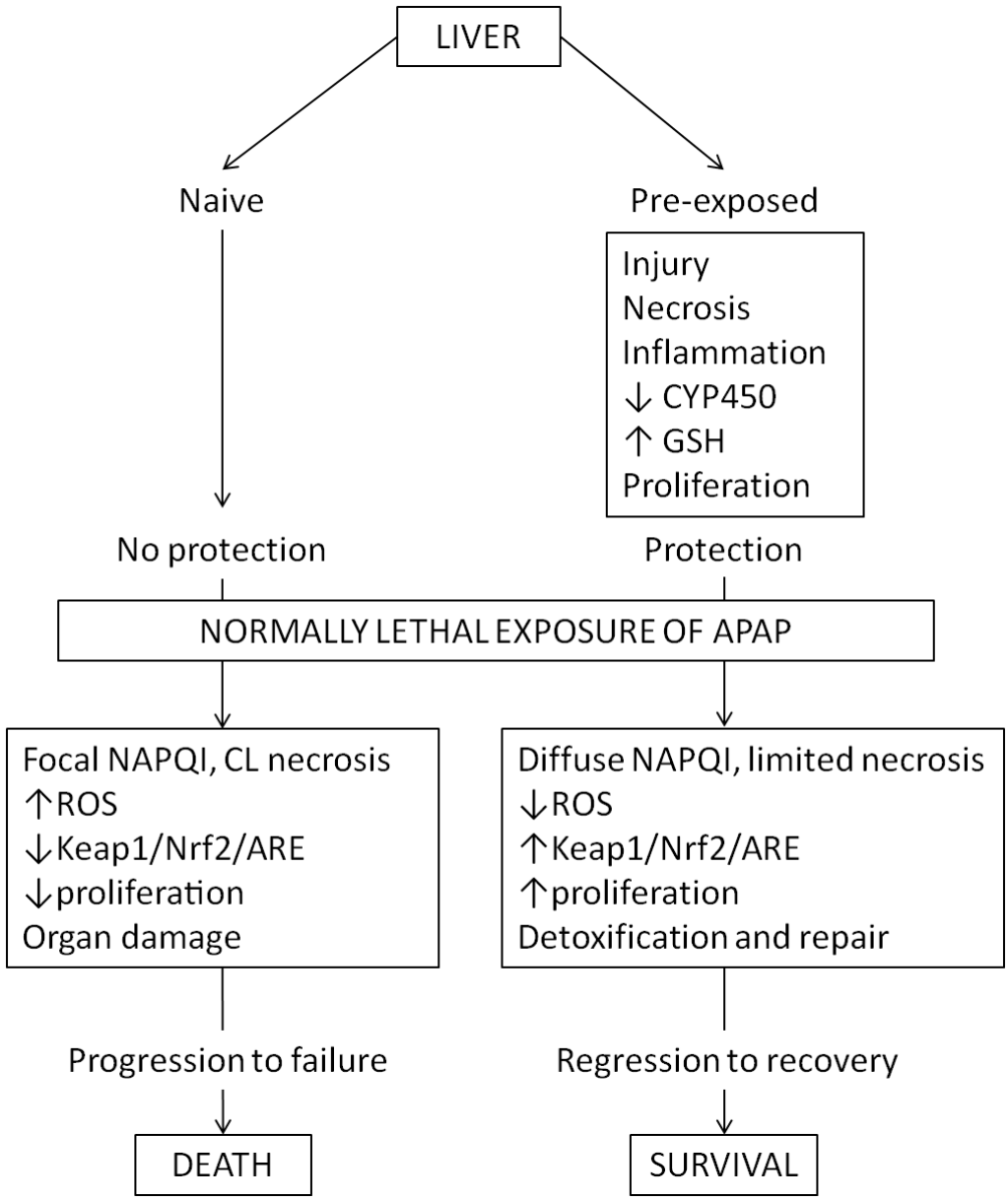

Figure 1.5: APAP-induced autoprotection in rodents

Legend: Where animals are naive to APAP (left side) and receive a toxic challenge, injury progresses in a well-characterised pattern. Intracellular accumulation of the reactive metabolite NAPQI in CYP450-rich centrilobular (CL) regions causes oxidative stress and suppresses the antioxidant response mediated by Nrf2. The naive liver is quickly overwhelmed by widespread necrosis, and the organ fails. If animals have received an injurious prior exposure to APAP (right side), this pre-exposure initiates protective changes in the liver, detectable as reduced CYP450, increased GSH and cellular proliferation as the organ recovers. A subsequent toxic challenge is tolerated due to enhanced detoxification and repair processes. Injury arising from the second exposure regresses, the organ heals and the animal survives. (Shayiq et al. 1999; Dalhoff et al. 2001; Fan et al. 2014)

1.6. Aim

The aim of this thesis is to investigate the molecular mechanisms of adaptation to chemical stress in two preclinical models using the model hepatotoxin APAP. In the first experimental chapter, two preclinical models of repeated APAP exposure are characterised, and a global proteomic analysis of rat liver provides insight into the changes in abundance of a subset of proteins common to all animals throughout the duration of the timecourse. The second experimental chapter probes deeper into the molecular events surrounding adaptation to repeated exposure in the rat, interrogating proteomic data using pathway analysis software, and focusing on the role of the key enzyme involved in the bioactivation of APAP, CYP2E1, at different timepoints in the model through immunohistochemistry and liver microsome experiments. The final experimental chapter compares the regenerative response in the rat and mouse, probing for proteins identified as key to the process of adaptation in the work of previous chapters.

1.6.1. Hypothesis

Adaptation to repeat APAP exposures is a complex process involving multiple pathways and phases, commensurate with a sophisticated response across the liver to ensure survival upon re-exposure to subsequent normally noxious exposures.

Chapter 2: Rodent adaptation to repeat APAP exposure

Contents

2.1. Introduction

Adaptation to chemical stress can be induced by many pharmaceutical compounds. The process has important implications for both public health and drug development. The factors governing hepatic adaptation to the popular analgesic and antipyretic acetaminophen (paracetamol, APAP) represent valuable research avenues, since APAP toxicity represents a leading cause of emergency hospital admissions through accidental and intentional overdose. Knowledge of the mechanism of hepatic adaptation is limited, and the research focus to date has been on select proteins implicated in APAP metabolism.

In this chapter, data have been presented from a rodent model of hepatic adaptation to drug toxicity from a whole proteome perspective. Quantitative mass spectrometry has been used to show that the expression of 30 % of proteins detected in the rat liver is altered during adaptation to APAP. Genetic manipulation in mouse of a key protein which dictates how the liver adapts to chemical stress, Nrf2, has limited effect. It is therefore likely that the process of adaptation is far more sophisticated than was previously realised. These data give the first insight into the unexpected complexity and dynamic nature of the biological response to drug-induced liver injury.

2.1.1. Adaptation to chemical stress

Adaptation in a biological setting can be defined as a change in the phenotype of an organism that allows it to better survive in its environment following exposure to a noxious stimulus. In the setting of drug safety, some individuals may tolerate exposure to a potential toxin, some may develop a transient injury but adapt and recover, whilst it has been suggested that others fail to adapt and develop a serious adverse drug reaction (Watkins 2005). In humans, some volunteers administered a therapeutic dose of APAP displayed elevations in circulating liver enzymes (clinical markers of liver injury), which then

resolved (Borlak et al. 2013). Adaptation is therefore likely to be an important defensive mechanism to prevent progressive injury resulting from drug toxicity.

This phenomenon, sometimes termed "autoprotection", has been particularly investigated in order to gain insight into the complex problem of drug induced liver injury (DILI), which is probably the most important drug safety issue in pre-clinical and clinical drug development. A clearer mechanistic understanding of the processes driving both DILI and adaptation is necessary in order to design safer medicines. Adaptation to normally toxic successive doses of a drug has been shown to confer protection in the liver and also other organs following administration of a diverse range of compounds including carbon tetrachloride, thioacetamide, 2-butoxyethanol and S-1,2-dichlorovinyl-L-cysteine (Dambrauskas and Cornish 1970; Thakore and Mehendale 1991; Mangipudy et al. 1995; Sivarao and Mehendale 1995; Vaidya et al. 2003).

2.1.2. APAP-induced adaptation in the literature

The most widely studied drug that elicits adaptation is APAP (Buttar et al. 1976; Poulsen and Thomsen 1988; Shayiq et al. 1999; Dalhoff et al. 2001; Aleksunes et al. 2008a; O'Connor et al. 2013). Previous research into APAP adaptation has indicated that metabolic detoxification processes are activated, which alter the fate of subsequent exposures (O'Connor et al. 2013). Specific candidate proteins shown to be altered by the initial exposure of an adaptogenic protocol include CYP2E1 and CYP1A2 (Shayiq et al. 1999), both enzymes which are directly implicated in the bioactivation of APAP to its reactive metabolite NAPQI; also the basolateral efflux transporters MRP3 and MRP4 (Aleksunes et al. 2008a); and more recently, the xenobiotic detoxicant FMO3 (Rudraiah et al. 2014). Due to its regulatory role in protection from oxidative stress, the transcription factor Nrf2 has been implicated in adaptation to APAP. Nrf2 is necessary for the induction of MRP3 and MRP4 (Aleksunes et al. 2008b), and genetic activation of Nrf2 confers resistance to acute

APAP toxicity (Okawa et al. 2006). Additionally, data are accumulating which indicate that the phenotype of regenerating tissue exerts a hepatoprotective effect, as demonstrated by studies which have employed the antimitotic colchicine to restore susceptibility in rodent models of adaptation (Shayiq et al. 1999; Dalhoff et al. 2001; Aleksunes et al. 2008a).

2.1.3. Summary

Studies of adaptation to APAP have thus far been largely restricted to proteins with a likely direct role in APAP metabolism, for example, CYP2E1. APAP pretreatment has previously been associated with changes in metabolic detoxification processes, with implications for the metabolism of subsequent drug exposure. However, there has not yet been a whole proteome approach to the investigation of adaptation to APAP, so the full extent of the response has not been revealed to date.

In this study, rats and mice were exposed every 24 hours to low, medium or high doses of APAP, and clinical chemistry and necropsy were performed to characterise and validate the model. Although rats and mice both showed an adaptive response, the mouse group showed a greater degree of overt toxicity than the rat. Based on these data, livers from the rat high APAP exposure group were taken forward for proteomic analysis as a model of resistance to repeat APAP exposure. It is shown here that almost 30 % of the detected proteome is significantly altered during adaptation, indicating that the breadth of the effects of adaptation is much greater than previously thought. This has been confirmed by examination of adaptation in an Nrf2 null mouse model, which demonstrated that adaptation still occurs in the absence of this key cytoprotective transcription factor.

2.2. Methods

2.2.1. Materials

8-plex isobaric tags for relative and absolute quantification (iTRAQ) protein labelling kit/reagents were purchased from AB Sciex (Framingham, MA, USA). Sequencing grade trypsin was obtained from Promega UK (Southampton, Hants, UK). LC-MS grade dH_2O and methanol, ethylene diamine-tetracetic acid (EDTA), ammonium bicarbonate and potassium chloride were from Fisher Scientific (Loughborough, UK). All other reagents were of analytical grade and quality and purchased from Sigma (St. Louis, MO). Antibodies for NQO1, PCNA and β-actin were purchased from Abcam (Cambridge, UK; Cat. nos ab2346, ab29 and ab6276 respectively). Antibody for GSTP1 was from Assay Designs (Enzo Life Sciences, Farmingdale, NY) (Cat. No. MSA-102) and antibody for vimentin was from Sigma (Cat. No. V6389).

2.2.2. Animals

All animal work was undertaken by Almirall S.A. (Barcelona, Spain), including toxicological assessment as described in 2.2.4. Male Crl:WI (Han) rats and male Crl:CD1 (ICR) mice (6-8 weeks of age) were obtained from Charles River Laboratories (Lyon, France) and allowed 1 week to acclimatise prior to the study. Six animals were housed per cage, on a 12 h light/dark cycle (lights on 0800, lights off 2000), temperature of 22 ± 2 ^{o}C and humidity of 55 ± 15 %. Standard food and tap water were provided *ad libitum*. Care of animals was undertaken in compliance with the European Community Directive 86/609/CEE for the use of laboratory animals and with the Autonomous Catalan law (Decret 214/1997). All experimental procedures were approved by the Almirall Ethics Committee before initiation of the study.

2.2.3. Study design

APAP was dissolved in vehicle (0.5 % methylcellulose and 0.1 % Tween 80 in distilled water, 10 mL/kg) and administered by gavage without previous fasting period. Formulations were prepared daily and control animals received the vehicle solution alone. Rats received a dose of 500, 1000 or 1500 mg/kg, and mice received 250, 500 or 750 mg/kg. Animals (n = 6) received either a single dose of APAP at 0 h (for 2, 4, 6 or 24 h) or vehicle (for 2 or 24 h), or were dosed at 24 h intervals for up to 72 h, with sacrifices 24 h after each dose. An outline of the dosing protocol is shown in Figure 2.1.

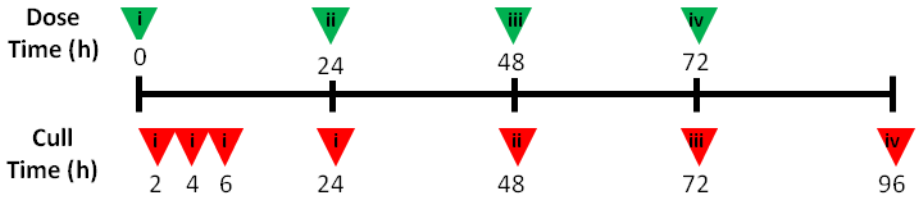

Figure 2.1: Study design for repeat APAP exposure in rat and mouse

Legend: Green triangles denote APAP administration. Rats received either 500, 1000 or 1500 mg/kg at each time point; mice received 250, 500 or 750 mg/kg. Red triangles indicate cull times. Animals were sacrificed at 2, 4, 6 and 24 h after the first dose, and at 24 hours after the last dose received in all other groups. Roman numerals denote the number of doses received.

Body weight was recorded daily during treatment to assess the general wellbeing of the animals. Terminal blood samples without previous fasting were collected from the retroorbital plexus under isoflurane anaesthesia (4 % induction, 1.5-3 % maintenance) into serum separator tubes for clinical chemistry analysis. Blood samples were centrifuged for 10 min at 3000 rpm and serum collected. After centrifugation, each sample was stored at -80 ^{o}C until analysis. Immediately after blood collection, animals were exsanguinated by cutting the abdominal aorta under isoflurane anaesthesia.

2.2.4. Toxicological assessment

A Synchron Clinical System cx7® (Beckman, Brea, CA) was used to determine alanine aminotansferase (ALT, IU/L) and aspartate aminotransferase (AST, IU/L). The liver and brain were weighed to calculate liver-to-brain weight ratios (in %) for each animal. Samples of liver were harvested and frozen in liquid nitrogen before storage at -80 ^{o}C. The hepatic median lobe was preserved in 10 % neutral buffered formalin, embedded in paraffin, sectioned and stained with haematoxylin and eosin (H&E) for subsequent histological blind examination under light microscopy. Distribution, incidence and score of hepatic lesions in each animal group were recorded according to the Predictive Safety Testing Consortium's "Recommended Histopathology Practices in Novel Liver Biomarker Qualification Studies". Scoring criteria are defined in Table 2.3.

2.2.5. Glutathione sample preparation

GSH analysis by mass spectrometry (MS) was performed by Dr. Joanne Walsh. Rat and mouse livers (n = 4 per treatment group) were homogenised using the method of Bouligand et al. with minor modifications (Bouligand et al. 2006). 50-100 mg of liver tissue was homogenised in acidic (pH 2) homogenisation buffer (1.15 % w/v potassium chloride, 1 mM EDTA and 2 mM batho-phenanthroline disulphonate in 0.1 % v/v formic acid (FA)) using a Mixer Mill 220 (Retsch, Haan, Germany) (30/s; 3 min). Samples were centrifuged (16 000 g, 15 min, 4 °C) and the supernatant retained. The pellets were reserved for protein concentration determination by the method of Lowry (Lowry et al. 1951).

GSH and GSSG (oxidised glutathione) standards (0.1-10 µM) were prepared from 1 mM stock solutions. 50 µL of internal standard (stable isotope labelled GSH [GSH-Gly($^{13}C_2$,^{15}N)]) was added to 50 µL of standards or homogenised samples. 50 µL of matrix (pooled mouse liver homogenate, 5 mg/mL protein) was also spiked into standards. In order to derivatise

the thiol groups, 100 µL of iodoacetamide (IAA) derivatisation solution [10 mM IAA in 10 mM ammonium bicarbonate with NH_3OH 0.5 % (v/v); pH 9.5] was added, and the solutions were incubated (1.5 h; room temperature (RT)). Reactions were performed in amber microfuge tubes for light sensitive samples (Eppendorf UK Ltd, Stevenage, UK).

50 µL of ice cold sulphosalicylic acid solution (10 % w/v) was added in order to stop the reaction and precipitate proteins. Samples and standards were vortexed and centrifuged (16 000 g, 15 min, 4 °C) before being filtered (1500 g, 20 min) using a 96 well MultiScreen filter plate (Millipore Ltd, Watford, UK). All solutions were made up to a final volume of 1 mL with 0.1 % (v/v) FA, and 100 µL transferred to a glass vial for LC-MS/MS analysis.

2.2.6. Glutathione LC-MS/MS analysis

The Dionex UltiMate 3000 High Performance Liquid Chromatography system (Thermo Fisher, UK Ltd, Surrey, UK) was used in combination with a Kinetex 2.6 µm C18 100 Å 100 x 2.1 mm column (Phenomenex, Macclesfield, UK), in order to achieve separation of analytes. The column oven was held at a temperature of 30 °C. The injection volume was 10 µL, with the syringe washed with 5 % methanol prior to each injection. The flow rate was 100 µL/min with mobile phases 0.1 % (v/v) FA in dH_2O (solvent A) and 0.1 % (v/v) FA in methanol (solvent B). The elution gradient (0 min, 0 % B; 0-5 min, 0-20 % B; 5-10 min, 20 % B; 10-15 min, 0 % B) had a total run time of 15 minutes. An ABSciex Q Trap mass spectrometer (ABSciex UK Ltd, Warrington, UK) was used for analyte detection using a multiple reaction monitoring (MRM) method. The parameters used for each analyte are detailed in Table 2.1

Analyte	Q1 mass	Q3 mass	DP (volts)	CE (volts)	CXP (volts)
CM-GSH	366.3	237.0	65.0	16.0	10.0
GSSG	613.4	355.2	83.0	32.0	10.0
CM-GSH-IS	369.1	84.0	71.0	53.0	2.0

Table 2.1: Parameters used for MS/MS analyte detection

DP = declustering potential; CE = collision energy; CXP = collision cell exit potential; CM = carboxymethyl; IS = internal standard.

2.2.7. iTRAQ labelling and mass spectrometric analysis of liver homogenates

Rat liver samples (n = 4 animals per timepoint, 1500 mg/kg group, ~100 mg wet weight) were homogenised in 0.5 M triethylammonium bicarbonate (TEAB)/0.1 % sodium dodecyl sulphate using a Mixer Mill 220 (Retsch, Haan, Germany), and centrifuged at 14000 g for 10 mins. Aliquots of each sample (100 µg protein) were denatured, reduced and sulphydryl groups were capped with methylmethane thiosulphate (MMTS) according to the manufacturer's 8-plex protocol (Life Technologies, Paisley, UK). The samples were digested with trypsin overnight, labelled with iTRAQ isobaric tags and mixed in equal proportions. Unbound reagent and trypsin were removed by cation exchange chromatography. Fractions were desalted using a macroporous C18 column (Agilent, Santa Clara, CA) on a Vision workstation and dried by centrifugation under vacuum (SpeedVac; Eppendorf, Stevenage, Herts, UK). Sample analysis was kindly performed by Dr. Roz Jenkins using a Triple TOF 5600 mass spectrometer (AB Sciex, Warrington, Cheshire, UK). Samples were delivered into the instrument by automated in-line liquid chromatography Eksigent NanoUltra cHiPLC System mounted with microfluidic trap and analytical column (15 cm × 75 µm) packed with ChromXP C18-CL 3 µm via a nano-electrospray source head and 10 µm inner diameter PicoTip (New Objective, Woburn, MA). The precolumn was washed for 10 min at 2 µL/min with 2 % acetonitrile (ACN)/0.1 % FA. A gradient from 2 % ACN/0.1 % FA (v/v) to 50 % ACN/0.1 % FA (v/v) in 90 min was applied at a flow rate of 300 nL/min.

The MS was operated in positive ion mode with survey scans of 250 ms, and with an MS/MS accumulation time of 100 ms for the 25 most intense ions (total cycle time 2.5 s). A threshold for triggering of MS/MS of 100 counts per second was used, together with dynamic exclusion for 12 s and rolling collision energy, adjusted for the use of iTRAQ reagent in the Analyst method. Information-dependent acquisition was powered by Analyst TF 1.5.1 software, using mass ranges of 400-1600 atomic mass units (amu) in MS and 100-1400 amu in MS/MS. The instrument was automatically calibrated after every fifth sample using a beta-galactosidase digest.

2.2.8. iTRAQ protein identification and statistical analyses

Liver samples from rats treated with 1500 mg/kg APAP or vehicle control were analysed across four iTRAQ runs with a comparator pooled sample included in each run for normalisation between iTRAQ experiments. Samples (n = 3 or 4) for each exposure group were randomised across the four runs to minimise label bias. Ratios for each iTRAQ label were obtained, using the common pool as the denominator. Data analysis was performed using ProteinPilot software (Version 3, Life Technologies, Paisley, UK). The data were analysed with MMTS as a fixed modification of cysteine and biological modifications. The SwissProt database was searched with a confidence interval of 95 % and also screened in reverse to facilitate false discovery rate (FDR) analysis. Proteins identified from peptides with more than 95 % confidence and a global FDR of less than 1 % were included in the statistical analysis.

The limma package within the R programming environment (Team, 2005) allowed simultaneous comparisons between multiple treatments using design and contrast matrices. This open source software generates a linear regression model to facilitate the analysis of differential protein expression. Mean fold changes were calculated and analysis conducted on the logged fold-change values. Unadjusted (raw) p values and p values

following FDR correction for multiple testing were determined. Volcano plots were generated, as was a heatmap of significantly changed proteins common to all animals, and principal component analysis (PCA) was performed.

2.2.9. Western immunoblotting

In order to confirm changes in key proteins identified by iTRAQ, buffered liver homogenates of standardised protein concentration (n = 4) were separated on a polyacrylamide gel. Resolved proteins were transferred onto nitrocellulose membrane (GE Healthcare, Little Chalfont, Buckinghamshire, UK) and Ponceau-S stained to confirm even protein loading before blocking with 10 % milk protein diluted in tris-buffered saline containing 0.05 % Tween 20 (TBS-T). Antibodies were diluted in TBS-T with the addition of 2 % milk protein and applied according to individual protocols (Table 2.2). All secondary antibodies were horseradish peroxidise (HRP)-conjugated. Membranes were treated with Western Lightning Plus Enhanced Chemiluminescence (Perkin Elmer, Waltham, MA) before exposure to X-ray film (GE Healthcare). Exposed films were scanned using a GS800 scanner (Bio-Rad, Hercules, CA) and relative band intensity was analysed using Quantity One software (Bio-Rad). Proteins of interest were normalised to actin, then expressed relative to the mean of the control group.

Protein	**GSTP1**	**NQO1**	**PCNA**	**Vimentin**	**Actin**
Manufacturer	Assay Designs	Abcam	Abcam	Sigma	Abcam
Code	msa-102	ab2346	ab29	v6389	ab6276
MW (kDa)	26	31	29	54	40
Host species	rabbit	goat	mouse	mouse	mouse
Block duration	overnight	30 min	30 min	30 min	overnight
Primary dilution	1:10 000	1:2000	1:2000	1:5000	1:20 000
Primary incubation	1h	overnight	overnight	overnight	30 min
Secondary dilution	1:10 000	1:5000	1:5000	1:5000	1:10 000
Secondary incubation	1h	1h	1h	1h	1h

Table 2.2: Antibody conditions for western immunoblot

2.2.10. Nrf2 knockout study

Data from a previously conducted study performed by Dr. Laura Randle was included due to its pertinence to the mechanism of adaptation to chemical stress. In Dr. Randle's study, the Nrf2-dependent response of the mouse to repeat APAP exposure was investigated. Mice (C57BL6J background) were treated daily with increasing doses of APAP in a recapitulation of the protocol described by Shayiq et al. (1999) (Figure 2.2).

Toxic challenge ↓

Pretreatment period (days) ←→

	1	2	3	4	5	6	7	8	9
A	150	150	300	300	450	450	600	600	1000
B	150	150	300	300	450	450	600	600	saline
C	saline	saline	saline	saline	saline	saline	saline	saline	1000
D	saline	saline	saline	saline	saline	saline	saline	saline	saline

Figure 2.2: Study design for repeat APAP exposure in Nrf2 knockout mice

Legend: In a study performed by Dr. Laura Randle, $Nrf2^{(+/+)}$ and $Nrf2^{(-/-)}$ mice were each assigned to groups A B C and D. Groups A and B received incremental doses of APAP every 24 h over a period of 8 days (range 150 – 600 mg/kg), with a final challenge on day 9 of 1000 mg/kg APAP or saline. Groups C and D received saline pretreatment and either toxic challenge or saline on day 9. Animals were culled 5 hours after dosing on day 9. All doses shown in mg/kg.

All experiments were undertaken in accordance with criteria outlined in a licence granted under the Animals (Scientific Procedures) Act 1986, and approved by the Animal Ethics Committee of the University of Liverpool. Generation of the Nrf2 knockout mouse and genotyping of progeny was performed as described previously (Itoh et al. 1997; McMahon et al. 2001). Non-fasted male littermate $Nrf2^{(+/+)}$ and $Nrf2^{(-/-)}$ mice of 10-12 weeks of age were used throughout the study. Mice were housed between 19 °C – 23 °C, under 12 h light/dark cycles and given free access to food and water. Dosing began at 10 am each day.

APAP 15 mg/mL or 30 mg/mL was freshly prepared in warmed saline (0.9 %) depending on the dose to be administered. After pilot dose ranging studies confirmed the dose dependent nature of APAP-induced hepatotoxicity, male $Nrf2^{(+/+)}$ mice and $Nrf2^{(-/-)}$ littermates received increasing daily doses of APAP (2 x 150 mg/kg, 2 x 300 mg/kg, 2 x 450 mg/kg, 2 x 600 mg/kg in 0.9 % saline, i.p.) over 8 days, or an equal volume of saline vehicle alone (0.9 %, i.p.) (n = 4 mice per treatment group). On day 9, both groups were further challenged with 1000 mg/kg APAP (0.9 % saline, i.p.) or saline (n = 4-8 mice per treatment group). Mice were culled by exposure to a rising concentration of CO_2 followed by cervical dislocation 5 h after the final toxic APAP dose on day 9 (approximately 3 pm) and survival data were analysed.

2.2.11. Data evaluation and statistical analysis

Clinical chemistry and toxicological data are expressed as mean plus standard error of the mean (SEM). Body weight, liver to brain ratio, and serum ALT and AST data for vehicle- and APAP-treated animals were compared to time-matched controls by one-way ANOVA with Tukey post-hoc test. Western immunoblotting, iTRAQ and GSH data were analysed using a one-way ANOVA with Dunnetts post-hoc test. The software used was GraphPad PRISM (version 6.03 for Windows, GraphPad Software, San Diego, USA). A p value < 0.05 was considered statistically significant.

2.3. Results

In this model of adaptation to repeat APAP exposure, rats were dosed orally with 500, 1000 or 1500 mg/kg APAP either once at 0 h with sacrifice at 2 h, 4 h, 6 h or 24 h; or at 24 hour intervals for up to 72 hours with sacrifices 24 hours after the final dose administered. Mice were also treated following an identical protocol but using doses of 250, 500 and 750 mg/kg (Figure 2.1).

2.3.1. Bodyweight

Bodyweight was monitored daily from the beginning of APAP administration to assess individual animal welfare throughout the dosing period.

2.3.1.1. Rat

No differences in bodyweight were observed in rats treated at 500 mg/kg compared to the corresponding vehicle group (Figure 2.3a). In contrast, bodyweight from rats treated at 1000 and 1500 mg/kg was significantly lower than that of control animals after 96 hours of daily APAP administration. No mortality was observed in rats at any dose tested.

2.3.1.2. Mouse

Mice treated with APAP at 250 mg/kg presented no reduction in bodyweight whereas treatment with both 500 and 750 mg/kg resulted in a loss of bodyweight which was significant after 48 hours of daily APAP administration, but animals recovered thereafter (Figure 2.3b). 1/48 mice in the 500 mg/kg group was found dead at 96 h; and 2/48 in the 750 mg/kg group were found dead, one at 48 h and one at 96 h.

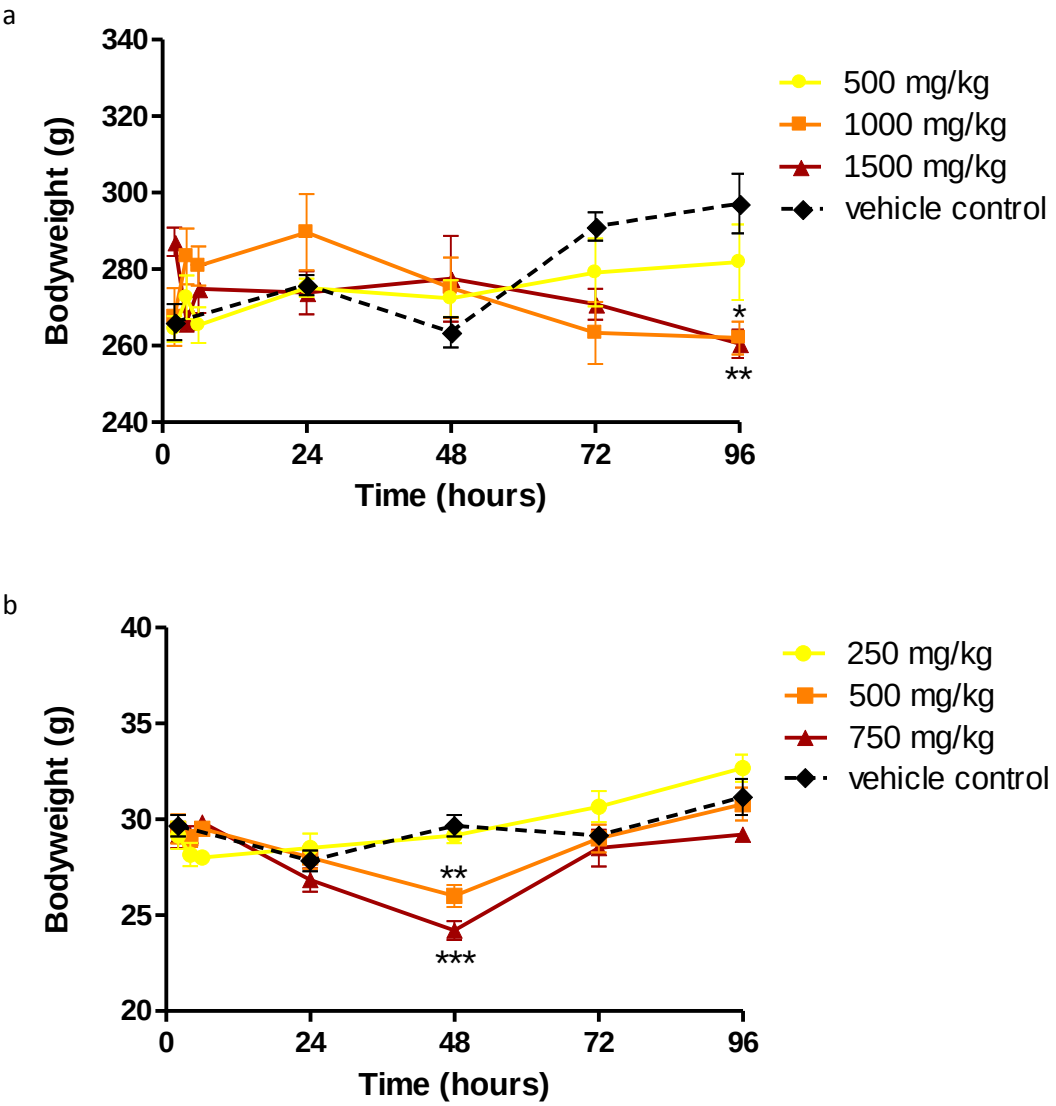

Figure 2.3: Bodyweight in rat and mouse

Legend: In rat (a), after 96 hours of daily APAP administration at 1000 and 1500 mg/kg, rats showed significantly lower bodyweight than time-matched control animals. No significant difference was seen at any other timepoint. In mouse (b) after 48 hours of daily APAP administration at either 500 or 750 mg/kg, mice showed significantly lower bodyweight than control animals. No significant difference was seen at any other timepoint.

2.3.2. Liver mass

Liver mass was calculated relative to brain mass in order to control for changes in growth over the study duration.

2.3.2.1. Rat

In rats, no statistical significance was seen when comparing liver to brain mass in each treatment group to ratios for control animals (Figure 2.4a).

2.3.2.2. Mouse

In mice, the relative mass of the liver was significantly decreased at 48 h in the 750 mg/kg group (Figure 2.4b).

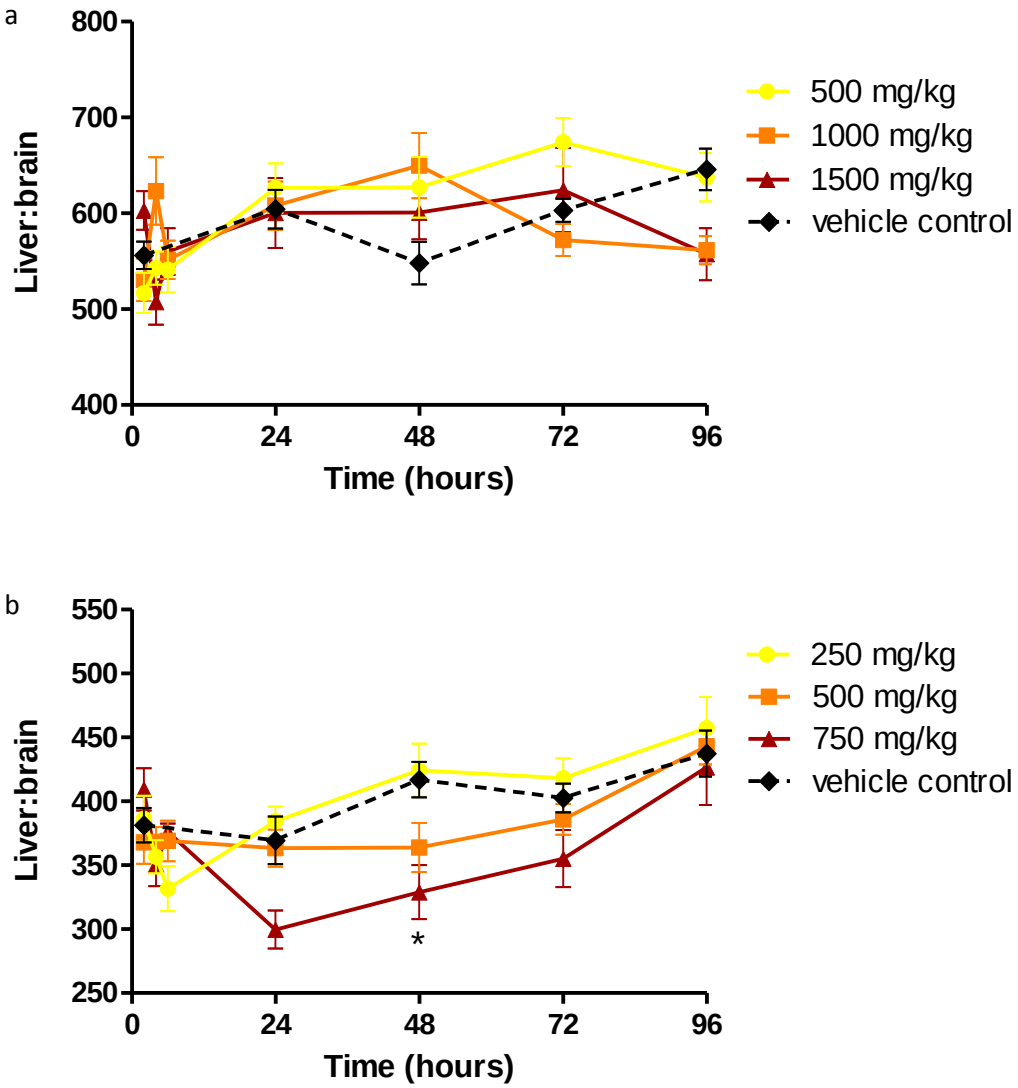

Figure 2.4: Liver to brain mass in mouse

Legend: In rat (a) when growth was controlled for by expressing liver mass relative to brain mass, no statistical significance was seen at any point. In mouse (b) after 48 hours of daily APAP administration at 750 mg/kg, mice showed significantly lower liver to brain mass ratio than control animals. No significant difference was seen at any other timepoint.

2.3.3. Histopathology

A histopathological review of liver samples was scored according to Table 2.3.

Score	Description	Observation
0	No injury	Histologically normal
1	Minimal	A microscopic change ranging from inconspicuous to barely noticeable but so minor, small, or infrequent as to warrant no more than the least assignable grade
2	Mild	A microscopic change that is a readily noticeable but not a prominent feature of the tissue and/or may be considered to be of no functional consequence
3	Moderate	A microscopic change that is a prominent but not a dominant feature of the tissue and/or may be considered to have limited impact on organ function
4	Marked	A microscopic change that is a dominant feature and may be an overwhelming component of the tissue and/or may be considered to cause significant tissue or organ dysfunction and/or represents an end-stage feature of the tissue (i.e. total organ failure)

Table 2.3: Histopathology scoring of tissue

2.3.3.1. Rat

Hepatic histological lesions seen after APAP administration in rats are presented in Table 2.4. Histologically, no apparent lesions were observed at 2, 4 or 6 h after a single APAP exposure. 24 h after the first administration, rats treated at all doses showed minimal hepatocellular eosinophilia in the centrilobular zone. Hepatic centrilobular necrosis was observed in 1/6 animals dosed at 1000 mg/kg, and presence of mild mixed inflammatory infiltrates in the same zone was observed in some animals treated at 1000 and 1500 mg/kg. Incidence of hepatic lesions peaked at 48 and 72 hours, notably in 1000 and 1500 mg/kg groups. Lesions were characterised by centrilobular mild hepatocellular eosinophilia and moderate to marked hepatocellular coagulative necrosis with associated mild mixed inflammatory cell infiltrates. Centrilobular hepatocellular eosinophilia and necrosis accompanied by mixed inflammatory infiltrates were still observed in some animals at 96 h, in particular at 1500 mg/kg. Representative H&E stained sections from rats treated with 1500 mg/kg APAP can be seen in Figure 2.5. Blinded and unblinded quantification areas of

necrosis across whole liver sections showed a significant 35 % loss of liver cells, predominantly hepatocytes, at 48 h only. No significant areas of necrosis were seen at subsequent timepoints (Table 2.5).

Experimental group		Dose (mg/kg)	Hepatocellular eosinophilia			Hepatocellular necrosis			Inflammatory cells		
			Distribution	Incidence	Score	Distribution	Incidence	Score	Distribution	Incidence	Score
Single dose	2 h	500									
		1000									
		1500									
	4 h	500									
		1000									
		1500									
	6 h	500									
		1000									
		1500									
	24 h	500	CL	3/6	1						
		1000	CL	4/6	1	CL	1/6	2	CL	2/6	1-2
		1500	CL	5/6	1-2				CL	3/6	1-2
Repeat dose	48 h	500	CL	3/6	0-1						
		1000	CL	6/6	1-2	CL	3/6	2	CL	6/6	1
		1500	CL	6/6	2	CL	6/6	3-4	CL	3/6	1-3
	72 h	500									
		1000	CL	5/6	1-2	CL	1/6	3			
		1500	CL	5/6	2	CL	5/6	3-4			
	96 h	500									
		1000	CL	2/6	1						
		1500	CL	2/6	2	CL	3/6	2-4	CL	2/6	2

Table 2.4: Main hepatic lesions observed after single or repeat APAP administration in rat

Legend: Numerical summary of the main hepatic lesions observed in the rat over 96 h experimental timecourse. Incidence of hepatic lesions peaked in animals which received 48 h or 72 h of daily APAP administration at 1000 and 1500 mg/kg. CL = centrilobular.

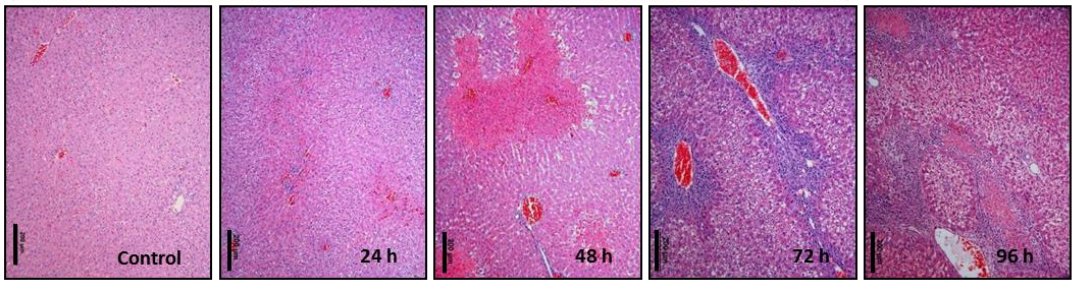

Figure 2.5: Representative images of H&E stained rat liver sections from each timepoint in the 1500 mg/kg dose group

Legend: Stained sections from the rat 1500 mg/kg APAP exposure timecourse showing the progression of tissue injury and recovery. Mild eosinophilia is visible in centrilobular regions at 24 h, and at 48 h centrilobular necrosis can be seen. Bar = 200 µm

Time (h)	% live cells	SEM
24	100	0.00
48	65**	3.54
72	96	2.13
96	95	2.89

Table 2.5: Quantification of area of necrosis in rats treated with 1500 mg/kg APAP

Legend: Regions of cell death presented as a percentage of total area of section analysed, following histopathological analysis of groups of animals at each timepoint in 1500 mg/kg group. 35 % cell death is seen after 48 h of APAP exposure, coincident with significant ALT release (Figure 2.9). Recovery to ~5 % cell death is seen at later timepoints.

2.3.3.2. Mouse

Hepatic histological lesions seen after APAP administration in mice are presented in Table 2.6. Histological examination of liver sections from mice that received a single administration of APAP showed minimal eosinophilia within centrilobular zones (2 h – 24 h). The main hepatic lesions appeared at 48 h, particularly in the 500 and 750 mg/kg dose groups, and were characterised by the presence of areas of coagulative necrosis in centrilobular zones with associated mixed inflammatory cell infiltrates. Additionally, hepatocellular eosinophilia and hypertrophy were seen. At 72 h and 96 h (500 and 750 mg/kg), some animals still presented extensive areas of necrosis accompanied by mononuclear inflammatory cells whereas others did not present any relevant hepatic lesions. Representative H&E stained sections from mice treated with 750 mg/kg APAP can be seen in Figure 2.6.

Experimental group		Dose (mg/kg)	Hepatocellular eosinophilia			Hepatocellular necrosis			Inflammatory cells		
			Distribution	Incidence	Score	Distribution	Incidence	Score	Distribution	Incidence	Score
Single dose	2 h	250									
		500	CL	1/6	1						
		750	CL	5/6	1						
	4 h	250	D	3/6	1						
		500	CL	4/6	1						
		750	CL	6/6	1						
	6 h	250	CL, P, D	5/6	1						
		500	P	5/6	1						
		750	CL	6/6	1						
	24 h	250	CL	1/6	1						
		500	CL	5/6	1						
		750	CL, D	5/6	1						
Repeat dose	48 h	250									
		500	CL, D	5/6	2-3	CL	2/6	2-4			
		750	CL	1/6	3	CL	4/6	4			
	72 h	250	CL	1/6	1						
		500	CL	5/6	1-2	CL	3/6	2-3	CL	4/6	1-3
		750	CL	5/6	1	CL	2/6	3-4	CL	3/6	1-3
	96 h	250									
		500	CL	2/6	1	CL	1/6	4	CL	1/6	1
		750	CL	3/6	2	CL	3/6	2-4	CL	1/6	1

Table 2.6: Main hepatic lesions observed after single or repeat APAP administration in mouse

Legend: Numerical summary of main hepatic lesions observed in the mouse over experimental timecourse. Incidence of hepatic lesions peaked in animals which received 48 h of daily APAP administration at 500 and 750 mg/kg. CL = centrilobular, P = periportal, D = diffuse.

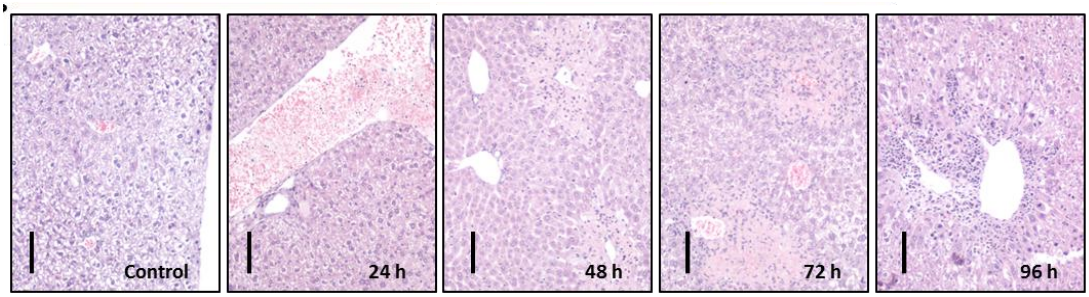

Figure 2.6: Representative images of H&E stained mouse liver sections from each timepoint in the 750 mg/kg dose group

Legend: Stained sections from the mouse 750 mg/kg APAP exposure timecourse showing the progression of tissue injury and recovery. At 48 h centrilobular necrosis can be seen, accompanied by inflammatory cell infiltrate and hepatocellular hypertrophy. Bar = 200 µm

2.3.4. Clinical chemistry

2.3.4.1. Rat

In rats, a single dose of APAP did not affect serum transaminases at 2, 4 or 6 h (data not shown). Both ALT (Figure 2.7a) and AST (Figure 2.7b) increased markedly at 48 h in the 1500 mg/kg dose group. At 72 h and 96 h, levels of both transaminases returned to baseline values. Rats displayed a peak serum ALT rise 40-fold above time-matched vehicle controls, from 40.8 IU/L to 1643.2 IU/L at 48 h; and a 45-fold serum AST rise over control, from 66.7 IU/L to 2987.5 IU/L at 48 h. Both biomarkers returned to normal levels by 96 h.

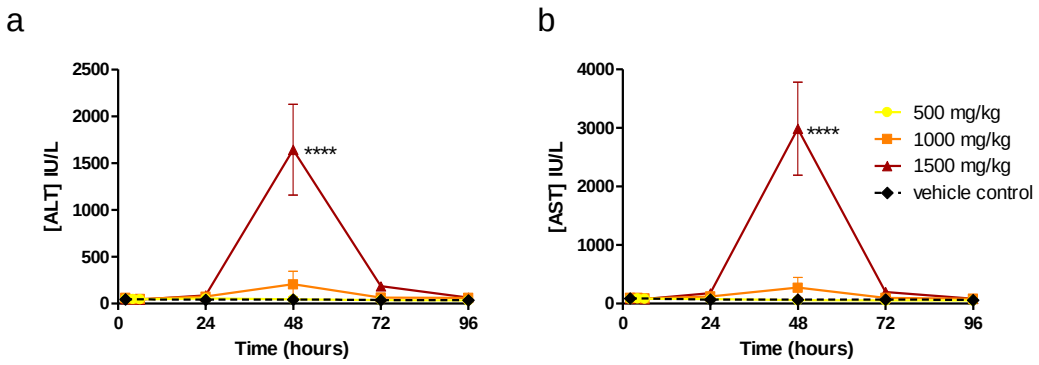

Figure 2.7: Serum transaminases in rat

Legend: Serum ALT and AST levels were determined in terminal blood samples from rats at all time points. Both biomarkers were significantly elevated after 48 h of 1500 mg/kg APAP, and both biomarkers thereafter returned to baseline levels. (n = 6)

2.3.4.2. Mouse

In mice, a single dose of APAP did not affect serum transaminases at 2, 4 or 6 h (data not shown). Both ALT (Figure 2.8a) and AST (Figure 2.8b) increased markedly at 48 h in the 750 mg/kg dose group. At 72 h and 96 h, levels of both transaminases returned to baseline values. Mice displayed a peak serum ALT rise 200-fold above time-matched vehicle controls, from 43.3 IU/L to 8666.2 IU/L at 48 h; and a 67-fold serum AST rise over control, from 75.2 IU/L to 5035.6 IU/L at 48 h. Both biomarkers returned to normal levels by 96 h.

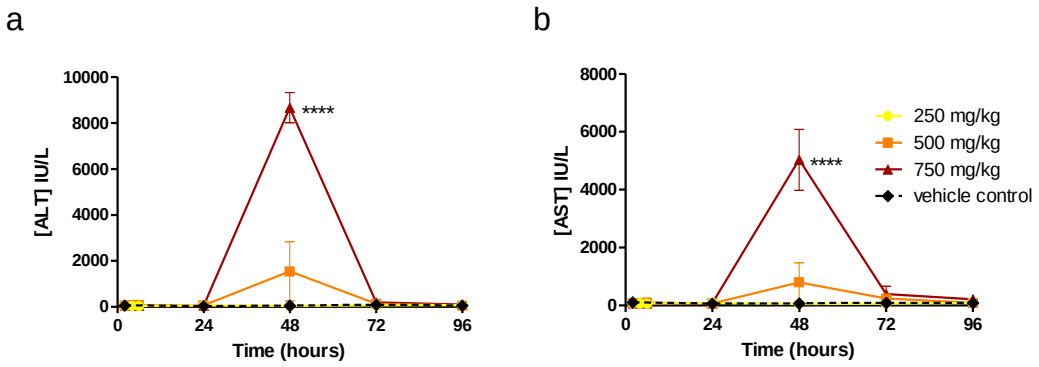

Figure 2.8: Serum transaminases in mouse

Legend: Serum ALT and AST levels were determined in terminal blood samples from mice at all time points. Both biomarkers were significantly elevated after 48 h of 750 mg/kg APAP, and both biomarkers thereafter returned to baseline levels. (n = 6)

2.3.5. Hepatic glutathione

Reduced GSH was measured by mass spectrometry in whole liver samples taken from rat and mouse models. Both models showed initial depletion of GSH at 2, 4, and 6 h after the first exposure to APAP; thereafter, responses diverged.

2.3.5.1. Rat liver glutathione

After an initial depletion at 4 h, GSH values fell further still after 24 h of either 1000 or 1500 mg/kg APAP. By 48 h of exposure, 500 and 1000 mg/kg groups had recovered to values consistent with control, and 1500 mg/kg animals showed significantly elevated values, which fell back to levels consistent with 24 h measurement by 96 h. In contrast, GSH in the 500 mg/kg group were significantly elevated above control values at 72 and 96 h (Figure 2.9).

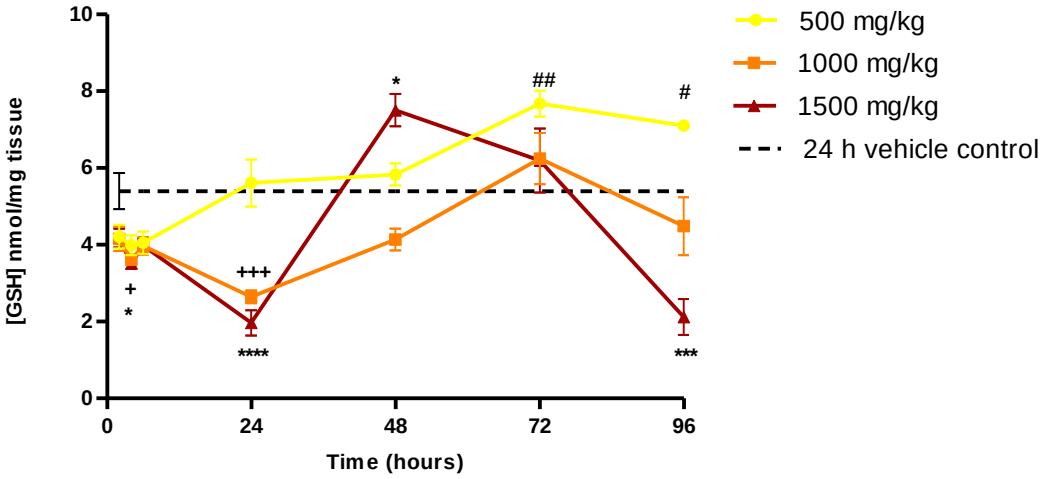

Figure 2.9: GSH in rat

Legend: Analysis of hepatic GSH in rat shows significant depletion at 4h in rats that received 1000 or 1500 mg/kg APAP. GSH remained low in these groups after 24 h of exposure. At the peak of toxicity, after 48 h of exposure, GSH is elevated in the 1500 mg/kg group alone. Thereafter in this group it falls significantly below control values by 96h. #, + and * denote significance for 500, 1000 and 1500 mg/kg group respectively. (n = 4)

2.3.5.2. Mouse

Although the trend was one of loss of GSH at early timepoints, significance was only seen in the 250 mg/kg group at 2 and 4 h. Thereafter no significant deviation from control values was detected at any later timepoint (Figure 2.10).

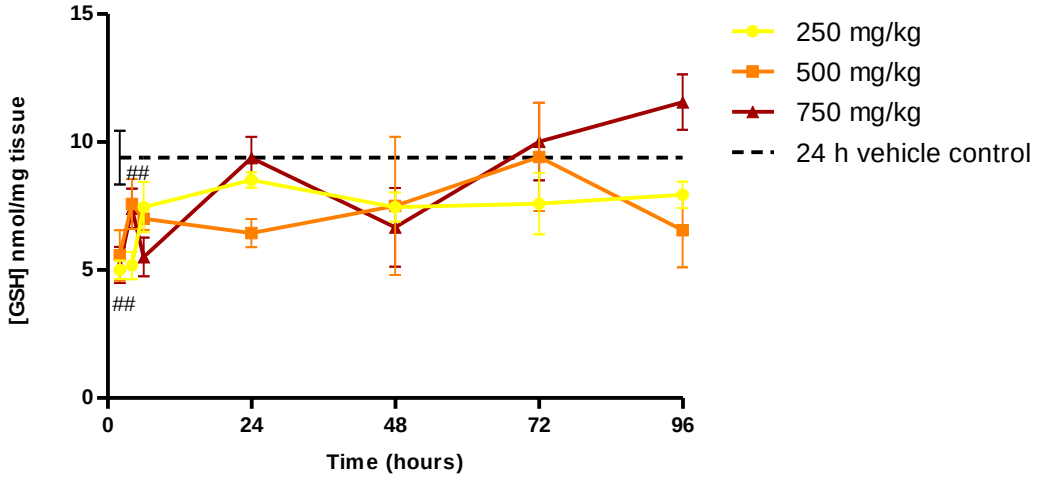

Figure 2.10: GSH in mouse

Legend: Analysis of hepatic GSH in mouse shows significant depletion at 2 and 4 h in animals that received 250 mg/kg APAP. Thereafter, no significant mean deviation from control values is seen. # denotes significance for 250 mg/kg group. (n = 4)

2.3.6. Quantitative mass spectrometry

Based on the results of the clinical chemistry and histopathology analyses, the rat was selected for further investigation. iTRAQ analysis was performed in order to assess the changing phenotype of the rat liver during adaptation to repeat APAP exposure. This technique allows unambiguous identification and quantification of proteins expressed in a complex tissue matrix, and presents a snapshot of the hepatoproteome at each of the timepoints examined. Global proteomic analysis of rat liver tissue identified 2181 unique proteins, of which 1169 were common to all animals and all time points, and were therefore amenable to statistical analysis. Lists of significantly perturbed proteins can be seen in Supplementary Tables 1a-d.

2.3.6.1. Volcano plots and Principal Component Analysis

Global changes at each timepoint have been visualised as volcano plots, in which significance (y) is plotted against fold change (x), allowing the most changed proteins to be easily identified. Although changes can be seen at 24 h (Figure 2.11a), at 48 h (Figure 2.11b, peak toxicity) the volcano plots show the most disparate protein abundance, as indicated by the number of red points (FDR ≤ 0.05) and blue points ($p < 0.05$) in the plot. Large numbers of protein changes are still observed at 72 h (Figure 2.11c) and 96 h (Figure 2.11d). Whilst some proteins in this analysis were increased in abundance as a consequence of dosing, the majority of significantly altered proteins were less abundant when compared to control animals, indicated by red points clustering on the left side of each plot. PCA was performed to identify the proteins contributing to the most apparent differences in the data set as a whole. Comparing principal component (PC) 1 to PC 4 allowed separation of data points into three distinct groups, thereby identifying groups of proteins contributing to the major differences between these groups (Figure 2.11e, Supplementary Table 2). Numerical descriptions of significant changes are shown in Table 2.7, showing that almost 30 % of the detected proteome is altered by repeat APAP exposure.

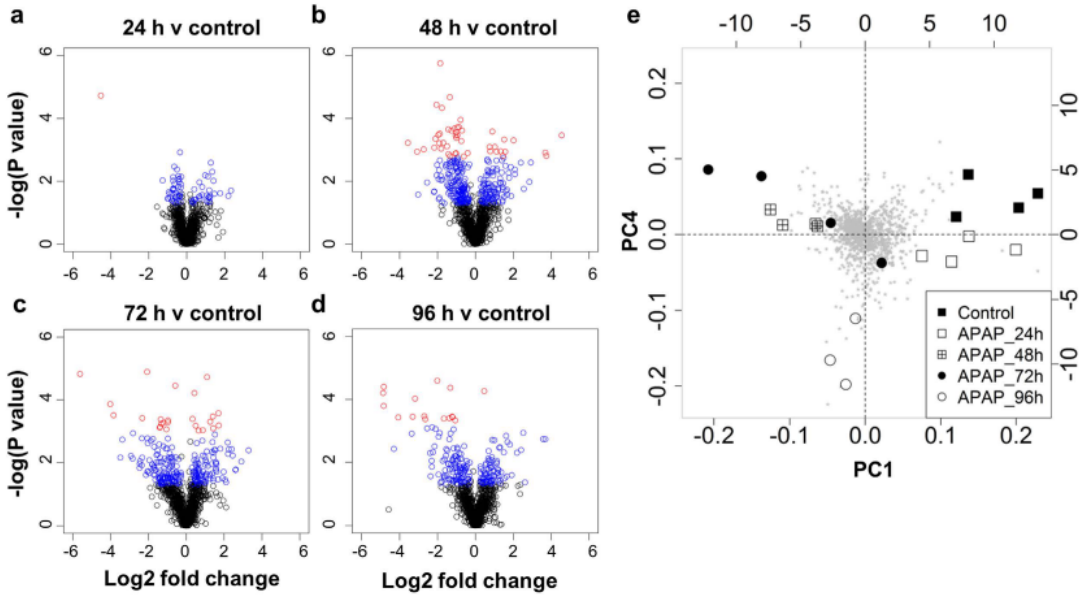

Figure 2.11: Analysis of trends in the rat proteomic data set

Legend: Volcano plots show changes in abundance against significance, allowing changed proteins to be visually identified. **a)** At 24 h, only one protein has significance after adjustment for FDR (shown in red). **b)** At 48 h this number has risen to forty-six; **c)** at 72 h it is twenty-five; **d)** at 96 h, it is sixteen. **e)** A PCA plot allowing identification of groups of proteins contributing to the most apparent differences seen in the data set. Control animals, and those receiving single exposures can be seen to the top right of the plot; repeat exposures at 48 h and 72 h cluster to the top left and 96 h clusters to the bottom of the plot. (n = 3-4)

Timepoint (h)	Doses	Proteins increased abundance ($p < 0.05$)	Proteins decreased abundance ($p < 0.05$)	Total	Percentage of quantifiable proteome different relative to control
24	1	30	43	73	6.24
48	2	116	199	315	26.95
72	3	111	145	256	21.90
96	4	86	125	211	18.05

Table 2.7: Numerical description of significant changes at each timepoint

Legend: Relative changes in protein abundance in rat liver in response to repeat APAP exposure. The number of proteins that were increased or decreased in abundance in rat liver at each timepoint compared to control animals is indicated. The total number of changed proteins is expressed as a percentage of the total number of proteins quantified in the analysis (1169).

2.3.6.2. Heatmapping and validation western immunoblotting

The subset of 1169 proteins common to all animals at every timepoint is expressed as a heatmap (Figure 2.12). This demonstrates similarity in protein expression levels between control and single dose livers (24 h). By contrast, the profile of the same proteins in the repeat dose livers (48 h and 72 h) appears markedly changed. By 96 h a further shift in the protein expression profile is seen, consistent with the clustering shown using PCA in Figure 2.11e.

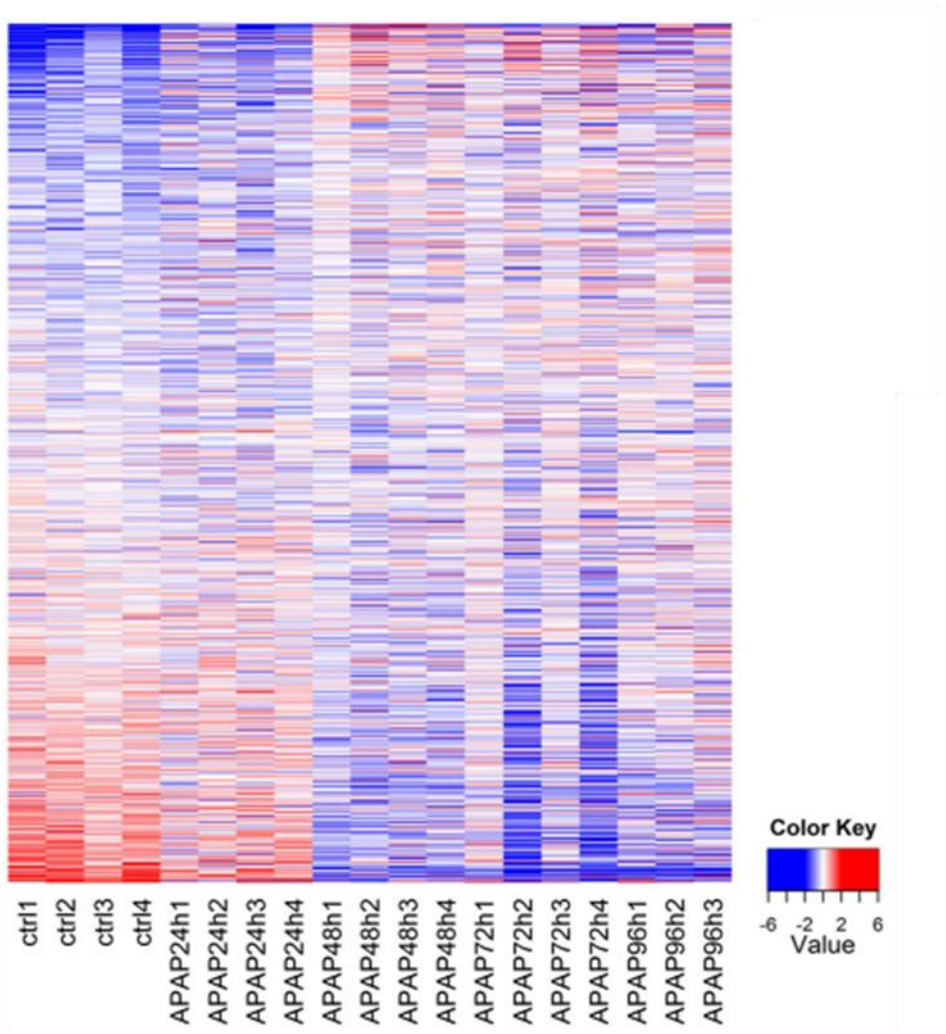

Figure 2.12: Heat map of proteins common to all animals at all timepoints

Legend: Heat map representing the 1169 proteins common to all samples and all time-points identified distinct changes in protein abundance in repeat-dosed animals (red indicates increased abundance, blue indicates decreased abundance).

These observations are supported by immunoblot data obtained from four proteins (Figure 2.13), selected from the iTRAQ mass spectrometric data for their different properties as sentinels of metabolic function or regeneration: GSTP1 (glutathione-s-transferase pi), NQO1, PCNA (Proliferating cell nuclear antigen), and vimentin. NQO1 and GSTP1 are important enzymes in the detoxification of NAPQI, the toxic metabolite of APAP. PCNA is a marker of replication (Galand and Degraef 1989), and indicates a surge in proliferative activity in the rat livers which peaks at 72 h. Vimentin is a classical marker of progenitor cells and is upregulated in cells that are undergoing epithelial to mesenchymal transition, a process implicated in wound healing and organ fibrosis (Eckes et al. 2000).

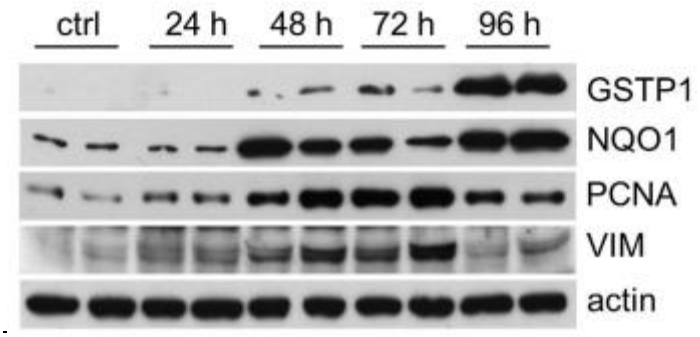

Figure 2.13: Validation of selected significantly perturbed proteins by western immunoblot

Legend: Representative images of western immunoblots for selected significantly perturbed proteins GSTP1, NQO1 and vimentin (VIM) are presented, showing n = 2 animals for each protein of interest. Actin is included as a loading control.

Comparison of western immunoblot data of liver lysates for these selected significantly perturbed proteins with data obtained for the same proteins by MS analysis demonstrated a positive correlation, validating the techniques employed (Figure 2.14).

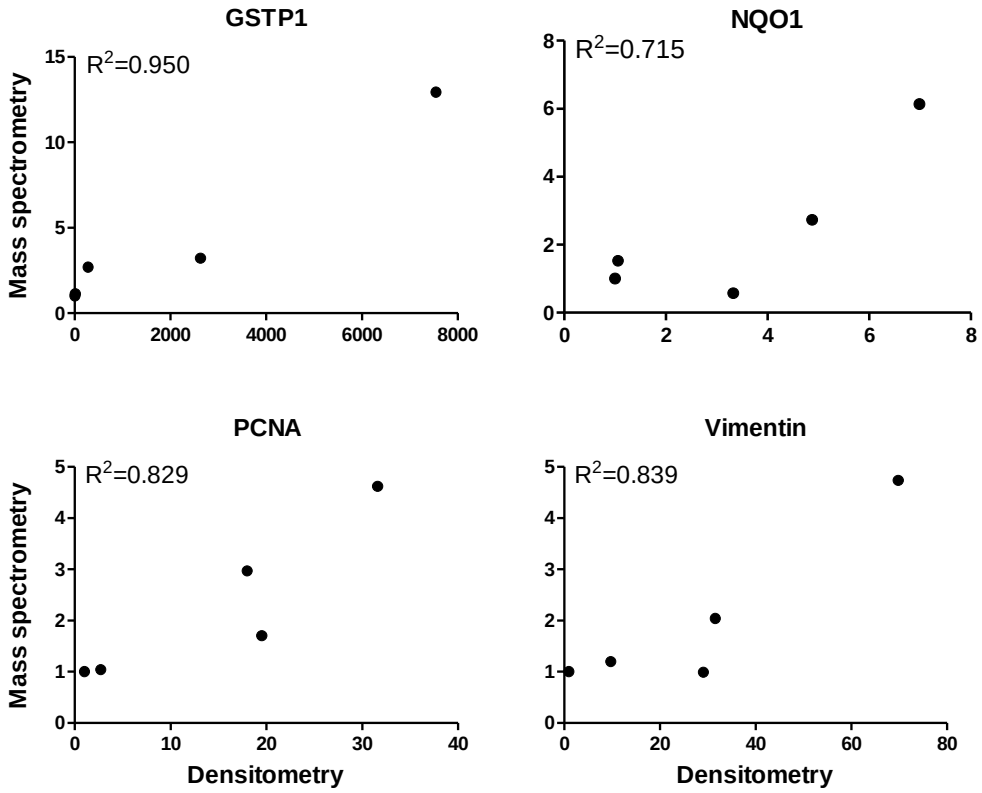

Figure 2.14: Correlation of immunoblot and mass spectrometric data

Legend: For each protein shown in Figure 2.13, densitometric values for abundance have been plotted against mass spectrometric, generating correlation plots showing positive association.

2.3.7. Hepatotoxic assessment of $Nrf2^{(+/+)}$ and $Nrf2^{(-/-)}$ mice

In Dr. Randle's study, after 8 days pretreatment with increasing doses of APAP, $Nrf2^{(+/+)}$ and $Nrf2^{(-/-)}$ mice were given a toxic challenge, and survival at 5 h post dose was quantified (Figure 2.15). In $Nrf2^{(+/+)}$ animals, a toxic challenge in naive animals resulted in 50 % mortality. The same toxic challenge in the APAP pretreatment group caused no mortality, demonstrating the protective effect of pretreatment in wild type animals.

In $Nrf2^{(-/-)}$ animals, a toxic challenge administered to naive animals was 100 % lethal, reflecting increased susceptibility caused by the silencing of the Nrf2 mediated oxidative

stress response. However, APAP pretreatment allowed 50 % of the Nrf2$^{(-/-)}$ animals to survive a toxic challenge that was 100 % lethal after saline pretreatment, demonstrating that Nrf2-mediated transcription is not the only mechanism of adaptation to toxic insult in this model, and indicating that the processes underpinning adaptation exhibit redundancy.

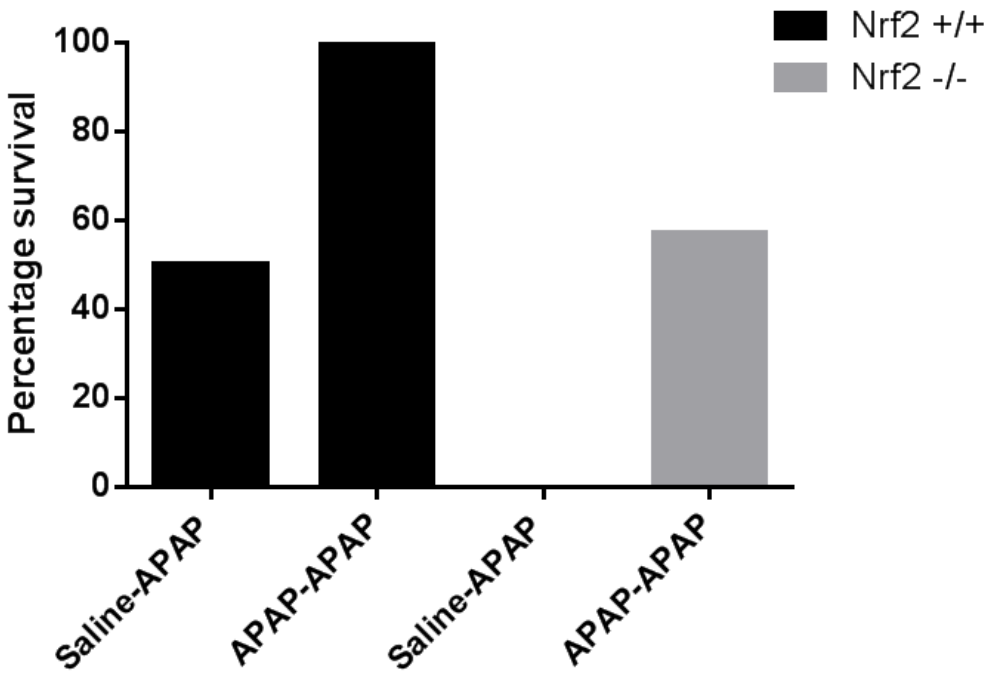

Figure 2.15: Effect of pretreatment on survival of toxic challenge in Nrf2$^{(+/+)}$ and Nrf2$^{(-/-)}$ mice

Legend: Hepatotoxic assessment of Nrf2$^{(+/+)}$ and Nrf2$^{(-/-)}$ mice after a toxic APAP challenge in saline or APAP pretreated mice. In Dr. Randle's experiment, Nrf2$^{(+/+)}$ and Nrf2$^{(-/-)}$ mice were dosed daily with a single i.p. dose of APAP (150-600 mg/kg) or saline vehicle control over 8 days before a 5 h toxic APAP challenge (1 g/kg). Survival was observed 5 h after the toxic dose and plotted as percentage survival.

2.4. Discussion

DILI is a major problem both in the clinic and for the pharmaceutical industry. Our relative lack of understanding of the physiological and toxicological mechanisms involved can lead to the loss of potentially effective drugs during development. APAP poisoning is itself also a significant clinical problem (Larson et al. 2005). Furthermore, APAP is probably the most extensively characterised hepatotoxin in pre-clinical models, and therefore provides a means to interrogate the various processes of adaptation and regeneration in the liver, which are also relevant to humans and may be applicable to other drugs associated with DILI.

2.4.1. Summary of findings

In this chapter, adaptation has been demonstrated in both rat and mouse models of repeated exposure to APAP, suggesting that the phenomenon of adaptation is not species-selective, but rather is a conserved process with relevance to humans. The two species were investigated because of their widespread use in preclinical toxicity testing; because of their similarity to aspects of human APAP hepatotoxicity (Bushel et al. 2007; Kienhuis et al. 2009; McGill et al. 2012a; Hadi et al. 2013); and because the mouse is more amenable to genetic modification in order test the role of specific genes in the process. Both species were dosed using an identical experimental protocol, and the doses were chosen in order to monitor adaptation across a range of sub-toxic, threshold toxic and overtly toxic doses of APAP, to ensure that the drug exposure is relevant to what may occur in humans. Animals were dosed either once at 0 h with sacrifice at 2, 4, 6, or 24 h; or at 24 h intervals for up to 72 h with sacrifice 24 h after the final exposure (Figure 2.1). No mortality was seen in the rat model, and three animals died in the mouse model – one treated with 500 mg/kg (threshold toxicity) was found dead at 96 h; and two treated with 750 mg/kg (overt toxicity) were found dead, one at 48 h and one at 96 h. Significant loss of bodyweight was

seen in both models, but only after 96 h of treatment at 1000 and 1500 mg/kg in rat (Figure 2.3a), and at 48 h of treatment at 500 and 750 mg/kg in the mouse (Figure 2.3b). However, when growth was controlled for by expressing liver mass relative to brain mass, no significant deviation from control was seen in the rat (Figure 2.4a), and in the mouse, significance was only observed after 48 h of treatment at 750 mg/kg (Figure 2.4b). This suggested that, although growth rates may have been affected by APAP exposure, significant liver tissue loss only arose in the mouse 750 mg/kg (overt toxicity) group, which was supported by histopathology and toxicology observations.

Hepatotoxicity in each model was assessed by histopathological analysis (Tables 2.4-2.6; Figures 2.5 and 2.6), alongside the classical serum biomarkers of liver injury, ALT and AST (Figures 2.7 and 2.8). At overtly toxic exposures, both models showed significant hepatocellular injury. At 48 h, mice treated with 750 mg/kg exhibited peak ALT and AST elevations of 200 and 67 fold above vehicle controls compared to 40 and 45 fold elevations respectively in rats treated with 1500 mg/kg. Both markers had returned to baseline levels by 72 h, despite ongoing daily exposure. Basal serum transaminase values are seen to be approximately equivalent in rats and mice. Assuming that intracellular transaminase is also therefore equivalent, the mice showed a greater degree of tissue injury than the rats. Histological analysis was consistent with these observations, showing significant cellular injury in both models after 48 h of APAP, with a greater degree of tissue degeneration in the mouse. Liver damage resolved over the ensuing timepoints, with limited observable fresh injury in either model.

Analysis of hepatic GSH in each model revealed depletion at 4 h after the initial exposure in 1000 and 1500 mg/kg groups in the rat (Figure 2.9), which fell further still by 24 h of exposure. This was in contrast to the mouse (Figure 2.10), in which significant depletion was seen at 4 and 6 h after initial exposure, but interestingly only in the 250 mg/kg (sub-

toxic) group. By 24 h of exposure, no significant deviation from control GSH values was seen, and this remained the case for the duration of the timecourse. In the rat, however, animals exposed to 1500 mg/kg for 48 h (overt toxicity) showed significant GSH elevation, which fell over successive timepoints to a value consistent with the depletion seen at 24 h of exposure. In the 1000 mg/kg group, despite depletion at 4 h post initial exposure, no further significant change was seen. The 500 mg/kg (sub-toxic) group, although initially unaffected by exposure, showed significant elevations in GSH after 72 h and 96 h of exposure.

The rat model was taken forward for proteomic analysis due to the animal's greater resistance to toxicity and higher propensity for adaptation. Although ALT levels were significantly elevated in both models at 48 h, the degree of overt liver tissue degeneration observed at the time point was lower in the rat, thus allowing robust proteomic analysis. In the rat model, observations were therefore likely to be of physiological adaptation phenomena rather than consequences of severe toxicity. Proteomic analysis of livers from rats exposed to 1500 mg/kg APAP identified 2181 unique proteins. Of those, 1169 were found to be common to all animals at all timepoints, and were therefore taken forward for statistical and *in silico* analysis. Analysis of this subset of detected proteins showed a gross alteration in abundance in animals that had received multiple doses compared to control and single-dosed animals (Figures 2.11 and 2.12). Although some proteins increased in abundance as a consequence of dosing, the majority became less abundant (Table 2.7), and at the peak of toxicity, almost 30 % of the detected proteome was significantly altered, showing the breadth of impact upon hepatic phenotype of adaptation to repeat APAP exposure. In order to validate the proteomic findings, four significantly perturbed proteins were selected from the dataset and probed in liver homogenate by western immunoblot (Figure 2.13). These data correlated closely with the original findings (Figure 2.14), increasing the degree of confidence in the results.

Adaptation in the mouse was contextualised by the presentation of pertinent work performed by Dr. Laura Randle. Dr. Randle's study investigated the effects of genetic manipulation of a well characterised mediator of the cellular stress response, Nrf2 (Figure 2.15). Whilst $Nrf2^{(-/-)}$ mice showed a greater susceptibility to APAP toxicity compared to wild types (reflecting the importance of the Nrf2 mediated response to oxidative stress in the liver), following pretreatment with APAP an adaptive response was still evident in the absence of Nrf2, albeit to a lesser degree. Nrf2-mediated transcription is therefore not the only mechanism of adaptation to repeated toxic insult in this model, and provides a demonstration that the process of adaptation involves more of the hepatoproteome than previously thought.

The work presented in this chapter shows that hepatotoxicity upon exposure to APAP initiates a complex and dynamic adaptive change in the liver involving large numbers of proteins. As well as engendering protection from subsequent basally noxious exposures, the change seems to support injury resolution whilst maintaining critical organ function. Collectively these processes ensure survival.

2.4.2. Relation of findings to literature

Adaptation has been demonstrated previously in rodents using a range of compounds including carbon tetrachloride, thioacetamide, 2-butoxyethanol and S-1,2-dichlorovinyl-L-cysteine (Dambrauskas and Cornish 1970; Thakore and Mehendale 1991; Mangipudy et al. 1995; Sivarao and Mehendale 1995; Vaidya et al. 2003) as well as the classic hepatotoxicant APAP (Strubelt et al. 1979; Poulsen and Thomsen 1988; Shayiq et al. 1999; Kim et al. 2009). Consistent with previous studies, data in this chapter show the typical hepatocellular centrilobular injury characteristic of APAP injury. In the rat model of APAP autoprotection, significant hepatotoxicity was only observed at a dose of 1500 mg/kg, confirming that the rat is relatively resistant to APAP toxicity as reported earlier (Buttar et al. 1976; Strubelt et

al. 1979; Poulsen and Thomsen 1988). While hepatotoxicity was evident at 48 h, significantly less or no necrosis was observed at 72 and 96 h, despite repeated exposure to APAP. Liver function was maintained at these points, as assessed by serum transaminases. These observations demonstrate an adaptive response in this model, protecting the liver from further injury, and this adaptation involves changes in a large proportion of the expressed hepatoproteome.

Observations of changes in GSH after initial APAP exposure in the overt toxicity groups in this study (Figures 2.9 and 2.10) seem to be in keeping with those reported by McGill et al. (2012b) in a paper which compared changes in total liver GSH over a 24 h period following an intraperitoneal administration of APAP. In this publication, both species showed initial GSH depletion at 1 and 3 h post exposure. At 24 h, GSH levels in the mouse had recovered back to pre-exposure values, whereas GSH in the rat had not. However, some of the GSH data presented here, particularly with respect to later timepoints and lower doses, are challenging to interpret. The publication cited above highlights the short latency between oxidative insult, GSH depletion and subsequent recovery. It is therefore possible that GSH observations in the present study are inadequately resolved due to the 24 h lapse between dosing and sampling in all except the initial exposures.

However, it is interesting that the early pattern of GSH loss and repletion in the mouse model are further supported by Fan et al. (2014), who also explored the role of Nrf2 in the process of liver regeneration after acute toxicity. This group showed Nrf2 to be induced by APAP toxicity, with concomitant increases in a panel of gene products regulated by the transcription factor. Whilst adaptation has been shown in the present work to occur even in the absence of Nrf2, its genetic ablation attenuates the adaptive response. Collectively these data suggest that, whilst Nrf2 is an important element of the adaptive response to liver injury, it is by no means the only mechanism through which the liver defends itself.

Expanding further the theme of liver regeneration, proliferating liver is known to show enhanced resistance to toxicity (Chanda et al. 1995; Shayiq et al. 1999; Dalhoff et al. 2001). Consistent with the findings presented here in Figure 2.13, rats which had been pretreated with APAP showed a regenerative response, determined through expression of PCNA in hepatocytes, upon a second toxic challenge (Dalhoff et al. 2001). This publication also showed that new hepatocytes have a greater capacity for GSH production, allowing regenerating liver to detoxify NAPQI more efficiently. In the present work, significantly elevated GSH was measured after 48 h of APAP in the rat 1500 mg/kg group, which correlated with the onset of increased PCNA expression, but pursuing this association further would enable clearer relationships to be established in this model.

2.4.3. Implications of findings and questions raised

Adaptation is a poorly-characterised phenomenon, and initial data shown here suggest it to be a much wider ranging process than previously thought, involving a large percentage of proteins in the liver in a complex and dynamic phenotypic change. Review of the literature indicates that adaptation protects the liver from subsequent noxious exposures, facilitates repair of hepatocellular injury, and preserves critical organ functions. Characterisation of the models presented here are in keeping with this definition of adaptation, permitting rodents to survive repeated overtly toxic APAP exposures. Further interrogation of these models may facilitate a clearer understanding of the processes influencing an organism's ability to adapt to chemical stress. In turn, this knowledge will have important implications for the management of human liver injury.

One of the key questions raised by the work presented here is whether the phenotypic changes seen in the rat liver are due to true differential regulation, or simply a consequence of catastrophic loss of hepatocyte mass resulting from drug exposure. The hypothesis that the selective destruction of centrilobular hepatocytes after APAP exposure

leaves only cells which are less vulnerable to subsequent injury is worthy of further investigation, and will be addressed by some of the work presented in the next chapter.

Chapter 3: Hepatic adaptation to chemical stress in the rat

Contents

3.1. Introduction

Work in the preceding chapter has begun to characterise the effects of daily exposure to APAP (paracetamol, acetaminophen) in two preclinical species. Both rat and mouse show interesting responses with some clear similarities (onset of toxicity, transaminase release, centrilobular tissue injury consistent with known APAP pharmacology). In rats that have received an overtly toxic daily exposure of 1500 mg/kg APAP, a global analysis of the hepatoproteome has identified gross shifts in the expression of a subset of detected proteins that were common to all rat livers at all timepoints.

Susceptibility to toxicity can be seen as a function of a number of factors in an organism, including i) the ability to reduce exposure to the toxin through constitutive detoxification processes; ii) the ability to adapt phenotypically to exposure; and iii) the ability to form new healthy tissue through regeneration. Rats are known to be less susceptible to toxicity than mice (Gregus et al. 1988; McGill et al. 2012b). Rats have a higher capacity than mice for detoxification through GSH conjugation, and therefore a greater capacity to buffer oxidative stress (Grover and Sims 1964). They have been shown to have a robust propensity for adaptation to chemical stress, examined through numerous studies of both autoprotection (Buttar et al. 1976; Strubelt et al. 1979; Poulsen and Thomsen 1988) and heteroprotection (Sato and Lieber 1981; Chanda et al. 1995). Rats also exhibit a concerted proliferative response following ablation of liver tissue by surgical or chemical means (Roberts et al. 1983; Zhang et al. 1999; Kurumiya et al. 2000). Because they are susceptible to liver injury by APAP overexposure, and yet exhibit a clear propensity for adaptation to chemical stress, rats present a valid model for the investigation of hepatic adaptation to repeat APAP exposure.

3.1.1. Further analysis of rat proteomic data

In order to clarify the nature of the adaptive response to repeat APAP challenge, in this chapter the proteomic data were analysed in greater detail. The rat's response to repeat APAP dosing was probed using pathway analysis software. This enabled identification of canonical pathways perturbed by dosing, and the contribution specific proteins made to the changes seen.

3.1.2. Use of microsomes to investigate metabolism

Data generated by the proteomic analysis have indicated alterations in abundance of a large number of proteins including key drug metabolising enzymes. However, this provided no context of the subtleties of enzyme activity regulation *in vivo*. It was therefore of value to examine change in the activity of these enzymes in response to dosing. One method available to researchers for investigating phase I metabolic activity in animal liver is the use of microsomes. Liver microsomes do not naturally occur *in vivo*, but are vesicular fragments of endoplasmic reticulum which can be isolated when hepatocytes are disrupted and subjected to ultracentrifugation. When physiological conditions are recapitulated in an *in vitro* microsomal incubation, enzymes within the microsomes retain metabolic activity and will transform any substrates present, allowing activity levels to be assessed.

Subsequent to the pathway analysis outlined above, microsomes from a subset of rat livers were prepared and incubated with either APAP or chlorzoxazone (CZX) to test the ability of each liver to break down APAP by any enzymatic pathway, and to specifically probe the activity of CYP2E1, respectively. An excess of GSH allowed the highly unstable APAP metabolite NAPQI to be trapped as a GSH conjugate via a nonenzymatic reaction, resulting in the product APAP-GSH. An NADPH regenerating system was employed in order to

ensure the essential cofactor was present in excess for the entire duration of the microsomal incubations.

3.1.3. Selection of subset of animals for microsome study

In order to examine the metabolic consequences of repeated APAP exposure, a subset of rat livers were selected from which to create microsomes. Alongside livers from 2 h vehicle control treated animals, livers from the 48 h APAP group (2 doses at 1500 mg/kg) and 96 h APAP group (4 doses at 1500 mg/kg) were chosen. These two groups have both received repeated APAP exposure, but crucially, the 48 h APAP group exhibited acute toxicity whereas the 96 h APAP group did not.

3.1.4. Use of immunohistochemistry to investigate protein localisation

Immunohistochemistry (IHC) allows the visualisation of distribution of a protein or proteins of interest across a mounted section of tissue. The technique exploits the relationship between antigens present in tissues and their corresponding antibodies. Further to findings from the proteomic analysis and microsomal enzyme activity studies, IHC was employed to examine the tissue distribution of the key CYP450 in APAP metabolism, CYP2E1.

3.1.5. Summary

Observations in the preceding chapter show the destruction of CYP450-rich tissue in centrilobular regions which typify APAP-induced liver injury in the rat repeat exposure model. Proteomic analysis identified changes in protein abundance which were not restricted to a small number of proteins or known pathways, and these changes will be explored in more depth using computer software. Further experimental work is included to validate the proteomic findings, and particular focus has been applied to the role of

CYP2E1 in the evolution of toxicity and adaptation. Work in this chapter aims to examine the abundance, enzymatic activity and tissue distribution of CYP2E1, and relate these findings to earlier data.

3.2. Methods

3.2.1. Materials

For preparation and incubation of microsomes, NADPH regenerating system was purchased from Corning (Woburn, MA). Parent drugs for LC-MS/MS analysis were obtained from Sigma-Aldrich (Gillingham, UK); internal standards from Toronto Research Chemicals (Toronto, Canada) and Alsachim (Illkirch-Graffenstaden, France). Metabolites were obtained from the same sources. Sources and concentrations of analytes and internal standards are given in Tables 3.1 and 3.2 respectively.

Compound	Abbreviation	Supplier	Product Code	Stock (mM)
Acetaminophen	APAP	SA	A7085	50
3-Cysteinylacetaminophen Trifluoroacetic Acid Salt	APAP-Cys	TRC	C994750	20
4-Acetamidophenyl β-D-Glucuronide	APAP-Gluc	SA	A4438	50
Acetaminophen Glutathione Disodium Salt	APAP-GSH	TRC	A161223	5
3-Methoxy Acetaminophen	APAP-MeO	TRC	M226050	50
3-(N-Acetyl-L-cystein-S-yl) Acetaminophen Disodium Salt	APAP-NAC	TRC	A172100	10
Acetaminophen sulphate potassium salt	APAP-Sulph	SA	89604	5

Table 3.1: Sources of analytes and stock solution concentrations

Compound	Abbreviation	Supplier	Product Code	Stock (mM)
Acetaminophen-D_4	D_4-APAP	ALSACHIM	C1235	10
3-[N-Acetyl-L-cystein-S-yl] Acetaminophen-D_5 Sodium Salt (Major)	D_5-APAP-NAC	TRC	A172102	5
3-Cysteinylacetaminophen-D_5 (major), Trifluoroacetic Acid Salt	D_5-APAP-Cys	TRC	C994752	5
4-Acetamidophenyl β-D-Glucuronide-D_3 Sodium Salt	D_3-APAP-Gluc	TRC	A158502	5
4-Acetaminophen-D_3 Sulphate Potassium Salt	D_3-APAP-Sulph	TRC	A161232	10

Table 3.2: Sources of internal standards and stock solution concentrations

For conducting IHC, sodium citrate buffer was obtained from Dako (Ely, UK). Avidin/biotin blocking kit was from Abcam (Cambridge, UK). SignalStain Boost IHC Detection Reagent (rabbit HRP) was from Cell Signaling Technology (Boston, MA). Entellan was from Merck

(Kenilworth, NJ). Antibody against glutamine synthetase (GS) was from Abcam (Cambridge, UK) All other reagents were of analytical grade and quality and purchased from Sigma (St. Louis, MO).

3.2.2. Ingenuity Pathway Analysis

Pathway analysis was performed using Ingenuity Pathway Analysis (Qiagen, Venlo, Limburg, Netherlands). Accession numbers for all proteins detected were uploaded to Ingenuity along with experimental observations (p value and log ratio). Significance cutoff was set at 0.05 using unadjusted p values, directional fold change was set (i.e. up/down), and the reference dataset was the user-defined proteome. Protein lists for each time point and directional change were compared, and analysed using the canonical pathways tool which maps proteins identified to classical pathways.

3.2.3. Preparation of rat liver microsomes

Pieces of frozen liver approximately 500 mg in mass were taken from stored samples and homogenised using a motor-driven homogeniser in ice cold 0.067 M phosphate buffer, pH 7.4, with the addition of 1.15 % (w/v) KCl. Using a Beckman UL60 ultracentrifuge and TI70.1 rotor, homogenates were spun at 4 ^{o}C for 25 minutes at 115,000 rpm to remove cellular debris. The pellet was discarded and the supernatant spun for a further 65 minutes at 37,000 rpm in order to pellet the microsomes. The supernatant was discarded, and the pellet containing the microsomal fraction was homogenised in phosphate buffer with KCl using a Wheaton 2 mL manual glass homogeniser. The resuspended pellet was centrifuged a third time for 65 minutes at 37,000 rpm, and resuspended in < 1mL phosphate buffer (without KCl). Aliquots were taken for protein determination using the method of Lowry, and also for spectrophotometric determination of CYP450 activity. Samples were snap frozen before transfer to -80 ^{o}C.

3.2.4. Spectrophotometric analysis of microsomes

Once the microsome preparation protocol had been completed, each sample was analysed spectrophotometrically in order to confirm the presence of active CYP450. Based on the methods of Omura and Sato (1964), microsome samples were standardised to a protein concentration of 1 mg/mL with phosphate buffer. Sodium dithionite crystals were added, and CO was bubbled through the suspension for one minute. Samples were transferred to a cuvette and read at 450 nm.

Isolation of microsomes and spectrophotometric analysis was performed on all livers from each named group, and the highest yielding samples from control (n = 4), 48 h APAP (n = 3), and 96 h APAP (n = 3) were taken forward for microsomal incubation, giving ten *in vivo* conditions in total.

3.2.5. Incubation of microsomes with APAP

Microsomes from individual animals were incubated in duplicate in glass vials in a shaking water bath at 37 ^{o}C in accordance with the tables shown below (Tables 3.3 and 3.4). APAP was dissolved in phosphate buffer. An excess of GSH was present in each reaction (1 mM final concentration), as was an appropriate concentration of NADPH regeneration substrates A and B. Reactions were stopped by addition of the withdrawn incubate fraction to an equal volume of ice cold ACN containing the evaporation standard fluconazole (prepared in 200 µL capacity microcentrifuge tubes and kept on ice) at 0.5 h, 1 h, and 4 h post addition of microsomes to incubation solution. Stopped incubates were immediately frozen at -80 ^{o}C pending analysis.

Tube	Condition*	Buffer	Drug	A	B	GSH (100 mM)	Microsomes	Total
A	C1	186	2	0	0	2	10	200
B	C2	186	2	0	0	2	10	200
C	0 1	176	0	10	2	2	10	200
D	0 2	176	0	10	2	2	10	200
E	L1	174	2	10	2	2	10	200
F	L2	174	2	10	2	2	10	200
G	M1	174	2	10	2	2	10	200
H	M2	174	2	10	2	2	10	200
I	H1	174	2	10	2	2	10	200
J	H2	174	2	10	2	2	10	200

Table 3.3: Composition of each microsomal condition in microlitres for APAP incubations

*Refer to Table 3.4 for description of condition abbreviation

Condition	Abbreviation	Description
APAP-free	0	APAP-free incubation to control for spontaneous metabolite generation
Low APAP	L	10 µM APAP added to incubation
Medium APAP	M	100 µM APAP added to incubation
High APAP	H	1 mM APAP added to incubation
No NADPH	C	1 mM APAP but no NADPH regeneration solutions included to control for passive turnover

Table 3.4: Key to microsomal incubation conditions for APAP turnover experiment

3.2.6. Incubation of microsomes with CZX

Microsomes from individual animals were incubated in duplicate in glass vials in a shaking water bath at 37 ^{o}C in accordance with the table shown below (Tables 3.5 and 3.6). CZX was dissolved in methanol. An excess of GSH was present in each reaction (1 mM final concentration), as was an appropriate concentration of NADPH regeneration substrates A and B. Reactions were stopped by addition of the withdrawn incubate fraction to an equal volume of ice cold ACN containing the evaporation standard fluconazole (prepared in 200 µL capacity microcentrifuge tubes and kept on ice) at 5, 10, 15, 20, 30, 45, 60 and 90 minutes post addition of microsomes to incubation solution. Stopped incubates were immediately frozen at -80 ^{o}C pending analysis.

Tube	Condition*	Buffer	Drug/veh	A	B	GSH (100 mM)	Microsomes	Total
A	p1	71.4	21	10.5	2.1	21	84	210
B	p2	71.4	21	10.5	2.1	21	84	210
C	c1	36	9	0	0	9	36	90
D	c2	36	9	0	0	9	36	90
E	v1	30.6	9	4.5	0.9	9	36	90
F	v2	30.6	9	4.5	0.9	9	36	90

Table 3.5: Composition of each microsomal condition for CZX incubations

*Refer to Table 3.6 for description of condition abbreviation

Condition	Abbreviation	Description
CZX	P	1 µM chlorzoxazone in methanol added to incubation – 0.1% final vehicle concentration
NADPH control	C	1 µM chlorzoxazone but no NADPH regeneration solutions included to control for passive turnover
Vehicle control	V	Methanol alone (0.1 %) added to incubation to control for vehicle effects

Table 3.6: Key to microsomal incubation conditions for CZX turnover experiment

3.2.7. Analysis of incubates by LC-MS/MS

Mass spectrometric analysis of microsomal incubates was kindly performed by Dr. Mark Bayliss using the methods described below. Test samples were treated with ACN to remove matrix-based interferences. They were diluted with water prior to analysis by LC-MS/MS on a Sciex API 4000 (Warrington, UK) equipped with a Turbo V™ electrospray source (ESI). The gradients were based on mobile phases containing 0.1 % v/v FA in both water (A) and ACN (B). Drugs and metabolites were detected using MRM.

3.2.7.1. Measurement of APAP and its major metabolites

Separations were performed on a 2.6 µm Kinetex® XBC18 column (50 x 2.1 mm internal diameter) obtained from Phenomenex (Macclesfield, UK), at a temperature of 40 °C and a flow-rate of 0.5 mL/min. The following gradient was used: 0 min 0 % B, 0.3 min 0 % B then 2.3 min 50 % B. The column was flushed with 100 % B, and then returned to 0 % B using a

flow-rate of 0.7 mL/min, giving a programmed cycle time of 4.2 minutes. A panel of deuterated internal standards was employed (Table 3.2). The MS was operated in negative ion mode for measuring all but one of the putative major metabolites and high concentrations of APAP. It was operated in positive ion mode for measuring the remaining metabolite and low concentrations of APAP.

3.2.7.2. Measurement of chlorzoxazone and its putative major metabolite, 6-hydroxy chlorzoxazone

Separations were performed on a 2.7 µM Halo® C18 column (50 x 2.1 mm internal diameter) obtained from HiChrom (Reading, UK), and at a temperature of 40 °C and a flow-rate of 0.6 mL/min. The following gradient was used: 0 min 5 % B, 0.5 min 5 % B, 1.5 min 95 % B, 2 min 95 % B, 2.1 min 5 % B and 2.6 min 5 % B. D^4-diclofenac was employed as the internal standard. The MS was operated in negative ion mode.

3.2.8. CYP2E1 localisation via immunohistochemistry

Immunohistochemical staining for CYP2E1 was carried out by Dr. Mariona Auli at Almirall S. A. Formalin-fixed, paraffin-embedded liver sections were cut at 3 µm. Sections were mounted on poly-L-lysine coated slides, air-dried, then deparaffinised in xylene, and hydrated through graded alcohols to distilled water. Endogenous peroxidase activity was blocked using 3 % H_2O_2 in methanol for 20 min. After washing in Tris-buffered saline (TBS), slides were transferred into a slide holder containing sodium citrate buffer and heated in a pressure cooker for 5 min for antigen retrieval. After 30 min cooling to RT, slides were rinsed in TBS containing 0.05 % Tween 20 (TBS-T) and endogenous avidin/biotin binding sites blocked. Slides were then washed in TBS-T and incubated at RT with 20 % normal goat serum in TBS-T for 1 h to block nonspecific binding. Slides were further incubated overnight (4 ^{o}C) with rabbit anti CYP2E1 monoclonal antibody at a working dilution of 1:1750 in 20 % normal goat serum/TBS-T. The primary antibody was omitted for negative controls.

SignalStain Boost IHC Detection Reagent was used as secondary antibody (1 h, RT). The reaction was developed using 3', 3'-diaminobenzidine (DAB) tetrahydrochloride as chromogen. Sections were counterstained with Harris haematoxylin, dehydrated and mounted using Entellan.

3.2.9. Western immunoblot

Western immunoblots were performed according to the method described in Chapter 2, section 2.2.9. GS antibody was used at a dilution of 1:20 000 for 1 h at RT, and secondary (anti-rabbit) was 1:10 000 overnight at 4 ^{o}C. CYP2E1 antibody was generously provided by Magnus Ingelman Sundberg (Karolinska Institute, Sweden) and used at a dilution of 1:20 000 for 1 h at RT, and secondary (anti-rabbit) was 1:10 000 overnight at 4 ^{o}C.

3.2.10. Data evaluation and statistical analysis

Western immunoblot data were analysed as described in Chapter 2, section 2.2.11. Microsomal data were analysed in GraphPad PRISM (V6.03 for Windows, GraphPad Software, San Diego, CA) using an ordinary two-way ANOVA with Dunnett's post-hoc test. Statistical analysis of proteomic data was performed by Dr. Joanne Walsh using a linear model in the R programming environment (ANOVA with Dunnett's post-hoc test). Error bars on charts represent SEM.

Mathematical modelling of microsomal enzyme activity data was generously performed by Dr. Steven Webb, University of Liverpool. Literature estimates for K_m are reported to be 30-300 times larger (Muzeeb et al. 2005; Guo et al. 2014) than the CZX concentration considered (1 µM). It was therefore possible to adopt linear kinetics for CYP2E1 activity (enzyme velocity = α[S], where [S] = CZX concentration and $\alpha = V_{max}/K_m$) instead of the full nonlinear Michaelis-Menten form. Solving the resulting first order ordinary differential equation yielded the following expression for 6'-OH CZX formation versus time (using

notation [P](t) to denote concentration at time t (min)): $[P](t) = [S](0)(1-\exp(-\alpha t/V))$, where [S](0) = initial CZX concentration (1 μM) and V is the sample volume (0.02 mL). A Levenberg Marquardt (non-linear regression) algorithm was used to then find best fit values for $\alpha = V_{max}/K_m$ for control, 48 h APAP and 96 h APAP groups. In each group, estimates shown here for $\alpha = V_{max}/K_m$ were found to lie within acceptable literature ranges. Under the assumption that enzyme-substrate binding affinity ($1/K_m$) is unaffected by microsomal conditions, ratios of α estimates were then used to compare relative enzyme activities.

3.3. Results

3.3.1. Identification of perturbed canonical pathways

In the previous chapter, a global proteomic analysis of liver tissue from rats which had received a daily 1500 mg/kg (overtly toxic) exposure to APAP was described. Within this data set, 1169 proteins were found to be common to all animals at all examined timepoints. Using Ingenuity Pathway Analysis it was possible to assign these detected proteins to accepted canonical biochemical pathways and rank the pathways in order of most perturbed across the timecourse. The top 25 most perturbed canonical pathways are presented below (Figure 3.1, and lists of proteins are provided in Supplementary Table 3), and values shown on the heatmap are the negative log of p values. All significant changes are in red blocks, and the intensity of the shading corresponds with the degree of significance. The left panel shows significant difference of increased protein abundance, and the right panel shows significant difference of decreased protein abundance. Consistent with data presented in Chapter 2 (Figures 2.13 and 2.14; Table 2.7), the protein changes indicate a trend towards widescale decreased abundance, particularly in the 48 h APAP group, reflecting the peak observed incidence of centrilobular injury.

A subset of proteins assigned to the canonical pathways '*LPS/IL-1 mediated inhibition of RXR function*' (identified as the most perturbed pathway) and '*Xenobiotic metabolism signalling*' (highly relevant to drug toxicity) have also been displayed as a heatmap in order to identify the contribution of specific proteins to the process of adaptation (Figure 3.2).

Figure 3.1: Ingenuity identification of top 25 most perturbed canonical pathways across timecourse

	(-log)p INCREASED abundance proteins				(-log)p DECREASED abundance proteins				Total
CANONICAL PATHWAY	24	48	72	96	24	48	72	96	Proteins
LPS/IL-1 Mediated Inhibition of RXR Function	0.32	0	0	1.64	3.91	13.59	9.16	10.01	34
Superpathway of Melatonin Degradation	1.86	0.33	0	1.98	1.68	10.78	5.14	5.49	17
Melatonin Degradation I	1.92	0.36	0	2.06	1.73	9.92	5.34	5.7	16
Dopamine Degradation	0	0	0	0.83	2.58	9.14	5.43	7.29	9
NRF2-mediated Oxidative Stress Response	1.86	4.26	1.77	9.53	0	3.11	2.33	0.55	27
γ-linolenate Biosynthesis II (Animals)	0	0	0	0.92	4.53	6.69	4.4	6.21	7
Xenobiotic Metabolism Signaling	0.74	1.76	0.7	2.46	0.59	6.89	4.78	3.94	34
Serotonin Degradation	0.82	0.36	0	2.09	1.75	7.61	4.31	3.53	15
Nicotine Degradation II	1.85	0.33	0	2.94	0	7.11	3.06	4.32	16
Fatty Acid β-oxidation I	0	0	0	1.6	2.19	7.29	4.4	3.41	11
EIF2 Signaling	0.45	7.71	3.58	4.95	1.79	0	0	0	19
Estrogen Biosynthesis	0.93	0	0	0.56	0	7.59	3.86	5.32	11
Acute Phase Response Signaling	6.13	6.57	3.73	0.8	0	0	0	0.23	21
Nicotine Degradation III	1.94	0.36	0	3.13	0	6.47	2.36	2.55	18
Bile Acid Biosynthesis, Neutral Pathway	0	0	0	2.15	1.21	5.17	2.99	4.6	7
Fatty Acid Activation	0	0	0	1.07	3.09	4.51	3.5	3.66	5
Thyroid Hormone Metabolism II (via Conj'n &or Degr'n)	1.08	0.59	0	1.71	2.3	3.94	3.44	2.45	8
Mitochondrial L-carnitine Shuttle Pathway	0	0	0	2.15	2.76	3.79	2.99	3.14	6
Aryl Hydrocarbon Receptor Signaling	0.45	2.46	2.79	2.35	0	3.04	2.08	1.15	20
Bupropion Degradation	1.06	0	0	0.69	0	6.27	2.25	3.56	8
Acetone Degradation I (to Methylglyoxal)	1.06	0	0	0.69	0	6.27	2.25	3.56	8
Glutathione-mediated Detoxification	0	0.57	0.63	2.85	0	5.01	3.36	1.38	9
Aldosterone Signaling in Epithelial Cells	0.56	8.06	3.46	1.33	0	0	0	0	13
PXR/RXR Activation	0	0	0	0.36	0	5.3	3.56	3.84	12
Superpathway of Cholesterol Biosynthesis	0	0	0	0	2.22	2.7	0.49	7.57	8

Chapter 3: Hepatic adaptation to chemical stress in the rat

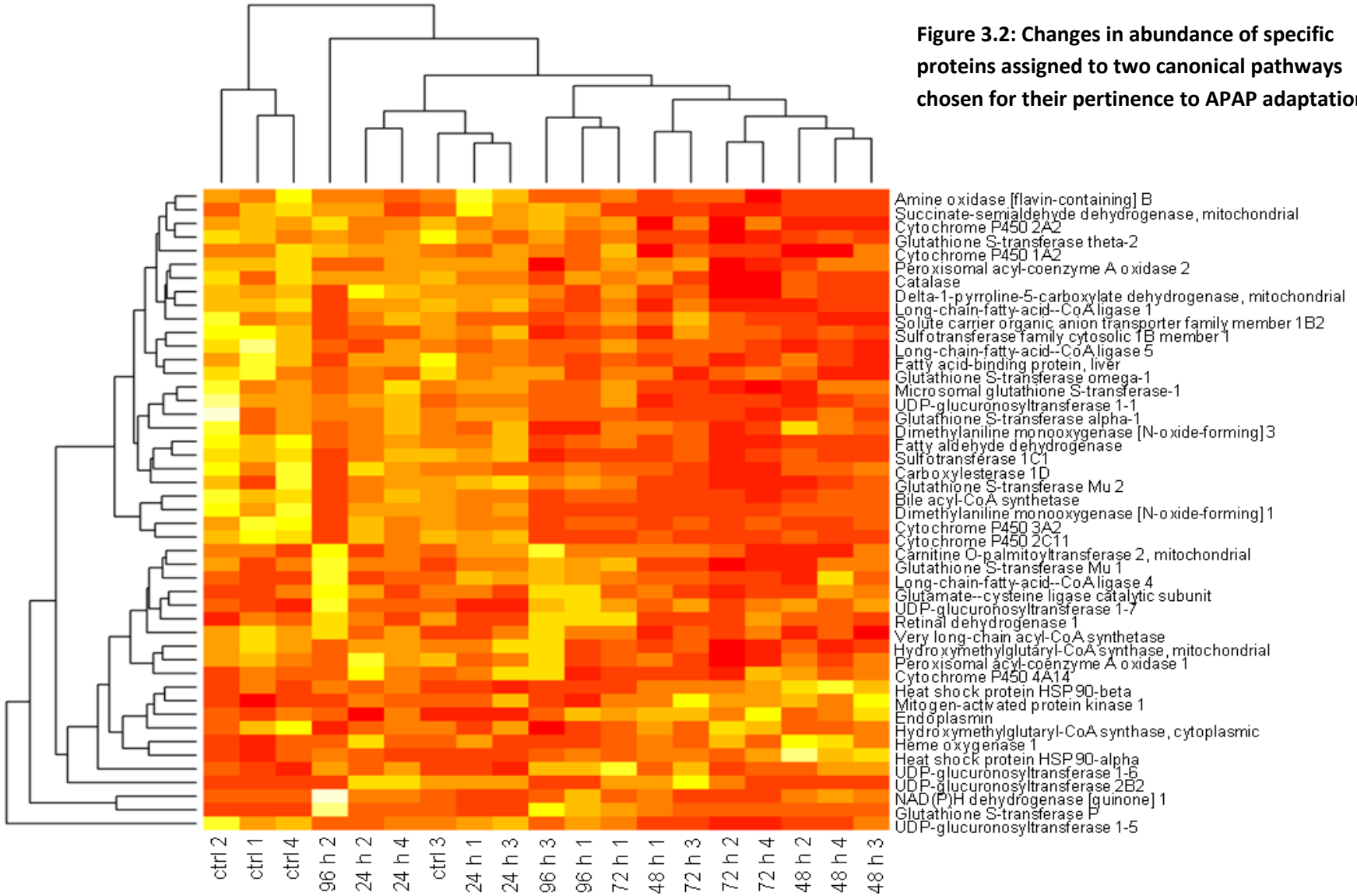

Figure 3.2: Changes in abundance of specific proteins assigned to two canonical pathways chosen for their pertinence to APAP adaptation

Chapter 3: Hepatic adaptation to chemical stress in the rat

Figure 3.1: Ingenuity identification of top 25 most perturbed canonical pathways across timecourse

Legend: Top 25 most perturbed canonical pathways over 96 h timecourse of repeat APAP exposure. Values shown are negative log (p) and significant changes are shown in red. The left hand panel shows increased abundance proteins, and the right hand panel shows decreased abundance. The total number of significantly perturbed proteins for each canonical pathway is shown on the far right. There is some redundancy in these pathways.

Figure 3.2: Changes in abundance of specific proteins assigned to two canonical pathways chosen for their pertinence to APAP adaptation

Legend: Heat map of perturbed proteins assigned to '*LPS/IL1 mediated inhibition of RXR function*' and '*Xenobiotic metabolism signaling*' pathways, presented in hierarchical clusters using paired Euclidean distances. Red denotes increased abundance and yellow denotes decreased abundance. Reflecting the data shown in section 2.3.6.1, Figure 2.11, control and single dose (24 h APAP) animals cluster away from repeat dosed animals

3.3.2. Shifts in abundance of drug metabolism proteins across the timecourse

Changes in drug metabolism proteins seen in the 48 h APAP group (as indicated by Ingenuity Pathway Analysis) were then explored in more depth (Figure 3.3). Phase I, II, and III drug metabolising proteins exhibited a trend towards decreased abundance after two successive doses. Thirteen out of the twenty-three CYP450s identified, the single most important set of proteins that govern how the liver initially processes a drug, were found to be present at lower abundance at 48 h. This included CYP2E1, which is largely expressed in the centrilobular region of the liver; and CYP2C6, which is expressed across all zones of the liver (36 % and 30 % of control values, respectively), although both of these proteins increased after 96 h. The majority of detected phase I and II proteins decreased during the process of adaptation to APAP. Notable exceptions to this loss of abundance are NQO1, which recycles APAP's toxic metabolite NAPQI back to APAP (Moffit et al. 2007); and GSTP1, which quenches electrophiles such as NAPQI through conjugation with glutathione (Ketterer et al. 1983). Both enzymes were more abundant at 48 h (273 % and 269 % of control values respectively, Figure 3.3c). The changes in the phenotype of the liver shown here after two and four successive doses of APAP may profoundly influence the fate of subsequent doses.

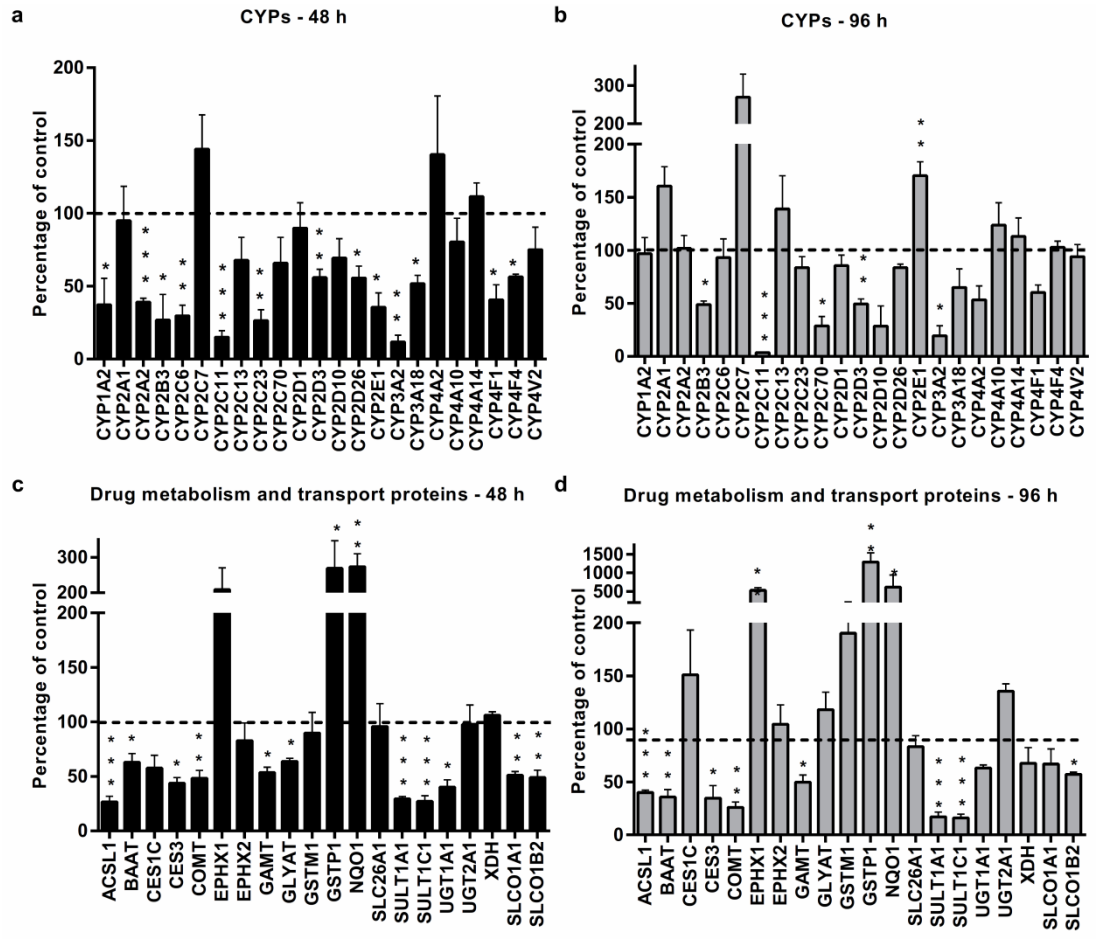

Figure 3.3: Changes in phase I, II and III drug metabolising proteins in 48 h and 96 h APAP groups compared to vehicle control treated animals

Legend: Phase I drug metabolising proteins show widescale decreased abundance at 48 h (a) with some recovery by 96 h (b) when compared to vehicle control values (dashed line). Similar trends are seen when looking at phase II/III proteins at 48 h (c) and 96 h (d). Notable exceptions to the trend of decreased abundance are CYP2E1 at 96 h, pertinent to APAP metabolism; and GSTP1 and NQO1 at both 48 h and 96 h, involved in detoxification.

3.3.3. Albumin as a clinical marker of hepatic function

In an effort to further explore the biological significance of the observed changes, expression in the liver of the clinical marker of function, albumin, was analysed (Figure 3.4). Over the timecourse, it can be seen that despite the dramatic losses of some proteins in response to dosing, hepatic albumin itself does not significantly deviate from control values. In the context of clinical chemistry data from Chapter 2, and along with results for

phase I, II and III proteins shown in section 3.3.2, this lends further weight to the hypothesis that the liver is undergoing an active change in phenotype in order to adapt to repeat exposure.

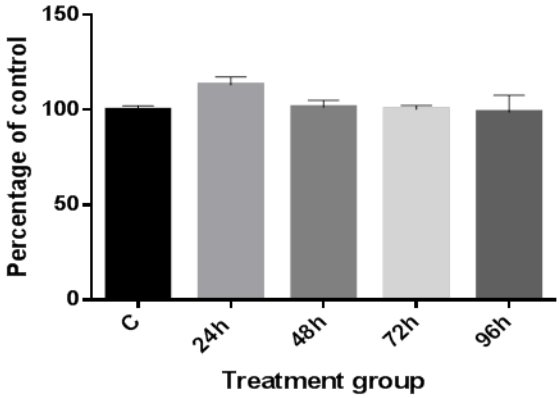

Figure 3.4: Intracellular expression of albumin across the timecourse

Legend: Expression of albumin in rat livers across 96 h repeat APAP exposure timecourse. No significant deviation from control value is seen.

3.3.4. Microsomal analysis of drug metabolism

In order to validate data gathered by global proteomic analysis and clarify the nature of the hepatic response to repeat APAP exposure, microsomes were made from remaining frozen rat liver tissue. Livers were selected from the 2 h vehicle control treated group, and the 48 h and 96 h APAP groups.

3.3.4.1. Spectral properties of microsomes

Cytochrome P450 enzymes have unique spectral properties. Under reducing conditions, a pink compound is formed when the enzyme binds to carbon monoxide (hence 'P'), with absorption in the 450 nm range.

Animal no.	Treatment group	CYP450* (nmol/mg)	Protein (mg/ml)
1	2h Vehicle	0.22	16.25
2	2h vehicle	0.40	15.16
3	2h vehicle	0.46	10.72
4	2h vehicle	0.33	19.09
106	48 h APAP	0.19	5.27
107	48 h APAP	0.35	7.00
108	48 h APAP	0.23	6.00
154	96 h APAP	0.42	10.17
155	96 h APAP	0.43	11.40
156	96 h APAP	0.28	10.47

Table 3.7: CYP450 concentration and protein concentration of microsomal preparations

*CYP450 concentration was calculated using the equation
[CYP450] nmol/mg protein = ([protein] mg/ml x 1000 x net absorbance)/91
Where 91 is the molar extinction coefficient of CYP450

Values for microsome preparations taken forward are shown in Table 3.7. The reference range for adult rat liver microsomes is 0.4-1.0 nmol/mg (Gibson and Skett 2001). Perhaps unsurprisingly given the storage duration of the samples in question (>3 years at -80 ^{o}C), concentrations were at or below the low end of this range. However, when taking protein concentration and sample mass into consideration, there was a sufficient quantity of each sample to permit small-scale microsomal incubations

3.3.4.2. Microsomal formation of APAP-GSH

A large number of CYP450s are expressed in the liver, and substrate specificity overlaps extensively. Although supratherapeutic APAP is primarily metabolised by CYP2E1, other P450s including CYP1A2 are also involved (Patten et al. 1993). Examining the formation of APAP-GSH provides biologically relevant information as to the turnover of the drug in the liver without giving specific identity to the CYP450s involved. Figure 3.5 shows the formation of APAP-GSH in each of the microsomal conditions that control, 48 h APAP and 96 h APAP tissue were exposed to. A statistically significant difference is seen in the highest microsomal concentration of APAP, 1 mM. In this condition, significantly more APAP-GSH is generated by the 96 h APAP tissue when compared to control and 48 h APAP,

showing perhaps surprisingly that metabolism of APAP is not diminished by the destruction of centrilobular regions, and is in fact increased after 96 h of repeated exposures.

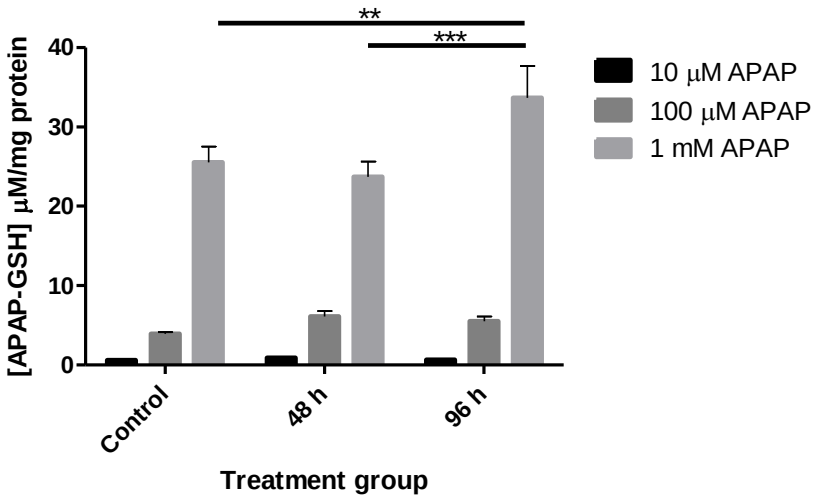

Figure 3.5: Microsomal formation of APAP-GSH in rat

Legend: Control, 48 h and 96 h microsomes were incubated with APAP to examine the turnover of test drug. Three concentrations of APAP were used, and significance is seen in the top dose group (1 mM). More adduct is formed at 96 h than control or 48 h.

3.3.4.3. Microsomal formation of 6'-OH CZX

Alongside investigation of APAP metabolism, incubations of microsome preparations with CZX were also conducted. CZX is a probe substrate which is specific for CYP2E1, and generation of the metabolite 6'-OH CZX indicates the degree of activity of CYP2E1 in the livers examined. Figure 3.6 shows the turnover of 1 µM CZX by liver microsomes from 2 h vehicle treated animals, as well as 48 h APAP and 96 h APAP treatment groups. Compared to control animals, CYP2E1 activity is significantly reduced in the 48 h APAP group, coincident with maximal hepatocellular injury. In the 96 h APAP group the opposite is observed, and CYP2E1 activity is significantly increased compared to the control group.

These observations of both increased APAP metabolism and CYP2E1 enzyme activity in the 96 h APAP group are unexpected, given that no further significant toxicity is seen at later timepoints despite ongoing exposure to APAP.

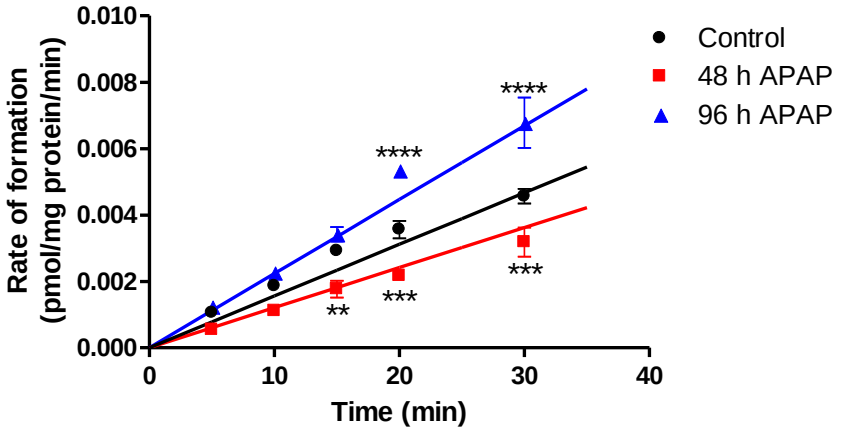

Figure 3.6: Microsomal turnover of the CYP2E1 probe substrate chlorzoxazone in rat

Legend: Rate of formation of 6'-OH CZX by control, 48 h APAP and 96 h APAP microsomes. CYP2E1 activity is reduced in the 48 h APAP group compared to control. The rate of formation of 6'-OH CZX is increased in the 96 h APAP group.

3.3.5. Localisation of Cytochrome P450 2E1 during liver injury, adaptation and regeneration

Bioactivation of APAP by CYP2E1 results in the generation of the toxic metabolite NAPQI. In an attempt to understand the mechanism by which CYP2E1 increases in abundance and activity at later timepoints without exacerbating cellular toxicity, IHC was employed to examine the spatial shifts in CYP2E1 expression across rat liver sections.

Immunohistochemical detection of CYP2E1 distribution in fixed liver sections revealed a change in localisation of expression through the timecourse (Figure 3.7). Basally, CYP2E1 is mainly expressed in centrilobular regions. Upon APAP challenge, CYP2E1 staining became diffuse and extended into midzonal regions. 2 doses produced acute centrilobular necrosis, with markedly reduced CYP2E1 staining in centrilobular regions. At later timepoints, staining extended diffusely into periportal regions which were CYP2E1-negative in control

animals. At the final timepoint (96 h), half of the animals presented a similar diffuse staining of periportal regions, and half of the animals presented staining similar to control animals.

A strong positive correlation has been seen between the different detection methods used to examine CYP2E1 abundance. Positive association has been shown between densitometric and MS data (Figure 3.8a), and visual comparison of densitometry to IHC stain intensity reveals remarkably similar patterns of abundance over the timecourse. The pattern of loss and repletion of CYP2E1 is in contrast to the changes in abundance of GS, chosen as a comparator sentinel of centrilobular hepatocytes. Western immunoblot (Figure 3.8b) reveals that, as with CYP2E1, in the 48 h APAP group a dramatic loss of the protein is seen. Thereafter, whilst CYP2E1 expression recovers, GS expression does not. This indicates that the process of adaptation is a selective one.

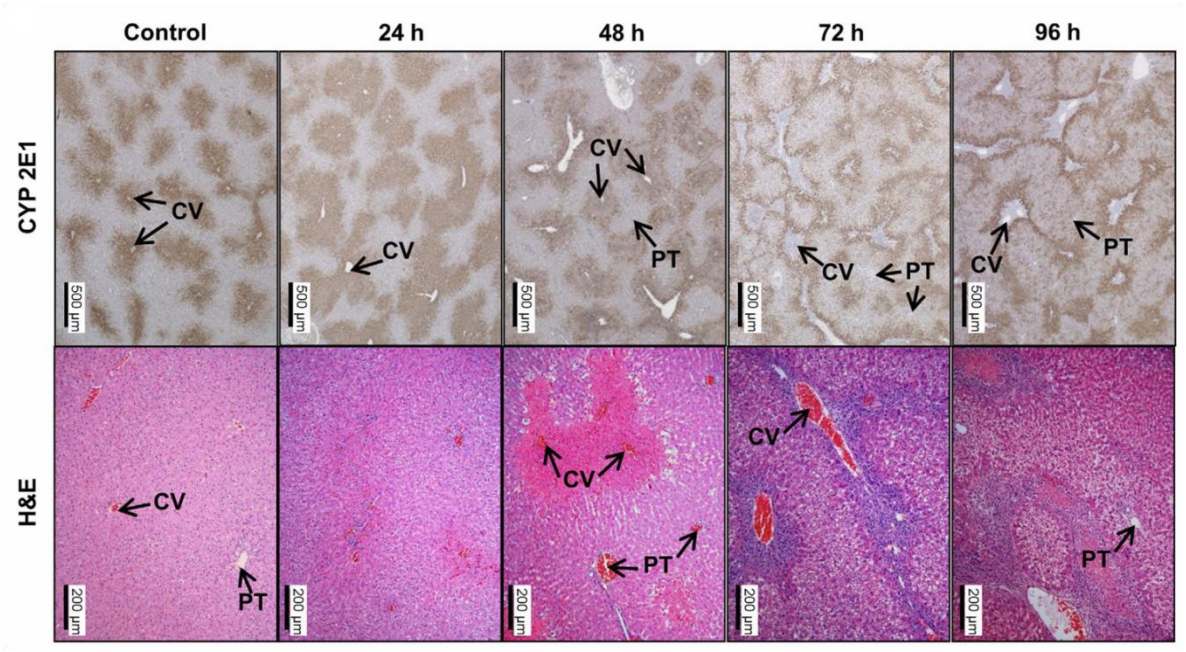

Figure 3.7: Change in localisation of CYP2E1 in response to treatment

Legend: Sectioned and stained rat liver from all treatment groups across 96 h repeat APAP exposure study. Upper panels show IHC for CYP2E1 (brown stain on grey background). Lower panels show H&E staining of tissue sections showing tissue injury and recovery. CV denotes central vein, PT denotes portal triad.

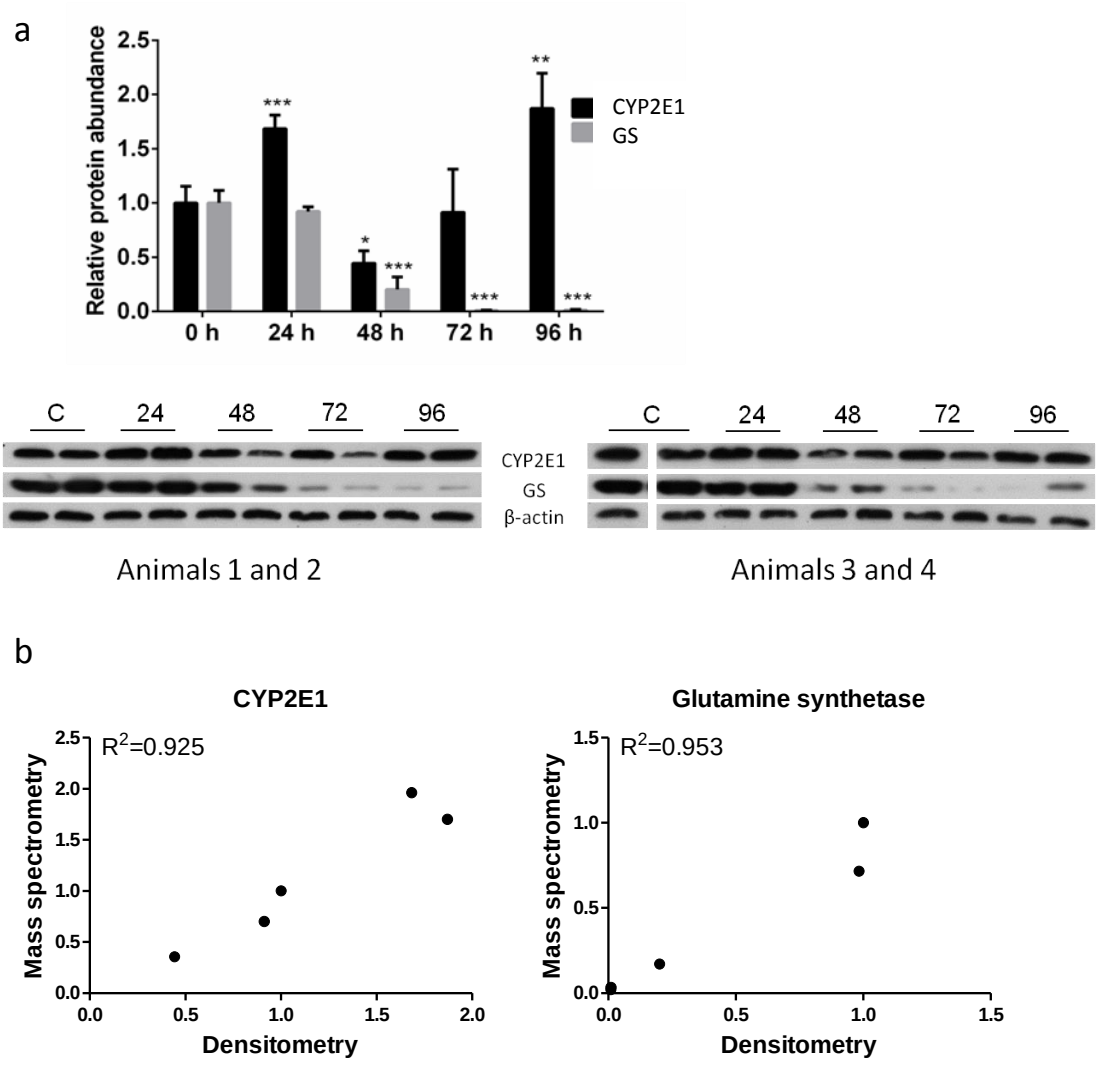

Figure 3.8: Relative abundance of CYP2E1 and GS, and correlation of MS and densitometric quantification methods

Legend: a) Densitometric analysis of western immunoblot data for basally perivenous CYP2E1 and GS, with representative images below. Left panel shows animals 1 and 2 from each treatment group, right panel shows animals 3 and 4. NB Lane 2 of right panel was left intentionally blank and has been digitally cropped for ease of interpretation of figure.

b) Positive correlation is seen between densitometric and mass spectrometric data for target proteins CYP2E1 and GS.

3.4. Discussion

The rat has been shown to be an appropriate model for the examination of hepatic adaptation to repeat APAP exposure. In this chapter, the proteomic data from the rat repeat APAP exposure model have been analysed in greater depth, identifying both expected and unexpected canonical pathways as being pertinent to the process of adaptation. Alongside this, the activity and distribution of CYP2E1 in rat liver from the model have also been explored, showing the breadth, dynamism and complexity of the process of adaptation to repeat APAP exposure.

3.4.1. Summary of findings and relation to literature

Ingenuity analysis of proteomic data allowed mapping of differentially expressed proteins onto canonical pathways (Figure 3.1), revealing the breadth of the adaptive process, and the extent of loss of protein abundance over the timecourse. Although Figure 3.1, showing the top 25 most perturbed canonical pathways, indicates widespread loss of protein abundance particularly at the peak of toxicity, a number of pathways showed increased abundance, including '*acute phase response signalling*', '*Nrf2-mediated oxidative stress response*' and '*glutathione-mediated detoxification*' which are all well-characterised reactions to toxic injury.

The result of heat mapping the proteins implicated in two key pathways identified by Ingenuity ('*LPS/IL1 mediated inhibition of RXR function*' and '*Xenobiotic metabolism signaling*'; Figure 3.2) validated data shown in the preceding chapter: the proteomic profile of repeat dosed animals diverges from that of control and single dosed animals, as is seen in section 2.3.6.1. The scope of this divergence again reinforces the notion that the adaptive changes to metabolism in the liver seen after repeat exposure to APAP are likely to profoundly influence the fate of subsequent xenobiotic exposures.

Beyond confirming existing knowledge that several CYPs relevant to APAP metabolism are down-regulated upon repeat APAP exposure, it can be seen here that liver tissue from repeat dosed rats shows a significantly reduced abundance of proteins across all phases of drug metabolism (Figure 3.3). This reduction in expression may represent a key facet of adaptation, providing an environment which facilitates compensatory hyperplastic activity, thereby preserving critical function. At the peak of toxicity, the mean of all detected CYP450s is reduced to approximately 60 % of control values. This change in phenotype is likely to be, at least partly, a consequence of the changing cell population in the liver over time. The initial toxic insult clearly destroys vulnerable hepatocytes at the centre of the lobule. CYP450 enzymes show predominantly centrilobular expression, and the differential expression of CYP450s in intact zones may account for the overall change seen at 48 h. Nevertheless, a number of CYP450s are pan-zonally expressed in rat liver (Oinonen and Lindros 1998), and of the ones that are also identified in the present work (CYP1A, 2B, 2C6 and 2C7 - a close homologue of the pan-zonal CYPEtOH2 (Foster et al. 1986; Wojcik et al. 1988; Omiecinski et al. 1990; Bühler et al. 1992)), all are significantly less abundant in the 48 h APAP group, dropping to around 30 % of control (with the exception of CYP2C7 which is not significantly changed by repeat APAP exposure). This suggests an active change in the phenotype of intact cells, as has been previously postulated, indicating a global dedifferentiation resulting in decreased liver-specific protein expression as part of an adaptive response to injury (Ito et al. 1991; Kurumiya et al. 2000), rather than a passive destruction of CYP450-rich tissue.

To further elucidate the complex mechanism of adaptation, CYP2E1 activity and localisation in response to repeat APAP exposure was examined. Consistent with proteomic data obtained for CYP2E1 abundance, microsomal activity assays showed a loss of CYP2E1 activity in the 48 h APAP group which was contemporary with the onset of acute injury (Figure 3.6), although overall formation of APAP-GSH by any pathway (Figure 3.5) was not

diminished at this timepoint. Despite continued APAP exposure, however, the 96 h APAP group exhibited a rebound of both expression and activity of CYP2E1, alongside an increase in turnover of APAP to APAP-GSH. This was not consistent with the fall in toxicity observed after 48 h of APAP.

The microsomal data suggests that other factors must be involved in the process of adaptation, since CYP2E1 is more active in the 96 h APAP group which would result in greater formation of NAPQI, but a corresponding increase in cellular injury in this group is not seen. Examination of the tissue distribution of CYP2E1 provides something of a clue to how this may happen. Immunohistochemical staining of liver sections from each treatment group revealed a diffuse redistribution of CYP2E1 into basally CYP2E1-negative regions (Figure 3.7). Importantly, the pattern of loss and restoration seen with total liver CYP2E1 was not observed for another similarly perivenous enzyme, GS (Figure 3.8), suggesting that this process is selective. From these observations it is hypothesised that diffuse re-expression of CYP2E1 may perhaps prevent the intracellular threshold of NAPQI toxicity being reached, thereby avoiding the initiation of further waves of cell death at later timepoints. Furthermore, in the regions where NAPQI is generated after redistribution of CYP2E1 expression, there are known to be higher intracellular concentrations of the reducing buffer GSH (Sastre et al. 1992). This phenomenon of CYP2E1 redistribution as an adaptive response has been seen after treatment with carbon tetrachloride (Irie et al. 2010) and ethanol (Bertola et al. 2013), but has not been detected previously after treatment with any pharmaceutical compound.

Figure 3.1, which identifies the top 25 most perturbed canonical pathways, also indicates other pathways which could be relevant to the process of adaptation. For example '*EIF2 signalling'*, which may indicate increased transcriptional activity; '*aryl hydrocarbon receptor*

signalling' which not only regulates CYP450 expression but also has a role in regulation of progenitor cell recruitment (Procházková et al. 2011); and '*aldosterone signalling'* which has recently been linked with the processes of proliferation and fibrosis in liver injury (Parlakgumus et al. 2013).

3.4.2. Implications of findings and questions raised

Adaptation in the rat model of repeat APAP exposure has been established through the lack of variance in expression of the clinical marker of hepatic function albumin, as well as that of the transaminases ALT and AST (shown in the preceding chapter) at later timepoints. The preferential restitution of CYP2E1 over GS tells of the selective nature of the process. In this model, Ingenuity identification of canonical pathways perturbed by dosing revealed a set of proteins that are greatly dysregulated in the process of adaptation, which contribute to future hypothesis generation. Data shown in this chapter demonstrate that the process of adaptation is not only temporal in scope but also spatial, as re-expression of CYP2E1 in a diffuse pattern may be an important element of the ability of these rats to withstand ongoing exposure. It is possible that other proteins pertinent to adaptation are also altered spatially, and this may have an impact on the liver's function with regard to processing xenobiotics.

Based on the degree of overt liver tissue degeneration seen in the mouse in Chapter 2, the process of adaptation is less easy to validate in the mouse model. The work in the final experimental chapter will therefore explore patterns of similarity and difference between the two rodent models.

Chapter 4: The regenerative response in rats and mice is incompletely conserved

Contents

4.1. Introduction

Both rats and mice are used extensively preclinically, and there are established differences in the way each species processes xenobiotics (Bogaards et al. 2000; Martignoni et al. 2006). Furthermore, acetaminophen (APAP) toxicity is known to vary considerably among preclinical species (Davis et al. 1974; Ioannides et al. 1983; Gregus et al. 1988; McGill et al. 2012b).

As stated in the previous experimental chapters, rats can tolerate far higher exposures to APAP than mice can, and this relates to the way the drug is processed by each species. Rats and mice show differences in the expression profile of CYP450 enzymes, although APAP-metabolising enzymes CYP2E1 and CYP1A2 are highly conserved among rat, mouse and human (Martignoni et al. 2006). Other differences are seen when comparing rates of GSH depletion and restitution on exposure to APAP (Davis et al. 1974; McGill et al. 2012b), and also the accumulation of products of APAP metabolism in the urine and bile (Gregus et al. 1988). It is therefore vital to thoroughly evaluate the characterised preclinical species and select the best available model of specific aspects of human drug toxicity.

4.1.1. Markers of toxicity

In order to compare the initial toxic effects of APAP in the livers of rats and mice, three markers were selected. CYP2E1 was chosen because of its role in the generation of the toxic metabolite NAPQI. CYP1A2 was investigated because of its similar centrilobular distribution and lesser role in APAP metabolism. GS was also compared as a sentinel of perivenous hepatocytes (Häussinger et al. 1991), but one without involvement in APAP toxicity.

4.1.2. Markers of adaptation

The canonical pathway entitled '*Nrf2-mediated oxidative stress response pathway*' was identified as significantly differentially regulated in rats the preceding chapter (Figure 3.2), and the transcription factor itself plays an important role in regulating the phenotypic response to cellular stress due to its interaction with the ARE, a promoter governing transcription of a panel of cytoprotective genes. However, as a function of this role, Nrf2 is both highly transient and present at very low abundance. Nrf2 rarely exists in an unbound state, free of its cytosolic repressor, Keap1, or molecules associated with either proteosomal degradation or transcription of nuclear DNA. It therefore presents a technical challenge to detect directly.

Both GCLC, the catalytic subunit of the glutathione synthetic enzyme glutamate-cysteine ligase, and the quinone reductase NQO1, arise from transcripts downstream of the ARE. Expression of these genes is therefore accepted as being regulated by Nrf2 (Wild et al. 1999; Jaiswal 2000). The abundance of these enzymes has been examined in both models in order to indirectly probe the activation state of Nrf2.

4.1.3. Markers of regeneration

To examine the regenerative response in the rat and mouse repeat APAP exposure models, two established markers of cellular proliferation were selected. PCNA is a sliding clamp which encircles DNA during the genome replication phase of the cell cycle (Smith 2013). Global proteomic analysis identified PCNA as one of the most significantly increased abundance proteins in the 72 h APAP group (Chapter 2, section 2.3.6.2; Supplementary Table 1c). Ki67 is a protein of unknown biological function that is strictly associated with all active phases of the cell cycle (Scholzen and Gerdes 2000). Since turnover of hepatocytes

in the quiescent liver is low (Klochendler et al. 2012), any increase in proliferative activity will be easily detected and confirmed using two independent markers.

4.1.4. Summary

Data shown in Chapter 2 explored some of the toxicological responses to repeat APAP exposure in rats and mice, identifying a number of similarities. Chapter 2 also highlighted some potentially important differences between the two models; in particular, GSH depletion (Figures 2.11 and 2.12) and the degree of tissue degeneration (Figures 2.7 and 2.8). Chapter 3 interrogated the complexity of the adaptive response in the rat, showing selective loss of the drug metabolism phenotype, and also alterations in the distribution and expression of CYP2E1 over the time course. Guided by the findings of the preceding chapters, the present chapter aims to identify some of the biochemical responses to repeat APAP exposure that may account for the interspecies differences observed.

4.2. Methods

4.2.1. Materials

CYP1A2, PCNA, GS, NQO1 and Ki67 antibodies were from Abcam (Cambridge, Cambs, UK; Cat. no. ab22717 (mouse), ab29 (mouse), ab49873 (rabbit), ab2346 (goat) and ab16667 (rabbit) respectively). Vimentin antibody was from Sigma (St. Louis, MO; cat. no. V6389, mouse). CYP2E1 antibody, raised in rabbit, was a kind donation from Magnus Ingelman-Sundberg, Karolinska Institute, Sweden. All other reagents were of analytical grade and quality and purchased from Sigma (St. Louis, MO).

4.2.2. Western immunoblot

Western immunoblot was performed as described in Chapter 2, section 2.2.9. Samples were prepared from livers taken from rats in the 1500 mg/kg APAP group and mice in the 750 mg/kg group (n = 4). CYP1A2 antibody (ab22717, Abcam, UK) was used at a dilution of 1:3000 overnight at 1 h at 4 ^{o}C, and secondary (anti-mouse) was 1:10 000 for 1 h at 4 ^{o}C. GCLC (ab53179, Abcam, UK) was used at a dilution of 1:10 000, in this case using bovine serum albumin as a blocking and non-specific binding agent. Secondary antibody (anti-rabbit) was 1:5000 for 1 h at RT.

Alongside immunoblot analysis of samples from individual animals, in some instances rat and mouse liver samples from each dose group (n = 4) were also pooled and resolved on the same gel to facilitate comparison of responses. These have been clearly indicated.

4.2.3. Immunohistochemistry

Ki67 IHC was performed as described in Chapter 3, section 3.2.8, with the following modifications: For antigen retrieval, slides were heated in a pressure cooker for 4 cycles of 3 min heat followed by cooling until depressurisation occurred; and slides were incubated

overnight (4 ^{o}C) with anti-Ki67 antibody at a working dilution of 1:200 in 20 % normal goat serum/TBS-T.

4.2.4. Statistical analysis

Statistical analysis was performed as described in Chapter 2, section 2.2.11

4.3. Results

4.3.1. Toxicity

The onset of toxicity can be seen as the initial phase in the repeat APAP exposure model, and has been characterised by toxicological assessment in Chapter 2. Some clear similarities between the two rodent models have been demonstrated in this way, particularly with regard to the pattern of hepatocellular injury and transaminase release; however, the mouse model exhibited a greater degree of overt tissue degeneration over the experimental timecourse. In an attempt to clarify the animals' response to the toxic phase of exposure, western immunoblot has been performed to detect three enzymes which inform the evolution of this phase. The assays have been performed on lysates from individual animals, which were then analysed densitometrically to permit statistical analysis (Figure 4.1). The assays were also performed on samples which had been pooled according to treatment group in order to allow intra-gel comparison of the two models (Figure 4.2).

CYP2E1 and CYP1A2 are both directly implicated in APAP metabolism, and were seen to be substantially depleted in the 48 h APAP group in both models, reflecting peak hepatocellular injury. CYP2E1 diminished to 44 % of control in rat in this group, and in mouse it fell to 8 %. Consistent with data from the rat shown in Chapter 3 (Figure 3.8), there was a 120 % increase of CYP2E1 in mouse at 24 h APAP, although in contrast to the rat data (which showed CYP2E1 was 187 % of pooled control at 96 h) there was no apparent rebound in the 96 h group. CYP1A2 fell to 18 % and 7 % of control in rat and mouse 48 h APAP groups respectively. The pattern of loss and recovery of CYP1A2 in the two models was closely conserved.

GS, a marker of perivenous hepatocytes, showed a similar pattern to CYP2E1 and CYP1A2, with significant loss of abundance observed in the 48 h APAP groups for both rat and

mouse (20 % and 1 % of controls respectively). In the rat, GS was quantified at 1 % of control in both the 72 h and 96 h APAP groups. The mouse model showed partial recovery of expression in 72 h and 96 h APAP groups. These later treatment groups were quantified at 48 % and 39 % respectively.

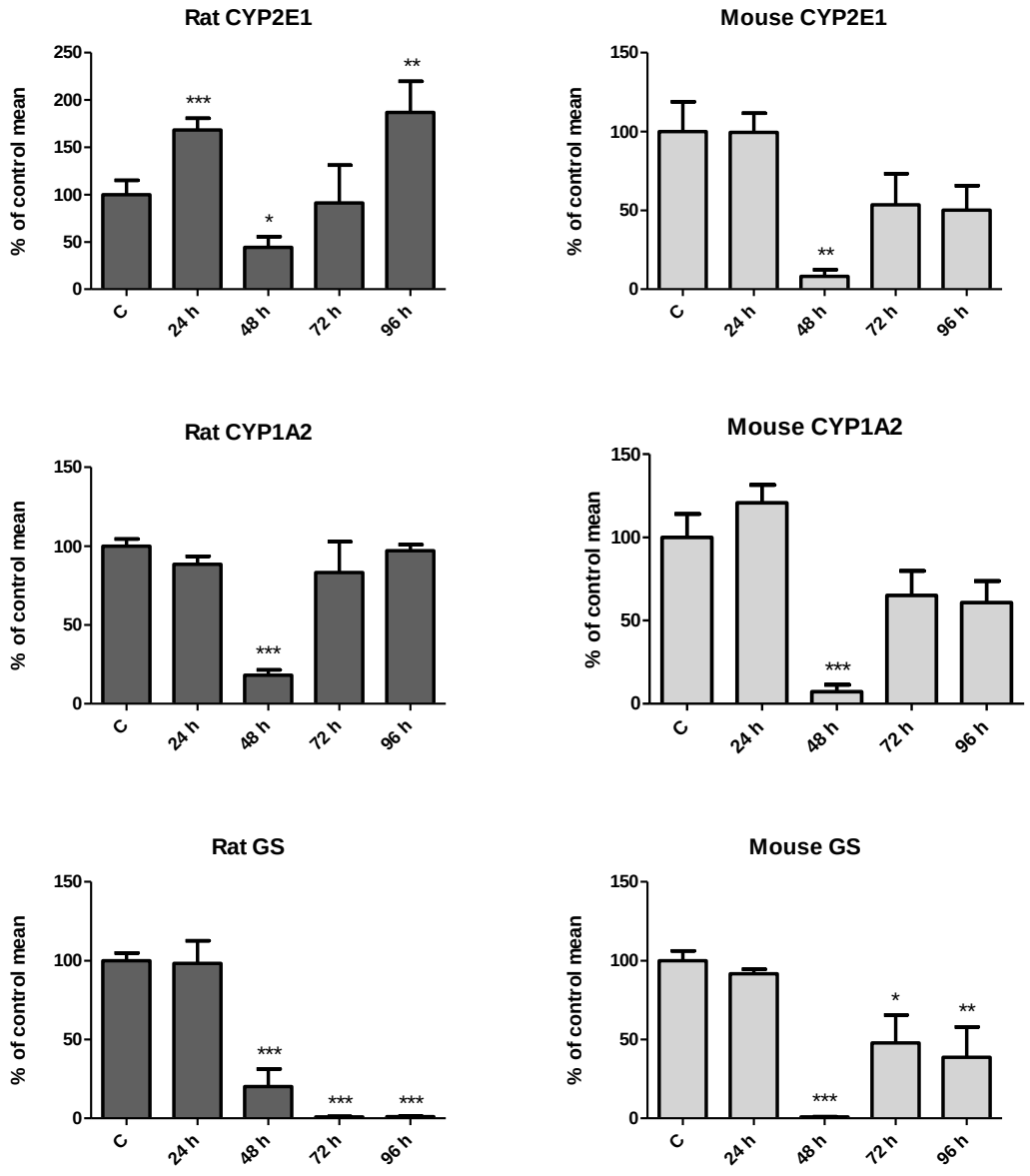

Figure 4.1: Densitometric analysis of western immunoblot data for perivenous enzymes

Legend: Densitometric analysis of western immunoblots comparing CYP2E1, CYP1A2 and GS in liver lysates (n = 4 animals) from each treatment group in both the rat and mouse models of repeat APAP exposure. Densitometric values are normalised to actin and expressed as a percentage of the mean of control group animals. In all instances, a reduction in expression is seen in the 48 h APAP treatment group, corresponding to loss of cells from the perivenous region.

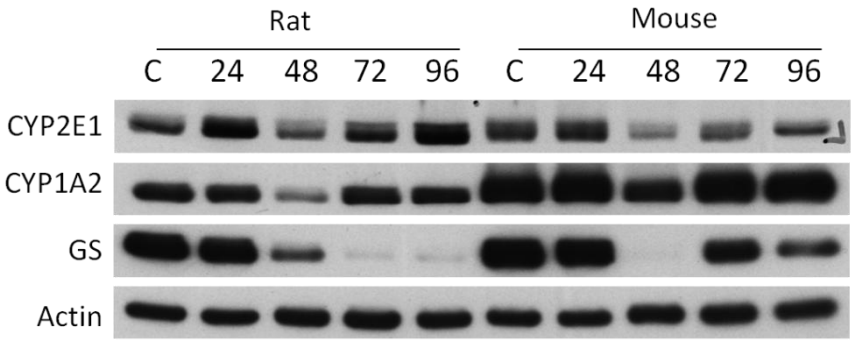

Figure 4.2: Western immunoblot of perivenous enzymes in rat and mouse – pooled samples

Legend: Representative western immunoblots comparing CYP1A2, CYP2E1 and GS in pooled liver lysates from each treatment group in both the rat and mouse models of repeat APAP exposure. Pooled n = 4 animals per lane.

4.3.2. Detoxification and phenotypic adaptation

The analysis of proteomic data described in Chapter 3 identified the Nrf2-mediated oxidative stress response pathway as being significantly perturbed by daily APAP exposure in rats, and therefore implicated in the processes of detoxification and phenotypic adaptation. Since the transcription factor Nrf2 itself was not detectable in the proteomic data set and could not reliably be detected by western immunoblot, GCLC and NQO1 were probed in individual (Figure 4.3) and pooled (Figure 4.4) liver lysates as surrogate markers of Nrf2 activation.

GCLC, the rate-limiting factor in repletion of GSH, was not markedly altered by dosing, except in the rat 96 h APAP group, where a significant increase to 195 % of pooled control was seen. In mouse, although a loss was seen in the 48 h APAP group, GCLC was not significantly changed in any dosing group.

In rats, an increase in abundance of NQO1 was seen from 48 h onwards, reflecting the recycling of NAPQI back to APAP. Significance was seen in the 48 h APAP group (488 % of control) and 96 h APAP group (699 % of control). This was not mirrored in the mouse: as seen with GCLC data, a loss of NQO1 was seen in the 48 h APAP group, although none of the groups showed statistical significance.

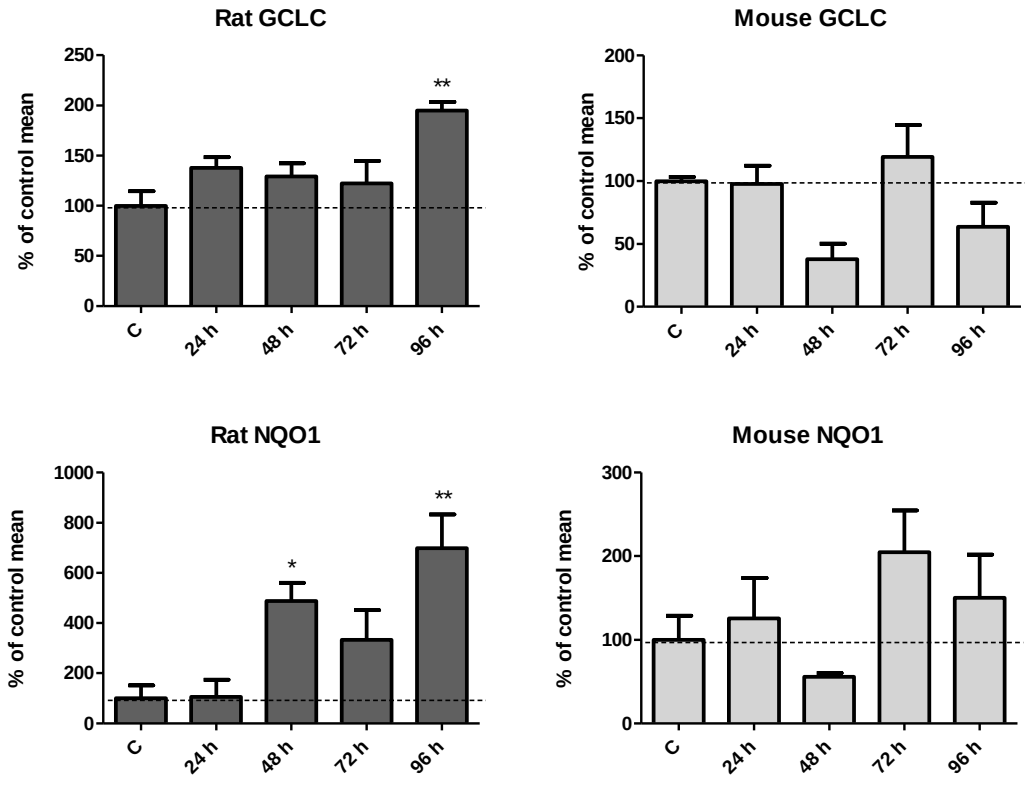

Figure 4.3: Densitometric analysis of western immunoblot data for APAP detoxification enzymes

Legend: Densitometric analysis of western immunoblots comparing GCLC and NQO1 in liver lysates (n = 4 animals) from each treatment group in both the rat and mouse models of repeat APAP exposure. Densitometric values are normalised to actin and expressed as a percentage of the mean of control group animals. Dashed line indicates control value.

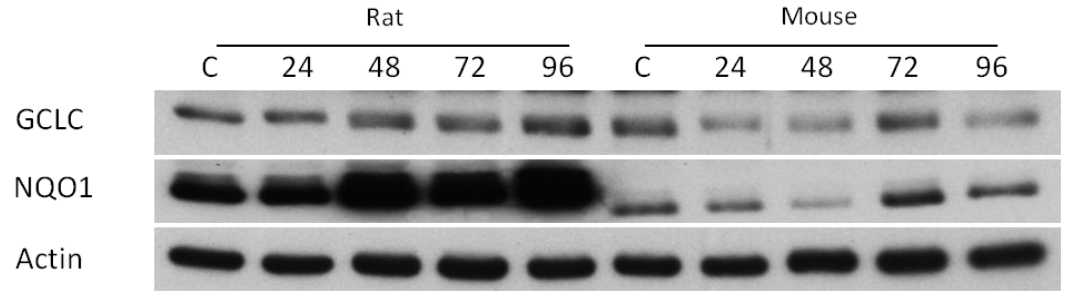

Figure 4.4: Western immunoblot of APAP detoxification enzymes in rat and mouse – pooled samples

Legend: Western immunoblots comparing GCLC and NQO1 in pooled liver lysates from each treatment group in both the rat and mouse models of repeat APAP exposure. Pooled n = 4 animals per lane.

4.3.3. Regenerative changes

A large part of an organism's ability to adapt to repeated APAP toxicity lies in its capacity for swift and organised liver regeneration. Review of the proteomic data shown in earlier chapters showed that, in the 72 h APAP group, proteins associated with cell cycle, proliferation and repair pathways were over-represented. One of the most prominent proteins at 72 h was the cytoskeletal protein vimentin, which is a marker of mesenchymal cells and is vital for cell migration and tissue remodelling (Eckes 2000). This observation was confirmed by western immunoblot (Figure 4.5). Basally close to the limit of detection, vimentin rises to almost 7000 % of control values after 72 h of daily APAP exposure.

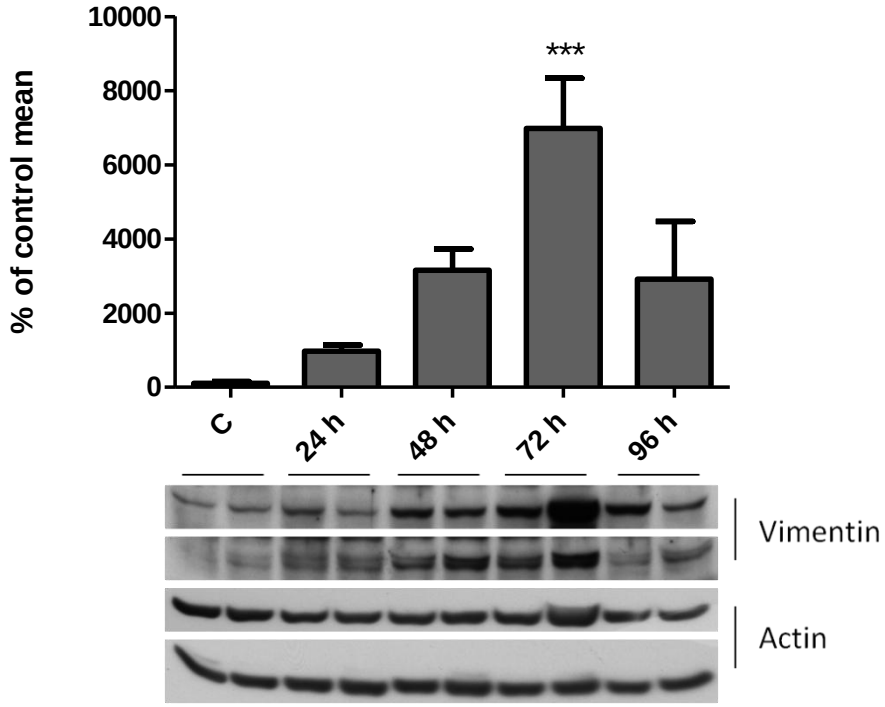

Figure 4.5: Densitometric analysis of immunoblot data for vimentin expression in rat

Legend: Densitometric analysis of western immunoblots for vimentin in liver lysates (n = 4 animals, representative immunoblots shown) from each treatment group in the rat model of repeat exposure. Densitometric values are normalised to actin and expressed as a percentage of the mean of control group animals. N. B.: Actin is itself slightly elevated in the 72 h APAP group, which may be a consequence of tissue remodelling.

In order to compare the regenerative responses of rat and mouse, the marker of cell cycling and tissue repair, PCNA, was examined in individual (Figure 4.6) and pooled liver lysates (Figure 4.7) in each treatment group. In rat, a significant increase in PCNA abundance was observed in all repeat exposure groups, peaking in the 72 h APAP group at 3162 % of control. In mouse, the emergent picture was very different, with an initial loss of expression in the 24 h APAP group, then a trend towards increased abundance at later timepoints, albeit without statistical significance.

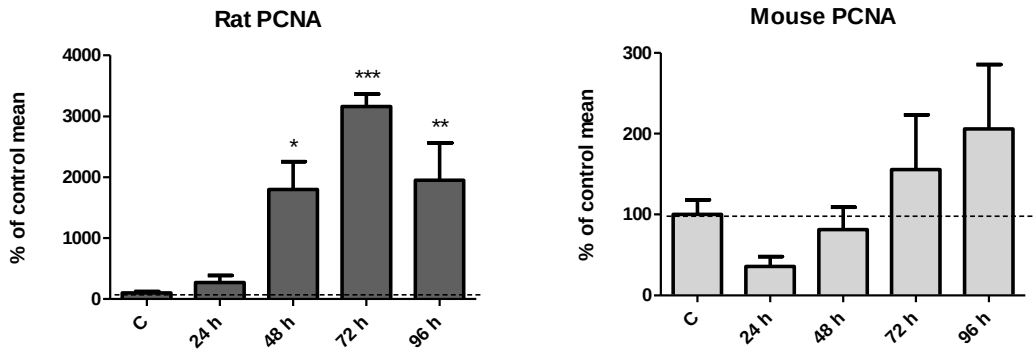

Figure 4.6: Densitometric analysis of western immunoblot data for PCNA expression in rat and mouse

Legend: Densitometric analysis of western immunoblots comparing PCNA in liver lysates (n = 4 animals) from each treatment group in both the rat and mouse models of repeat APAP exposure. Densitometric values are normalised to actin and expressed as a percentage of the mean of control group animals.

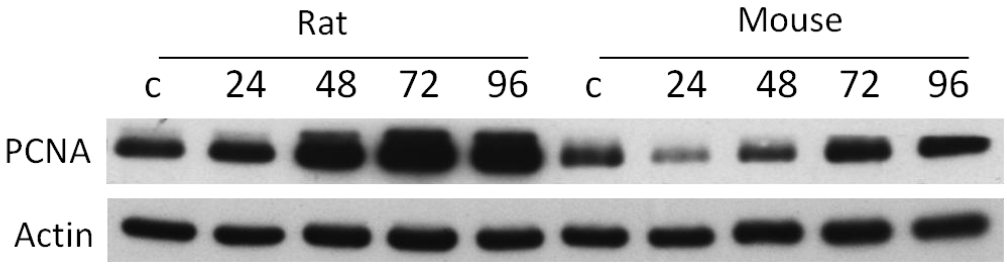

Figure 4.7: Western immunoblot of PCNA in rat and mouse – pooled samples

Legend: Western immunoblots comparing PCNA expression in pooled liver lysates from each treatment group in both the rat and mouse models of repeat APAP exposure. Pooled n = 4 animals per lane.

In the rat model, the change in expression of PCNA (Figure 4.6) was seen to be closely consistent with that seen for vimentin (Figure 4.5), and an analysis of correlation is shown (Figure 4.8) which shows a significant R^2 value of 0.938.

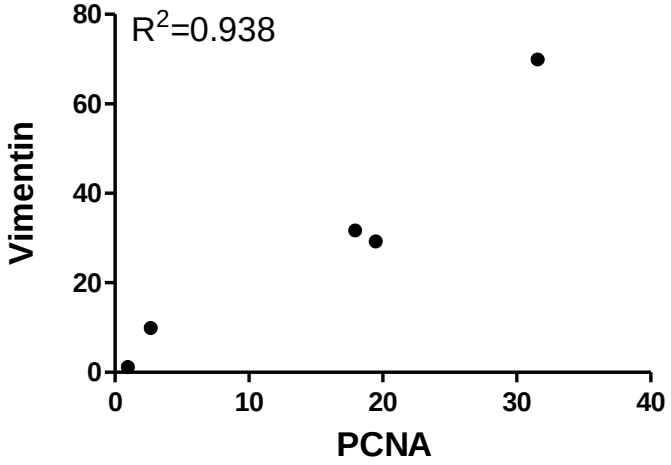

Figure 4.8: Correlation of densitometric data for vimentin and PCNA in rat

Legend: A strong correlation is seen between the protein expression profile of markers of tissue repair and remodelling, vimentin and PCNA, in rat liver lysates.

IHC was used in Chapter 3 to track the tissue distribution of CYP2E1, identifying a spatial element to the process of adaptation in rats. To gain an additional dimension of understanding of the regenerative response in each model, here the marker of replication Ki67 was also investigated by IHC in rats and mice. Although software permitting quantitative image analysis was not available, visual assessment of the slides from each treatment group suggested a remarkably similar pattern of expression between PCNA and Ki67 in each model. Representative images are shown in Figure 4.9. The rat again shows an early and robust increase in cells expressing Ki67, closely reflecting the profile seen for vimentin in Figure 4.5 and PCNA in Figure 4.6. Positively stained cells were observed throughout the sections, with greatest densities seen in the perivenous regions, corresponding to areas that had sustained prior tissue injury and cell death. In the mouse,

mitotic events appeared basally more common. They diminished in the 24 h APAP group before gradually increasing in the 96 h APAP group, again both diffusely throughout the section and in higher densities surrounding central veins. Observations for Ki67 staining were consistent with the abundance of PCNA (Figure 4.6) in both models. A detailed image comparing Ki67 staining in rat and mouse liver at 72 h is presented in Figure 4.10, showing the concerted proliferative response in the rat compared to the absence of immunogen in the mouse tissue.

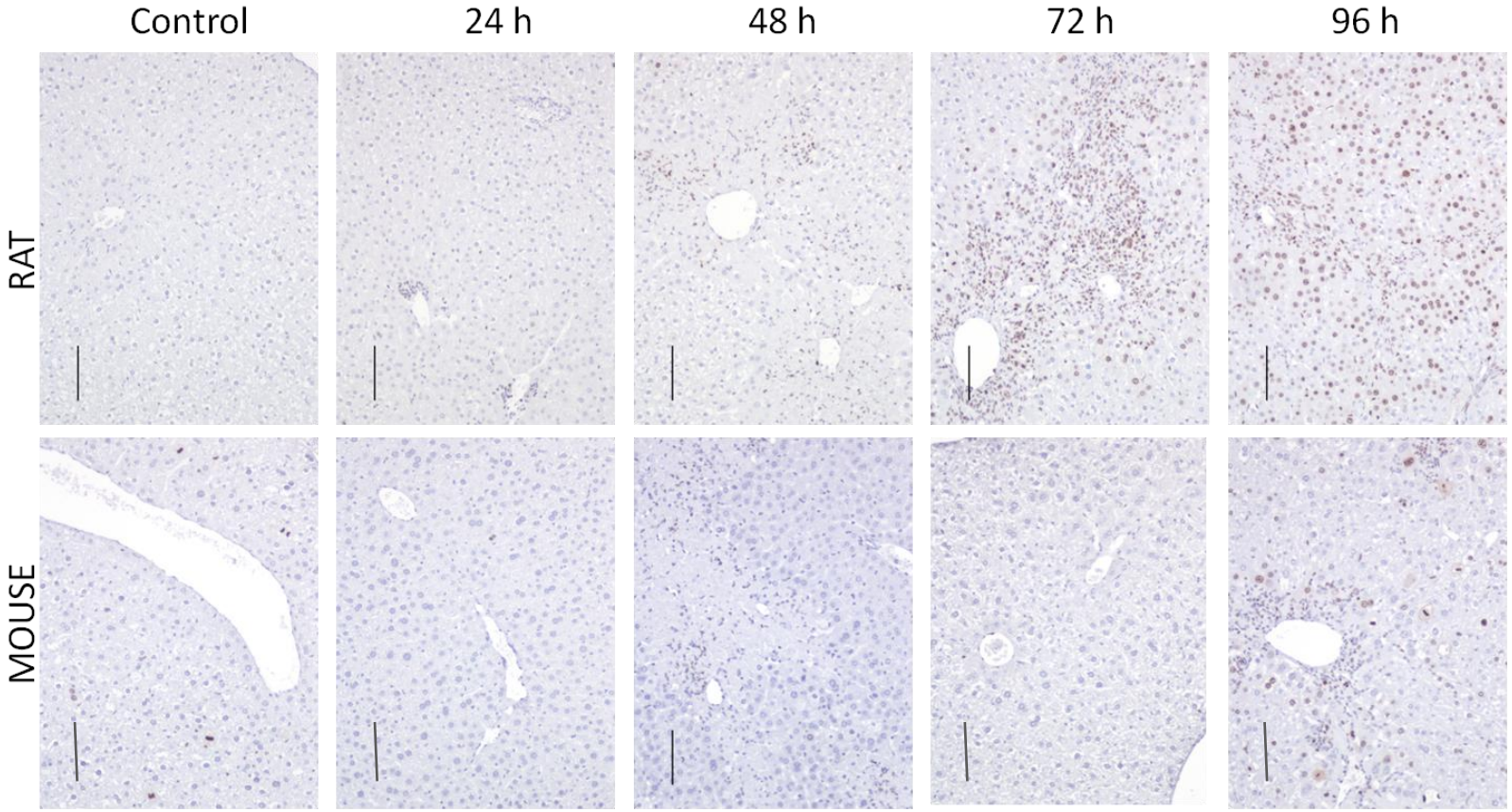

Figure 4.9: Ki67 staining in rat and mouse

Legend: Representative image from each treatment group in the rat and mouse model, showing liver sections stained for the replication marker Ki67. Immunogen is brown against a blue haematoxylin counterstain. Although more mitotic events were observed basally in the mouse, the rat showed a greater ability to mount a proliferative response to tissue injury. Bar = 100 µm.

Chapter 4: The regenerative response in rats and mice is incompletely conserved

Figure 4.10: Detail of Ki67 staining in rat and mouse 72 h APAP treatment groups

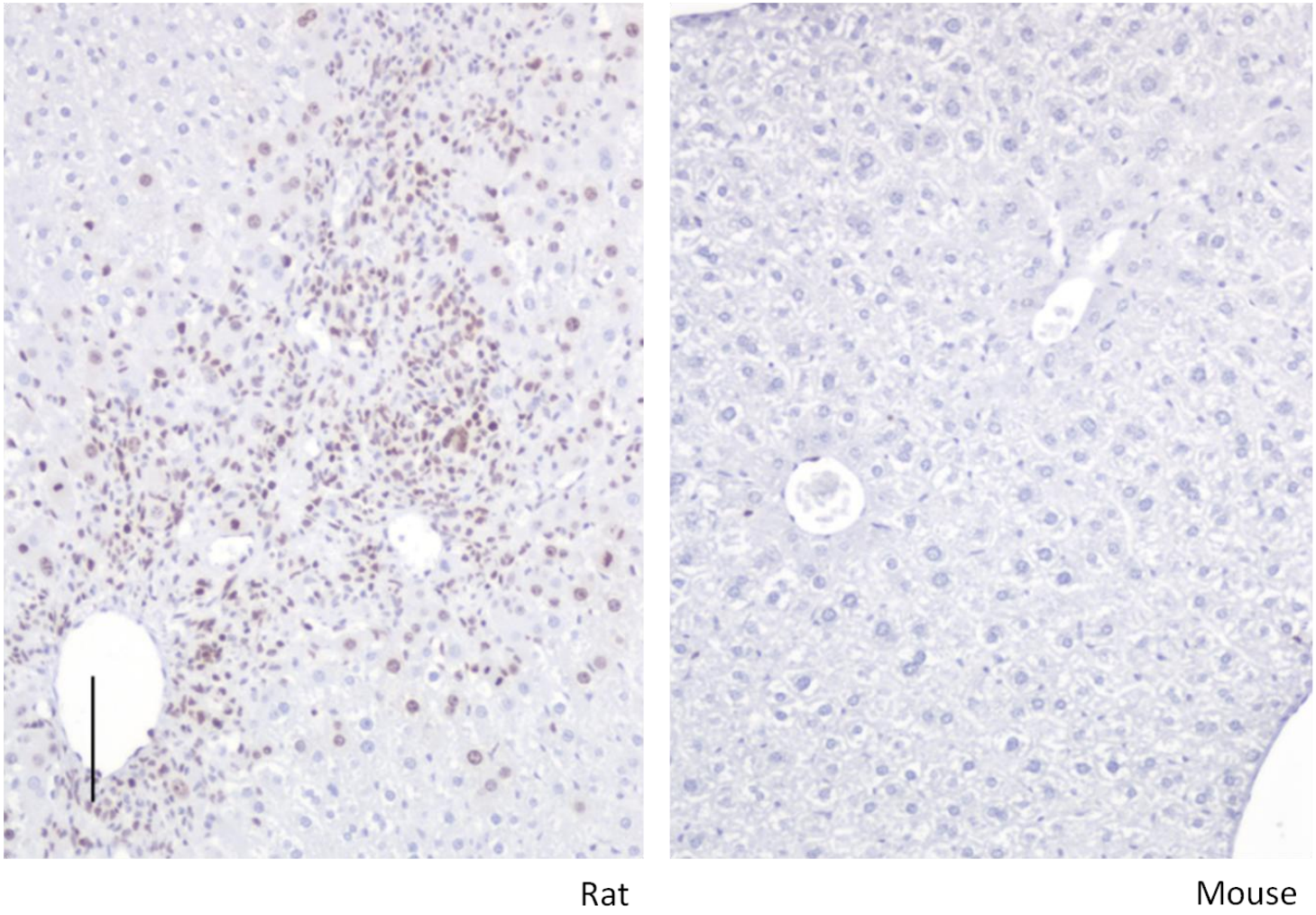

Legend: Detail of Ki67 staining in rat and mouse 72 h APAP treatment groups showing the abundance of actively replicating cells in the rat, in particular in the region surrounding the central vein. This is in stark contrast to the same group in the mouse model, showing absence of immunogen in mouse tissue. Immunogen is brown against blue haematoxylin counterstain. Bar = 100 µm.

Chapter 4: The regenerative response in rats and mice is incompletely conserved

4.4. Discussion

Data presented in earlier chapters show the gross change in hepatic phenotype in the rat in response to repeated APAP exposure. Data shown in Chapter 3 suggest that the drug metabolising phenotype of the liver is suppressed in favour of a proteome supporting essential functions and repair. In this chapter, the response of rats and mice to repeated APAP exposure was compared over a 96 h period. Rats received 1500 mg/kg daily and mice received 750 mg/kg daily. In both models, significant toxicity was seen in the 48 h APAP group. Selected markers of toxicity, adaptation and regeneration were examined in each model, revealing differences at every point in the process (Table 4.1). Understanding the way each species behaves in response to repeated chemical stress is necessary to make an appropriate choice for preclinical modelling of drug toxicity and liver regeneration.

	RAT	**MOUSE**
TOXICITY	Loss of all markers at 48 h; Induction of CYP2E1 at 24 h and 96 h	Loss of all markers at 48 h; recovery of GS expression at 72 and 96 h
ADAPTATION	Induction of Nrf2-dependent proteins	No induction of Nrf2-dependent proteins
REGENERATION	Robust proliferative response, peaking at 72 h	No significant proliferative response

Table 4.1: Summary of key differences identified in rat and mouse responses to repeat APAP exposure

Legend: Despite initial similarities between the two models in terms of characteristic APAP-induced hepatocellular injury, after repeated exposures the responses of rats and mice diverge.

4.4.1. Summary of findings and relation to literature

Consistent with data shown in Chapter 2, some clear similarities exist between the two models of repeat APAP exposure investigated. Both rats and mice in the 48 h APAP group

showed a marked loss of CYP2E1 and CYP1A2 as a consequence of repeat exposure, reflecting destruction of the CYP450-rich centrilobular regions of the liver. However, the robust induction of CYP2E1 seen in the rat 24 h APAP and 96 h APAP groups was not reflected by the mouse cohorts. Comparison of GS abundance revealed a picture that was initially similar, with loss of the marker of perivenous hepatocytes in the 48 h APAP group in both models. Interestingly, the mouse 72 h APAP group showed rapid partial restitution of GS despite ongoing tissue injury, in contrast to the rat model, which had not recovered GS expression by the end of the time course (Figure 4.1). It is unclear at this point which cells could be responsible for the re-expression of GS in the mouse, since data shown in Chapter 2 (Section 2.3.3.2) showed that some animals continued to sustain extensive tissue injury in each dose group.

Activation of Nrf2 is an important step in the process of detoxification and restoration of redox equilibrium pursuant to oxidative stress. It has previously been demonstrated in both the rat (Ahmed et al. 2011) and the mouse (Goldring et al. 2004) in response to APAP exposure. Data presented in Figure 4.3 suggest more effective Nrf2 activation in rat than in mouse. This observation is in keeping with the rats' known greater resistance to toxicity, and is supported by findings shown in Chapter 3 which identified the involvement of the Nrf2-mediated response to oxidative stress in the rat (Figure 3.1).

However, the use of surrogate markers is not without pitfalls, and in order to have greater confidence in these findings it would be valuable to ascertain experimentally a number of additional factors to assist with interpretation of the data. These factors include i) the degree of temporal lag between Nrf2 activation and detectable upregulation of downstream gene products in these models; ii) the degree of crosstalk between Nrf2 and other transcription factors that interact with the ARE upstream of the surrogate markers in

question; and iii) the degree of upregulation that constitutes biological significance in this context.

A model of APAP-induced liver injury examined by Fan et al. (2014) displayed elevated NQO1 at the protein level 48 h after exposure. These data are consistent with findings for the rat model in the present work, reinforcing the notion that Nrf2 is activated in the process of adaptation in the rat. The findings are in contrast to the mouse model which in this repeat exposure context does not exhibit elevated NQO1, suggesting that either Nrf2 is not activated in this context, or its activity is suppressed as a consequence of repeat APAP exposure.

Whilst it is tempting to conclude that Nrf2 activation alone is responsible for the induction of NQO1 and GCLC in the rat model presented here, it must be borne in mind that crosstalk between different transcription factors and the ARE have been documented. Besides Nrf2, the transcription factors Jun, Fos and Fra also bind to the ARE and influence the transcription of ARE-governed genes (Venugopal and Jaiswal 1996). Furthermore, the Fos protein Fra1 has been shown to protect mice from APAP-induced liver injury (Hasenfuss et al. 2014). Collectively, these observations raise the possibility that, despite the fact that the Nrf2-mediated oxidative stress response pathway was identified through pathway mapping, the upregulation of detoxification proteins seen here in the rat may be driven by other transcriptional pathways besides Nrf2.

The cytoskeletal protein vimentin was probed by immunoblot in the rat (Figure 4.5) and findings were consistent with proteomic data (Chapter 2, Figure 2.13). Vimentin is strongly associated with mesenchymal cells and wound healing (Eckes et al. 2000), but is also established as a marker of dedifferentiating primary hepatocytes in culture (Schuetz et al. 1988). The latter association may lend further weight to the observations that mature

hepatocytes re-entering mitosis undergo phenotypic dedifferentiation in a manner very similar to that seen in cultured primary cells (Ito et al. 1991), and that this dedifferentiation is part of the liver's strategy to limit further toxicity in the aftermath of extensive liver injury.

A similar profile of expression to that seen with vimentin is also seen when PCNA is examined in the rat (Figure 4.6) and in fact, correlation between the two markers of regeneration is close (Figure 4.8). PCNA expression in the mouse, however, is very different. Although statistical significance was not seen, immunoblot data showed an initial loss of expression of PCNA, with a trend towards increased expression at later time points in some animals, which peaked in the 96 h APAP group. Image analysis was not performed on Ki67 IHC, but visual evaluation of the data obtained using this assay seemed to be in keeping with the profile of expression of PCNA in both models (Figure 4.9). A stark visual contrast is notable between rat and mouse in the 72 h APAP group. In this group the rats showed the greatest increase in abundance of proteins contributing to repair and regeneration, according to the proteomic data. Figure 4.10 shows a large number of Ki67 immunopositive cells in the rat liver, particularly clustering around the centrilobular region. In the mouse, stained liver from the equivalent experimental group shows an almost complete absence of Ki67 immunopositive cells, suggesting that tissue remodelling processes in the mouse model are very different.

4.4.2. Implications of findings and questions raised

Although there are some common responses to repeat APAP exposure in the models explored, striking differences have been identified at every phase of toxicity, adaptation and regeneration in repeat dosed mice and rats. These differences are particularly apparent when comparing Nrf2 activation and tissue remodelling activity. Something is known of how rats are adapting to repeated APAP exposure in this model by virtue of the

analysis of proteomic data conducted in the previous chapter. What remain less clear are the mechanisms by which the mice are able to withstand a similar stress.

Although controversy exists over the mode of cell death in APAP overdose, necrosis is generally accepted as the predominant mechanism (Jaeschke et al. 2014). Necrosis is characterised by cell swelling and lysis, vacuolation, karyorrhexis and karyolysis (Gujral et al. 2002). Both species suffer an initial depletion of absolute cell number, and whereas the rat has been shown to initiate a strong regenerative response in the immediate aftermath of cellular injury, when judged by the same criteria, the mouse does not. However, with the exception of three animals that were found dead, the mice in this study were able to withstand repeat exposure over the time period examined. How therefore is the mouse liver adapting and regenerating?

Using knockout animals, Nrf2 has recently been identified as a novel regulator of hepatocyte mitosis (Zou et al. 2015). Although the mouse cohort in the present work was not deficient in Nrf2, mice showed an apparent lack of activation of Nrf2 under these experimental conditions. Given that the mice also failed to initiate a significant mitotic response, these observations seem in accord with the findings of the publication. Using an inducer of Nrf2 may therefore be valuable in stimulating hepatocyte mitosis and treating APAP-induced liver injury.

It is also worth noting here that, whilst PCNA and Ki67 are validated markers of DNA replication, in this context DNA replication does not necessarily equate to cell division. A peculiarity of hepatocytes is their propensity for polyploidy. Around 70 % of all mature hepatocytes in rodents are tetraploid (Fausto and Campbell 2003). It would seem therefore that hepatocytes do not necessarily undergo conventional cell division. As well as polyploidy, a significant number of hepatocytes are binucleate, and it is thought that these binucleate cells represent a functional reserve (Wheatley 1972). It has been

observed that the number of binucleate cells diminishes after partial hepatectomy (Wheatley 1972), so it is possible that one facet of recovery in the mouse is reductive cell division, whereby a binucleate parent cell gives rise to two mononucleate daughter cells.

Consistent with observations made in Chapter 2, section 2.3.3.2, further research has shown that in mice, the initial response to loss of liver tissue is hypertrophy (Miyaoka et al. 2012). This physical enlargement of remaining hepatocytes to reconstitute organ mass was shown to precede proliferation, and proliferation would only occur if hypertrophy was insufficient to restore mass. In 30 % partial hepatectomy (a cell loss roughly equivalent with that seen at the peak of toxicity in the present model), hepatocyte division was not observed (Miyaoka et al. 2012). So perhaps another facet of the mouse's strategy for survival could be explored by interrogating hepatocyte volume, nuclear number and ploidy in response to APAP toxicity.

In some ways the mouse is considered a closer analogue of human APAP toxicity than the rat (Jaeschke et al. 2014), and yet as discussed here there are still many facets of the mouse's adaptation to repeated exposure that are poorly understood. What is clear is that although some common features exist between rats and mice, other elements of the process of adaptation are unique to each species. Furthermore, adaptation is incredibly intricate and complex, and the work presented here merely scratches the surface of the process. Reviewing the data, it seems impossible to attribute adaptation to a single pathway or group of molecules – an appropriate biological characteristic since an organism's survival can depend on it.

Chapter 5: Concluding Discussion

Contents

5.1. Summary of model and key findings

The aim of this thesis was to investigate the molecular mechanisms of adaptation to chemical stress using the model hepatotoxin acetaminophen (APAP). In the first experimental chapter, two preclinical models of repeated APAP exposure have been characterised through clinically accepted toxicological and histopathological assessments, establishing APAP-induced toxicity in the high dose APAP exposure groups in both rat and mouse models. A global proteomic analysis of rat liver has given insight into the changes in abundance of a subset of proteins common to all rats throughout the duration of the repeat exposure study, demonstrating that the process of adaptation to repeat APAP exposure is not mediated by a single enzyme or pathway, but rather by a dynamic shift in expression of a large number of hepatic proteins.

The second experimental chapter probed deeper into the molecular events surrounding adaptation to repeat exposure in the rat, and interrogated the proteomic data using pathway analysis software. This interrogation mapped significantly differentially abundant proteins onto established canonical pathways, and permitted the identification of phenotypic shifts in response to dosing. These phenotypic shifts gave an indication of what may constitute adaptation. A graphical summary of the model is shown in Figure 5.1. Other work in this chapter focused on the role of APAP's major bioactivator, CYP2E1, at different time points in the rat high dose APAP exposure model through immunohistochemistry and liver microsome experiments. This work identified a marked change in both spatial and temporal expression of CYP2E1, and alterations in the enzyme's activity which did not seem to correlate with the degree of toxicity seen at the timepoints examined.

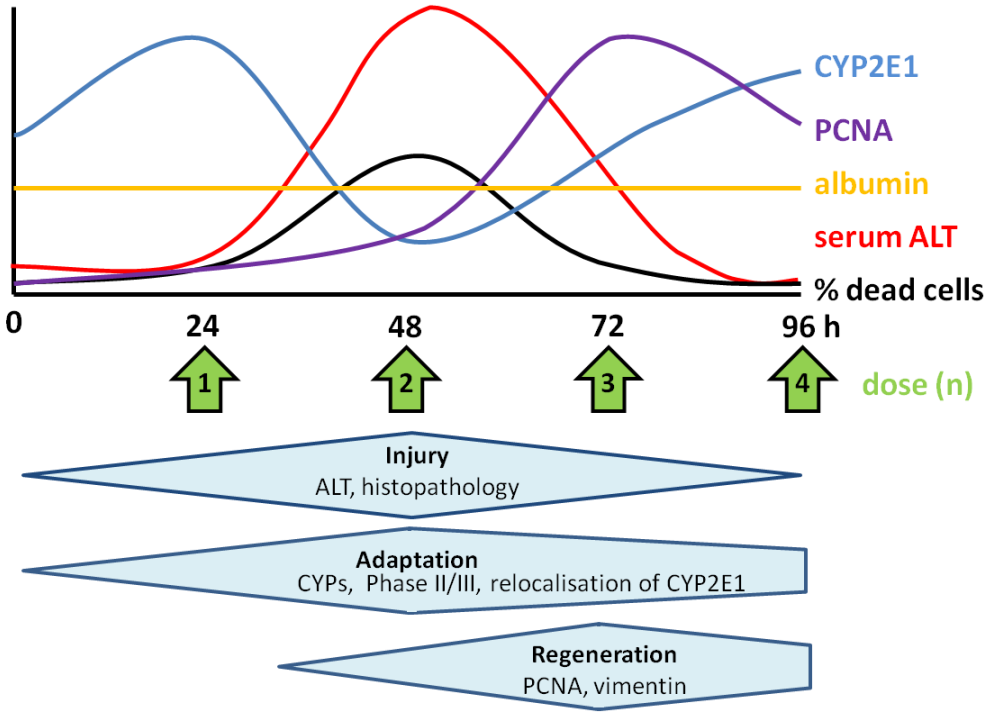

Figure 5.1: Graphical summary of the rat model of adaptation to APAP

Legend: Visual representation of key observations made of the rat's response to repeat APAP exposure. Cell death and ALT release is seen at 48 h, preceded by an increase in CYP2E1 abundance, although the clinical marker of liver function albumin remains unaffected throughout. Cellular injury rapidly resolves, as phenotypic shifts alter the drug metabolism profile of the liver and initiate proliferative activity to restore lost tissue.

The final experimental chapter compared and contrasted the regenerative response in the rat and mouse high dose APAP exposure groups, probing for proteins identified as key to the processes of toxicity, adaptation and regeneration based on the work of previous chapters. Whilst common observations were made, differences between the two models were observed in every equivalent time point. Both models showed loss of centrilobular hepatocytes, but the mouse model displayed partial restoration of expression of GS, accepted as a sentinel of immediately perivenous hepatocytes. The Nrf2-mediated oxidative stress response is known to be conserved between murine models and man, but under these experimental conditions, the rat seemed to mount an oxidative stress response to liver injury, demonstrated through analysis of the surrogate markers of Nrf2

activation GCLC and NQO1. The mouse, on the other hand, did not show significant elevation of these markers. The rat was also shown to have a far greater capacity for proliferative activity than the mouse, raising questions concerning which other mechanisms might mediate the mouse's adaptation and survival.

5.1.1. Relation of findings to hypothesis

The original hypothesis was that adaptation to repeat APAP exposures is a complex process involving multiple pathways and phases, commensurate with a sophisticated response across the liver to ensure survival upon re-exposure to subsequent normally noxious exposures. Data presented here from the rat model fully support the hypothesis, showing that there is a great breadth of hepatic responses, and that these responses are dynamic and concerted, effectively protecting the animal from sustaining further injury whilst preserving critical hepatic function. In the mouse, although adaptation has been demonstrated, initial analyses presented here suggest that some of the mechanisms underpinning adaptation in the mouse may be markedly different to those seen in the rat. As the mouse is in some regards accepted to be a closer model of human APAP toxicity, further characterisation of these mechanisms and their divergence from what is known of the rat may shed light on the processes of human adaptation to chemical stress. Understanding the consequences of failure in any of these processes would enable the development of improved strategies for clinical management of APAP-induced liver injury.

5.2. Limitations of study and opportunities for further research

As with any scientific study, the data presented here must be interpreted within the context and the limitations of the experimental framework. The original animal studies were conceived, designed and conducted by Almirall S. A. as a means of modelling acute liver failure. Since the animals in each of the studies did not succumb to liver failure as a result of repeat APAP exposure, but rather adapted to the exposure and became resistant to its effect, the study presented a valuable opportunity to investigate the process of adaptation.

5.2.1. Choice of experimental timepoints

The initial objectives of the studies informed the choice of timepoint for dosing and sacrificing the animals. Consequently, the timepoints examined in this thesis were not necessarily the most appropriate with which to characterise the many facets of adaptation. Analysis of the study data has shown that the hepatic response over the 96 hour period is highly dynamic. It is possible that some of the more subtle responses may have been missed due to their transient nature. A good example of this is the transcription factor Nrf2, which is known to be transiently induced within 1-2 hours of stress *in vivo* (Goldring et al. 2004). Therefore an attempt to recapitulate any of this work might include a number of sampling points after each administration in order to capture the more transient changes in phenotype.

5.2.2. Selection of proteomic data for analysis

Any proteins that were not detected in all liver samples from every group in the rat 1500 mg/kg proteomic analysis were excluded from the data analysis. Although this decision was taken in order to permit robust statistical analysis, excluding proteins which did not appear in all dose groups may, again, have resulted in some important changes being

overlooked. Any proteins that were basally undetectable in some samples but present in others have been excluded from the analysis, as well as any that were expressed by only some of the animals in any given exposure group. A subsequent evaluation of the model may reveal new leads in the search for mediators of adaptation. Re-examination of raw data alongside immunostained histological specimens may highlight additional relevant responses, selectively identifying potential contributions of non-parenchymal cells to adaptation.

5.2.3. Duration of experimental timecourse

Although what constitutes 'chronic' exposure in an animal model can vary greatly depending on both the species and pharmaceutical agent in question, the International Conference on Harmonization (ICH) Guidance for Industry makes recommendations on preclinical repeated dose toxicity testing. A minimum study duration of 2 weeks is suggested, which can be extended to several months dependent on the anticipated duration of treatment in humans (ICH 2010). The Organisation for Economic Co-operation and Development (OECD) assert that repeated dose oral toxicity testing in rodents (where adverse effects may occur after multiple or continuous exposures) should be performed for 28 days with a 14 day washout period (OECD 2008), and sub-chronic oral toxicity testing (where toxicity may occur after repeated or continuous exposure for up to 10 % of the organism's lifespan (ISO 2006)) should be carried out for 90 days (OECD 1998).

The first study to identify the phenomenon of adaptation to APAP (Buttar et al. 1976) looked at sub-acute exposure, defined in the paper as twice-daily exposure for a period of seven days. Data from these animals were compared to an acute exposure group which received a single treatment. Following on from the hepatoprotective effects observed in this study, a subsequent publication (Strubelt et al. 1979) sought to elucidate the mechanisms of the phenomenon. This work found that after a sub-acute exposure

consisting of four daily doses, with a further exposure on the sixth day, again, adaptation had occurred. Also of interest in the work presented by Strubelt was the notion that these hepatoprotective changes persisted beyond the duration of exposure, as animals which received a final exposure on day six of this study showed only a partial reversal of the hepatic adaptations that APAP induced. Since these publications, more recent studies have shown that longer term exposures continue to confer protection in animal models (Poulsen and Thomsen 1988; Dalhoff et al. 2001).

From the clinical perspective, adaptation to long-term APAP exposure is described in a number of publications including a case study in which a clinician developed tolerance to a prescription opioid/APAP formulation with no liver injury (Shayiq et al. 1999). Furthermore, an analysis of a multicentre retrospective study of repeated supratherapeutic ingesters of APAP revealed that just over one third of the subjects identified as such experienced hepatotoxicity, suggesting that the remainder were able to either tolerate or adapt to repeated exposure despite often complex sociomedical backgrounds (Alhelail et al. 2011). However, little data exist concerning whether these protective changes persist in the aftermath of treatment.

The duration of the present work is in keeping with the animal studies cited above which explore the adaptive effects of APAP exposure; yet, in this context, the current work falls into the broad grey area between acute and chronic exposure. Although not a preclinical trial and therefore not the subject of industry guidelines, when viewed in such a context the model of adaptation presented in this thesis may have been somewhat limited by its duration. Whilst 4 days of bolus dosing is in some regards a reasonable reflection of a human therapeutic APAP exposure to medicate minor illness or injury, given the dynamic nature of the responses provoked by repeat exposure it would be worthwhile assessing whether the detected changes continue to evolve over a longer time period. Doing so

would also enable researchers to ascertain the duration of the hepatoprotective changes after the initial exposure.

5.2.4. Controlling for food consumption

A further factor that should be considered in the interpretation of data is whether the animals were consuming food normally. Rats and mice in the work presented here had unrestricted access to standard laboratory rodent feed for the duration of the study, but data for food consumption was not recorded when the study was conducted. Tissue injury and inflammation cause sickness behaviour, a hallmark of which is anorexia (Maes et al. 2012). Some animals may have stopped eating after the initial APAP exposure due to the degree of liver injury sustained. This means that they would have received subsequent doses in an effectively fasted state, which may be confounding the results. A recent study focusing on nutritional state as a risk factor for toxicity arising from ongoing exposure to therapeutic doses of APAP (Kondo et al. 2012) found that rats which had their food intake restricted to mimic chronic human undernourishment were more susceptible to APAP induced liver injury than rats fed *ad libitum*. Rats in the restricted feed group showed reduced liver GSH. GSH production is dependent on dietary availability of sulphur-containing amino acids (Tateishi et al. 1981; Glazenburg et al. 1983), which could potentially have become limited in animals in the present study. Loss of abundance of GSH has direct implications for an organism's ability to neutralise APAP's reactive metabolite NAPQI, and the influence of GSH abundance on the process of adaptation is one which may merit further exploration.

Most researchers agree that hepatic GSH depletion is the critical trigger for acetaminophen hepatotoxicity (Bessems and Vermeulen 2001). In the context of current understanding of GSH and APAP metabolism (and as has been shown in Chapter 2), it is likely to be the loss of GSH upon initial exposure to APAP that initiates a transcriptional shift in the liver which

comprises part of the adaptive process. Depletion of GSH by the reactive metabolite NAPQI in this model of adaptation may indeed be a necessary step to prime the liver for adaptation. Arguably, based on what is known of APAP toxicity, if GSH is not depleted by the initial exposure, the degree of toxicity is insufficient to warrant adaptation. Interestingly though, the Glazenburg study referenced above found that, despite extreme restriction of dietary sulphur with concomitant reduction of hepatic GSH to just 20 % of that of control rats, formation of APAP-GSH was unaffected. This suggests that upon APAP exposure, GSH can be synthesised rapidly and in significant quantities even under dietary restriction. This may relate to the observation in the present work of a sudden increase in GSH measured at 48 h in the rat, coincident with peak APAP toxicity, which later fell (Chapter 2, Figure 2.9). In contrast, a subsequent rodent study showed that insufficient dietary sulphur resulted in increased susceptibility to APAP toxicity, and the protective effect of reduced CYP450 formation (as a consequence of suppressed protein synthesis) was insufficient to offset the potentiating effect of the reduced ability to detoxify NAPQI (Price and Jollow 1989). In humans, however, short-term restriction of dietary sulphur did not affect the elimination of APAP at therapeutic doses (Mannery et al. 2010). It is clear that further research into the interplay between GSH and APAP will be necessary in order to understand how the various factors outlined here interact, tipping the physiological scale in favour of susceptibility or resistance to injury.

5.2.5. Influence of non-parenchymal cells

A further element that has not been specifically probed here is the influence of non-parenchymal cells upon the process of adaptation. As has been seen in Chapter 3 from IHC data, the contribution to the liver mass from non-parenchymal cells increases over time. This is due to infiltration of immune cells and expansion of small, densely staining cells (presumed, but not demonstrated, to be fibroblasts) in areas where hepatocytes have been

lost; as well as the loss by cell death of the hepatocytes themselves. Whilst these cells are likely to have been excluded from the proteomic data if their contribution both differed from that of the parenchyma and was basally undetectable, it would be valuable to identify all the cell types mediating the adaptive process.

Performing stains for individual cell types in liver sections as suggested in section 5.2.2 would be a valid initial step, and one which might help to identify changes in the subpopulations of, for example, endothelial cells, macrophages and fibroblasts. The use of laser capture microdissection (Espina et al. 2006) in subsequent work would permit the excision and analysis of specific cells from liver tissue sections. Use of immunostains to assist in identification would enable the separation of hepatocytic proteins from the contribution of non-parenchymal cells, and facilitate the examination of hepatocytes from different zones of the liver in order to characterise the adaptive phenotype in regions both proximal and distal to the foci of injury.

5.2.6. Identity of repopulating cells

APAP-induced injury can cause loss of hepatocytes on a significant scale. In the aftermath of injury in the rat model we see 'foci of regeneration' (Chapter 4, Figure 4.10): high concentrations of Ki67-positive cells in and around the spaces where hepatocytes have been lost through APAP toxicity. IHC data shows some of the cells re-entering mitosis are clearly identifiable by morphological characteristics as mature hepatocytes, but there is at least one further population of cells focused around centrilobular regions and consisting of small, densely staining bodies whose identity is unknown. Referring back to literature presented in the general introduction, there are thought to be two mechanisms of cellular restitution after liver injury. One relies on mature hepatocytes re-entering the cell cycle, and the other is mediated by the expansion and differentiation of multipotent cells

(referred to here as liver progenitor cells, or LPCs) from the areas in proximity to the bile ducts, presented as the streaming liver hypothesis.

Controversy continues to reign over exactly which populations of cells contribute to the repopulation of a previously damaged liver with phenotypically mature hepatocytes, and under which circumstances different populations do so. Recent publications in this field have become ever more eloquent, using genetic manipulation to trace the fate of different cell populations in the liver. A high-profile paper appearing in Nature Genetics used fate-tracing techniques to label LPCs, establishing the involvement of stem-cell-derived cells in both homeostatic and reconstitutive activity in the liver (Furuyama et al. 2011).

In the same year, a second publication sought to test the findings of Furuyama et al., but rather than labelling LPCs, this group labelled mature hepatocytes of mouse livers in order to determine loss of reporter signal either in response to injury or as a normal homeostatic mechanism (Malato et al. 2011). Its findings were in definite contrast to the work by Furuyama et al. despite using the same mediators of clean (2/3 partial hepatectomy) and toxic (CCl_4) injury. The authors speculate that the experimental protocol employed in the preceding publication resulted in low-level toxicity which may have recruited LPCs, thereby confounding results.

The following year, again using fate tracing methods, Gastroenterology published a paper which concluded that chronic injury is repaired by LPCs but acute injury is not (Español-Suñer et al. 2012). These findings reinforced the established streaming liver hypothesis, which proposed that stem cells are only recruited if the mitotic capacity of mature hepatocytes is impaired in some way.

Further confounding issues in the same year, a work was presented which expanded on previous publications exploring hypertrophy and unconventional cell division as an organ-

specific method of recovery from injury (Miyaoka et al. 2012). The authors of this paper argued that the accepted paradigm for liver regeneration was too simplistic, since these factors were not acknowledged.

In 2013, a publication was presented showing that under conditions of both toxic injury and partial hepatectomy, widespread interconversion was seen between hepatocytes and biliary epithelial cells (Yanger et al. 2013). The following year, the same group published data showing that, after toxic liver injury, virtually all new cells were derived from existing hepatocytes (Yanger et al. 2014).

It should be noted that the data presented above are all gathered from mouse models, since mice are so much more amenable to genetic manipulation. Publications in this research area remain sparse for rat and human. However, when reviewing the work presented in this thesis in the context of current literature, it seems probable that the rat model of adaptation presented herein is one in which repopulation of the liver is achieved predominantly through mitotic activity of existing hepatocytes. The injury is chemical in nature, and exposure is not sustained over a long period of time. The animals used were young, with no experimental impairments to their mitotic capacity, so it seems unlikely that there would be any involvement of LPCs in the repair process. The accumulation of literature portraying the intricate phenomenon of regeneration is at present reminiscent of the Indian proverb concerning blind men describing an elephant, each part intricately rendered and yet seemingly at odds with other descriptions of the same beast. Perhaps, then, until it is clear how each of these beautifully detailed investigations fit together to form a complete representation, the most important point to consider is the functional change that regenerating liver exhibits. Regardless of the cell type mediating recovery, literature shows that increased cellular proliferation in the liver has been associated with enhanced resistance to toxicity via alterations in expression of xenobiotic metabolising

enzymes; and that blocking proliferation using the antimitotic colchicine abrogates resistance (Shayiq et al. 1999; Dalhoff et al. 2001; Aleksunes et al. 2008a). This change in phenotype described has important implications for the fate of subsequent exposures to any xenobiotic.

5.3. Further considerations in the investigation of adaptation

5.3.1. Evidence for hepatic functional reserve

Expanding on the paper cited above by Miyaoka et al. describing both cellular hypertrophy and unconventional cell division as mediators of hepatocellular restitution (Miyaoka et al. 2012), the concept of hepatic functional reserve may prove pertinent to the bigger picture of adaptation. The liver has a profound ability to compensate for injury, and it is established clinically that by the time symptoms of liver injury arise, the degree of damage to the organ is likely to be severe (Asrani and Kamath 2013). Several possible mechanisms for functional reserve can be identified in the literature.

As an alternative interpretation of 'functional heterogeneity', the idea that a subset of hepatocytes in the liver are transcriptionally inactive or incompletely active was proposed in 2011 in a study that examined acetylated histones as markers of active gene transcription (Shi et al. 2011). This group found that in human cirrhosis, as the parenchyma was lost through disease progression, the ratio of cells positive for markers of transcription gradually increased. These findings correlated with work performed in a mouse partial hepatectomy model which showed that remaining cells after surgery were extensively activated, and this activation was independent of regenerative activity.

Widespread incidence of hepatocytic aneuploidy has been documented in rodents and humans (Duncan et al. 2010, 2012), and is thought to act as a 'survival of the fittest' mechanism in the liver, allowing rapid adaptation to stress through selection of the strongest phenotype. Proliferating hepatocytes produce a highly diverse population of daughter cells, allowing rapid adaptation to noxious stimuli.

Although the functional consequence of adaptation has been described in the work presented, establishing the means by which adaptation and regeneration occur is by no

means as simple as examining the frequency of mitotic events. Any of the mechanisms summarised here could be active in the rodent models presented. In the rat model, mitotic events are implicated in adaptation, and evidence of mature hepatocytes dividing to restore cell number and mass has been presented histologically. Given the critical importance of adaptation to the organism's survival, it is likely that there is redundancy in the process and as such, other mechanisms may also be implicated in this model.

The mouse model, interrogated at lower resolution, hints at alternative predominant processes, since mitotic events were seen to be comparatively rare. The concepts presented by Miyaoka et al. concerning cell division in the absence of DNA replication as well as cellular hypertrophy; those proposed by Shi et al. relating to a cellular reserve of transcriptionally inactive hepatocytes; and those concerning genetic heterogeneity discussed by Duncan et al. may all be contributing to the mouse's apparent ability to adapt to repeated APAP toxicity in the absence of concerted mitotic activity.

5.3.2. Novel modes of inter-cell communication

Liver cells are able to secrete and recapture extracellular vesicles, often referred to in the literature as exosomes. Recent research has identified the importance of these actively secreted vesicles, which contain small molecules that impart information to recipient cells or tissues. Exosomes were first demonstrated to contain genetic information in 2007 (Valadi et al. 2007), and are detectable in a wide range of biofluids, making them an attractive target for biomarker identification. The discovery that nucleic acids can be transferred between cells has engendered a paradigm shift in the current understanding of gene regulation. It is now generally accepted that exosomal traffic presents a means of post-transcriptional gene regulation.

Hepatocytes are known to secrete exosomes (Conde-Vancells et al. 2008), and both the abundance and the cargo of these vesicles are changed in response to liver injury (Royo and Falcon-Perez 2012). A key constituent of hepatocyte-derived exosomes is the liver-specific microRNA miR-122 which is emerging as a sensitive and specific early biomarker of liver injury, as well as a post-transcriptional regulator of the hepatic phenotype. miR-122 has been characterised as a biomarker of APAP-induced liver injury in preclinical models (Wang et al. 2009) and also in humans (Starkey Lewis et al. 2011; Ward et al. 2014), where data suggest it may be an improvement on the gold standard biomarker of hepatocellular injury, ALT.

Less clear thus far is whether miR-122 may play a part in mediating adaptation to toxicity. miR-122 represents about 70 % of the liver's total microRNA content. It is completely conserved in all the species it has been identified in, and has a wide range of endogenous targets within major pathways including tumour suppression, cholesterol metabolism and iron homeostasis (Jopling 2012). Experiments using human hepatocellular carcinoma cells show that miR-122 is necessary for maintaining the hepatic phenotype (Coulouarn et al. 2009); and yet, in a chimpanzee model of chronic hepatitis C infection, gene silencing resulting in its progressive loss did not seem to cause liver toxicity (Lanford et al. 2010).

A time-dependent loss of miR-122 from liver tissue has been shown in a mouse model of APAP induced liver injury (Starkey Lewis, unpublished data), and loss of miR-122 from liver cells is implicated in tissue remodelling and fibrosis associated with steatohepatitis (Csak et al. 2015). Given that microRNAs influence at least one third of all human transcripts (Lakner et al. 2011) it seems unlikely that the liver-specific miR-122 would not be involved in some part of the process of adaptation. In humans, an association has been seen between elevated miR-122 in both liver tissue and serum, and spontaneous recovery from acute liver failure (John et al. 2014). The authors of this paper noted previous research that

has shown haemoxygenase-1 (HO-1) to inhibit proliferation, differentiation and antiapoptotic pathways, suggesting this enzyme may negatively influence liver regeneration. The HO-1 transcript is negatively regulated by miR-122, and patients in the John et al. study who spontaneously recovered from acute liver failure presented with significantly higher miR-122 and lower HO-1 than those who required intervention.

The question is therefore exactly what role miR-122 plays in mediating adaptation to injury. Direct links between miR-122 and the processes of adaptation and regeneration are limited, but circumstantially an association exists through exosomes. In mouse models of ischaemia reperfusion injury and partial hepatectomy, exosomes originating from hepatocytes have been shown to mediate repair and regeneration (Nojima et al. 2016). In the models characterised in the present work, it would be fascinating to query the involvement of exosome-mediated intercellular communication in adaptation to chemical stress.

In the present model, hepatocytes that have sustained toxic injury in the initial hours after APAP exposure may be actively secreting exosomes (potentially containing, amongst other molecules, miR-122) in response to the chemical stress and redox perturbation brought about by the accumulation of NAPQI. These exosomes are known to be released into the bloodstream, and have also been identified in bile (Masyuk et al. 2010). When reviewing this nascent field, an emergent hypothesis is that between centrilobular and periportal hepatocytes, communication pathways exist which are mediated by biliary exosomes and which help regulate adaptation. In this way, perhaps centrilobular cells could release a distress signal which would be detected by cells further along the portocentral axis which are initially unaffected by direct toxicity. The distress signal could conceivably contain information on the nature of the insult that the originating cells were suffering, and what

phenotypic changes may be necessary in order for the organ as a whole to become more resilient in the face of subsequent exposures.

5.4. Concluding remarks

5.4.1. Refining *in vivo* models of human adaptation to APAP

Laboratory rodents differ from humans in many ways, in particular their limited genetic diversity and the closely controlled influence of diet and environment. Rodents are the preferred choice for preclinical modelling of DILI, but alternative *in vivo* models have historically been utilised and are continually being developed. Primates have historically been used for experimental work due to their high degree of genetic identity with humans, but improvements in the human understanding of their capacity to suffer has meant that, on ethical grounds, primates are now subjected to preclinical testing with far less frequency. Pigs in particular have been successfully employed in the modelling of APAP-induced acute liver failure, and to trial interventions aiming to prolong survival or permit liver recovery (Lee et al. 2013) but the practicalities of working with such large mammals can make this work prohibitively complex and expensive. The development of genetic modification methods over recent decades means that humanised rodents now hold the promise of a more faithful reflection of human drug metabolism (Patterson et al. 2012); and the zebrafish, although perhaps a less obvious choice for modelling human toxicity and adaptation, has been shown to be comparable to established rodent models (Driessen et al. 2015)

Because of the complexity of the *in vivo* response to xenobiotics, the possibility of successfully recapitulating human liver adaptation in its global form in a single model seems remote. However, judicious selection of model organisms alongside increasingly sophisticated *in vitro* and *in silico* models is allowing ever more authentic representation of the processes underpinning human physiology and pathophysiology.

5.4.2. Relevance of model to human adaptation

The *in vivo* models presented in this thesis perhaps most closely reflect repeated supratherapeutic APAP use in humans with vulnerability to toxicity. Obviously, one would not expect to see such hepatocellular damage as the model showed at true therapeutic exposures in healthy humans, but many people have compromised liver function arising from a wide variety of causes. These may be related to underlying organ pathology, for example, viral hepatitis; or due to malnutrition, alcoholism or co-ingestion of other pharmaceutical substances (Alhelail et al. 2011). Additionally, accidental overexposure is common (Dart and Bailey 2007).

In the clinic, the Rumack-Matthew nomogram is used as a means of predicting patients at significant risk of developing hepatotoxicity arising from a single APAP exposure (Rumack and Matthew 1975). In cases of toxicity arising from repeat supratherapeutic ingestion, the Rumack-Matthew nomogram cannot be used; however, the likelihood of clinically significant hepatotoxicity is currently estimated based on AST, ALT, and serum APAP levels (O'Malley and O'Malley 2015). Whilst use of this nomogram has undoubtedly prevented many patients progressing to liver failure in the aftermath of APAP overdose, it is limited by the assumption of equal susceptibility in all patients.

Reports in the literature document an association between dental pain and increased risk of APAP poisoning through unintentional overexposure (Vogel et al. 2011). The authors suggest that dental pain is likely to be both ongoing and increasing in severity if treatment is not sought, leading to longer-term and potentially escalating exposures to APAP. They also point out the well-documented association between starvation and APAP toxicity, with particular regard to the limitations chronic toothache may place on food consumption.

Therapeutic exposures have also been shown to be toxic in some instances, though controversy exists. Whilst a multicentre randomised study found no effect of therapeutic APAP in newly abstinent alcoholics over a three-day treatment (Kuffner et al. 2007), a case report of a female alcohol-dependent patient presenting with acute liver injury after taking APAP with therapeutic intent is highlighted (Manchanda et al. 2013). Despite the limitations of case reporting, this publication is reviewed with interest because the APAP exposure described therein is perhaps more relevant to the issue of human vulnerability to toxicity. The patient in question had taken therapeutic APAP (prescribed for neck pain) for one month prior to clinical intervention for liver injury, and again for a further two weeks with similar consequences despite warnings to avoid APAP. Since APAP is routinely prescribed for management of ongoing mild to moderate pain, these durations of exposure are relevant when considering human toxicity arising from therapeutic APAP use. The case also highlights the importance of communication between healthcare providers, as APAP was prescribed a second time despite known alcoholism and administration of treatment for APAP poisoning.

Taking the work presented in this thesis forward, examining rodent blood for markers of adaptation, and then comparing findings to patient data and blood samples from clinical studies will assist in the translation of findings in rodent models to humans. An improved understanding of the biomolecular signatures associated with both liver toxicity and adaptive and regenerative events, as has been contributed to in some small capacity by the work presented in this thesis, will aid in the clinical management of not just binary acute/chronic toxicity admissions, but also the management of APAP medication in humans with vulnerability to toxicity.

5.4.3. Summary

APAP poisoning, through intentional or accidental means, remains a significant public health problem. An individual's susceptibility to liver injury is influenced by both genetic and environmental risk factors. It is therefore imperative that the mechanisms underpinning both the evolution of toxicity in the liver, and the defensive strategies the organ employs in response to chemical insult are characterised.

The process of adaptation to repeated exposures of this model hepatotoxin is incredibly intricate and complex, and the work presented here barely scratches the surface of a breathtaking symphony of molecular activity. The response is clearly not limited to proteins associated, even broadly, with drug metabolism, and there is a high degree of redundancy in the response. It seems impossible to attribute adaptation to a single pathway or group of molecules – an appropriate biological characteristic since an organism's survival can depend on it. With sustained endeavours in this fascinating field, it is possible that, in years to come, fine manipulation of adaptive and regenerative processes in human patients will permit vastly improved outcomes for the types of people who are currently in danger of significant morbidity and mortality from not only APAP toxicity, but also by extension, many other types of liver injury.

To adapt is to survive.

Bibliography

Bibliography

Acharya M, Lau-Cam CA. Comparison of the protective actions of N-acetylcysteine, hypotaurine and taurine against acetaminophen-induced hepatotoxicity in the rat. J Biomed Sci. 2010;17(Suppl 1):S35.

Ahmed MME, Wang T, Luo Y, Ye S, Wu Q, Guo Z, et al. Aldo-keto reductase-7A protects liver cells and tissues from acetaminophen-induced oxidative stress and hepatotoxicity. Hepatology. 2011;54(4):1322–32.

Albano E, Rundgren M, Harvison PJ, Nelson SD, Moldéus P. Mechanisms of N-acetyl-p-benzoquinone imine cytotoxicity. Mol Pharmacol. 1985;28(3):306–11.

Aleksunes LM, Campion SN, Goedken MJ, Manautou JE. Acquired resistance to acetaminophen hepatotoxicity is associated with induction of multidrug resistance-associated protein 4 (Mrp4) in proliferating hepatocytes. Toxicol Sci. 2008 a;104(2):261–73.

Aleksunes LM, Goedken M, Manautou JE. Up-regulation of NAD(P)H quinone oxidoreductase 1 during human liver injury. World J Gastroenterol. 2006;12(12):1937–40.

Aleksunes LM, Slitt AL, Maher JM, Augustine LM, Goedken MJ, Chan JY, et al. Induction of Mrp3 and Mrp4 transporters during acetaminophen hepatotoxicity is dependent on Nrf2. Toxicol Appl Pharmacol. 2008 b;226(1):74–83.

Alhelail MA, Hoppe JA, Rhyee SH, Heard KJ. Clinical course of repeated supratherapeutic ingestion of acetaminophen. Clin Toxicol (Phila). 2011;49(2):108–12.

Amens B. Dietary carcinogens and anticarcinogens. Science. 1983;221:1256.

Antoine DJ, Williams DP, Park BK. Understanding the role of reactive metabolites in drug-induced hepatotoxicity: state of the science. Expert Opin Drug Metab Toxicol. 2008;4(11):1415–27.

Asrani SK, Kamath PS. Natural history of cirrhosis. Current gastroenterology reports. Springer; 2013;15(2):1–6.

Bertola A, Mathews S, Ki SH, Wang H, Gao B. Mouse model of chronic and binge ethanol feeding (the NIAAA model). Nat Protoc. 2013;8(3):627–37.

Bessems JG, Vermeulen NP. Paracetamol (acetaminophen)-induced toxicity: molecular and biochemical mechanisms, analogues and protective approaches. Crit Rev Toxicol. 2001;31(1):55–138.

Björnsson E, Olsson R. Outcome and prognostic markers in severe drug-induced liver disease. Hepatology. Wiley Online Library; 2005;42(2):481–9.

Bogaards JJ, Bertrand M, Jackson P, Oudshoorn MJ, Weaver RJ, van Bladeren PJ, et al. Determining the best animal model for human cytochrome P450 activities: a comparison of mouse, rat, rabbit, dog, micropig, monkey and man. Xenobiotica. 2000;30(12):1131–52.

Borlak J, Chatterji B, Londhe KB, Watkins PB. Serum acute phase reactants hallmark healthy individuals at risk for acetaminophen-induced liver injury. Genome Med. 2013;5(9):86.

Bouligand J, Deroussent A, Paci A, Morizet J, Vassal G. Liquid chromatography-tandem mass spectrometry assay of reduced and oxidized glutathione and main precursors in mice liver. Journal of Chromatography B. Elsevier; 2006;832(1):67–74.

Bühler R, Lindros KO, Nordling A, Johansson I, Ingelman-Sundberg M. Zonation of cytochrome P450 isozyme expression and induction in rat liver. Eur J Biochem. 1992;204(1):407–12.

Bushel P, Heinloth A, Li J, Huang L, Chou J, Boorman G, et al. Blood gene expression signatures predict exposure levels. Proceedings of the National Academy of Sciences. National Acad Sciences; 2007;104(46):18211–6.

Buttar HS, Nera EA, Downie RH. Serum enzyme activities and hepatic triglyceride levels in acute and subacute acetaminophen-treated rats. Toxicology. 1976;6(1):9–20.

Cardin R, Piciocchi M, Bortolami M, Kotsafti A, Barzon L, Lavezzo E, et al. Oxidative damage in the progression of chronic liver disease to hepatocellular carcinoma: an intricate pathway. World journal of gastroenterology: WJG. Baishideng Publishing Group Inc; 2014;20(12):3078–86.

Chanda S, Mangipudy RS, Warbritton A, Bucci TJ, Mehendale HM. Stimulated hepatic tissue repair underlies heteroprotection by thioacetamide against acetaminophen-induced lethality. Hepatology. 1995;21(2):477–86.

Chen W, Koenigs LL, Thompson SJ, Peter RM, Rettie AE, Trager WF, et al. Oxidation of acetaminophen to its toxic quinone imine and nontoxic catechol metabolites by baculovirus-expressed and purified human cytochromes P450 2E1 and 2A6. Chem Res Toxicol. 1998;11(4):295–301.

Cho H-Y, Reddy SPM, Yamamoto M, Kleeberger SR. The transcription factor NRF2 protects against pulmonary fibrosis. FASEB J. 2004;18(11):1258–60.

Conde-Vancells J, Rodriguez-Suarez E, Embade N, Gil D, Matthiesen R, Valle M, et al. Characterization and comprehensive proteome profiling of exosomes secreted by hepatocytes. Journal of proteome research. ACS Publications; 2008;7(12):5157–66.

Copple IM, Goldring CE, Jenkins RE, Chia AJL, Randle LE, Hayes JD, et al. The hepatotoxic metabolite of acetaminophen directly activates the Keap1-Nrf2 cell defense system. Hepatology. 2008;48(4):1292–301.

Copple IM, Goldring CE, Kitteringham NR, Park BK. The keap1-nrf2 cellular defense pathway: mechanisms of regulation and role in protection against drug-induced toxicity. Adverse Drug Reactions. Springer; 2010. p. 233–66.

Coulouarn C, Factor VM, Andersen JB, Durkin ME, Thorgeirsson SS. Loss of miR-122 expression in liver cancer correlates with suppression of the hepatic phenotype and gain of metastatic properties. Oncogene. Nature Publishing Group; 2009;28(40):3526–36.

Csak T, Bala S, Lippai D, Satishchandran A, Catalano D, Kodys K, et al. microRNA-122 regulates hypoxia-inducible factor-1 and vimentin in hepatocytes and correlates with fibrosis in diet-induced steatohepatitis. Liver International. Wiley Online Library; 2015;35(2):532–41.

Cullinan SB, Gordan JD, Jin J, Harper JW, Diehl JA. The Keap1-BTB protein is an adaptor that bridges Nrf2 to a Cul3-based E3 ligase: oxidative stress sensing by a Cul3-Keap1 ligase. Molecular and cellular biology. Am Soc Microbiol; 2004;24(19):8477–86.

Dahlin DC, Miwa GT, Lu AY, Nelson SD. N-acetyl-p-benzoquinone imine: a cytochrome P-450-mediated oxidation product of acetaminophen. Proc Natl Acad Sci USA. 1984;81(5):1327–31.

Dahlin DC, Nelson SD. Synthesis, decomposition kinetics, and preliminary toxicological studies of pure N-acetyl-p-benzoquinone imine, a proposed toxic metabolite of acetaminophen. Journal of medicinal chemistry. ACS Publications; 1982;25(8):885–6.

Dalhoff K, Laursen H, Bangert K, Poulsen HE, Anderson ME, Grunnet N, et al. Autoprotection in acetaminophen intoxication in rats: the role of liver regeneration. Pharmacol Toxicol. 2001;88(3):135–41.

Dambrauskas T, Cornish HH. Effect of pretreatment of rats with carbon tetrachloride on tolerance development. Toxicol Appl Pharmacol. 1970;17(1):83–97.

Dart RC, Bailey E. Does therapeutic use of acetaminophen cause acute liver failure? Pharmacotherapy: The Journal of Human Pharmacology and Drug Therapy. Wiley Online Library; 2007;27(9):1219–30.

Davis DC, Potter WZ, Jollow DJ, Mitchell JR. Species differences in hepatic glutathione depletion, covalent binding and hepatic necrosis after acetaminophen. Life Sci. 1974;14(11):2099–109.

Dayoub R, Vogel A, Schuett J, Lupke M, Spieker SM, Kettern N, et al. Nrf2 activates augmenter of liver regeneration (ALR) via antioxidant response element and links oxidative stress to liver regeneration. Mol Med. 2013;19:237–44.

Dhalla NS, Temsah RM, Netticadan T. Role of oxidative stress in cardiovascular diseases. Journal of hypertension. LWW; 2000;18(6):655–73.

Dinkova-Kostova AT, Holtzclaw WD, Cole RN, Itoh K, Wakabayashi N, Katoh Y, et al. Direct evidence that sulfhydryl groups of Keap1 are the sensors regulating induction of phase 2 enzymes that protect against carcinogens and oxidants. Proceedings of the National Academy of Sciences. National Acad Sciences; 2002;99(18):11908–13.

Dollé L, Best J, Mei J, Al Battah F, Reynaert H, van Grunsven LA, et al. The quest for liver progenitor cells: a practical point of view. J Hepatol. 2010;52(1):117–29.

Donato MT, Gómez-Lechón MJ, Jover R, Nakamura T, Castell JV. Human hepatocyte growth factor down-regulates the expression of cytochrome P450 isozymes in human hepatocytes in primary culture. J Pharmacol Exp Ther. 1998;284(2):760–7.

Dong H, Haining RL, Thummel KE, Rettie AE, Nelson SD. Involvement of human cytochrome P450 2D6 in the bioactivation of acetaminophen. Drug Metab Dispos. 2000;28(12):1397–400.

Driessen M, Vitins AP, Pennings JL, Kienhuis AS, van de Water B, van der Ven LT. A transcriptomics-based hepatotoxicity comparison between the zebrafish embryo and established human and rodent in vitro and in vivo models using cyclosporine A, amiodarone and acetaminophen. Toxicology letters. Elsevier; 2015;232(2):403–12.

Duncan AW, Hanlon Newell AE, Smith L, Wilson EM, Olson SB, Thayer MJ, et al. Frequent aneuploidy among normal human hepatocytes. Gastroenterology. 2012;142(1):25–8.

Duncan AW, Taylor MH, Hickey RD, Newell AEH, Lenzi ML, Olson SB, et al. The ploidy conveyor of mature hepatocytes as a source of genetic variation. Nature. Nature Publishing Group; 2010;467(7316):707–10.

Eckes B, Colucci-Guyon E, Smola H, Nodder S, Babinet C, Krieg T, et al. Impaired wound healing in embryonic and adult mice lacking vimentin. J Cell Sci. 2000;113 (Pt 13):2455–62.

Español-Suñer R, Carpentier R, Van Hul N, Legry V, Achouri Y, Cordi S, et al. Liver progenitor cells yield functional hepatocytes in response to chronic liver injury in mice. Gastroenterology. 2012;143(6):1564–1575.e7.

Espina V, Wulfkuhle JD, Calvert VS, VanMeter A, Zhou W, Coukos G, et al. Laser-capture microdissection. Nat Protoc. 2006;1(2):586–603.

Fagan E, Wannan G. Reducing paracetamol overdoses. BMJ: British Medical Journal. BMJ Group; 1996;313(7070):1417.

Fan X, Chen P, Tan H, Zeng H, Jiang Y, Wang Y, et al. Dynamic and coordinated regulation of KEAP1-NRF2-ARE and p53/p21 signaling pathways is associated with acetaminophen injury responsive liver regeneration. Drug Metabolism and Disposition. ASPET; 2014;42(9):1532–9.

Fausto N, Campbell JS. The role of hepatocytes and oval cells in liver regeneration and repopulation. Mech Dev. 2003;120(1):117–30.

Favre C, Monti JA, Scapini C, Pellegrino J, Carnovale CE, Carrillo MC. Putrescine decreases cytochrome P450 3A4 levels during liver regeneration in the rat. J Hepatol. 1998;28(4):700–8.

Foster JR, Elcombe CR, Boobis AR, Davies DS, Sesardic D, McQuade J, et al. Immunocytochemical localization of cytochrome P-450 in hepatic and extra-hepatic tissues of the rat with a monoclonal antibody against cytochrome P-450 c. Biochem Pharmacol. 1986;35(24):4543–54.

Fujiyoshi M, Ozaki M. Molecular mechanisms of liver regeneration and protection for treatment of liver dysfunction and diseases. J Hepatobiliary Pancreat Sci. 2011;18(1):13–22.

Furuyama K, Kawaguchi Y, Akiyama H, Horiguchi M, Kodama S, Kuhara T, et al. Continuous cell supply from a Sox9-expressing progenitor zone in adult liver, exocrine pancreas and intestine. Nat Genet. 2011;43(1):34–41.

Galand P, Degraef C. Cyclin/PCNA immunostaining as an alternative to tritiated thymidine pulse labelling for marking S phase cells in paraffin sections from animal and human tissues. Cell Tissue Kinet. 1989;22(5):383–92.

Gibson GG, Skett P. Introduction to drug metabolism. Nelson Thornes; 2001.

Glazenburg EJ, Jekel-Halsema I, Scholtens E, Baars AJ, Mulder GJ. Effects of variation in the dietary supply of cysteine and methionine on liver concentration of glutathione and“ active sulfate”(PAPS) and serum levels of sulfate, cystine, methionine and taurine: relation to the metabolism of acetaminophen. J Nutr. 1983;113(7):1363–73.

Goldring CE, Kitteringham NR, Elsby R, Randle LE, Clement YN, Williams DP, et al. Activation of hepatic Nrf2 in vivo by acetaminophen in CD-1 mice. Hepatology. Wiley Online Library; 2004;39(5):1267–76.

Gregus Z, Madhu C, Klaassen CD. Species variation in toxication and detoxication of acetaminophen in vivo: a comparative study of biliary and urinary excretion of acetaminophen metabolites. J Pharmacol Exp Ther. 1988;244(1):91–9.

Grover PL, Sims P. Conjugations with glutathione. Distribution of glutathione S-aryltransferase in vertebrate species. Biochem J. 1964;90(3):603–6.

Grunnet N, Tygstrup N, Dich J. Autoprotection against acetaminophen toxicity in cultured rat hepatocytes: the effect of pretreatment and growth factors. Pharmacol Toxicol. 2003;93(3):135–41.

Gujral JS, Knight TR, Farhood A, Bajt ML, Jaeschke H. Mode of cell death after acetaminophen overdose in mice: apoptosis or oncotic necrosis? Toxicol Sci. 2002;67(2):322–8.

Guo S, Liu Y, Lin Z, Tai S, Yin S, Liu G. Effects of eleutheroside B and eleutheroside E on activity of cytochrome P450 in rat liver microsomes. BMC Complement Altern Med. 2014;14:1.

Hadi M, Dragovic S, van Swelm R, Herpers B, van de Water B, Russel FG, et al. AMAP, the alleged non-toxic isomer of acetaminophen, is toxic in rat and human liver. Archives of toxicology. Springer; 2013;87(1):155–65.

Hailfinger S, Jaworski M, Braeuning A, Buchmann A, Schwarz M. Zonal gene expression in murine liver: lessons from tumors. Hepatology. Wiley Online Library; 2006;43(3):407–14.

Hargus SJ, Martin BM, George JW, Pohl LR. Covalent modification of rat liver dipeptidyl peptidase IV (CD26) by the nonsteroidal anti-inflammatory drug diclofenac. Chemical research in toxicology. ACS Publications; 1995;8(8):993–6.

Hasenfuss SC, Bakiri L, Thomsen MK, Hamacher R, Wagner EF. Activator protein 1 transcription factor fos-related antigen 1 (fra-1) is dispensable for murine liver fibrosis, but modulates xenobiotic metabolism. Hepatology. Wiley Online Library; 2014;59(1):261–73.

Häussinger D, Lamers W, Moorman A. Hepatocyte heterogeneity in the metabolism of amino acids and ammonia. Enzyme. 1991;46(1-3):72–93.

Hawton K, Bergen H, Simkin S, Arensman E, Corcoran P, Cooper J, et al. Impact of different pack sizes of paracetamol in the United Kingdom and Ireland on intentional overdoses: a comparative study. BMC Public Health. 2011;11:460.

Hinson JA, Monks TJ, Hong M, Highet RJ, Pohl LR. 3-(glutathion-S-yl) acetaminophen: a biliary metabolite of acetaminophen. Drug Metabolism and Disposition. ASPET; 1982;10(1):47–50.

Hinson JA, Roberts DW, James LP. Mechanisms of acetaminophen-induced liver necrosis. Handb Exp Pharmacol. 2010;(196):369–405.

Hodgson E. A textbook of modern toxicology. John Wiley \& Sons; 2004.

Hong F, Sekhar KR, Freeman ML, Liebler DC. Specific patterns of electrophile adduction trigger Keap1 ubiquitination and Nrf2 activation. Journal of Biological Chemistry. ASBMB; 2005;280(36):31768–75.

ICH. Nonclinical Safety Studies for the Conduct of Human Clinical Trials and Marketing Authorization for Pharmaceuticals. ICH M3 (R2). International Conference on Harmonization. 2010. p. 303–12.

Ioannides C, Steele CM, Parke DV. Species variation in the metabolic activation of paracetamol to toxic intermediates: role of cytochromes p-450 and p-448. Toxicol Lett. 1983;16(1-2):55–61.

Irie H, Asano-Hoshino A, Sekino Y, Nogami M, Kitagawa T, Kanda H. Striking LD50 variation associated with fluctuations of CYP2E1-positive cells in hepatic lobule during chronic CCl4 exposure in mice. Virchows Arch. 2010;456(4):423–31.

ISO. Biological evaluation of medical devices — Part 11: Tests for systemic toxicity. 2006;

Ito Y, Hayashi H, Taira M, Tatibana M, Tabata Y, Isono K. Depression of liver-specific gene expression in regenerating rat liver: a putative cause for liver dysfunction after hepatectomy. J Surg Res. 1991;51(2):143–7.

Itoh K, Chiba T, Takahashi S, Ishii T, Igarashi K, Katoh Y, et al. An Nrf2/small Maf heterodimer mediates the induction of phase II detoxifying enzyme genes through antioxidant response elements. Biochemical and biophysical research communications. Elsevier; 1997;236(2):313–22.

Jaeschke H, Xie Y, McGill MR. Acetaminophen-induced liver injury: from animal models to humans. Journal of clinical and translational hepatology. Xia \& He Publishing Limited; 2014;2(3):153.

Jaiswal AK. Regulation of genes encoding NAD(P)H:quinone oxidoreductases. Free Radic Biol Med. 2000;29(3-4):254–62.

Jancova P, Anzenbacher P, Anzenbacherova E, others. Phase II drug metabolizing enzymes. Biomedical Papers. Biomedical Papers; 2010;154(2):103–16.

John K, Hadem J, Krech T, Wahl K, Manns MP, Dooley S, et al. MicroRNAs play a role in spontaneous recovery from acute liver failure. Hepatology. Wiley Online Library; 2014;60(4):1346–55.

Jollow D, Thorgeirsson S-S, Potter WZ, Hashimoto M, Mitchell J. Acetaminophen-induced hepatic necrosis. VI. Metabolic disposition of toxic and nontoxic doses of acetaminophen. Pharmacology. 1973;12(4-5):251–71.

Jopling C. Liver-specific microRNA-122: Biogenesis and function. RNA biology. Taylor \& Francis; 2012;9(2):137–42.

Josephy P. The molecular toxicology of acetaminophen. Drug Metab Rev. 2005;37(4):581–94.

Jungermann K, Katz N. Functional specialization of different hepatocyte populations. Physiol Rev. 1989;69(3):708–64.

Karvellas CJ, Safinia N, Auzinger G, Heaton N, Muiesan P, O'Grady J, et al. Medical and psychiatric outcomes for patients transplanted for acetaminophen-induced acute liver failure: a case-control study. Liver Int. 2010;30(6):826–33.

Kera Y, Penttilä KE, Lindros KO. Glutathione replenishment capacity is lower in isolated perivenous than in periportal hepatocytes. Biochem J. 1988;254(2):411–7.

Ketterer B, Coles B, Meyer DJ. The role of glutathione in detoxication. Environ Health Perspect. 1983;49:59–69.

Kienhuis AS, van de Poll MC, Wortelboer H, van Herwijnen M, Gottschalk R, Dejong CH, et al. Parallelogram approach using rat-human in vitro and rat in vivo toxicogenomics predicts acetaminophen-induced hepatotoxicity in humans. Toxicological sciences. Soc Toxicology; 2009;107(2):544–52.

Killpack D. Liver microanatomy - Transparent wash [Internet]. 2016 [cited 2016 Jan]. Available from: http://illuminationstudios.com/archives/150

Kim SJ, Lee MY, Kwon DY, Kim SY, Kim YC. Alteration in metabolism and toxicity of acetaminophen upon repeated administration in rats. J Pharmacol Sci. 2009;111(2):175–81.

Klochendler A, Weinberg-Corem N, Moran M, Swisa A, Pochet N, Savova V, et al. A transgenic mouse marking live replicating cells reveals in vivo transcriptional program of proliferation. Dev Cell. 2012;23(4):681–90.

Kondo K, Yamada N, Suzuki Y, Toyoda K, Hashimoto T, Takahashi A, et al. Enhancement of acetaminophen-induced chronic hepatotoxicity in restricted fed rats: a nonclinical approach to acetaminophen-induced chronic hepatotoxicity in susceptible patients. J Toxicol Sci. 2012;37(5):911–29.

Kretzrommel A, Boelsterli U. Diclofenac covalent protein binding is dependent on acyl glucuronide formation and is inversely related to P450-mediated acute cell injury in cultured rat hepatocytes. Toxicology and applied pharmacology. Elsevier; 1993;120(1):155–61.

Kuffner EK, Green JL, Bogdan GM, Knox PC, Palmer RB, Heard K, et al. The effect of acetaminophen (four grams a day for three consecutive days) on hepatic tests in alcoholic patients-a multicenter randomized study. BMC Med. 2007;5:13.

Kurumiya Y, Nozawa K, Sakaguchi K, Nagino M, Nimura Y, Yoshida S. Differential suppression of liver-specific genes in regenerating rat liver induced by extended hepatectomy. J Hepatol. 2000;32(4):636–44.

Lakner AM, Bonkovsky HL, Schrum LW. microRNAs: fad or future of liver disease. World journal of gastroenterology: WJG. Baishideng Publishing Group Co., Ltd.; 2011;17(20):2536.

Lamlé J, Marhenke S, Borlak J, von Wasielewski R, Eriksson CJP, Geffers R, et al. Nuclear factor-eythroid 2-related factor 2 prevents alcohol-induced fulminant liver injury. Gastroenterology. 2008;134(4):1159–68.

Lanford RE, Hildebrandt-Eriksen ES, Petri A, Persson R, Lindow M, Munk ME, et al. Therapeutic silencing of microRNA-122 in primates with chronic hepatitis C virus infection. Science. American Association for the Advancement of Science; 2010;327(5962):198–201.

Larson AM, Polson J, Fontana RJ, Davern TJ, Lalani E, Hynan LS, et al. Acetaminophen-induced acute liver failure: results of a United States multicenter, prospective study. Hepatology. Wiley Online Library; 2005;42(6):1364–72.

Lee KC, Palacios Jimenez C, Alibhai H, Chang Y-M, Leckie PJ, Baker LA, et al. A reproducible, clinically relevant, intensively managed, pig model of acute liver failure for testing of therapies aimed to prolong survival. Liver International. Wiley Online Library; 2013;33(4):544–51.

Lee WM. Drug-induced hepatotoxicity. New England Journal of Medicine. Mass Medical Soc; 2003;349(5):474–85.

Li S, Tan H-Y, Wang N, Zhang Z-J, Lao L, Wong C-W, et al. The Role of Oxidative Stress and Antioxidants in Liver Diseases. International journal of molecular sciences. Multidisciplinary Digital Publishing Institute; 2015;16(11):26087–124.

Limaye PB, Bhave VS, Palkar PS, Apte UM, Sawant SP, Yu S, et al. Upregulation of calpastatin in regenerating and developing rat liver: role in resistance against hepatotoxicity. Hepatology. 2006;44(2):379–88.

Liu J, Wu KC, Lu Y-F, Ekuase E, Klaassen CD. Nrf2 protection against liver injury produced by various hepatotoxicants. Oxid Med Cell Longev. 2013;2013:305861.

Liu M, Grigoryev DN, Crow MT, Haas M, Yamamoto M, Reddy SP, et al. Transcription factor Nrf2 is protective during ischemic and nephrotoxic acute kidney injury in mice. Kidney Int. 2009;76(3):277–85.

Liu Z-X, Kaplowitz N. Role of innate immunity in acetaminophen-induced hepatotoxicity. Informa UK Ltd London, UK; 2006;

Lowry OH, Rosebrough NJ, Farr AL, Randall RJ, others. Protein measurement with the Folin phenol reagent. J biol Chem. 1951;193(1):265–75.

Lu SC. Regulation of glutathione synthesis. Molecular aspects of medicine. Elsevier; 2009;30(1):42–59.

Maes M, Berk M, Goehler L, Song C, Anderson G, Ga\lecki P, et al. Depression and sickness behavior are Janus-faced responses to shared inflammatory pathways. BMC medicine. BioMed Central Ltd; 2012;10(1):66.

Malato Y, Naqvi S, Schürmann N, Ng R, Wang B, Zape J, et al. Fate tracing of mature hepatocytes in mouse liver homeostasis and regeneration. J Clin Invest. 2011;121(12):4850–60.

Manchanda A, Cameron C, Robinson G. Beware of paracetamol use in alcohol abusers: a potential cause of acute liver injury. NZ Med J. 2013;126:80–4.

Mangipudy RS, Chanda S, Mehendale HM. Hepatocellular regeneration: key to thioacetamide autoprotection. Pharmacol Toxicol. 1995;77(3):182–8.

Mannery YO, Ziegler TR, Park Y, Jones DP. Acetaminophen elimination half-life in humans is unaffected by short-term consumption of sulfur amino acid-free diet. Journal of Pharmacology and Experimental Therapeutics. ASPET; 2010;333(3):948–53.

Martignoni M, Groothuis GMM, de Kanter R. Species differences between mouse, rat, dog, monkey and human CYP-mediated drug metabolism, inhibition and induction. Expert Opin Drug Metab Toxicol. 2006;2(6):875–94.

Masyuk AI, Huang BQ, Ward CJ, Gradilone SA, Banales JM, Masyuk TV, et al. Biliary exosomes influence cholangiocyte regulatory mechanisms and proliferation through interaction with primary cilia. American Journal of Physiology-Gastrointestinal and Liver Physiology. Am Physiological Soc; 2010;299(4):G990–G999.

McGill MR, Sharpe MR, Williams CD, Taha M, Curry SC, Jaeschke H. The mechanism underlying acetaminophen-induced hepatotoxicity in humans and mice involves mitochondrial damage and nuclear DNA fragmentation. J Clin Invest. 2012 a;122(4):1574–83.

McGill MR, Williams CD, Xie Y, Ramachandran A, Jaeschke H. Acetaminophen-induced liver injury in rats and mice: comparison of protein adducts, mitochondrial dysfunction, and oxidative stress in the mechanism of toxicity. Toxicol Appl Pharmacol. 2012 b;264(3):387–94.

McMahon M, Itoh K, Yamamoto M, Chanas SA, Henderson CJ, McLellan LI, et al. The Cap "n"Collar basic leucine zipper transcription factor Nrf2 (NF-E2 p45-related factor 2) controls both constitutive and inducible expression of intestinal detoxification and glutathione biosynthetic enzymes. Cancer research. AACR; 2001;61(8):3299–307.

Miller JA. Carcinogenesis by chemicals: an overview—GHA Clowes memorial lecture. Cancer research. AACR; 1970;30(3):559–76.

Mitchell J, Jollow D, Potter W, Davis D, Gillette J, Brodie B. Acetaminophen-induced hepatic necrosis. I. Role of drug metabolism. Journal of Pharmacology and Experimental Therapeutics. ASPET; 1973 a;187(1):185–94.

Mitchell J, Jollow D, Potter W, Gillette J, Brodie B. Acetaminophen-induced hepatic necrosis. IV. Protective role of glutathione. Journal of Pharmacology and Experimental Therapeutics. ASPET; 1973 b;187(1):211–7.

Miyaoka Y, Ebato K, Kato H, Arakawa S, Shimizu S, Miyajima A. Hypertrophy and unconventional cell division of hepatocytes underlie liver regeneration. Curr Biol. 2012;22(13):1166–75.

Moffit JS, Aleksunes LM, Kardas MJ, Slitt AL, Klaassen CD, Manautou JE. Role of NAD(P)H:quinone oxidoreductase 1 in clofibrate-mediated hepatoprotection from acetaminophen. Toxicology. 2007;230(2-3):197–206.

Muzeeb S, Pasha MK, Basha SJS, Mullangi R, Srinivas NR. Effect of 1-aminobenzotriazole on the in vitro metabolism and single-dose pharmacokinetics of chlorzoxazone, a selective CYP2E1 substrate in Wistar rats. Xenobiotica. 2005;35(8):825–38.

Nojima H, Freeman CM, Schuster RM, Japtok L, Kleuser B, Edwards MJ, et al. Hepatocyte exosomes mediate liver repair and regeneration via sphingosine-1-phosphate. Journal of hepatology. Elsevier; 2016;64(1):60–8.

O'Brien PJ, Slaughter MR, Swain A, Birmingham JM, Greenhill RW, Elcock F, et al. Repeated acetaminophen dosing in rats: adaptation of hepatic antioxidant system. Hum Exp Toxicol. 2000;19(5):277–83.

O'Connor MA, Koza-Taylor P, Campion SN, Aleksunes LM, Gu X, Enayetallah AE, et al. Analysis of changes in hepatic gene expression in a murine model of tolerance to acetaminophen hepatotoxicity (autoprotection). Toxicol Appl Pharmacol. 2013;

O'Malley G, O'Malley R. Acetaminophen Poisoning [Internet]. 2015 [cited 2016 Jan]. Available from: http://www.merckmanuals.com/professional/injuries;-poisoning/poisoning/acetaminophen-poisoning

OECD. OECD Guideline for the Testing of Chemicals 408. 1998 [cited 2016 Jan]; Available from: http://www.oecd-ilibrary.org/docserver/download/9740801e.pdf?expires=1452539238&id=id&accname=guest&checksum=3AE2FF693575095D296133FACEA39608

OECD. OECD Guidelines for the Testing of Chemicals 407. 2008 [cited 2016 Jan]; Available from: https://ntp.niehs.nih.gov/iccvam/suppdocs/feddocs/oecd/oecdtg407-2008.pdf

Oinonen T, Lindros KO. Zonation of hepatic cytochrome P-450 expression and regulation. Biochem J. 1998;329 (Pt 1):17–35.

Okawa H, Motohashi H, Kobayashi A, Aburatani H, Kensler TW, Yamamoto M. Hepatocyte-specific deletion of the keap1 gene activates Nrf2 and confers potent resistance against acute drug toxicity. Biochem Biophys Res Commun. 2006;339(1):79–88.

Omiecinski CJ, Hassett C, Costa P. Developmental expression and in situ localization of the phenobarbital-inducible rat hepatic mRNAs for cytochromes CYP2B1, CYP2B2, CYP2C6, and CYP3A1. Mol Pharmacol. 1990;38(4):462–70.

Omura T, Sato R. THE CARBON MONOXIDE-BINDING PIGMENT OF LIVER MICROSOMES. I. EVIDENCE FOR ITS HEMOPROTEIN NATURE. J Biol Chem. 1964;239:2370–8.

Ostapowicz G, Fontana RJ, Schiødt FV, Larson A, Davern TJ, Han SHB, et al. Results of a prospective study of acute liver failure at 17 tertiary care centers in the United States. Ann Intern Med. 2002;137(12):947–54.

Overturf K, al-Dhalimy M, Ou CN, Finegold M, Grompe M. Serial transplantation reveals the stem-cell-like regenerative potential of adult mouse hepatocytes. Am J Pathol. 1997;151(5):1273–80.

Park BK, Kitteringham NR, Maggs JL, Pirmohamed M, Williams DP. The role of metabolic activation in drug-induced hepatotoxicity. Annu Rev Pharmacol Toxicol. 2005;45:177–202.

Park BK, Pirmohamed M, Kitteringham NR. The role of cytochrome P450 enzymes in hepatic and extrahepatic human drug toxicity. Pharmacol Ther. 1995;68(3):385–424.

Parlakgumus A, Colakoglu T, Kayaselcuk F, Colakoglu S, Ezer A, Calıskan K, et al. Two drugs with paradoxical effects on liver regeneration through antiangiogenesis and antifibrosis: Losartan and Spironolactone: a pharmacologic dilemma on hepatocyte proliferation. J Surg Res. 2013;179(1):60–5.

Patten CJ, Thomas PE, Guy RL, Lee M, Gonzalez FJ, Guengerich FP, et al. Cytochrome P450 enzymes involved in acetaminophen activation by rat and human liver microsomes and their kinetics. Chemical research in toxicology. ACS Publications; 1993;6(4):511–8.

Patterson AD, Shah YM, Matsubara T, Krausz KW, Gonzalez FJ. Peroxisome proliferator-activated receptor alpha induction of uncoupling protein 2 protects against acetaminophen-induced liver toxicity. Hepatology. Wiley Online Library; 2012;56(1):281–90.

Pirmohamed M, Breckenridge AM, Kitteringham NR, Park BK. Fortnightly review: adverse drug reactions. BMJ: British Medical Journal. BMJ Group; 1998;316(7140):1295.

Poulsen HE, Thomsen P. Long-term administration of toxic doses of paracetamol (acetaminophen) to rats. Liver. 1988;8(3):151–6.

Price VF, Jollow DJ. Effects of sulfur-amino acid-deficient diets on acetaminophen metabolism and hepatotoxicity in rats. Toxicol Appl Pharmacol. 1989;101(2):356–69.

Primiano T, Sutter TR, Kensler TW. Redox regulation of genes that protect against carcinogens. Comparative Biochemistry and Physiology Part B: Biochemistry and Molecular Biology. Elsevier; 1997;118(3):487–97.

Procházková J, Kabátková M, Bryja V, Umannová L, Bernatík O, Kozubík A, et al. The interplay of the aryl hydrocarbon receptor and β-catenin alters both AhR-dependent transcription and Wnt/β-catenin signaling in liver progenitors. Toxicol Sci. 2011;122(2):349–60.

Randle LE, Goldring CEP, Benson CA, Metcalfe PN, Kitteringham NR, Park BK, et al. Investigation of the effect of a panel of model hepatotoxins on the Nrf2-Keap1 defence response pathway in CD-1 mice. Toxicology. 2008;243(3):249–60.

Reisman SA, Aleksunes LM, Klaassen CD. Oleanolic acid activates Nrf2 and protects from acetaminophen hepatotoxicity via Nrf2-dependent and Nrf2-independent processes. Biochemical pharmacology. Elsevier; 2009 a;77(7):1273–82.

Reisman SA, Csanaky IL, Aleksunes LM, Klaassen CD. Altered disposition of acetaminophen in Nrf2-null and Keap1-knockdown mice. Toxicol Sci. 2009 b;109(1):31–40.

Roberts E, Ahluwalia MB, Lee G, Chan C, Sarma DS, Farber E. Resistance to hepatotoxins acquired by hepatocytes during liver regeneration. Cancer Res. 1983;43(1):28–34.

Royo F, Falcon-Perez JM. Liver extracellular vesicles in health and disease. Journal of extracellular vesicles. Co-Action Publishing; 2012;1.

Rudraiah S, Rohrer PR, Gurevich I, Goedken MJ, Rasmussen T, Hines RN, et al. Tolerance to Acetaminophen Hepatotoxicity in the Mouse Model of Autoprotection Is Associated with Induction of Flavin-Containing Monooxygenase-3 (FMO3) in Hepatocytes. Toxicol Sci. 2014;141(1):263–77.

Rumack BH, Matthew H. Acetaminophen poisoning and toxicity. Pediatrics. Am Acad Pediatrics; 1975;55(6):871–6.

Sastre J, Rodriguez JV, Pallardó FV, Gasco E, Asensi M, Ferrer JV, et al. Effect of aging on metabolic zonation in rat liver: acinar distribution of GSH metabolism. Mech Ageing Dev. 1992;62(2):181–90.

Sato C, Lieber CS. Mechanism of the preventive effect of ethanol on acetaminophen-induced hepatoxicity. J Pharmacol Exp Ther. 1981;218(3):811–5.

Scholzen T, Gerdes J. The Ki-67 protein: from the known and the unknown. J Cell Physiol. 2000;182(3):311–22.

Schuetz EG, Li D, Omiecinski CJ, Muller-Eberhard U, Kleinman HK, Elswick B, et al. Regulation of gene expression in adult rat hepatocytes cultured on a basement membrane matrix. Journal of cellular physiology. Wiley Online Library; 1988;134(3):309–23.

Shayiq RM, Roberts DW, Rothstein K, Snawder JE, Benson W, Ma X, et al. Repeat exposure to incremental doses of acetaminophen provides protection against acetaminophen-induced lethality in mice: an explanation for high acetaminophen dosage in humans without hepatic injury. Hepatology. 1999;29(2):451–63.

Shi Y, Sun H, Bao J, Zhou P, Zhang J, Li L, et al. Activation of inactive hepatocytes through histone acetylation: a mechanism for functional compensation after massive loss of hepatocytes. Am J Pathol. 2011;179(3):1138–47.

Sim SC, Ingelman-Sundberg M. The Human Cytochrome P450 Allele Nomenclature Committee Web Site. Cytochrome P450 Protocols. Springer; 2006. p. 183–91.

Sivarao DV, Mehendale HM. 2-Butoxyethanol autoprotection is due to resiliance of newly formed erythrocytes to hemolysis. Arch Toxicol. 1995;69(8):526–32.

Smith JM. PCNA: The Sliding Clamp that Tethers Essential Binding Partners to the DNA Template During Replication and Repair. JAMA. 2013;310(1):16–7.

Smith M, Loveridge N, Wills E, Chayen J. The distribution of glutathione in the rat liver lobule. Biochem J. 1979;182:103–8.

Starkey Lewis PJ, Dear J, Platt V, Simpson KJ, Craig DG, Antoine DJ, et al. Circulating microRNAs as potential markers of human drug-induced liver injury. Hepatology. Wiley Online Library; 2011;54(5):1767–76.

Strubelt O, Siegers CP, Völpel M, Younes M. Studies on the mechanism of paracetamol-induced protection against paracetamol hepatotoxicity. Toxicology. 1979;12(2):121–33.

Surh Y-J, Kundu JK, Na H-K. Nrf2 as a master redox switch in turning on the cellular signaling involved in the induction of cytoprotective genes by some chemopreventive phytochemicals. Planta medica. 2008;74(13):1526–39.

Tateishi N, HIGASHI T, NARUSE A, HIKITA K, SAKAMOTO Y. Relative contributions of sulfur atoms of dietary cysteine and methionine to rat liver glutathione and proteins. Journal of biochemistry. Jpn Biochemical Soc; 1981;90(6):1603–10.

Thakore KN, Mehendale HM. Role of hepatocellular regeneration in CCl4 autoprotection. Toxicol Pathol. 1991;19(1):47–58.

Timbrell J. Principles of biochemical toxicology. CRC Press; 1999.

Tufts. How the Tufts Center for the Study of Drug Development Pegged the Cost of a New Drug at $2.6 Billion. 2014;

Tygstrup N, Jensen SA, Kroga B, Pietrangelo A, Shafritz DA. Expression of messenger RNA for liver functions following 70\% and 90\% hepatectomy. Journal of hepatology. Elsevier; 1996;25(1):72–8.

Vaidya VS, Shankar K, Lock EA, Bucci TJ, Mehendale HM. Role of tissue repair in survival from s-(1,2-dichlorovinyl)-L-cysteine-induced acute renal tubular necrosis in the mouse. Toxicol Sci. 2003;74(1):215–27.

Valadi H, Ekström K, Bossios A, Sjöstrand M, Lee JJ, Lötvall JO. Exosome-mediated transfer of mRNAs and microRNAs is a novel mechanism of genetic exchange between cells. Nature cell biology. Nature Publishing Group; 2007;9(6):654–9.

Valko M, Leibfritz D, Moncol J, Cronin MT, Mazur M, Telser J. Free radicals and antioxidants in normal physiological functions and human disease. The international journal of biochemistry \& cell biology. Elsevier; 2007;39(1):44–84.

Venugopal R, Jaiswal AK. Nrf1 and Nrf2 positively and c-Fos and Fra1 negatively regulate the human antioxidant response element-mediated expression of NAD (P) H: quinone oxidoreductase1 gene. Proceedings of the National Academy of Sciences. National Acad Sciences; 1996;93(25):14960–5.

Vogel J, Heard KJ, Carlson C, Lange C, Mitchell G. Dental pain as a risk factor for accidental acetaminophen overdose: a case-control study. The American journal of emergency medicine. Elsevier; 2011;29(9):1125–9.

Wang K, Zhang S, Marzolf B, Troisch P, Brightman A, Hu Z, et al. Circulating microRNAs, potential biomarkers for drug-induced liver injury. Proceedings of the National Academy of Sciences. National Acad Sciences; 2009;106(11):4402–7.

Ward J, Kanchagar C, Veksler-Lublinsky I, Lee RC, McGill MR, Jaeschke H, et al. Circulating microRNA profiles in human patients with acetaminophen hepatotoxicity or ischemic hepatitis. Proceedings of the National Academy of Sciences. National Acad Sciences; 2014;111(33):12169–74.

Watkins PB. Idiosyncratic liver injury: challenges and approaches. Toxicol Pathol. 2005;33(1):1–5.

Wheatley D. Binucleation in mammalian liver: Studies on the control of cytokinesis in vivo. Experimental cell research. Elsevier; 1972;74(2):455–65.

Wild AC, Moinova HR, Mulcahy RT. Regulation of γ-glutamylcysteine synthetase subunit gene expression by the transcription factor Nrf2. Journal of Biological Chemistry. ASBMB; 1999;274(47):33627–36.

Wojcik E, Dvorak C, Chianale J, Traber PG, Keren D, Gumucio JJ. Demonstration by in situ hybridization of the zonal modulation of rat liver cytochrome P-450b and P-450e gene expression after phenobarbital. J Clin Invest. 1988;82(2):658–66.

Xu C, Li CY-T, Kong A-NT. Induction of phase I, II and III drug metabolism/transport by xenobiotics. Arch Pharm Res. 2005;28(3):249–68.

Xu W, Hellerbrand C, Köhler UA, Bugnon P, Kan Y-W, Werner S, et al. The Nrf2 transcription factor protects from toxin-induced liver injury and fibrosis. Lab Invest. 2008;88(10):1068–78.

Yanger K, Knigin D, Zong Y, Maggs L, Gu G, Akiyama H, et al. Adult hepatocytes are generated by self-duplication rather than stem cell differentiation. Cell Stem Cell. 2014;15(3):340–9.

Yanger K, Zong Y, Maggs LR, Shapira SN, Maddipati R, Aiello NM, et al. Robust cellular reprogramming occurs spontaneously during liver regeneration. Genes Dev. 2013;27(7):719–24.

Zhang BH, Gong DZ, Mei MH. Protection of regenerating liver after partial hepatectomy from carbon tetrachloride hepatotoxicity in rats: role of hepatic stimulator substance. J Gastroenterol Hepatol. 1999;14(10):1010–7.

Zou Y, Hu M, Lee J, Nambiar SM, Garcia V, Bao Q, et al. Nrf2 is essential for timely M phase entry of replicating hepatocytes during liver regeneration. American Journal of Physiology-Gastrointestinal and Liver Physiology. Am Physiological Soc; 2015;308(4):G262–G268.

Supplementary Data

Supplementary Data

Supplementary Table 1A: *iTRAQ-based proteomic comparison of liver proteins in vehicle control- and APAP-treated rats (24h timepoint).* Proteins with expression that was different (raw P < 0.05) between control and APAP-treated rats at 24h are listed. Mean expression values relative to a common pool are given for n=4 animals. Proteins are ordered according to the ratio between the 24h and control groups (lowest to highest) such that proteins with expression that was most markedly reduced at 24h appear at the top of the list.

[a]Average number of peptides used for quantification across the four individual iTRAQ runs.
[b]Uncorrected raw p value.

Uniprot Accession	Name	Peptides[a]	Vehicle control		24h		24h/ctrl	p value[b]
			Mean	SD	Mean	SD	Ratio	
Proteins reduced at 24h								
P49890	Estrogen sulfotransferase, isoform 6	18	3.22	0.91	0.14	0.07	**0.04**	<0.001
P05369	Farnesyl pyrophosphate synthase	27	1.5	0.39	0.62	0.21	**0.42**	0.009
O35760	Isopentenyl-diphosphate Delta-isomerase 1	4	1.38	0.41	0.69	0.27	**0.5**	0.035
O88813	Long-chain-fatty-acid--CoA ligase 5	28	1.89	0.67	0.97	0.31	**0.52**	0.036
Q9ES38	Bile acyl-CoA synthetase	26	2.8	0.86	1.45	0.44	**0.52**	0.022
P52847	Sulfotransferase family cytosolic 1B member 1	16	1.97	0.42	1.06	0.43	**0.54**	0.025
P36510	UDP-glucuronosyltransferase 2A1	3	1.35	0.34	0.75	0.29	**0.56**	0.033
P63174	60S ribosomal protein L38	5	0.96	0.24	0.56	0.24	**0.58**	0.041
Q9WUS0	Adenylate kinase isoenzyme 4, mitochondrial	14	1.38	0.19	0.81	0.26	**0.59**	0.024
Q4V8F9	Hydroxysteroid dehydrogenase-like protein 2	9	0.95	0.24	0.56	0.16	**0.59**	0.041
P15083	Polymeric immunoglobulin receptor	16	1.2	0.24	0.73	0.1	**0.61**	0.007
Q6AXX6	Redox-regulatory protein PAMM	8	1.54	0.33	0.94	0.1	**0.61**	0.01
P16970	ATP-binding cassette sub-family D member 3	13	1.69	0.46	1.03	0.07	**0.61**	0.018
P02692	Fatty acid-binding protein, liver	69	1.94	0.49	1.18	0.12	**0.61**	0.017
P62271	40S ribosomal protein S18	13	1.05	0.27	0.66	0.2	**0.63**	0.043
P09527	Ras-related protein Rab-7a	11	0.96	0.11	0.61	0.09	**0.63**	0.003
P00173	Cytochrome b5	31	1.37	0.2	0.88	0.21	**0.64**	0.018
P27605	Hypoxanthine-guanine phosphoribosyltransferase	12	1.35	0.2	0.87	0.18	**0.64**	0.012
Q7TQM4	Sterol O-acyltransferase 2	5	1.32	0.32	0.87	0.15	**0.66**	0.034
P29411	GTP:AMP phosphotransferase, mitochondrial	7	1.41	0.24	0.94	0.28	**0.66**	0.049
P54921	Alpha-soluble NSF attachment protein	10	1.22	0.29	0.81	0.07	**0.66**	0.023
P10867	L-gulonolactone oxidase	18	2	0.36	1.35	0.29	**0.67**	0.03
P97612	Fatty-acid amide hydrolase 1	26	1.67	0.31	1.15	0.2	**0.69**	0.033

P57093	Phytanoyl-CoA dioxygenase, peroxisomal	10	1.36	0.22	0.95	0.21	**0.7**	0.04
Q5XIM9	T-complex protein 1 subunit beta	31	0.97	0.08	0.68	0.09	**0.7**	0.004
P11507	Sarcoplasmic/endoplasmic reticulum calcium ATPase 2	30	1.01	0.1	0.75	0.09	**0.74**	0.007
P50237	Sulfotransferase 1C1	27	1.95	0.15	1.44	0.3	**0.74**	0.029
Q9WUW9	Sulfotransferase 1C2A	5	1.2	0.17	0.89	0.09	**0.74**	0.015
P04646	60S ribosomal protein L35a	3	1.04	0.06	0.78	0.16	**0.75**	0.041
O88941	Mannosyl-oligosaccharide glucosidase	12	1.12	0.13	0.85	0.08	**0.76**	0.008
Q68FP2	Serum paraoxonase/lactonase 3	16	1.43	0.1	1.09	0.15	**0.76**	0.011
P29314	40S ribosomal protein S9	13	0.86	0.1	0.65	0.05	**0.76**	0.009
P06214	Delta-aminolevulinic acid dehydratase	35	1.5	0.26	1.15	0.08	**0.76**	0.027
P97562	Peroxisomal acyl-coenzyme A oxidase 2	38	1.45	0.15	1.13	0.15	**0.78**	0.029
Q03336	Regucalcin	45	1.98	0.18	1.54	0.25	**0.78**	0.03
P85108	Tubulin beta-2A chain	72	1.11	0.05	0.87	0.06	**0.78**	0.001
P18445	60S ribosomal protein L27a	9	0.86	0.08	0.68	0.08	**0.79**	0.023
Q5XI32	F-actin-capping protein subunit beta	11	1.03	0.11	0.82	0.12	**0.8**	0.045
P61107	Ras-related protein Rab-14	9	1.11	0.14	0.89	0.04	**0.8**	0.016
Q497B0	Omega-amidase NIT2	34	1.58	0.09	1.28	0.13	**0.81**	0.013
P41562	Isocitrate dehydrogenase [NADP] cytoplasmic	59	1.21	0.08	1	0.07	**0.82**	0.007
Q920J4	Thioredoxin-like protein 1	8	1.12	0.11	0.94	0.06	**0.84**	0.026
Q68FS4	Cytosol aminopeptidase	53	1.52	0.14	1.33	0.06	**0.88**	0.044
Proteins increased at 24h								
P08541	UDP-glucuronosyltransferase 2B2	37	0.46	0.87	2.34	0.85	**5.05**	0.02
P02091	Hemoglobin subunit beta-1	179	0.44	0.2	2.03	1.54	**4.58**	0.029
P38918	Aflatoxin B1 aldehyde reductase member 3	42	0.2	0.17	0.69	0.31	**3.4**	0.024
P13221	Aspartate aminotransferase, cytoplasmic	30	0.51	0.2	1.35	0.49	**2.66**	0.01
Q62651	Delta(3,5)-Delta(2,4)-dienoyl-CoA isomerase, mitochondrial	17	0.62	0.2	1.59	0.44	**2.55**	0.005
O70199	UDP-glucose 6-dehydrogenase	38	0.32	0.1	0.77	0.16	**2.42**	0.003
P06866	Haptoglobin	21	0.33	0.15	0.77	0.28	**2.35**	0.033
O09171	Betaine--homocysteine S-methyltransferase 1	123	1.06	0.39	2.49	1.05	**2.35**	0.028
P09034	Argininosuccinate synthase	95	0.7	0.51	1.62	0.48	**2.32**	0.045
P08649	Complement C4	30	0.52	0.34	1.2	0.15	**2.31**	0.046
P23562	Band 3 anion transport protein	17	0.9	0.23	2.02	0.98	**2.24**	0.033
P27139	Carbonic anhydrase 2	18	0.68	0.32	1.52	0.49	**2.23**	0.032
P20059	Hemopexin	24	0.45	0.12	0.98	0.25	**2.16**	0.007

P13255	Glycine N-methyltransferase	37	0.86	0.37	1.83	0.71	**2.14**	0.044
Q68FT5	Betaine--homocysteine S-methyltransferase 2	82	0.99	0.45	2.08	0.57	**2.1**	0.028
P48508	Glutamate--cysteine ligase regulatory subunit	9	0.68	0.26	1.39	0.4	**2.05**	0.041
P05182	Cytochrome P450 2E1	29	0.89	0.14	1.74	0.48	**1.96**	0.006
Q6URK4	Heterogeneous nuclear ribonucleoprotein A3	20	0.56	0.07	0.99	0.29	**1.76**	0.027
Q63416	Inter-alpha-trypsin inhibitor heavy chain H3	10	0.81	0.25	1.31	0.25	**1.62**	0.036
P20817	Cytochrome P450 4A14	23	1.06	0.19	1.71	0.45	**1.61**	0.03
Q58FK9	Kynurenine--oxoglutarate transaminase 3	23	1.01	0.27	1.61	0.18	**1.59**	0.011
P13635	Ceruloplasmin	19	0.67	0.2	1.05	0.07	**1.57**	0.031
P25409	Alanine aminotransferase 1	19	0.85	0.09	1.13	0.14	**1.32**	0.018
Q63584	Transmembrane emp24 domain-containing protein 10	11	0.9	0.07	1.17	0.21	**1.31**	0.038
P38062	Methionine aminopeptidase 2	2	0.87	0.12	1.11	0.16	**1.28**	0.049
P21571	ATP synthase-coupling factor 6, mitochondrial	13	0.93	0.09	1.17	0.17	**1.25**	0.045
P85834	Elongation factor Tu, mitochondrial	26	1.01	0.12	1.23	0.13	**1.22**	0.045
P63086	Mitogen-activated protein kinase 1	5	0.83	0.08	1	0.11	**1.21**	0.041
Q9Z1W6	Protein LYRIC	7	1.17	0.14	1.38	0.06	**1.18**	0.037
P02770	Serum albumin	193	0.97	0.04	1.1	0.08	**1.13**	0.026

Supplementary Table 1B: *iTRAQ-based proteomic comparison of liver proteins in vehicle control- and APAP-treated rats (48h timepoint).* Proteins with expression that was different (raw P < 0.05) between control and APAP-treated rats at 48h are listed. Mean expression values relative to a common pool are given for n=4 animals. Proteins are ordered according to the ratio between the 48h and control groups (lowest to highest) such that proteins with expression that was most markedly reduced at 48h appear at the top of the list.
[a]Average number of peptides used for quantification across the four individual iTRAQ runs.
[b]Uncorrected raw p value.

			Vehicle control		48h		48h/ctrl	
Uniprot Accession	Name	Peptides[a]	Mean	SD	Mean	SD	Ratio	p value[b]
Proteins reduced at 48h								
P49890	Estrogen sulfotransferase, isoform 6	18	3.22	0.91	0.27	0.17	**0.08**	0.001
P05183	Cytochrome P450 3A2	15	2.49	0.97	0.29	0.23	**0.12**	0.001
P08683	Cytochrome P450 2C11	51	2.53	0.52	0.38	0.23	**0.15**	0.001
P09606	Glutamine synthetase	17	2.73	0.78	0.47	0.3	**0.17**	0.011
P08010	Glutathione S-transferase Mu 2	70	1.42	0.86	0.31	0.15	**0.22**	0.022
Q9ES38	Bile acyl-CoA synthetase	26	2.8	0.86	0.62	0.24	**0.22**	0.001
P02761	Major urinary protein	22	2.27	0.42	0.52	0.23	**0.23**	<0.001
P10867	L-gulonolactone oxidase	18	2	0.36	0.48	0.09	**0.24**	<0.001
P16232	Corticosteroid 11-beta-dehydrogenase isozyme 1	21	2.55	0.83	0.62	0.31	**0.24**	0.006
P02692	Fatty acid-binding protein, liver	69	1.94	0.49	0.48	0.32	**0.25**	0.003
P52847	Sulfotransferase family cytosolic 1B member 1	16	1.97	0.42	0.51	0.15	**0.26**	<0.001
Q8VHE9	All-trans-retinol 13,14-reductase	10	1.54	0.84	0.4	0.2	**0.26**	0.009
P55051	Fatty acid-binding protein, brain	9	1.61	0.57	0.42	0.47	**0.26**	0.037
P24470	Cytochrome P450 2C23	25	1.53	0.32	0.41	0.23	**0.26**	0.004
P13107	Cytochrome P450 2B3	27	1.48	0.55	0.4	0.52	**0.27**	0.033
P18163	Long-chain-fatty-acid--CoA ligase 1	78	1.54	0.13	0.41	0.16	**0.27**	0.001
P50237	Sulfotransferase 1C1	27	1.95	0.15	0.53	0.2	**0.27**	<0.001
P36365	Dimethylaniline monooxygenase [N-oxide-forming] 1	13	2.34	0.94	0.64	0.17	**0.27**	0.002
Q03336	Regucalcin	45	1.98	0.18	0.55	0.06	**0.28**	<0.001
O88813	Long-chain-fatty-acid--CoA ligase 5	28	1.89	0.67	0.53	0.3	**0.28**	0.007
Q64638	UDP-glucuronosyltransferase 1-5	25	3.79	1.58	1.08	0.77	**0.28**	0.009
P30839	Fatty aldehyde dehydrogenase	36	1.74	0.55	0.5	0.08	**0.29**	0.001
P17988	Sulfotransferase 1A1	30	1.99	0.34	0.58	0.09	**0.29**	<0.001
P05178	Cytochrome P450 2C6	20	1.67	0.62	0.5	0.24	**0.3**	0.009
P14141	Carbonic anhydrase 3	70	1.99	1.3	0.59	0.26	**0.3**	0.046
P09811	Glycogen phosphorylase, liver form	76	1.4	0.26	0.43	0.13	**0.31**	0.001
P00502	Glutathione S-transferase	51	1.57	1.21	0.5	0.35	**0.32**	0.05

	alpha-1							
P12928	Pyruvate kinase isozymes R/L	61	1.64	0.53	0.55	0.19	**0.34**	0.003
Q64232	Very-long-chain enoyl-CoA reductase	35	1.76	0.41	0.6	0.22	**0.34**	0.003
O35077	Glycerol-3-phosphate dehydrogenase [NAD+], cytoplasmic	39	1.45	0.42	0.51	0.07	**0.35**	0.001
Q64611	Cysteine sulfinic acid decarboxylase	25	1.81	0.7	0.64	0.15	**0.35**	0.003
P05182	Cytochrome P450 2E1	29	0.89	0.14	0.32	0.17	**0.36**	0.013
P15865	Histone H1.4	19	1.04	0.35	0.38	0.12	**0.36**	0.008
P31210	3-oxo-5-beta-steroid 4-dehydrogenase	51	1.07	0.22	0.39	0.3	**0.36**	0.014
Q5U2Q3	Ester hydrolase C11orf54 homolog	12	2	0.36	0.74	0.38	**0.37**	0.006
Q497B0	Omega-amidase NIT2	34	1.58	0.09	0.59	0.13	**0.37**	<0.001
P04799	Cytochrome P450 1A2	7	1.32	0.36	0.49	0.48	**0.37**	0.024
Q6AYT9	Acyl-coenzyme A synthetase ACSM5, mitochondrial	14	1.53	0.3	0.57	0.17	**0.37**	0.001
Q07071	Glucokinase regulatory protein	27	1.71	0.64	0.65	0.23	**0.38**	0.015
P43278	Histone H1.0	4	1.51	0.31	0.58	0.19	**0.38**	0.003
P16638	ATP-citrate synthase	65	1.93	0.71	0.74	0.12	**0.38**	0.003
Q4KLP0	Probable 2-oxoglutarate dehydrogenase E1 component DHKTD1, mitochondrial	35	1.59	0.56	0.61	0.22	**0.39**	0.006
P15149	Cytochrome P450 2A2	35	1.28	0.09	0.5	0.07	**0.39**	<0.001
P97612	Fatty-acid amide hydrolase 1	26	1.67	0.31	0.65	0.19	**0.39**	0.002
P18757	Cystathionine gamma-lyase	37	1.4	0.63	0.55	0.21	**0.39**	0.021
P19112	Fructose-1,6-bisphosphatase 1	72	1.71	0.38	0.67	0.16	**0.39**	0.002
Q5PPL3	Sterol-4-alpha-carboxylate 3-dehydrogenase, decarboxylating	20	1.74	0.46	0.69	0.25	**0.4**	0.008
P05545	Serine protease inhibitor A3K	34	1.5	0.5	0.6	0.28	**0.4**	0.016
P00884	Fructose-bisphosphate aldolase B	129	1.31	0.33	0.52	0.16	**0.4**	0.005
Q64550	UDP-glucuronosyltransferase 1-1	29	1.54	0.7	0.62	0.21	**0.4**	0.016
P29147	D-beta-hydroxybutyrate dehydrogenase, mitochondrial	42	1.4	0.23	0.56	0.18	**0.4**	0.002
P33274	Cytochrome P450 4F1	14	1.35	0.35	0.55	0.28	**0.41**	0.029
P27867	Sorbitol dehydrogenase	26	1.21	0.44	0.5	0.1	**0.41**	0.011
Q02253	Methylmalonate-semialdehyde dehydrogenase [acylating], mitochondrial	124	1.22	0.24	0.51	0.06	**0.42**	<0.001
Q9Z339	Glutathione S-transferase omega-1	10	1.42	0.4	0.59	0.32	**0.42**	0.025
P55159	Serum paraoxonase/arylesterase 1	17	1.68	0.55	0.71	0.06	**0.42**	0.003
P17764	Acetyl-CoA	60	1.28	0.07	0.54	0.26	**0.42**	0.014

	acetyltransferase, mitochondrial							
Q63357	Myosin-Id	93	1.01	0.12	0.43	0.22	**0.42**	0.014
Q4KLZ6	Bifunctional ATP-dependent dihydroxyacetone kinase/FAD-AMP lyase (cyclizing)	64	1.7	0.39	0.72	0.23	**0.43**	0.005
Q6AYT0	Quinone oxidoreductase	9	1.37	0.36	0.59	0.21	**0.43**	0.017
Q07523	Hydroxyacid oxidase 2	8	1.99	0.34	0.87	0.24	**0.44**	0.002
P16303	Carboxylesterase 3	33	1.85	0.85	0.81	0.19	**0.44**	0.03
P22791	Hydroxymethylglutaryl-CoA synthase, mitochondrial	106	1.46	0.4	0.65	0.26	**0.44**	0.01
Q62730	Estradiol 17-beta-dehydrogenase 2	17	1.72	0.47	0.76	0.36	**0.44**	0.034
P13803	Electron transfer flavoprotein subunit alpha, mitochondrial	50	1.29	0.23	0.59	0.25	**0.46**	0.011
Q63150	Dihydropyrimidinase	29	1.41	0.17	0.64	0.32	**0.46**	0.02
P24329	Thiosulfate sulfurtransferase	41	1.33	0.2	0.61	0.08	**0.46**	<0.001
P46953	3-hydroxyanthranilate 3,4-dioxygenase	25	1.42	0.4	0.66	0.06	**0.47**	0.003
Q6DGG1	Alpha/beta hydrolase domain-containing protein 14B	12	1.36	0.25	0.64	0.14	**0.47**	0.002
P57113	Maleylacetoacetate isomerase	36	1.58	0.34	0.74	0.14	**0.47**	0.002
P97532	3-mercaptopyruvate sulfurtransferase	23	1.27	0.28	0.61	0.09	**0.48**	0.001
Q5FVQ4	Malectin	8	1.39	0.58	0.67	0.31	**0.48**	0.043
P52759	Ribonuclease UK114	51	1.29	0.41	0.62	0.23	**0.48**	0.035
P02696	Retinol-binding protein 1	13	1.29	0.23	0.62	0.15	**0.48**	0.003
P22734	Catechol O-methyltransferase	46	1.49	0.39	0.72	0.22	**0.48**	0.009
P08011	Microsomal glutathione S-transferase 1	25	1.57	0.62	0.76	0.34	**0.48**	0.044
A0JPQ8	Alkylglycerol monooxygenase	6	1.64	0.2	0.8	0.12	**0.49**	<0.001
Q498D5	Regulator of microtubule dynamics protein 2	8	1.34	0.14	0.65	0.21	**0.49**	0.003
P30713	Glutathione S-transferase theta-2	19	1.34	0.31	0.65	0.1	**0.49**	0.002
Q9QZX8	Solute carrier organic anion transporter family member 1B2	3	1.36	0.4	0.67	0.19	**0.49**	0.009
Q7TP52	Carboxymethylenebutenolidase homolog	16	1.79	0.45	0.88	0.32	**0.49**	0.018
P27605	Hypoxanthine-guanine phosphoribosyltransferase	12	1.35	0.2	0.66	0.12	**0.49**	0.001
P25093	Fumarylacetoacetase	48	1.45	0.12	0.71	0.12	**0.49**	<0.001
Q02974	Ketohexokinase	25	1.56	0.28	0.77	0.07	**0.5**	<0.001
Q5BK17	Iodotyrosine dehalogenase 1	4	1.75	0.28	0.87	0.22	**0.5**	0.004
P57093	Phytanoyl-CoA dioxygenase, peroxisomal	10	1.36	0.22	0.68	0.18	**0.5**	0.004
Q66HG4	Aldose 1-epimerase	5	1.37	0.18	0.7	0.27	**0.51**	0.008
P46720	Solute carrier organic	4	1.41	0.3	0.72	0.1	**0.51**	0.003

	anion transporter family member 1A1							
Q63060	Glycerol kinase	20	1.68	0.28	0.87	0.19	**0.51**	0.002
Q68FP2	Serum paraoxonase/lactonase 3	16	1.43	0.1	0.74	0.11	**0.51**	<0.001
P10760	Adenosylhomocysteinase	54	1.29	0.2	0.67	0.25	**0.51**	0.011
P23680	Serum amyloid P-component	4	1.61	0.24	0.83	0.08	**0.52**	<0.001
P23457	3-alpha-hydroxysteroid dehydrogenase	48	1.51	0.36	0.78	0.33	**0.52**	0.048
P10860	Glutamate dehydrogenase 1, mitochondrial	118	1.63	0.34	0.84	0.15	**0.52**	0.005
Q64581	Cytochrome P450 3A18	8	1.5	0.57	0.78	0.17	**0.52**	0.019
P06214	Delta-aminolevulinic acid dehydratase	35	1.5	0.26	0.78	0.14	**0.52**	0.002
B0BNE5	S-formylglutathione hydrolase	23	1.32	0.33	0.69	0.25	**0.52**	0.02
Q562C4	Methyltransferase-like protein 7B	8	1.63	0.7	0.85	0.17	**0.52**	0.028
P08461	Dihydrolipoyllysine-residue acetyltransferase component of pyruvate dehydrogenase complex, mitochondrial	11	1.13	0.26	0.59	0.06	**0.52**	0.005
P41562	Isocitrate dehydrogenase [NADP] cytoplasmic	59	1.21	0.08	0.63	0.15	**0.52**	0.002
Q63270	Cytoplasmic aconitate hydratase	36	1.21	0.2	0.64	0.21	**0.52**	0.01
P70712	Kynureninase	19	1.41	0.32	0.74	0.13	**0.52**	0.005
Q5I0M2	Nicotinate-nucleotide pyrophosphorylase [carboxylating]	11	1.28	0.42	0.67	0.27	**0.53**	0.041
P62959	Histidine triad nucleotide-binding protein 1	8	1.59	0.36	0.84	0.2	**0.53**	0.008
Q9WUS0	Adenylate kinase isoenzyme 4, mitochondrial	14	1.38	0.19	0.73	0.38	**0.53**	0.026
O89000	Dihydropyrimidine dehydrogenase [NADP+]	12	1.36	0.32	0.72	0.32	**0.53**	0.03
P00173	Cytochrome b5	31	1.37	0.2	0.73	0.3	**0.53**	0.02
P10868	Guanidinoacetate N-methyltransferase	16	1.58	0.51	0.85	0.15	**0.53**	0.018
Q6P6R2	Dihydrolipoyl dehydrogenase, mitochondrial	25	1.16	0.23	0.62	0.23	**0.54**	0.023
P11915	Non-specific lipid-transfer protein	31	1.23	0.23	0.66	0.31	**0.54**	0.049
Q03248	Beta-ureidopropionase	30	1.21	0.25	0.66	0.11	**0.54**	0.005
P11884	Aldehyde dehydrogenase, mitochondrial	98	1.17	0.24	0.64	0.16	**0.55**	0.011
P04762	Catalase	160	1.35	0.36	0.74	0.27	**0.55**	0.038
P0C2X9	Delta-1-pyrroline-5-carboxylate dehydrogenase, mitochondrial	43	1.3	0.1	0.71	0.09	**0.55**	<0.001
P11348	Dihydropteridine reductase	27	1.29	0.44	0.71	0.15	**0.55**	0.039
Q9WVK7	Hydroxyacyl-coenzyme A dehydrogenase,	54	1.22	0.31	0.68	0.18	**0.55**	0.026

	mitochondrial							
P10634	Cytochrome P450 2D26	57	1.53	0.31	0.85	0.25	**0.56**	0.022
P12938	Cytochrome P450 2D3	46	1.52	0.33	0.85	0.17	**0.56**	0.01
P38652	Phosphoglucomutase-1	58	1.05	0.17	0.59	0.13	**0.56**	0.007
P51869	Cytochrome P450 4F4	14	1.42	0.51	0.8	0.05	**0.56**	0.038
P19643	Amine oxidase [flavin-containing] B	29	1.3	0.32	0.74	0.03	**0.56**	0.003
Q5FVQ8	NLR family member X1	9	1.14	0.25	0.65	0.26	**0.57**	0.046
P84817	Mitochondrial fission 1 protein	2	1.28	0.25	0.74	0.09	**0.58**	0.004
P07953	6-phosphofructo-2-kinase/fructose-2,6-bisphosphatase 1	13	1.47	0.11	0.85	0.09	**0.58**	<0.001
P97524	Very long-chain acyl-CoA synthetase	34	1.53	0.35	0.89	0.25	**0.58**	0.021
P07896	Peroxisomal bifunctional enzyme	45	1.24	0.32	0.72	0.22	**0.58**	0.038
Q5XIC0	Enoyl-CoA delta isomerase 2, mitochondrial	14	1.2	0.24	0.71	0.24	**0.59**	0.046
Q5HZY2	GTP-binding protein SAR1b	13	1.22	0.23	0.72	0.11	**0.59**	0.004
Q0VGK3	Glycerate kinase	16	1.22	0.15	0.72	0.29	**0.59**	0.043
P38718	Mitochondrial pyruvate carrier 2/Brain protein 44	3	1.35	0.43	0.79	0.18	**0.59**	0.041
P16617	Phosphoglycerate kinase 1	54	1.09	0.24	0.65	0.19	**0.59**	0.031
P00481	Ornithine carbamoyltransferase, mitochondrial	57	1.3	0.19	0.77	0.12	**0.59**	0.003
P81155	Voltage-dependent anion-selective channel protein 2	10	1.09	0.22	0.65	0.24	**0.59**	0.039
Q68FS4	Cytosol aminopeptidase	53	1.52	0.14	0.9	0.19	**0.59**	0.003
P48500	Triosephosphate isomerase	33	1.17	0.32	0.69	0.22	**0.59**	0.04
Q68FU3	Electron transfer flavoprotein subunit beta	29	1.17	0.22	0.7	0.2	**0.6**	0.025
P00507	Aspartate aminotransferase, mitochondrial	73	1.07	0.15	0.64	0.19	**0.6**	0.016
Q6UPE1	Electron transfer flavoprotein-ubiquinone oxidoreductase, mitochondrial	36	1.12	0.12	0.67	0.07	**0.6**	0.001
P51635	Alcohol dehydrogenase [NADP+]	24	1.25	0.27	0.75	0.15	**0.6**	0.014
P27364	3 beta-hydroxysteroid dehydrogenase type 5	19	1.41	0.31	0.85	0.06	**0.6**	0.004
Q6P6V0	Glucose-6-phosphate isomerase	32	1.23	0.31	0.74	0.15	**0.6**	0.025
Q9QZH8	Arylacetamide deacetylase	6	1.64	0.55	0.99	0.15	**0.6**	0.034
Q6AXX6	Redox-regulatory protein PAMM	8	1.54	0.33	0.93	0.25	**0.6**	0.026
P56574	Isocitrate dehydrogenase [NADP], mitochondrial	27	1.1	0.24	0.67	0.18	**0.61**	0.037
P49432	Pyruvate dehydrogenase E1 component subunit beta, mitochondrial	16	1.2	0.3	0.73	0.2	**0.61**	0.034
Q6I7R3	Isochorismatase domain-containing protein 1	10	1.44	0.23	0.87	0.12	**0.61**	0.005

P08503	Medium-chain specific acyl-CoA dehydrogenase, mitochondrial	26	1.49	0.32	0.91	0.22	**0.61**	0.017
P30904	Macrophage migration inhibitory factor	22	1.31	0.21	0.8	0.19	**0.61**	0.018
P41034	Alpha-tocopherol transfer protein	16	1.28	0.15	0.78	0.03	**0.61**	<0.001
Q562C9	1,2-dihydroxy-3-keto-5-methylthiopentene dioxygenase	8	1.34	0.34	0.82	0.16	**0.61**	0.025
P31044	Phosphatidylethanolamine-binding protein 1	22	1.26	0.27	0.78	0.15	**0.62**	0.018
P07153	Dolichyl-diphosphooligosaccharide--protein glycosyltransferase subunit 1	56	1.08	0.27	0.67	0.21	**0.62**	0.049
P05369	Farnesyl pyrophosphate synthase	27	1.5	0.39	0.93	0.14	**0.62**	0.024
P35738	2-oxoisovalerate dehydrogenase subunit beta, mitochondrial	13	1.23	0.12	0.76	0.23	**0.62**	0.016
Q5M875	17-beta-hydroxysteroid dehydrogenase 13	22	1.09	0.17	0.68	0.1	**0.62**	0.005
P50137	Transketolase	80	1.15	0.2	0.72	0.16	**0.62**	0.016
P11951	Cytochrome c oxidase subunit 6C-2	4	1.03	0.2	0.64	0.26	**0.63**	0.05
Q920P0	L-xylulose reductase	12	1.44	0.45	0.91	0.05	**0.63**	0.028
P20070	NADH-cytochrome b5 reductase 3	26	1.62	0.42	1.02	0.32	**0.63**	0.043
P51650	Succinate-semialdehyde dehydrogenase, mitochondrial	10	1.21	0.32	0.76	0.06	**0.63**	0.019
Q63276	Bile acid-CoA:amino acid N-acyltransferase	57	1.25	0.27	0.79	0.2	**0.63**	0.026
Q5PQT3	Glycine N-acyltransferase	22	1.05	0.24	0.67	0.06	**0.64**	0.016
Q9QYU4	Thiomorpholine-carboxylate dehydrogenase	9	1.31	0.25	0.84	0.17	**0.64**	0.017
P25235	Dolichyl-diphosphooligosaccharide--protein glycosyltransferase subunit 2	46	1.18	0.28	0.76	0.15	**0.64**	0.028
P85971	6-phosphogluconolactonase	12	1.56	0.23	1.02	0.1	**0.65**	0.003
P97562	Peroxisomal acyl-coenzyme A oxidase 2	38	1.45	0.15	0.94	0.22	**0.65**	0.021
P29266	3-hydroxyisobutyrate dehydrogenase, mitochondrial	23	1.21	0.17	0.79	0.15	**0.65**	0.01
Q1HCL7	NAD kinase domain-containing protein 1	17	1.25	0.18	0.82	0.05	**0.66**	0.002
Q923K9	APOBEC1 complementation factor	10	1.09	0.26	0.72	0.16	**0.66**	0.04
P18297	Sepiapterin reductase	11	1.36	0.27	0.9	0.17	**0.66**	0.017
P32089	Tricarboxylate transport protein, mitochondrial	11	1.11	0.09	0.74	0.17	**0.67**	0.015
Q6P7R8	Estradiol 17-beta-dehydrogenase 12	6	1.15	0.2	0.77	0.1	**0.67**	0.013
P07633	Propionyl-CoA carboxylase beta chain,	23	1.21	0.18	0.81	0.17	**0.67**	0.017

	mitochondrial							
P85973	Purine nucleoside phosphorylase	41	1.12	0.2	0.75	0.12	**0.67**	0.016
P15999	ATP synthase subunit alpha, mitochondrial	122	1.05	0.08	0.71	0.16	**0.68**	0.012
O88767	Protein DJ-1	16	1.21	0.2	0.82	0.16	**0.68**	0.025
P14942	Glutathione S-transferase alpha-4	12	0.99	0.12	0.67	0.12	**0.68**	0.008
Q9JM53	Apoptosis-inducing factor 1, mitochondrial	27	1.24	0.13	0.85	0.2	**0.69**	0.026
P07872	Peroxisomal acyl-coenzyme A oxidase 1	42	1.33	0.25	0.92	0.17	**0.7**	0.046
Q923M1	Mitochondrial peptide methionine sulfoxide reductase	3	1.19	0.24	0.84	0.12	**0.7**	0.024
Q6AYQ8	Acylpyruvase FAHD1, mitochondrial	10	1.15	0.22	0.81	0.11	**0.71**	0.039
Q6P7Q4	Lactoylglutathione lyase	8	1.19	0.21	0.85	0.16	**0.71**	0.046
Q5XIH7	Prohibitin-2	29	1.66	0.28	1.21	0.24	**0.73**	0.046
P52873	Pyruvate carboxylase, mitochondrial	134	1.16	0.13	0.86	0.14	**0.74**	0.018
Q5M7T9	Threonine synthase-like 2	6	1.26	0.23	0.94	0.11	**0.74**	0.037
P12336	Solute carrier family 2, facilitated glucose transporter member 2	5	1.16	0.21	0.86	0.09	**0.74**	0.038
P46462	Transitional endoplasmic reticulum ATPase	71	1.14	0.18	0.85	0.11	**0.75**	0.034
Q64380	Sarcosine dehydrogenase, mitochondrial	41	1.28	0.19	0.96	0.15	**0.75**	0.047
Q8CG45	Aflatoxin B1 aldehyde reductase member 2	22	1.11	0.05	0.84	0.07	**0.75**	0.001
P97700	Mitochondrial 2-oxoglutarate/malate carrier protein	7	1.15	0.19	0.87	0.05	**0.75**	0.016
Q68FT1	Ubiquinone biosynthesis protein COQ9, mitochondrial	9	1.01	0.06	0.77	0.08	**0.76**	0.004
Q7TMA5	Apolipoprotein B-100	29	1.09	0.21	0.83	0.08	**0.76**	0.047
P97519	Hydroxymethylglutaryl-CoA lyase, mitochondrial	14	0.99	0.09	0.77	0.14	**0.78**	0.036
Q641Y0	Dolichyl-diphosphooligosaccharide--protein glycosyltransferase 48 kDa subunit	16	1.18	0.12	0.92	0.13	**0.78**	0.032
P80067	Dipeptidyl peptidase 1	12	1.09	0.19	0.86	0.04	**0.79**	0.039
Q9JLA3	UDP-glucose:glycoprotein glucosyltransferase 1	28	0.97	0.06	0.78	0.06	**0.8**	0.003
P26453	Basigin	7	1.15	0.14	0.96	0	**0.84**	0.028
Q05096	Myosin-Ib	94	1.03	0.04	0.87	0.08	**0.84**	0.013
P84903	Stromal interaction molecule 1	5	1.03	0.03	0.91	0.09	**0.88**	0.047
Proteins increased at 48h								
P42930	Heat shock protein beta-1	10	0.12	0.11	2.87	1.41	**23.49**	<0.001
Q07439	Heat shock 70 kDa protein 1A/1B	56	0.21	0.2	2.77	1.5	**13.39**	0.002
P38918	Aflatoxin B1 aldehyde	42	0.2	0.17	1.55	0.68	**7.6**	0.003

	reductase member 3							
P01048	T-kininogen 1	15	0.25	0.21	1.83	0.91	**7.21**	0.01
P02764	Alpha-1-acid glycoprotein	6	0.31	0.37	1.83	0.22	**5.87**	0.017
P06866	Haptoglobin	21	0.33	0.15	1.74	0.81	**5.26**	0.003
P82995	Heat shock protein HSP 90-alpha	74	0.47	0.29	2	0.82	**4.25**	0.006
P05370	Glucose-6-phosphate 1-dehydrogenase	15	0.38	0.22	1.63	0.36	**4.24**	0.004
O70199	UDP-glucose 6-dehydrogenase	38	0.32	0.1	1.28	0.34	**4.04**	0.001
Q66HA8	Heat shock protein 105 kDa	23	0.47	0.24	1.72	0.21	**3.64**	0.004
P02680	Fibrinogen gamma chain	17	0.54	0.24	1.86	0.65	**3.43**	0.008
P20059	Hemopexin	24	0.45	0.12	1.53	0.73	**3.37**	0.005
P06762	Heme oxygenase 1	5	0.57	0.28	1.82	0.76	**3.21**	0.027
P06399	Fibrinogen alpha chain	39	0.5	0.29	1.58	0.31	**3.18**	0.019
P09006	Serine protease inhibitor A3N	19	0.61	0.19	1.82	0.67	**3**	0.003
P04961	Proliferating cell nuclear antigen	4	0.41	0.07	1.21	0.37	**2.97**	0.001
O89049	Thioredoxin reductase 1, cytoplasmic	17	0.42	0.29	1.19	0.36	**2.87**	0.031
P13383	Nucleolin	21	0.47	0.15	1.33	0.13	**2.87**	<0.001
P11980	Pyruvate kinase isozymes M1/M2	19	0.44	0.09	1.23	0.38	**2.81**	0.002
P17475	Alpha-1-antiproteinase	39	0.47	0.18	1.31	0.57	**2.77**	0.012
P62982	Ubiquitin-40S ribosomal protein S27a	23	0.5	0.3	1.38	0.33	**2.73**	0.018
P05982	NAD(P)H dehydrogenase [quinone] 1	8	0.5	0.12	1.37	0.37	**2.73**	0.002
P07150	Annexin A1	12	0.55	0.23	1.47	0.49	**2.7**	0.015
P05371	Clusterin	6	0.56	0.31	1.52	0.52	**2.7**	0.041
P04906	Glutathione S-transferase P	12	0.26	0.22	0.7	0.41	**2.69**	0.045
O35821	Myb-binding protein 1A	15	0.53	0.17	1.4	0.25	**2.63**	0.002
P14480	Fibrinogen beta chain	25	0.52	0.24	1.36	0.55	**2.63**	0.026
Q3B8Q1	Nucleolar RNA helicase 2	7	0.48	0.2	1.26	0.26	**2.62**	0.005
P13084	Nucleophosmin	14	0.51	0.21	1.29	0.17	**2.53**	0.011
P63018	Heat shock cognate 71 kDa protein	106	0.6	0.12	1.51	0.35	**2.5**	0.001
P06761	78 kDa glucose-regulated protein	112	0.69	0.25	1.7	0.5	**2.47**	0.008
P52631	Signal transducer and activator of transcription 3	10	0.64	0.3	1.57	0.46	**2.45**	0.011
P08430	UDP-glucuronosyltransferase 1-6	40	0.58	0.23	1.37	0.48	**2.34**	0.017
D4A4T9	Cysteine and histidine-rich domain-containing protein 1	3	0.86	0.23	2	1.03	**2.32**	0.046
Q62812	Myosin-9	161	0.57	0.26	1.31	0.35	**2.3**	0.018
P63029	Translationally-controlled tumor protein	9	0.69	0.2	1.52	0.27	**2.2**	0.004
P05765	40S ribosomal protein S21	10	0.55	0.32	1.21	0.25	**2.2**	0.032
P62961	Nuclease-sensitive element-binding protein 1	22	0.71	0.33	1.55	0.19	**2.17**	0.025
P05197	Elongation factor 2	70	0.71	0.15	1.55	0.27	**2.17**	0.001

O35814	Stress-induced-phosphoprotein 1	24	0.72	0.16	1.54	0.71	**2.15**	0.031
P34058	Heat shock protein HSP 90-beta	80	0.77	0.18	1.65	0.41	**2.14**	0.005
B0BNA5	Coactosin-like protein	3	0.6	0.19	1.27	0.44	**2.11**	0.022
Q63525	Nuclear migration protein nudC	9	0.51	0.16	1.05	0.42	**2.05**	0.035
P31000	Vimentin	32	0.51	0.15	1.03	0.26	**2.04**	0.012
Q62651	Delta(3,5)-Delta(2,4)-dienoyl-CoA isomerase, mitochondrial	17	0.62	0.2	1.26	0.5	**2.03**	0.026
O35763	Moesin	19	0.58	0.12	1.18	0.14	**2.03**	0.001
Q6AYC2	Immunity-related GTPase family M protein	3	0.71	0.25	1.43	0.29	**2.02**	0.017
P50503	Hsc70-interacting protein	14	0.69	0.32	1.39	0.5	**2.02**	0.047
P13221	Aspartate aminotransferase, cytoplasmic	30	0.51	0.2	1.01	0.37	**1.99**	0.043
Q9JJ19	Na(+)/H(+) exchange regulatory cofactor NHE-RF1	13	0.7	0.17	1.37	0.43	**1.95**	0.021
Q6URK4	Heterogeneous nuclear ribonucleoprotein A3	20	0.56	0.07	1.08	0.26	**1.91**	0.004
Q1JU68	Eukaryotic translation initiation factor 3 subunit A	23	0.66	0.17	1.26	0.26	**1.91**	0.007
Q07936	Annexin A2	15	0.61	0.2	1.13	0.38	**1.87**	0.036
P26772	10 kDa heat shock protein, mitochondrial	13	0.72	0.29	1.34	0.12	**1.87**	0.016
Q9Z2G8	Nucleosome assembly protein 1-like 1	5	0.72	0.14	1.35	0.24	**1.87**	0.005
Q5M9G3	Caprin-1	4	0.88	0.24	1.65	0.58	**1.87**	0.035
P45592	Cofilin-1	14	0.65	0.06	1.21	0.16	**1.86**	<0.001
P70619	Glutathione reductase (Fragment)	8	0.68	0.17	1.25	0.29	**1.85**	0.014
O35987	NSFL1 cofactor p47	14	0.71	0.37	1.29	0.21	**1.82**	0.036
Q5BJY9	Keratin, type I cytoskeletal 18	82	0.77	0.29	1.35	0.23	**1.76**	0.04
P69897	Tubulin beta-5 chain	75	0.53	0.17	0.92	0.2	**1.75**	0.027
Q63617	Hypoxia up-regulated protein 1	55	0.66	0.13	1.16	0.17	**1.74**	0.005
O88600	Heat shock 70 kDa protein 4	28	0.73	0.13	1.26	0.11	**1.72**	0.001
P41777	Nucleolar and coiled-body phosphoprotein 1	4	0.65	0.19	1.11	0.13	**1.71**	0.023
P13635	Ceruloplasmin	19	0.67	0.2	1.14	0.22	**1.7**	0.028
P11442	Clathrin heavy chain 1	103	0.77	0.1	1.28	0.15	**1.67**	0.001
P30009	Myristoylated alanine-rich C-kinase substrate	12	0.5	0.17	0.84	0.1	**1.67**	0.032
Q8K1Q0	Glycylpeptide N-tetradecanoyltransferase 1	5	0.87	0.15	1.45	0.34	**1.66**	0.016
P62425	60S ribosomal protein L7a	13	0.7	0.2	1.16	0.15	**1.65**	0.012
P48721	Stress-70 protein, mitochondrial	67	0.75	0.14	1.23	0.25	**1.64**	0.015
P63102	14-3-3 protein zeta/delta	26	0.63	0.11	1.03	0.17	**1.63**	0.006
Q68FR6	Elongation factor 1-gamma	21	0.73	0.08	1.19	0.2	**1.63**	0.002
P20673	Argininosuccinate lyase	42	0.69	0.14	1.13	0.27	**1.62**	0.035
P04276	Vitamin D-binding	15	0.78	0.14	1.24	0.33	**1.6**	0.031

	protein							
P63039	60 kDa heat shock protein, mitochondrial	161	0.87	0.3	1.39	0.34	**1.6**	0.049
Q9EPH8	Polyadenylate-binding protein 1	24	0.82	0.14	1.3	0.36	**1.59**	0.038
P08082	Clathrin light chain B	3	0.67	0.13	1.07	0.1	**1.59**	0.005
P11232	Thioredoxin	7	0.69	0.12	1.1	0.3	**1.58**	0.032
P19945	60S acidic ribosomal protein P0	24	0.68	0.12	1.08	0.14	**1.58**	0.007
P62634	Cellular nucleic acid-binding protein	5	0.71	0.18	1.11	0.08	**1.56**	0.012
P28064	Proteasome subunit beta type-8	6	0.76	0.16	1.18	0.22	**1.56**	0.019
P02401	60S acidic ribosomal protein P2	31	0.71	0.09	1.11	0.16	**1.56**	0.004
B5DFC8	Eukaryotic translation initiation factor 3 subunit C	14	0.85	0.12	1.31	0.1	**1.55**	0.002
Q5RKI1	Eukaryotic initiation factor 4A-II	22	0.84	0.12	1.31	0.11	**1.55**	0.002
P81795	Eukaryotic translation initiation factor 2 subunit 3	11	0.77	0.09	1.19	0.31	**1.54**	0.021
O08629	Transcription intermediary factor 1-beta	8	0.82	0.21	1.24	0.22	**1.51**	0.036
Q62667	Major vault protein	19	0.77	0.08	1.13	0.16	**1.47**	0.007
P38656	Lupus La protein homolog	7	0.83	0.16	1.21	0.16	**1.47**	0.017
Q4V7C6	GMP synthase [glutamine-hydrolyzing]	7	0.78	0.19	1.15	0.13	**1.47**	0.025
Q5XIU5	Proteasome inhibitor PI31 subunit	2	0.85	0.2	1.25	0.18	**1.46**	0.027
P62250	40S ribosomal protein S16	13	0.83	0.17	1.22	0.18	**1.46**	0.022
Q08163	Adenylyl cyclase-associated protein 1	9	0.85	0.23	1.23	0.2	**1.45**	0.044
P04256	Heterogeneous nuclear ribonucleoprotein A1	18	0.86	0.02	1.24	0.26	**1.45**	0.012
A0JPM9	Eukaryotic translation initiation factor 3 subunit J	5	0.8	0.22	1.16	0.16	**1.45**	0.047
Q6AXS5	Plasminogen activator inhibitor 1 RNA-binding protein	12	0.72	0.16	1.05	0.19	**1.45**	0.036
Q6P799	Seryl-tRNA synthetase, cytoplasmic	14	0.84	0.15	1.21	0.26	**1.45**	0.045
Q07205	Eukaryotic translation initiation factor 5	10	0.8	0.11	1.13	0.18	**1.4**	0.023
P62815	V-type proton ATPase subunit B, brain isoform	14	0.82	0.2	1.14	0.15	**1.39**	0.042
Q9EQS0	Transaldolase	15	0.73	0.09	0.99	0.13	**1.37**	0.012
P63086	Mitogen-activated protein kinase 1	5	0.83	0.08	1.12	0.14	**1.36**	0.009
P38650	Cytoplasmic dynein 1 heavy chain 1	51	0.76	0.07	1.03	0.14	**1.36**	0.011
Q63347	26S protease regulatory subunit 7	15	0.88	0.06	1.19	0.18	**1.35**	0.013
P62859	40S ribosomal protein S28	7	0.79	0.14	1.07	0.16	**1.35**	0.036
Q6P502	T-complex protein 1 subunit gamma	34	0.92	0.14	1.24	0.09	**1.34**	0.013

Q63945	Protein SET	9	0.77	0.15	1.03	0.15	**1.34**	0.049
Q4FZY0	EF-hand domain-containing protein D2	4	0.84	0.13	1.08	0.15	**1.3**	0.043
Q6P7P5	Basic leucine zipper and W2 domain-containing protein 1	7	0.79	0.14	1.03	0.09	**1.3**	0.041
P68511	14-3-3 protein eta	15	0.85	0.1	1.09	0.12	**1.29**	0.02
P12001	60S ribosomal protein L18	9	0.83	0.13	1.07	0.09	**1.29**	0.025
P38659	Protein disulfide-isomerase A4	45	0.86	0.14	1.09	0.09	**1.27**	0.039
Q505J9	ATPase family AAA domain-containing protein 1	2	0.93	0.08	1.14	0.16	**1.24**	0.044
P29314	40S ribosomal protein S9	13	0.86	0.1	1.06	0.08	**1.24**	0.022
P18395	Cold shock domain-containing protein E1	3	0.82	0.11	1.01	0.01	**1.22**	0.026
Q9ER24	Ataxin-10	4	0.91	0.08	1.1	0.05	**1.21**	0.009
Q6RUV5	Ras-related C3 botulinum toxin substrate 1	4	0.88	0.11	1.04	0.03	**1.18**	0.042
Q6AXS3	Protein DEK	4	0.93	0.12	1.09	0.05	**1.18**	0.043

Supplementary Table 1C: *iTRAQ-based proteomic comparison of liver proteins in vehicle control- and APAP-treated rats (72h timepoint).* Proteins with expression that was different (raw P < 0.05) between control and APAP-treated rats at 72h are listed. Mean expression values relative to a common pool are given for n=4 animals. Proteins are ordered according to the ratio between the 72h and control groups (lowest to highest) such that proteins with expression that was most markedly reduced at 72h appear at the top of the list.
[a]Average number of peptides used for quantification across the four individual iTRAQ runs.
[b]Uncorrected raw p value.

Uniprot Accession	Name	Peptides[a]	Vehicle control		72h		72h/ctrl	p value[b]
			Mean	SD	Mean	SD	Ratio	
Proteins reduced at 72h								
P09606	Glutamine synthetase	17	2.73	0.78	0.06	0.03	**0.02**	<0.001
P08683	Cytochrome P450 2C11	51	2.53	0.52	0.16	0.09	**0.06**	<0.001
P49890	Estrogen sulfotransferase, isoform 6	18	3.22	0.91	0.22	0.15	**0.07**	<0.001
P14141	Carbonic anhydrase 3	70	1.99	1.3	0.18	0.2	**0.09**	0.007
P36365	Dimethylaniline monooxygenase [N-oxide-forming] 1	13	2.34	0.94	0.22	0.15	**0.1**	0.002
P02761	Major urinary protein	22	2.27	0.42	0.3	0.3	**0.13**	0.006
Q9ES38	Bile acyl-CoA synthetase	26	2.8	0.86	0.39	0.39	**0.14**	0.007
P17988	Sulfotransferase 1A1	30	1.99	0.34	0.28	0.16	**0.14**	0.001
P00502	Glutathione S-transferase alpha-1	51	1.57	1.21	0.28	0.27	**0.18**	0.015
Q03336	Regucalcin	45	1.98	0.18	0.36	0.38	**0.18**	0.011
P05183	Cytochrome P450 3A2	15	2.49	0.97	0.46	0.24	**0.18**	0.009
P16303	Carboxylesterase 3	33	1.85	0.85	0.36	0.33	**0.2**	0.012
Q64565	Alanine--glyoxylate aminotransferase 2, mitochondrial	28	1.26	0.46	0.25	0.14	**0.2**	0.002
P04182	Ornithine aminotransferase, mitochondrial	8	1.44	0.74	0.29	0.13	**0.2**	0.007
P50237	Sulfotransferase 1C1	27	1.95	0.15	0.39	0.17	**0.2**	<0.001
Q64611	Cysteine sulfinic acid decarboxylase	25	1.81	0.7	0.41	0.61	**0.23**	0.025
Q07523	Hydroxyacid oxidase 2	8	1.99	0.34	0.47	0.07	**0.24**	<0.001
P12928	Pyruvate kinase isozymes R/L	61	1.64	0.53	0.4	0.17	**0.24**	0.002
P14173	Aromatic-L-amino-acid decarboxylase	13	1.74	0.94	0.42	0.39	**0.24**	0.019
P10867	L-gulonolactone oxidase	18	2	0.36	0.49	0.28	**0.24**	0.002
P10860	Glutamate dehydrogenase 1, mitochondrial	118	1.63	0.34	0.4	0.35	**0.25**	0.019
Q64638	UDP-glucuronosyltransferase 1-5	25	3.79	1.58	0.97	0.93	**0.26**	0.022
P50169	Retinol dehydrogenase 3	30	1.54	0.61	0.4	0.27	**0.26**	0.008
P09811	Glycogen phosphorylase, liver form	76	1.4	0.26	0.38	0.15	**0.27**	0.002
P25093	Fumarylacetoacetase	48	1.45	0.12	0.41	0.29	**0.29**	0.012
Q5U2Q3	Ester hydrolase C11orf54 homolog	12	2	0.36	0.58	0.29	**0.29**	0.011
P02692	Fatty acid-binding	69	1.94	0.49	0.57	0.18	**0.29**	0.002

	protein, liver							
Q4KLP0	Probable 2-oxoglutarate dehydrogenase E1 component DHKTD1, mitochondrial	35	1.59	0.56	0.48	0.26	**0.3**	0.015
P55051	Fatty acid-binding protein, brain	9	1.61	0.57	0.49	0.4	**0.3**	0.024
Q4KLZ6	Bifunctional ATP-dependent dihydroxyacetone kinase/FAD-AMP lyase (cyclizing)	64	1.7	0.39	0.52	0.25	**0.31**	0.013
Q497B0	Omega-amidase NIT2	34	1.58	0.09	0.49	0.24	**0.31**	0.003
P23680	Serum amyloid P-component	4	1.61	0.24	0.5	0.34	**0.31**	0.014
P55159	Serum paraoxonase/arylesterase 1	17	1.68	0.55	0.53	0.36	**0.32**	0.025
P07872	Peroxisomal acyl-coenzyme A oxidase 1	42	1.33	0.25	0.43	0.28	**0.32**	0.017
P23457	3-alpha-hydroxysteroid dehydrogenase	48	1.51	0.36	0.49	0.41	**0.32**	0.035
P30839	Fatty aldehyde dehydrogenase	36	1.74	0.55	0.56	0.37	**0.32**	0.018
Q9QYU4	Thiomorpholine-carboxylate dehydrogenase	9	1.31	0.25	0.44	0.24	**0.33**	0.01
P16638	ATP-citrate synthase	65	1.93	0.71	0.65	0.21	**0.34**	0.006
P20070	NADH-cytochrome b5 reductase 3	26	1.62	0.42	0.57	0.21	**0.35**	0.005
Q920P0	L-xylulose reductase	12	1.44	0.45	0.51	0.18	**0.35**	0.004
Q07071	Glucokinase regulatory protein	27	1.71	0.64	0.6	0.35	**0.35**	0.029
P29147	D-beta-hydroxybutyrate dehydrogenase, mitochondrial	42	1.4	0.23	0.5	0.47	**0.36**	0.047
Q8CHM7	2-hydroxyacyl-CoA lyase 1	28	1.66	0.35	0.61	0.4	**0.36**	0.021
P11497	Acetyl-CoA carboxylase 1	44	1.46	0.57	0.53	0.18	**0.37**	0.01
P57113	Maleylacetoacetate isomerase	36	1.58	0.34	0.58	0.42	**0.37**	0.033
B0BNE5	S-formylglutathione hydrolase	23	1.32	0.33	0.49	0.16	**0.37**	0.003
Q6DGG1	Alpha/beta hydrolase domain-containing protein 14B	12	1.36	0.25	0.51	0.29	**0.37**	0.042
P12785	Fatty acid synthase	155	1.79	1.03	0.67	0.11	**0.38**	0.03
P12938	Cytochrome P450 2D3	46	1.52	0.33	0.57	0.11	**0.38**	0.001
Q9R063	Peroxiredoxin-5, mitochondrial	21	1.83	0.94	0.7	0.23	**0.38**	0.032
A0JPQ8	Alkylglycerol monooxygenase	6	1.64	0.2	0.63	0.19	**0.38**	0.001
P70712	Kynureninase	19	1.41	0.32	0.54	0.19	**0.38**	0.007
P70473	Alpha-methylacyl-CoA racemase	18	1.07	0.04	0.41	0.3	**0.39**	0.028
Q68FU3	Electron transfer flavoprotein subunit beta	29	1.17	0.22	0.46	0.24	**0.39**	0.01
P19112	Fructose-1,6-bisphosphatase 1	72	1.71	0.38	0.67	0.38	**0.39**	0.018
Q66HG4	Aldose 1-epimerase	5	1.37	0.18	0.54	0.12	**0.39**	<0.001
P24329	Thiosulfate sulfurtransferase	41	1.33	0.2	0.52	0.41	**0.39**	0.042

Q02253	Methylmalonate-semialdehyde dehydrogenase [acylating], mitochondrial	124	1.22	0.24	0.48	0.39	**0.39**	0.044
P00884	Fructose-bisphosphate aldolase B	129	1.31	0.33	0.52	0.39	**0.4**	0.047
P29411	GTP:AMP phosphotransferase, mitochondrial	7	1.41	0.24	0.56	0.11	**0.4**	0.001
O35077	Glycerol-3-phosphate dehydrogenase [NAD+], cytoplasmic	39	1.45	0.42	0.58	0.32	**0.4**	0.026
P97612	Fatty-acid amide hydrolase 1	26	1.67	0.31	0.67	0.5	**0.4**	0.037
P52873	Pyruvate carboxylase, mitochondrial	134	1.16	0.13	0.47	0.35	**0.4**	0.042
P22791	Hydroxymethylglutaryl-CoA synthase, mitochondrial	106	1.46	0.4	0.6	0.42	**0.41**	0.05
P05544	Serine protease inhibitor A3L	30	1.22	0.12	0.5	0.43	**0.41**	0.042
Q02974	Ketohexokinase	25	1.56	0.28	0.64	0.31	**0.41**	0.01
P18163	Long-chain-fatty-acid--CoA ligase 1	78	1.54	0.13	0.65	0.48	**0.42**	0.044
P22734	Catechol O-methyltransferase	46	1.49	0.39	0.63	0.37	**0.42**	0.034
Q62730	Estradiol 17-beta-dehydrogenase 2	17	1.72	0.47	0.74	0.42	**0.43**	0.029
P06214	Delta-aminolevulinic acid dehydratase	35	1.5	0.26	0.65	0.13	**0.43**	0.001
Q68FP2	Serum paraoxonase/lactonase 3	16	1.43	0.1	0.62	0.19	**0.43**	0.003
P08503	Medium-chain specific acyl-CoA dehydrogenase, mitochondrial	26	1.49	0.32	0.65	0.32	**0.44**	0.015
P05545	Serine protease inhibitor A3K	34	1.5	0.5	0.66	0.38	**0.44**	0.035
P13803	Electron transfer flavoprotein subunit alpha, mitochondrial	50	1.29	0.23	0.57	0.37	**0.44**	0.045
P30713	Glutathione S-transferase theta-2	19	1.34	0.31	0.6	0.26	**0.45**	0.02
P46720	Solute carrier organic anion transporter family member 1A1	4	1.41	0.3	0.63	0.23	**0.45**	0.008
P46953	3-hydroxyanthranilate 3,4-dioxygenase	25	1.42	0.4	0.64	0.26	**0.45**	0.03
P08009	Glutathione S-transferase Yb-3	53	1.1	0.29	0.5	0.26	**0.45**	0.03
Q64232	Very-long-chain enoyl-CoA reductase	35	1.76	0.41	0.8	0.41	**0.45**	0.045
O88813	Long-chain-fatty-acid--CoA ligase 5	28	1.89	0.67	0.87	0.36	**0.46**	0.029
P10760	Adenosylhomocysteinase	54	1.29	0.2	0.61	0.24	**0.47**	0.01
P41034	Alpha-tocopherol transfer protein	16	1.28	0.15	0.61	0.19	**0.47**	0.004
Q68G31	Phenazine biosynthesis-like domain-containing protein	16	1.23	0.55	0.59	0.13	**0.48**	0.023
P07953	6-phosphofructo-2-kinase/fructose-2,6-bisphosphatase 1	13	1.47	0.11	0.71	0.17	**0.48**	0.001

Q6AYT0	Quinone oxidoreductase	9	1.37	0.36	0.67	0.24	**0.49**	0.023
Q561R9	Beta-lactamase-like protein 2	11	1.2	0.24	0.59	0.18	**0.49**	0.008
P57093	Phytanoyl-CoA dioxygenase, peroxisomal	10	1.36	0.22	0.67	0.18	**0.5**	0.004
Q9Z339	Glutathione S-transferase omega-1	10	1.42	0.4	0.7	0.22	**0.5**	0.026
P62959	Histidine triad nucleotide-binding protein 1	8	1.59	0.36	0.8	0.3	**0.5**	0.031
P11348	Dihydropteridine reductase	27	1.29	0.44	0.65	0.25	**0.51**	0.044
Q99MS0	SEC14-like protein 2	16	1.32	0.14	0.67	0.11	**0.51**	0.001
Q63060	Glycerol kinase	20	1.68	0.28	0.86	0.16	**0.51**	0.002
P85971	6-phosphogluconolactonase	12	1.56	0.23	0.8	0.1	**0.51**	<0.001
Q63448	Peroxisomal acyl-coenzyme A oxidase 3	27	1.27	0.23	0.65	0.26	**0.51**	0.027
Q68FS4	Cytosol aminopeptidase	53	1.52	0.14	0.78	0.3	**0.51**	0.031
P16970	ATP-binding cassette sub-family D member 3	13	1.69	0.46	0.87	0.35	**0.52**	0.032
P45380	Sulfate anion transporter 1	3	1.09	0.35	0.57	0.21	**0.52**	0.029
Q9Z0V5	Peroxiredoxin-4	16	1.03	0.11	0.55	0.19	**0.53**	0.016
P52847	Sulfotransferase family cytosolic 1B member 1	16	1.97	0.42	1.04	0.26	**0.53**	0.007
Q66H45	Tetratricopeptide repeat protein 36	5	1.2	0.34	0.65	0.13	**0.54**	0.014
P43278	Histone H1.0	4	1.51	0.31	0.82	0.26	**0.54**	0.021
Q8CG45	Aflatoxin B1 aldehyde reductase member 2	22	1.11	0.05	0.6	0.27	**0.54**	0.042
Q6AXX6	Redox-regulatory protein PAMM	8	1.54	0.33	0.84	0.13	**0.55**	0.005
P30904	Macrophage migration inhibitory factor	22	1.31	0.21	0.73	0.3	**0.55**	0.032
P10868	Guanidinoacetate N-methyltransferase	16	1.58	0.51	0.88	0.23	**0.56**	0.03
P29117	Peptidyl-prolyl cis-trans isomerase F, mitochondrial	8	1.25	0.26	0.7	0.29	**0.56**	0.044
Q03626	Murinoglobulin-1	65	1.26	0.2	0.7	0.22	**0.56**	0.014
P51650	Succinate-semialdehyde dehydrogenase, mitochondrial	10	1.21	0.32	0.68	0.05	**0.56**	0.007
P14604	Enoyl-CoA hydratase, mitochondrial	35	1.08	0.04	0.62	0.23	**0.57**	0.03
Q6AYT9	Acyl-coenzyme A synthetase ACSM5, mitochondrial	14	1.53	0.3	0.88	0.16	**0.58**	0.007
P31044	Phosphatidylethanolamine-binding protein 1	22	1.26	0.27	0.74	0.22	**0.58**	0.034
Q8VID1	Dehydrogenase/reductase SDR family member 4	6	1.1	0.23	0.65	0.15	**0.59**	0.011
O89000	Dihydropyrimidine dehydrogenase [NADP+]	12	1.36	0.32	0.8	0.21	**0.59**	0.037
Q63150	Dihydropyrimidinase	29	1.41	0.17	0.83	0.22	**0.59**	0.008
P97852	Peroxisomal multifunctional enzyme type 2	47	1.2	0.09	0.71	0.3	**0.59**	0.04

P29266	3-hydroxyisobutyrate dehydrogenase, mitochondrial	23	1.21	0.17	0.71	0.12	**0.59**	0.003
Q5BK17	Iodotyrosine dehalogenase 1	4	1.75	0.28	1.04	0.24	**0.59**	0.013
P35738	2-oxoisovalerate dehydrogenase subunit beta, mitochondrial	13	1.23	0.12	0.73	0.24	**0.6**	0.02
Q6I7R3	Isochorismatase domain-containing protein 1	10	1.44	0.23	0.86	0.15	**0.6**	0.007
P27364	3 beta-hydroxysteroid dehydrogenase type 5	19	1.41	0.31	0.84	0.29	**0.6**	0.037
Q7TP48	Adipocyte plasma membrane-associated protein	10	1.55	0.48	0.94	0.13	**0.61**	0.035
O35952	Hydroxyacylglutathione hydrolase, mitochondrial	14	1.36	0.35	0.83	0.06	**0.61**	0.009
Q64380	Sarcosine dehydrogenase, mitochondrial	41	1.28	0.19	0.81	0.24	**0.63**	0.037
Q6AYQ8	Acylpyruvase FAHD1, mitochondrial	10	1.15	0.22	0.74	0.15	**0.64**	0.023
P46462	Transitional endoplasmic reticulum ATPase	71	1.14	0.18	0.73	0.23	**0.64**	0.041
P07633	Propionyl-CoA carboxylase beta chain, mitochondrial	23	1.21	0.18	0.79	0.21	**0.65**	0.037
Q9ES21	Phosphatidylinositide phosphatase SAC1	9	1.33	0.25	0.9	0.16	**0.67**	0.03
Q923M1	Mitochondrial peptide methionine sulfoxide reductase	3	1.19	0.24	0.81	0.15	**0.68**	0.027
Q505J8	Phenylalanine--tRNA ligase alpha subunit	31	0.99	0.1	0.67	0.12	**0.68**	0.007
B0BNG0	Tetratricopeptide repeat protein 35	11	1.31	0.3	0.89	0.14	**0.68**	0.028
P70552	GTP cyclohydrolase 1 feedback regulatory protein	5	1.09	0.21	0.75	0.09	**0.69**	0.02
P16617	Phosphoglycerate kinase 1	54	1.09	0.24	0.76	0.17	**0.69**	0.046
O88767	Protein DJ-1	16	1.21	0.2	0.84	0.12	**0.69**	0.021
P27605	Hypoxanthine-guanine phosphoribosyltransferase	12	1.35	0.2	0.96	0.15	**0.72**	0.025
Q64591	2,4-dienoyl-CoA reductase, mitochondrial	23	1.02	0.1	0.75	0.14	**0.73**	0.023
O35331	Pyridoxal kinase	13	1.22	0.21	0.91	0.13	**0.75**	0.045
P35433	Amidophosphoribosyltransferase	2	1.25	0.17	0.94	0.06	**0.75**	0.008
Q9R1Z0	Voltage-dependent anion-selective channel protein 3	8	1.17	0.16	0.9	0.11	**0.77**	0.027
P17625	Glycogen [starch] synthase, liver	5	1.1	0.11	0.85	0.16	**0.77**	0.048
B2RYT9	Translational activator of cytochrome c oxidase 1	3	1.1	0.1	0.88	0.13	**0.8**	0.042
Q641Y0	Dolichyl-diphosphooligosaccharide--protein glycosyltransferase 48 kDa subunit	16	1.18	0.12	0.97	0.07	**0.82**	0.021
Q6AY78	Solute carrier family 22	4	1	0.11	0.83	0.05	**0.82**	0.025

	member 18							
Q4G064	2-methoxy-6-polyprenyl-1,4-benzoquinol methylase, mitochondrial	6	1.07	0.1	0.89	0.07	**0.83**	0.027
Q8VI04	Isoaspartyl peptidase/L-asparaginase	7	0.99	0.07	0.83	0.04	**0.84**	0.006
Q9Z1N4	3'(2'),5'-bisphosphate nucleotidase 1	4	0.94	0.07	0.83	0.05	**0.88**	0.044
Proteins increased at 72h								
P01048	T-kininogen 1	15	0.25	0.21	1.91	0.92	**7.52**	0.009
P02764	Alpha-1-acid glycoprotein	6	0.31	0.37	1.91	0.33	**6.13**	0.017
P42930	Heat shock protein beta-1	10	0.12	0.11	0.67	0.33	**5.46**	0.006
P11980	Pyruvate kinase isozymes M1/M2	19	0.44	0.09	2.32	1.65	**5.28**	0.004
P31000	Vimentin	32	0.51	0.15	2.4	1.34	**4.74**	0.004
P04961	Proliferating cell nuclear antigen	4	0.41	0.07	1.88	1.39	**4.62**	0.005
P06866	Haptoglobin	21	0.33	0.15	1.51	0.53	**4.57**	0.002
P38918	Aflatoxin B1 aldehyde reductase member 3	42	0.2	0.17	0.87	0.66	**4.29**	0.042
Q07439	Heat shock 70 kDa protein 1A/1B	56	0.21	0.2	0.81	0.35	**3.93**	0.02
P30009	Myristoylated alanine-rich C-kinase substrate	12	0.5	0.17	1.9	1.07	**3.76**	0.031
P69897	Tubulin beta-5 chain	75	0.53	0.17	1.83	0.76	**3.48**	0.004
P11762	Galectin-1	4	0.73	0.12	2.38	0.75	**3.29**	0.001
P20059	Hemopexin	24	0.45	0.12	1.47	0.25	**3.26**	<0.001
P04906	Glutathione S-transferase P	12	0.26	0.22	0.84	0.56	**3.21**	0.034
P05370	Glucose-6-phosphate 1-dehydrogenase	15	0.38	0.22	1.16	0.21	**3.01**	0.011
P07150	Annexin A1	12	0.55	0.23	1.62	0.67	**2.96**	0.015
Q62812	Myosin-9	161	0.57	0.26	1.69	0.72	**2.96**	0.017
Q5XFX0	Transgelin-2	13	0.55	0.23	1.61	0.49	**2.95**	0.01
Q3B8Q1	Nucleolar RNA helicase 2	7	0.48	0.2	1.4	0.38	**2.9**	0.004
P07335	Creatine kinase B-type	11	0.64	0.11	1.83	0.58	**2.86**	0.001
P13383	Nucleolin	21	0.47	0.15	1.3	0.42	**2.8**	0.004
P17475	Alpha-1-antiproteinase	39	0.47	0.18	1.3	0.36	**2.74**	0.005
P06302	Prothymosin alpha	6	0.7	0.47	1.88	0.95	**2.7**	0.038
B0BNA5	Coactosin-like protein	3	0.6	0.19	1.63	0.51	**2.7**	0.007
Q07936	Annexin A2	15	0.61	0.2	1.62	0.92	**2.68**	0.032
P10960	Sulfated glycoprotein 1	14	0.6	0.11	1.62	0.42	**2.68**	0.001
P45592	Cofilin-1	14	0.65	0.06	1.73	0.41	**2.65**	<0.001
O35763	Moesin	19	0.58	0.12	1.51	0.45	**2.61**	0.002
P18437	Non-histone chromosomal protein HMG-17	3	0.51	0.22	1.31	0.52	**2.58**	0.022
O35821	Myb-binding protein 1A	15	0.53	0.17	1.36	0.37	**2.56**	0.005
O70199	UDP-glucose 6-dehydrogenase	38	0.32	0.1	0.8	0.29	**2.53**	0.011
P14480	Fibrinogen beta chain	25	0.52	0.24	1.24	0.41	**2.4**	0.033
Q9Z2G8	Nucleosome assembly protein 1-like 1	5	0.72	0.14	1.72	0.25	**2.39**	0.001
P16391	RT1 class I histocompatibility	6	0.6	0.37	1.43	0.26	**2.38**	0.024

	antigen, AA alpha chain							
P13084	Nucleophosmin	14	0.51	0.21	1.22	0.39	**2.38**	0.026
P13221	Aspartate aminotransferase, cytoplasmic	30	0.51	0.2	1.12	0.28	**2.22**	0.013
Q6URK4	Heterogeneous nuclear ribonucleoprotein A3	20	0.56	0.07	1.2	0.05	**2.14**	<0.001
P63102	14-3-3 protein zeta/delta	26	0.63	0.11	1.34	0.35	**2.13**	0.004
P52555	Endoplasmic reticulum resident protein 29	12	0.95	0.19	1.99	0.93	**2.09**	0.023
Q62667	Major vault protein	19	0.77	0.08	1.59	0.61	**2.06**	0.01
P13635	Ceruloplasmin	19	0.67	0.2	1.36	0.23	**2.03**	0.008
P82995	Heat shock protein HSP 90-alpha	74	0.47	0.29	0.95	0.23	**2.02**	0.044
P05197	Elongation factor 2	70	0.71	0.15	1.42	0.46	**2**	0.012
O35814	Stress-induced-phosphoprotein 1	24	0.72	0.16	1.44	0.63	**2**	0.025
P68255	14-3-3 protein theta	20	0.87	0.3	1.74	0.69	**2**	0.04
Q63525	Nuclear migration protein nudC	9	0.51	0.16	1.02	0.36	**1.99**	0.028
P24268	Cathepsin D	12	0.86	0.3	1.71	0.28	**1.97**	0.006
P34064	Proteasome subunit alpha type-5	15	0.63	0.31	1.22	0.3	**1.93**	0.042
P50503	Hsc70-interacting protein	14	0.69	0.32	1.3	0.28	**1.89**	0.042
Q66HD0	Endoplasmin	95	0.71	0.27	1.32	0.34	**1.86**	0.036
P29457	Serpin H1	11	0.81	0.17	1.51	0.45	**1.86**	0.019
Q68FR6	Elongation factor 1-gamma	21	0.73	0.08	1.33	0.22	**1.83**	0.001
P63018	Heat shock cognate 71 kDa protein	106	0.6	0.12	1.1	0.21	**1.82**	0.006
O54753	17-beta-hydroxysteroid dehydrogenase type 6	12	0.85	0.33	1.53	0.31	**1.8**	0.024
Q63617	Hypoxia up-regulated protein 1	55	0.66	0.13	1.19	0.1	**1.8**	0.002
P04639	Apolipoprotein A-I	20	0.82	0.28	1.46	0.27	**1.77**	0.035
P19945	60S acidic ribosomal protein P0	24	0.68	0.12	1.18	0.36	**1.73**	0.026
Q5BJY9	Keratin, type I cytoskeletal 18	82	0.77	0.29	1.3	0.16	**1.7**	0.043
Q5M9G3	Caprin-1	4	0.88	0.24	1.46	0.4	**1.65**	0.035
Q1JU68	Eukaryotic translation initiation factor 3 subunit A	23	0.66	0.17	1.07	0.24	**1.64**	0.026
P38656	Lupus La protein homolog	7	0.83	0.16	1.32	0.25	**1.6**	0.018
P62634	Cellular nucleic acid-binding protein	5	0.71	0.18	1.14	0.24	**1.6**	0.024
P62425	60S ribosomal protein L7a	13	0.7	0.2	1.11	0.13	**1.58**	0.015
P62828	GTP-binding nuclear protein Ran	8	0.8	0.17	1.26	0.28	**1.57**	0.022
P81795	Eukaryotic translation initiation factor 2 subunit 3	11	0.77	0.09	1.21	0.12	**1.57**	0.001
Q62651	Delta(3,5)-Delta(2,4)-dienoyl-CoA isomerase, mitochondrial	17	0.62	0.2	0.97	0.15	**1.56**	0.035
P62250	40S ribosomal protein S16	13	0.83	0.17	1.29	0.18	**1.56**	0.011
P11442	Clathrin heavy chain 1	103	0.77	0.1	1.2	0.25	**1.56**	0.011

P38650	Cytoplasmic dynein 1 heavy chain 1	51	0.76	0.07	1.18	0.32	**1.56**	0.018
O08557	N(G),N(G)-dimethylarginine dimethylaminohydrolase 1	11	0.68	0.19	1.04	0.2	**1.54**	0.033
P12346	Serotransferrin	78	0.76	0.13	1.16	0.31	**1.54**	0.049
P04644	40S ribosomal protein S17	17	0.8	0.26	1.23	0.19	**1.54**	0.041
Q08163	Adenylyl cyclase-associated protein 1	9	0.85	0.23	1.31	0.35	**1.54**	0.049
O08629	Transcription intermediary factor 1-beta	8	0.82	0.21	1.27	0.11	**1.54**	0.016
Q9JJ22	Endoplasmic reticulum aminopeptidase 1	8	0.93	0.14	1.39	0.37	**1.49**	0.038
Q9R0J8	Legumain	3	0.94	0.13	1.39	0.19	**1.48**	0.008
P69736	Endothelial differentiation-related factor 1	2	0.81	0.2	1.2	0.18	**1.48**	0.04
Q9JI85	Nucleobindin-2	17	1.02	0.17	1.5	0.32	**1.47**	0.029
P62853	40S ribosomal protein S25	9	0.76	0.12	1.12	0.19	**1.47**	0.014
Q63797	Proteasome activator complex subunit 1	26	0.81	0.15	1.19	0.1	**1.47**	0.009
Q9R1T1	Barrier-to-autointegration factor	3	0.9	0.25	1.32	0.13	**1.47**	0.026
Q4AEF8	Coatomer subunit gamma-1	18	0.85	0.23	1.24	0.09	**1.46**	0.026
P62752	60S ribosomal protein L23a	8	0.78	0.12	1.14	0.17	**1.46**	0.014
P23514	Coatomer subunit beta	30	0.88	0.12	1.27	0.3	**1.45**	0.04
P51583	Multifunctional protein ADE2	8	1.12	0.06	1.6	0.34	**1.43**	0.034
Q63945	Protein SET	9	0.77	0.15	1.1	0.08	**1.43**	0.012
Q8K1Q0	Glycylpeptide N-tetradecanoyltransferase 1	5	0.87	0.15	1.24	0.19	**1.42**	0.023
B5DFC8	Eukaryotic translation initiation factor 3 subunit C	14	0.85	0.12	1.2	0.19	**1.42**	0.018
Q5RJR8	Leucine-rich repeat-containing protein 59	21	0.8	0.14	1.14	0.14	**1.42**	0.021
P43244	Matrin-3	12	0.91	0.07	1.28	0.09	**1.41**	0.001
P25113	Phosphoglycerate mutase 1	20	0.92	0.1	1.3	0.25	**1.41**	0.024
P41123	60S ribosomal protein L13	16	0.76	0.1	1.06	0.13	**1.4**	0.011
Q3T1J1	Eukaryotic translation initiation factor 5A-1	13	0.84	0.08	1.16	0.22	**1.39**	0.021
P68511	14-3-3 protein eta	15	0.85	0.1	1.18	0.25	**1.39**	0.036
P21531	60S ribosomal protein L3	23	0.8	0.13	1.11	0.2	**1.39**	0.037
Q63584	Transmembrane emp24 domain-containing protein 10	11	0.9	0.07	1.23	0.26	**1.37**	0.03
P63086	Mitogen-activated protein kinase 1	5	0.83	0.08	1.12	0.12	**1.36**	0.006
Q641Z6	EH domain-containing protein 1	20	0.87	0.03	1.17	0.06	**1.35**	<0.001
P02401	60S acidic ribosomal protein P2	31	0.71	0.09	0.95	0.06	**1.34**	0.008

Q66H80	Coatomer subunit delta	13	0.91	0.15	1.22	0.16	**1.34**	0.03
P28023	Dynactin subunit 1	6	0.85	0.11	1.12	0.14	**1.31**	0.02
Q6RUV5	Ras-related C3 botulinum toxin substrate 1	4	0.88	0.11	1.14	0.14	**1.3**	0.025
Q62871	Cytoplasmic dynein 1 intermediate chain 2	6	0.89	0.15	1.14	0.13	**1.28**	0.048
Q5M7W5	Microtubule-associated protein 4	8	0.89	0.09	1.14	0.13	**1.27**	0.02
P85125	Polymerase I and transcript release factor	5	0.85	0.03	1.07	0.05	**1.26**	<0.001
P85972	Vinculin	35	0.85	0.1	1.07	0.15	**1.26**	0.047
Q8CFN2	Cell division control protein 42 homolog	8	0.93	0.1	1.14	0.08	**1.23**	0.014
P29314	40S ribosomal protein S9	13	0.86	0.1	1.03	0.09	**1.2**	0.048
Q5U211	Sorting nexin-3	5	0.93	0.08	1.07	0.08	**1.16**	0.04
Q62991	Sec1 family domain-containing protein 1	8	0.98	0.05	1.14	0.04	**1.16**	0.002
O35142	Coatomer subunit beta'	9	0.93	0.05	1.04	0.04	**1.11**	0.02

Supplementary Table 1D: *iTRAQ-based proteomic comparison of liver proteins in vehicle control- and APAP-treated rats (96h timepoint).* Proteins with expression that was different (raw P < 0.05) between control and APAP-treated rats at 96h are listed. Mean expression values relative to a common pool are given for n=3 animals. Proteins are ordered according to the ratio between the 96h and control groups (lowest to highest) such that proteins with expression that was most markedly reduced at 96h appear at the top of the list.
[a]Average number of peptides used for quantification across the four individual iTRAQ runs.
[b]Uncorrected raw p value.

Uniprot Accession	Name	Peptides[a]	Vehicle control		96h		96h/ctrl	p value[b]
			Mean	SD	Mean	SD	Ratio	
Proteins reduced at 96h								
P08683	Cytochrome P450 2C11	51	2.53	0.52	0.09	0.04	**0.03**	<0.001
P49890	Estrogen sulfotransferase, isoform 6	18	3.22	0.91	0.11	0.08	**0.03**	<0.001
P09606	Glutamine synthetase	17	2.73	0.78	0.1	0.03	**0.03**	<0.001
P14141	Carbonic anhydrase 3	70	1.99	1.3	0.1	0.08	**0.05**	0.004
Q07523	Hydroxyacid oxidase 2	8	1.99	0.34	0.12	0.08	**0.06**	<0.001
P36365	Dimethylaniline monooxygenase [N-oxide-forming] 1	13	2.34	0.94	0.24	0.05	**0.1**	<0.001
P02761	Major urinary protein	22	2.27	0.42	0.25	0.08	**0.11**	<0.001
P10867	L-gulonolactone oxidase	18	2	0.36	0.31	0.12	**0.15**	<0.001
P50237	Sulfotransferase 1C1	27	1.95	0.15	0.31	0.12	**0.16**	<0.001
P17988	Sulfotransferase 1A1	30	1.99	0.34	0.34	0.15	**0.17**	0.001
Q9ES38	Bile acyl-CoA synthetase	26	2.8	0.86	0.53	0.32	**0.19**	0.005
P05183	Cytochrome P450 3A2	15	2.49	0.97	0.48	0.42	**0.19**	0.028
P12785	Fatty acid synthase	155	1.79	1.03	0.36	0.07	**0.2**	0.009
P04182	Ornithine aminotransferase, mitochondrial	8	1.44	0.74	0.29	0.18	**0.2**	0.014
Q62730	Estradiol 17-beta-dehydrogenase 2	17	1.72	0.47	0.35	0.11	**0.2**	0.001
Q02769	Squalene synthase	8	1.7	0.55	0.36	0.14	**0.21**	0.005
P11497	Acetyl-CoA carboxylase 1	44	1.46	0.57	0.33	0.07	**0.22**	0.003
P16638	ATP-citrate synthase	65	1.93	0.71	0.45	0.01	**0.23**	0.001
Q03336	Regucalcin	45	1.98	0.18	0.49	0.08	**0.25**	<0.001
P05369	Farnesyl pyrophosphate synthase	27	1.5	0.39	0.39	0.35	**0.26**	0.025
P22734	Catechol O-methyltransferase	46	1.49	0.39	0.39	0.13	**0.26**	0.002
P52847	Sulfotransferase family cytosolic 1B member 1	16	1.97	0.42	0.53	0.15	**0.27**	0.001
P17425	Hydroxymethylglutaryl-CoA synthase, cytoplasmic	9	1.3	0.44	0.36	0.26	**0.28**	0.045
P19225	Cytochrome P450 2C70	19	1.56	0.65	0.45	0.35	**0.29**	0.041
P12928	Pyruvate kinase isozymes R/L	61	1.64	0.53	0.49	0.25	**0.3**	0.009
Q63060	Glycerol kinase	20	1.68	0.28	0.53	0.1	**0.31**	<0.001
Q9EQ76	Dimethylaniline monooxygenase [N-oxide-forming] 3	21	1.24	0.6	0.4	0.28	**0.32**	0.031
Q68FT5	Betaine--homocysteine S-methyltransferase 2	82	0.99	0.45	0.32	0.17	**0.32**	0.026

Q5PPL3	Sterol-4-alpha-carboxylate 3-dehydrogenase, decarboxylating	20	1.74	0.46	0.56	0.28	**0.32**	0.008
P07953	6-phosphofructo-2-kinase/fructose-2,6-bisphosphatase 1	13	1.47	0.11	0.49	0.34	**0.33**	0.018
O35760	Isopentenyl-diphosphate Delta-isomerase 1	4	1.38	0.41	0.47	0.11	**0.34**	0.006
P02692	Fatty acid-binding protein, liver	69	1.94	0.49	0.67	0.2	**0.34**	0.004
P16303	Carboxylesterase 3	33	1.85	0.85	0.64	0.38	**0.35**	0.05
P18757	Cystathionine gamma-lyase	37	1.4	0.63	0.48	0.19	**0.35**	0.026
Q63276	Bile acid-CoA:amino acid N-acyltransferase	57	1.25	0.27	0.45	0.15	**0.36**	0.004
P30839	Fatty aldehyde dehydrogenase	36	1.74	0.55	0.64	0.15	**0.37**	0.011
Q64611	Cysteine sulfinic acid decarboxylase	25	1.81	0.7	0.67	0.19	**0.37**	0.012
Q5FVR2	Thymidine phosphorylase	11	1.8	0.99	0.69	0.08	**0.38**	0.033
P11030	Acyl-CoA-binding protein	20	1.87	1.03	0.72	0.23	**0.38**	0.036
P20070	NADH-cytochrome b5 reductase 3	26	1.62	0.42	0.62	0.09	**0.38**	0.002
P06214	Delta-aminolevulinic acid dehydratase	35	1.5	0.26	0.58	0.07	**0.39**	<0.001
Q5I0J9	Putative L-aspartate dehydrogenase	17	1.35	0.44	0.53	0.12	**0.39**	0.017
P18163	Long-chain-fatty-acid--CoA ligase 1	78	1.54	0.13	0.61	0.06	**0.4**	<0.001
Q8CHM7	2-hydroxyacyl-CoA lyase 1	28	1.66	0.35	0.67	0.01	**0.4**	0.001
P08290	Asialoglycoprotein receptor 2	4	1.04	0.35	0.42	0.21	**0.4**	0.035
P57093	Phytanoyl-CoA dioxygenase, peroxisomal	10	1.36	0.22	0.55	0.23	**0.41**	0.012
P23680	Serum amyloid P-component	4	1.61	0.24	0.68	0.05	**0.43**	<0.001
Q5BK17	Iodotyrosine dehalogenase 1	4	1.75	0.28	0.75	0.42	**0.43**	0.017
Q64654	Lanosterol 14-alpha demethylase	9	1.45	0.43	0.63	0.09	**0.43**	0.008
Q68FS4	Cytosol aminopeptidase	53	1.52	0.14	0.66	0.12	**0.43**	<0.001
Q07071	Glucokinase regulatory protein	27	1.71	0.64	0.74	0.35	**0.43**	0.037
P08009	Glutathione S-transferase Yb-3	53	1.1	0.29	0.48	0.18	**0.44**	0.02
P55051	Fatty acid-binding protein, brain	9	1.61	0.57	0.71	0.31	**0.44**	0.041
P85973	Purine nucleoside phosphorylase	41	1.12	0.2	0.49	0.17	**0.44**	0.009
P14669	Annexin A3	17	1.09	0.27	0.49	0.12	**0.45**	0.007
P25409	Alanine aminotransferase 1	19	0.85	0.09	0.38	0.08	**0.45**	0.001
P27364	3 beta-hydroxysteroid dehydrogenase type 5	19	1.41	0.31	0.64	0.13	**0.45**	0.004
P10860	Glutamate dehydrogenase 1, mitochondrial	118	1.63	0.34	0.74	0.34	**0.45**	0.037
P97562	Peroxisomal acyl-coenzyme A oxidase 2	38	1.45	0.15	0.66	0.34	**0.46**	0.038

O88813	Long-chain-fatty-acid--CoA ligase 5	28	1.89	0.67	0.87	0.04	**0.46**	0.015
P24329	Thiosulfate sulfurtransferase	41	1.33	0.2	0.62	0.19	**0.47**	0.006
O89000	Dihydropyrimidine dehydrogenase [NADP+]	12	1.36	0.32	0.64	0.12	**0.47**	0.011
Q920P0	L-xylulose reductase	12	1.44	0.45	0.69	0.1	**0.48**	0.013
A0JPQ8	Alkylglycerol monooxygenase	6	1.64	0.2	0.78	0.08	**0.48**	<0.001
P00884	Fructose-bisphosphate aldolase B	129	1.31	0.33	0.64	0.1	**0.49**	0.006
P13107	Cytochrome P450 2B3	27	1.48	0.55	0.72	0.11	**0.49**	0.036
Q6AXX6	Redox-regulatory protein PAMM	8	1.54	0.33	0.75	0.24	**0.49**	0.015
Q4KLZ6	Bifunctional ATP-dependent dihydroxyacetone kinase/FAD-AMP lyase (cyclizing)	64	1.7	0.39	0.83	0.18	**0.49**	0.009
Q66H45	Tetratricopeptide repeat protein 36	5	1.2	0.34	0.59	0.21	**0.49**	0.036
P12938	Cytochrome P450 2D3	46	1.52	0.33	0.75	0.12	**0.5**	0.006
P10868	Guanidinoacetate N-methyltransferase	16	1.58	0.51	0.79	0.18	**0.5**	0.028
Q5I0M2	Nicotinate-nucleotide pyrophosphorylase [carboxylating]	11	1.28	0.42	0.64	0.13	**0.5**	0.035
Q5U2Q3	Ester hydrolase C11orf54 homolog	12	2	0.36	1.01	0.3	**0.51**	0.015
Q63150	Dihydropyrimidinase	29	1.41	0.17	0.72	0.33	**0.51**	0.021
Q9Z339	Glutathione S-transferase omega-1	10	1.42	0.4	0.72	0.28	**0.51**	0.048
Q63448	Peroxisomal acyl-coenzyme A oxidase 3	27	1.27	0.23	0.65	0.09	**0.51**	0.003
Q9WUS0	Adenylate kinase isoenzyme 4, mitochondrial	14	1.38	0.19	0.71	0.15	**0.52**	0.004
Q9WU49	Calcium-regulated heat stable protein 1	7	1.17	0.2	0.61	0.17	**0.52**	0.009
P70712	Kynureninase	19	1.41	0.32	0.74	0.08	**0.52**	0.008
P57113	Maleylacetoacetate isomerase	36	1.58	0.34	0.83	0.37	**0.53**	0.035
Q7TP48	Adipocyte plasma membrane-associated protein	10	1.55	0.48	0.83	0.07	**0.53**	0.026
P97612	Fatty-acid amide hydrolase 1	26	1.67	0.31	0.9	0.31	**0.54**	0.029
P00173	Cytochrome b5	31	1.37	0.2	0.76	0.14	**0.55**	0.005
Q6P7R8	Estradiol 17-beta-dehydrogenase 12	6	1.15	0.2	0.64	0.14	**0.56**	0.014
P55159	Serum paraoxonase/arylesterase 1	17	1.68	0.55	0.94	0.06	**0.56**	0.037
Q64232	Very-long-chain enoyl-CoA reductase	35	1.76	0.41	0.99	0.22	**0.56**	0.017
Q02974	Ketohexokinase	25	1.56	0.28	0.89	0.2	**0.57**	0.015
Q497B0	Omega-amidase NIT2	34	1.58	0.09	0.9	0.26	**0.57**	0.008
Q9QZH8	Arylacetamide deacetylase	6	1.64	0.55	0.93	0.07	**0.57**	0.038
Q9QZX8	Solute carrier organic anion transporter family member 1B2	3	1.36	0.4	0.78	0.05	**0.57**	0.021

P04937	Fibronectin	27	0.74	0.22	0.43	0.01	**0.58**	0.041
Q6AXM8	Serum paraoxonase/arylesterase 2	8	1.1	0.24	0.65	0.19	**0.59**	0.046
P52873	Pyruvate carboxylase, mitochondrial	134	1.16	0.13	0.68	0.14	**0.59**	0.005
B0BNG0	Tetratricopeptide repeat protein 35	11	1.31	0.3	0.77	0.15	**0.59**	0.022
P29147	D-beta-hydroxybutyrate dehydrogenase, mitochondrial	42	1.4	0.23	0.83	0.28	**0.59**	0.033
O35331	Pyridoxal kinase	13	1.22	0.21	0.73	0.2	**0.6**	0.032
P41034	Alpha-tocopherol transfer protein	16	1.28	0.15	0.77	0.15	**0.6**	0.008
P25093	Fumarylacetoacetase	48	1.45	0.12	0.88	0.24	**0.61**	0.015
Q498D5	Regulator of microtubule dynamics protein 2	8	1.34	0.14	0.83	0.34	**0.62**	0.044
Q9QYU4	Thiomorpholine-carboxylate dehydrogenase	9	1.31	0.25	0.81	0.25	**0.62**	0.039
Q06647	ATP synthase subunit O, mitochondrial	35	1.09	0.27	0.67	0.08	**0.62**	0.043
P0C2X9	Delta-1-pyrroline-5-carboxylate dehydrogenase, mitochondrial	43	1.3	0.1	0.81	0.23	**0.62**	0.016
P09456	cAMP-dependent protein kinase type I-alpha regulatory subunit	7	1.22	0.2	0.76	0.14	**0.62**	0.018
Q6DGG1	Alpha/beta hydrolase domain-containing protein 14B	12	1.36	0.25	0.85	0.2	**0.63**	0.031
P08503	Medium-chain specific acyl-CoA dehydrogenase, mitochondrial	26	1.49	0.32	0.94	0.13	**0.63**	0.024
P70473	Alpha-methylacyl-CoA racemase	18	1.07	0.04	0.68	0.19	**0.64**	0.024
Q5M876	Aspartoacylase-2	5	1.35	0.26	0.88	0.04	**0.65**	0.013
Q68FP2	Serum paraoxonase/lactonase 3	16	1.43	0.1	0.95	0.13	**0.66**	0.003
Q99MS0	SEC14-like protein 2	16	1.32	0.14	0.88	0.19	**0.67**	0.02
Q66HG4	Aldose 1-epimerase	5	1.37	0.18	0.93	0.13	**0.68**	0.015
Q6I7R3	Isochorismatase domain-containing protein 1	10	1.44	0.23	0.97	0.06	**0.68**	0.017
Q63524	Transmembrane emp24 domain-containing protein 2	8	1.29	0.21	0.89	0.09	**0.69**	0.018
P41562	Isocitrate dehydrogenase [NADP] cytoplasmic	59	1.21	0.08	0.88	0.15	**0.72**	0.014
P17764	Acetyl-CoA acetyltransferase, mitochondrial	60	1.28	0.07	0.93	0.15	**0.72**	0.009
Q9Z1W6	Protein LYRIC	7	1.17	0.14	0.87	0.05	**0.75**	0.011
P27605	Hypoxanthine-guanine phosphoribosyltransferase	12	1.35	0.2	1.01	0.06	**0.75**	0.035
Q64057	Alpha-aminoadipic semialdehyde dehydrogenase	55	1.17	0.2	0.89	0.07	**0.76**	0.05
P60892	Ribose-phosphate pyrophosphokinase 1	6	1.08	0.15	0.84	0.04	**0.78**	0.035
P85108	Tubulin beta-2A chain	72	1.11	0.05	0.88	0.12	**0.79**	0.021

O88941	Mannosyl-oligosaccharide glucosidase	12	1.13	0.13	0.89	0.1	**0.79**	0.044
P11507	Sarcoplasmic/endoplasmic reticulum calcium ATPase 2	30	1.01	0.1	0.81	0.07	**0.8**	0.028
Q7TQ16	Cytochrome b-c1 complex subunit 8	4	0.99	0.06	0.8	0.06	**0.81**	0.01
P35738	2-oxoisovalerate dehydrogenase subunit beta, mitochondrial	13	1.23	0.12	1.03	0.05	**0.84**	0.039
B2RYT9	Translational activator of cytochrome c oxidase 1	3	1.1	0.1	0.93	0.05	**0.84**	0.043
Q62920	PDZ and LIM domain protein 5	5	1	0.03	0.93	0.03	**0.93**	0.019
Proteins increased at 96h								
P04906	Glutathione S-transferase P	12	0.26	0.22	3.37	1.12	**12.94**	0.002
P38918	Aflatoxin B1 aldehyde reductase member 3	42	0.2	0.17	2.42	0.14	**11.89**	0.002
P05982	NAD(P)H dehydrogenase [quinone] 1	8	0.5	0.12	3.08	2.86	**6.14**	0.044
O70199	UDP-glucose 6-dehydrogenase	38	0.32	0.1	1.82	0.75	**5.76**	0.001
P07687	Epoxide hydrolase 1	54	0.4	0.19	2.11	0.48	**5.32**	0.004
P04903	Glutathione S-transferase alpha-2	51	0.54	0.23	2.46	0.87	**4.58**	0.005
O89049	Thioredoxin reductase 1, cytoplasmic	17	0.42	0.29	1.57	0.29	**3.78**	0.026
P08430	UDP-glucuronosyltransferase 1-6	40	0.58	0.23	2.06	0.36	**3.52**	0.003
Q9Z0U5	Aldehyde oxidase	52	0.68	0.2	2.21	0.58	**3.23**	0.002
P05370	Glucose-6-phosphate 1-dehydrogenase	15	0.38	0.22	1.2	0.33	**3.13**	0.028
P13383	Nucleolin	21	0.47	0.15	1.43	0.11	**3.07**	0.001
Q62651	Delta(3,5)-Delta(2,4)-dienoyl-CoA isomerase, mitochondrial	17	0.62	0.2	1.76	0.44	**2.83**	0.005
P48508	Glutamate--cysteine ligase regulatory subunit	9	0.68	0.26	1.74	0.31	**2.57**	0.021
P23965	Enoyl-CoA delta isomerase 1, mitochondrial	18	0.59	0.37	1.46	0.3	**2.5**	0.046
P18437	Non-histone chromosomal protein HMG-17	3	0.51	0.22	1.26	0.52	**2.49**	0.037
Q9Z2Y0	Glycine N-acyltransferase-like protein Keg1	6	0.79	0.21	1.94	0.24	**2.45**	0.003
O35547	Long-chain-fatty-acid--CoA ligase 4	9	0.78	0.11	1.88	0.58	**2.4**	0.003
P51647	Retinal dehydrogenase 1	29	0.85	0.45	2	0.05	**2.35**	0.04
Q99PS8	Histidine-rich glycoprotein	9	1.03	0.33	2.41	0.76	**2.34**	0.027
P13084	Nucleophosmin	14	0.51	0.21	1.17	0.03	**2.29**	0.036
P17475	Alpha-1-antiproteinase	39	0.47	0.18	1.08	0.28	**2.28**	0.022
P13221	Aspartate aminotransferase, cytoplasmic	30	0.51	0.2	1.15	0.05	**2.26**	0.016
Q3B8Q1	Nucleolar RNA helicase 2	7	0.48	0.2	1.06	0.16	**2.21**	0.021

Q64633	UDP-glucuronosyltransferase 1-7	23	0.72	0.2	1.58	0.26	**2.2**	0.009
Q9EQS0	Transaldolase	15	0.73	0.09	1.58	0.6	**2.18**	0.011
O35821	Myb-binding protein 1A	15	0.53	0.17	1.16	0.11	**2.17**	0.01
P19468	Glutamate--cysteine ligase catalytic subunit	22	0.87	0.17	1.74	0.13	**2.01**	0.002
P06761	78 kDa glucose-regulated protein	112	0.69	0.25	1.37	0.23	**1.99**	0.029
Q6P6S9	Ectonucleoside triphosphate diphosphohydrolase 5	12	0.79	0.26	1.55	0.4	**1.96**	0.026
P70619	Glutathione reductase (Fragment)	8	0.68	0.17	1.31	0.32	**1.94**	0.019
Q6P747	Heterochromatin protein 1-binding protein 3	4	0.91	0.19	1.75	0.51	**1.93**	0.019
P18886	Carnitine O-palmitoyltransferase 2, mitochondrial	21	0.84	0.19	1.59	0.48	**1.89**	0.037
P63102	14-3-3 protein zeta/delta	26	0.63	0.11	1.17	0.07	**1.85**	0.002
Q5M827	Pirin	3	0.78	0.33	1.45	0.2	**1.85**	0.048
P48721	Stress-70 protein, mitochondrial	67	0.75	0.14	1.39	0.32	**1.84**	0.013
P31210	3-oxo-5-beta-steroid 4-dehydrogenase	51	1.07	0.22	1.95	0.18	**1.83**	0.007
P41777	Nucleolar and coiled-body phosphoprotein 1	4	0.65	0.19	1.18	0.21	**1.82**	0.044
Q6URK4	Heterogeneous nuclear ribonucleoprotein A3	20	0.56	0.07	1.02	0.25	**1.82**	0.009
P63039	60 kDa heat shock protein, mitochondrial	161	0.87	0.3	1.58	0.22	**1.82**	0.027
P97584	Prostaglandin reductase 1	16	0.88	0.1	1.58	0.42	**1.8**	0.015
Q68FR9	Elongation factor 1-delta	19	0.75	0.2	1.35	0.43	**1.79**	0.04
P11442	Clathrin heavy chain 1	103	0.77	0.1	1.36	0.53	**1.78**	0.037
P61980	Heterogeneous nuclear ribonucleoprotein K	27	0.78	0.26	1.38	0.31	**1.77**	0.038
P04785	Protein disulfide-isomerase	89	0.89	0.3	1.57	0.32	**1.76**	0.046
P70580	Membrane-associated progesterone receptor component 1	18	0.87	0.2	1.51	0.25	**1.74**	0.015
Q9Z2G8	Nucleosome assembly protein 1-like 1	5	0.72	0.14	1.25	0.15	**1.73**	0.011
P24368	Peptidyl-prolyl cis-trans isomerase B	14	0.74	0.2	1.27	0.3	**1.72**	0.045
O35814	Stress-induced-phosphoprotein 1	24	0.72	0.16	1.23	0.31	**1.71**	0.029
P05182	Cytochrome P450 2E1	29	0.89	0.14	1.51	0.26	**1.7**	0.009
P04961	Proliferating cell nuclear antigen	4	0.41	0.07	0.69	0.16	**1.7**	0.021
P24268	Cathepsin D	12	0.86	0.3	1.47	0.32	**1.7**	0.046
P10960	Sulfated glycoprotein 1	14	0.6	0.11	1.02	0.19	**1.68**	0.013
Q6AXS5	Plasminogen activator inhibitor 1 RNA-binding protein	12	0.72	0.16	1.21	0.29	**1.66**	0.039
P62752	60S ribosomal protein L23a	8	0.78	0.12	1.26	0.07	**1.62**	0.004
P11232	Thioredoxin	7	0.69	0.12	1.11	0.05	**1.6**	0.009
P17178	Sterol 26-hydroxylase, mitochondrial	13	1.01	0.13	1.61	0.27	**1.6**	0.008

P19945	60S acidic ribosomal protein P0	24	0.68	0.12	1.08	0.16	**1.59**	0.017
Q9ER34	Aconitate hydratase, mitochondrial	46	0.78	0.23	1.23	0.08	**1.58**	0.029
Q1JU68	Eukaryotic translation initiation factor 3 subunit A	23	0.66	0.17	0.98	0.08	**1.5**	0.041
Q641Y8	ATP-dependent RNA helicase DDX1	12	0.73	0.13	1.09	0.15	**1.5**	0.025
P08082	Clathrin light chain B	3	0.67	0.13	1.01	0.09	**1.5**	0.022
P38656	Lupus La protein homolog	7	0.83	0.16	1.23	0.21	**1.49**	0.039
P62919	60S ribosomal protein L8	11	0.79	0.17	1.18	0.19	**1.49**	0.04
Q63797	Proteasome activator complex subunit 1	26	0.81	0.15	1.19	0.17	**1.48**	0.031
P62161	Calmodulin	20	0.78	0.14	1.15	0.13	**1.48**	0.024
O88600	Heat shock 70 kDa protein 4	28	0.73	0.13	1.07	0.05	**1.47**	0.011
O35244	Peroxiredoxin-6	32	0.87	0.2	1.27	0.11	**1.46**	0.045
P07151	Beta-2-microglobulin	3	0.81	0.1	1.17	0.17	**1.45**	0.012
Q68FR6	Elongation factor 1-gamma	21	0.73	0.08	1.05	0.24	**1.44**	0.044
P48679	Prelamin-A/C	35	0.78	0.07	1.12	0.25	**1.43**	0.043
Q9EPH8	Polyadenylate-binding protein 1	24	0.82	0.14	1.15	0.05	**1.4**	0.022
Q5M875	17-beta-hydroxysteroid dehydrogenase 13	22	1.09	0.17	1.51	0.14	**1.39**	0.024
Q05096	Myosin-Ib	94	1.03	0.04	1.42	0.01	**1.38**	<0.001
P14942	Glutathione S-transferase alpha-4	12	0.99	0.12	1.37	0.23	**1.38**	0.035
P04256	Heterogeneous nuclear ribonucleoprotein A1	18	0.86	0.02	1.15	0.2	**1.34**	0.019
P25113	Phosphoglycerate mutase 1	20	0.92	0.1	1.23	0.23	**1.33**	0.048
P02401	60S acidic ribosomal protein P2	31	0.71	0.09	0.93	0.11	**1.31**	0.042
B5DFC8	Eukaryotic translation initiation factor 3 subunit C	14	0.85	0.12	1.12	0.08	**1.31**	0.032
Q9Z0V6	Thioredoxin-dependent peroxide reductase, mitochondrial	10	0.87	0.13	1.13	0.1	**1.3**	0.045
P62853	40S ribosomal protein S25	9	0.76	0.12	0.97	0.05	**1.27**	0.045
Q3T1J1	Eukaryotic translation initiation factor 5A-1	13	0.84	0.08	1.03	0.04	**1.23**	0.016
Q924S5	Lon protease homolog, mitochondrial	27	1.01	0.1	1.23	0.1	**1.22**	0.033
Q9ER24	Ataxin-10	4	0.91	0.08	1.1	0.05	**1.21**	0.022
Q4G061	Eukaryotic translation initiation factor 3 subunit B	15	0.85	0.09	1.03	0.06	**1.21**	0.04
P61314	60S ribosomal protein L15	7	0.91	0.11	1.1	0.03	**1.21**	0.041
Q63584	Transmembrane emp24 domain-containing protein 10	11	0.9	0.07	1.08	0.03	**1.2**	0.014

Supplementary Table 2: Principle Component Analysis PC1 vs PC4 identifies a group of proteins which are highly expressed in rat livers after four daily doses of APAP (96 h group) and are therefore candidate proteins for further exploration of adaptation

Accession	Name
P04906	Glutathione S-transferase P
P05982	NAD(P)H dehydrogenase [quinone] 1
P38918	Aflatoxin B1 aldehyde reductase member 3
P04903	Glutathione S-transferase alpha-2
P07687	Epoxide hydrolase 1
Q9Z0U5	Aldehyde oxidase
P05179	Cytochrome P450 2C7
P06757	Alcohol dehydrogenase 1
Q99PS8	Histidine-rich glycoprotein
P50137	Transketolase
P08430	UDP-glucuronosyltransferase 1-6
O70199	UDP-glucose 6-dehydrogenase
O35547	Long-chain-fatty-acid--CoA ligase 4
P48508	Glutamate--cysteine ligase regulatory subunit
P31210	3-oxo-5-beta-steroid 4-dehydrogenase
P04905	Glutathione S-transferase Mu 1
P05182	Cytochrome P450 2E1
P05545	Serine protease inhibitor A3K
P51647	Retinal dehydrogenase 1
Q9Z2Y0	Glycine N-acyltransferase-like protein Keg1

Supplementary Table 3: Top 25 most perturbed canonical pathways, with lists of individual proteins contributing to the perturbation (Page 1/2)

LPS/IL-1 Mediated Inhibition of RXR Function	Superpathway of Melatonin Degradation	Melatonin Degradation I	Dopamine Degradation	NRF2-mediated Oxidative Stress Response	γ-linolenate Biosynthesis II (Animals)	Xenobiotic Metabolism Signaling	Serotonin Degradation	Nicotine Degradation II	Fatty Acid β-oxidation I	EIF2 Signaling	Estrogen Biosynthesis	Acute Phase Response Signaling
ACOX1	CYP1A2	CYP2E1	ALDH1A1	AKR1A1	ACSL1	MAPK1	AKR1A1	CYP2E1	ACADM	EIF3A	CYP1A2	APCS
ACOX2	CYP2C18	CYP1A2	ALDH2	AKR7A2	ACSL4	ALDH1A1	ALDH1A1	AOX1	ACSL1	EIF3B	CYP2C18	CP
ACSL1	CYP2C9	CYP2C18	ALDH3A2	AKR7A3	ACSL5	ALDH3A2	ALDH2	CYP1A2	ACSL4	EIF3C/EIF3CL	CYP2C9	FGA
ACSL4	CYP2D6	CYP2C9	ALDH4A1	AOX1	CYB5A	ALDH4A1	ALDH3A2	CYP2C18	ACSL5	EIF3J	CYP2D6	FGB
ACSL5	CYP2E1	CYP2D6	COMT	CAT	CYB5R3	ALDH5A1	ALDH4A1	CYP2C9	ECI1	EIF4A2	CYP2E1	FGG
ALDH1A1	CYP3A4	CYP3A4	MAOB	EPHX1	SLC27A2	CAT	DHRS4	CYP2D6	ECI2	EIF5	CYP3A4	FN1
ALDH3A2	CYP4F8	CYP4F8	Sult1a1	ERP29	SLC27A5	Ces1d	MAOB	CYP3A4	EHHADH	MAPK1	CYP4F8	HMOX1
ALDH4A1	CYP51A1	CYP51A1	SULT1B1	FMO1		CYP1A2	Sult1a1	CYP4F8	HADH	PABPC1	CYP51A1	HNRNPK
ALDH5A1	MAOB	Sult1a1	SULT1C3	GCLC		CYP2C9	SULT1B1	CYP51A1	HSD17B4	RPL15	HSD17B12	HP
CAT	Sult1a1	SULT1B1		GCLM		CYP3A4	SULT1C3	FMO1	SLC27A2	RPL18	HSD17B2	HRG
CPT2	SULT1B1	SULT1C3		GSR		FMO1	UGT1A1	FMO3	SLC27A5	RPL27A	HSD17B4	MAPK1
Cyp2a2	SULT1C3	UGT1A1		GSTA1		FMO3	UGT1A4	UGT1A1		RPL3		ORM1
CYP2C9	UGT1A1	UGT1A4		GSTA5		GCLC	UGT1A6	UGT1A4		RPL38		RBP1
CYP3A4	UGT1A4	UGT1A6		GSTM1		GSTA1	Ugt1a7c	UGT1A6		RPL8		SERPINA1
Cyp4a14	UGT1A6	Ugt1a7c		GSTM2		GSTA5	Ugt2b	Ugt1a7c		RPLP0		SERPINA3
FABP1	Ugt1a7c	Ugt2b		GSTO1		GSTM1		Ugt2b		RPLP2		STAT3
FMO1	Ugt2b			GSTP1		GSTM2				RPS16		TF
FMO3				GSTT2/GSTT2B		GSTO1				RPS18		
GSTA1				HMOX1		GSTP1				RPS21		
GSTA5				MAPK1		GSTT2/GSTT2B						
GSTM1				MGST1		HMOX1						
GSTM2				NQO1		HSP90AA1						
GSTO1				PPIB		HSP90AB1						
GSTP1				STIP1		HSP90B1						
GSTT2/GSTT2B				TXN		MAOB						
HMGCS1				TXNRD1		MGST1						
HMGCS2				VCP		NQO1						
MAOB						SULT1B1						
MGST1						SULT1C3						
SLC27A2						UGT1A1						
SLC27A5						UGT1A4						
SLCO1B3						UGT1A6						
SULT1B1						Ugt1a7c						
SULT1C3						Ugt2b						

Continued overleaf

Supplementary Table 3: Top 25 most perturbed canonical pathways, with lists of individual proteins contributing to the perturbation (Page 2/2)

Nicotine Degradation III	Bile Acid Biosynthesis, Neutral Pathway	Fatty Acid Activation	Thyroid Hormone Metabolism II (via Conjugation and/or Degradation)	Mitochondrial L-carnitine Shuttle Pathway	Aryl Hydrocarbon Receptor Signaling	Bupropion Degradation	Acetone Degradation I (to Methylglyoxal)	Glutathione-mediated Detoxification	Aldosterone Signaling in Epithelial Cells	PXR/RXR Activation	Superpathway of Cholesterol Biosynthesis
ALB	AKR1D1	ACSL1	Sult1a1	ACSL1	ALDH1A1	CYP1A2	CYP1A2	GSTA1	AHCY	ALDH1A1	ACAT1
AOX1	AMACR	ACSL4	SULT1B1	ACSL4	ALDH3A2	CYP2C18	CYP2C18	Gsta4	HSP90AA1	ALDH3A2	CYP51A1
C4A/C4B	BAAT	ACSL5	SULT1C3	ACSL5	ALDH4A1	CYP2C9	CYP2C9	GSTA5	HSP90AB1	CYP1A2	FDFT1
CYP1A2	CYP27A1	SLC27A2	UGT1A1	CPT2	ALDH5A1	CYP2D6	CYP2D6	GSTM1	HSP90B1	CYP2C9	FDPS
CYP2C18	CYP3A4	SLC27A5	UGT1A4	SLC27A2	CTSD	CYP2E1	CYP2E1	GSTM2	HSPA1A/HSPA1B	CYP3A4	HMGCS1
CYP2C9	SCP2		UGT1A6	SLC27A5	CYP1A2	CYP3A4	CYP3A4	GSTO1	HSPA5	GSTA1	HMGCS2
CYP2D6	SLC27A5		Ugt1a7c		GSTA1	CYP4F8	CYP4F8	GSTP1	HSPA8	GSTM1	IDI1
CYP2E1			Ugt2b		GSTA5	CYP51A1	CYP51A1	GSTT2/GSTT2B	HSPA9	GSTM2	NSDHL
CYP3A4					GSTM1			MGST1	HSPB1	HMGCS2	
CYP4F8					GSTM2				HSPD1	PRKAR1A	
CYP51A1					GSTO1				HSPE1	SLCO1B3	
HPX					GSTP1				HSPH1	UGT1A1	
ITIH3					GSTT2/GSTT2B				MAPK1		
UGT1A1					HSP90AA1						
UGT1A4					HSP90AB1						
UGT1A6					HSP90B1						
Ugt1a7c					HSPB1						
Ugt2b					MAPK1						
					MGST1						
					NQO1						

Supplementary Data

SCIENTIFIC REPORTS

OPEN

Adaptation to acetaminophen exposure elicits major changes in expression and distribution of the hepatic proteome

Received: 23 June 2015
Accepted: 12 October 2015
Published: 26 November 2015

R. Eakins[1,*], J. Walsh[1,*], L. Randle[2,*], R. E. Jenkins[1], I. Schuppe-Koistinen[3], C. Rowe[1], P. Starkey Lewis[1], O. Vasieva[4], N. Prats[5], N. Brillant[1], M. Auli[5], M. Bayliss[1], S. Webb[1], J. A. Rees[1], N. R. Kitteringham[1], C. E. Goldring[1] & B. K. Park[1]

Acetaminophen overdose is the leading cause of acute liver failure. One dose of 10–15 g causes severe liver damage in humans, whereas repeated exposure to acetaminophen in humans and animal models results in autoprotection. Insight of this process is limited to select proteins implicated in acetaminophen toxicity and cellular defence. Here we investigate hepatic adaptation to acetaminophen toxicity from a whole proteome perspective, using quantitative mass spectrometry. In a rat model, we show the response to acetaminophen involves the expression of 30% of all proteins detected in the liver. Genetic ablation of a master regulator of cellular defence, NFE2L2, has little effect, suggesting redundancy in the regulation of adaptation. We show that adaptation to acetaminophen has a spatial component, involving a shift in regionalisation of CYP2E1, which may prevent toxicity thresholds being reached. These data reveal unexpected complexity and dynamic behaviour in the biological response to drug-induced liver injury.

Acetaminophen (paracetamol, APAP) overdose is the leading cause of acute liver failure in the USA and UK, resulting in over 600 deaths a year in these countries[1,2]. Whilst a single dose of 10–15 g is likely to result in severe liver damage[3], prolonged exposure to acetaminophen has been shown to result in autoprotection in some patients, such that daily doses even in excess of 10 g have apparently little adverse effect. In one extreme example, APAP-induced autoprotection was demonstrated in an adult male addicted to the analgesic Percocet (APAP formulated with oxycodone), who consumed up to 65 g per day of APAP[4]. In addition, volunteers administered a daily therapeutic dose (4 g) of APAP displayed elevations in circulating liver enzymes (clinical markers of liver injury), which then resolved[5]. Autoprotection is therefore likely to be an important human defensive mechanism to prevent progressive injury resulting from drug toxicity.

Autoprotection to APAP has also been recapitulated in animal models: in mice, daily escalating doses can tolerize against liver damage within a week of treatment[4]. Our knowledge of the mechanism of hepatic adaptation is limited, and focus to date has been on select proteins implicated in APAP toxicity. APAP liver damage is caused by a metabolite – N-acetyl-p-benzoquinoneimine (NAPQI) – thus enzymes involved in the formation or detoxification of NAPQI are likely to be involved in the adaptive response. In particular, cytochrome P450 (CYP) 2E1 which activates APAP to NAPQI and the multidrug

[1]MRC Centre for Drug Safety Science, University of Liverpool, Liverpool L69 3GE, UK. [2]Liverpool John Moores University, Byrom Street, Liverpool, L3 3AF, UK. [3]Almirall S. A. R&D Centre, Barcelona, Spain. [4]Institute of Integrative Biology, University of Liverpool, Liverpool, L69 7ZL, UK. [5]AstraZeneca R&D, Innovative Medicines, Personalised Healthcare & Biomarkers, Translational Science Centre, Science for Life Laboratory, Solna, Sweden. *These authors contributed equally to this work. Correspondence and requests for materials should be addressed to G.C.E. (email: chrissy@liverpool.ac.uk)

resistance-associated proteins ABCC3 and ABCC4 (also known as MRP3 and MRP4), which transport APAP and other xenobiotics out of cells, have been implicated in the autoprotection[4,6]. Alternatively, proteins involved in the cell's natural defence systems, including those regulating glutathione (GSH), may underlie the adaptation. A recent microarray study also linked the expression of a number of novel genes to the development of tolerance to APAP[7]. Induction of flavin-containing monooxygenase-3 (FMO3), an enzyme identified in this study that has not previously been associated with APAP metabolism, was subsequently shown to be protective in an APAP autoprotection model[8].

Here, using a rat model, we have investigated this process and show that in fact the expression of as many as 30% of all proteins detected in the liver is altered during adaptation to APAP, and see a dramatic shift in the localisation of CYP2E1. This indicates that the process of adaptation to APAP-induced liver injury is more extensive and dynamic than previously thought.

Results

We examined two separate species, rat and mouse, for adaptation to repeat APAP exposure, in order to ensure that this is not a species-selective process and therefore more likely to be relevant to man. The two models were selected because of the similar sensitivity of the rat to human APAP hepatotoxicity[9–11], and because the mouse is more amenable to genetic modification in order to test the role of specific genes in the process. Rats were dosed orally with 500, 1000 or 1500 mg/kg APAP, and mice with 250, 500 or 750 mg/kg APAP. The doses were chosen in order to monitor autoprotection across a range of sub-toxic, threshold toxic and overtly toxic doses of APAP, to ensure that the drug exposure is relevant to what may occur in humans. Animals were either dosed once at 0 h with sacrifice at 2 h or 24 h, or at 24 h intervals for up to 72 h and sacrificed 24 h after the final dose administered. An outline of the dosing protocol is shown in Fig. 1a. At the 1500 mg/kg dose, at 48 h, rats exhibited rises in circulating liver enzymes, showing a peak serum alanine aminotransferase (ALT) rise 36-fold above vehicle controls, and a 33-fold serum aspartate aminotransferase (AST) rise over control (Fig. 1b,c). Both markers returned to normal levels by 96 h. Histopathology analyses were performed in order to validate the model of liver injury (representative images are shown, Fig. 1d). Although substantial hepatocellular damage was seen at 48 h, this injury had largely resolved by 72 h, despite the animals continuing to receive a daily toxic dose of APAP.

At the 750 mg/kg dose of APAP, at 48 h, mice also displayed a peak serum ALT rise, which reached 200-fold above vehicle controls, and a 67-fold serum AST rise over control (Fig. 1e,f). Both markers also returned to normal levels by 96 h. Although substantial hepatocellular damage was seen at 48 h (Fig. 1g), this injury had resolved considerably by 72 h, as in the rat model.

In order to reveal the breadth of change occurring in the liver during adaptation, we selected the rat model for comprehensive analysis using a global bioanalytical approach. While ALT levels were significantly elevated at 48 h in the rat (as they were in the mouse), indicative of substantial hepatocellular damage, the degree of overt liver tissue degeneration was low (in contrast to the mouse) as assessed by histopathology, thus allowing robust proteomic analysis. The technique of isobaric tags for relative and absolute quantification (iTRAQ) allows unambiguous identification and quantification of proteins expressed in a complex tissue matrix, and presents here a snapshot of the hepatoproteome at each of the time-points examined. Analysis of rat liver identified 2181 unique proteins, of which 1169 were common to all animals and all time-points, and were therefore amenable for statistical analysis and pathway mapping. Lists of significantly altered proteins are shown in Supplementary Tables 1a–d.

Global changes at each time-point were visualised as volcano plots (Fig. 2a–d), in which significance (y) is plotted against fold change (x). Although changes can be seen at 24 h (Fig. 2a), at 48 h (Fig. 2b; peak toxicity) the volcano plots show the greatest change in protein abundance, as indicated by the number of blue points (raw $p < 0.05$) and red points (FDR ≤ 0.05). Large numbers of protein changes are still observed at 72 h (Fig. 2c) and 96 h (Fig. 2d). Principal Component (PC) analysis was performed to identify the proteins contributing to the clearest differences in the data set as a whole (Fig. 2e). Comparing PC1 to PC4 allowed separation into three distinct groups (in Fig. 2e, see control and 24 h to the top right, 48 h and 72 h to top left, and 96 h to the bottom of the plot), thereby identifying groups of proteins contributing to the major differences between these groups (Fig. 2e). These proteins are listed in Supplementary Table 2. Numerical descriptions of significant changes are shown in Table 1.

The subset of 1169 proteins common to all animals at every time-point is expressed as a heat map (Fig. 2f), which demonstrates the similarity in protein expression levels between control and single dose livers (24 h). By contrast, the profile of the same proteins in the repeat dose livers (48 h and 72 h) appears markedly changed. By 96 h a further shift in the protein expression profile is seen, consistent with the clustering shown in Fig. 2e. These observations are consistent with immunoblot data carried out on four proteins (Fig. 2g), selected from the mass spectrometric data for their different properties as sentinels of metabolic function or regeneration: Glutathione S-transferase P1 (GSTP1), NAD(P)H dehydrogenase [quinone] 1 (NQO1), Proliferating cell nuclear antigen (PCNA), and vimentin (VIM). NQO1 and GSTP1 are important enzymes in the detoxification of NAPQI, the toxic metabolite of APAP. PCNA is a marker of replication[12], and indicates a surge in proliferative activity in the rats which peaks at 72 h. VIM is a classical marker of progenitor cells and is upregulated in cells that are undergoing epithelial to mesenchymal transition, a process implicated in wound healing and organ fibrosis[13,14]. Overall, the data indicate a much wider response in adaptation than has been posited previously, not only implicating proteins directly involved in APAP metabolism.

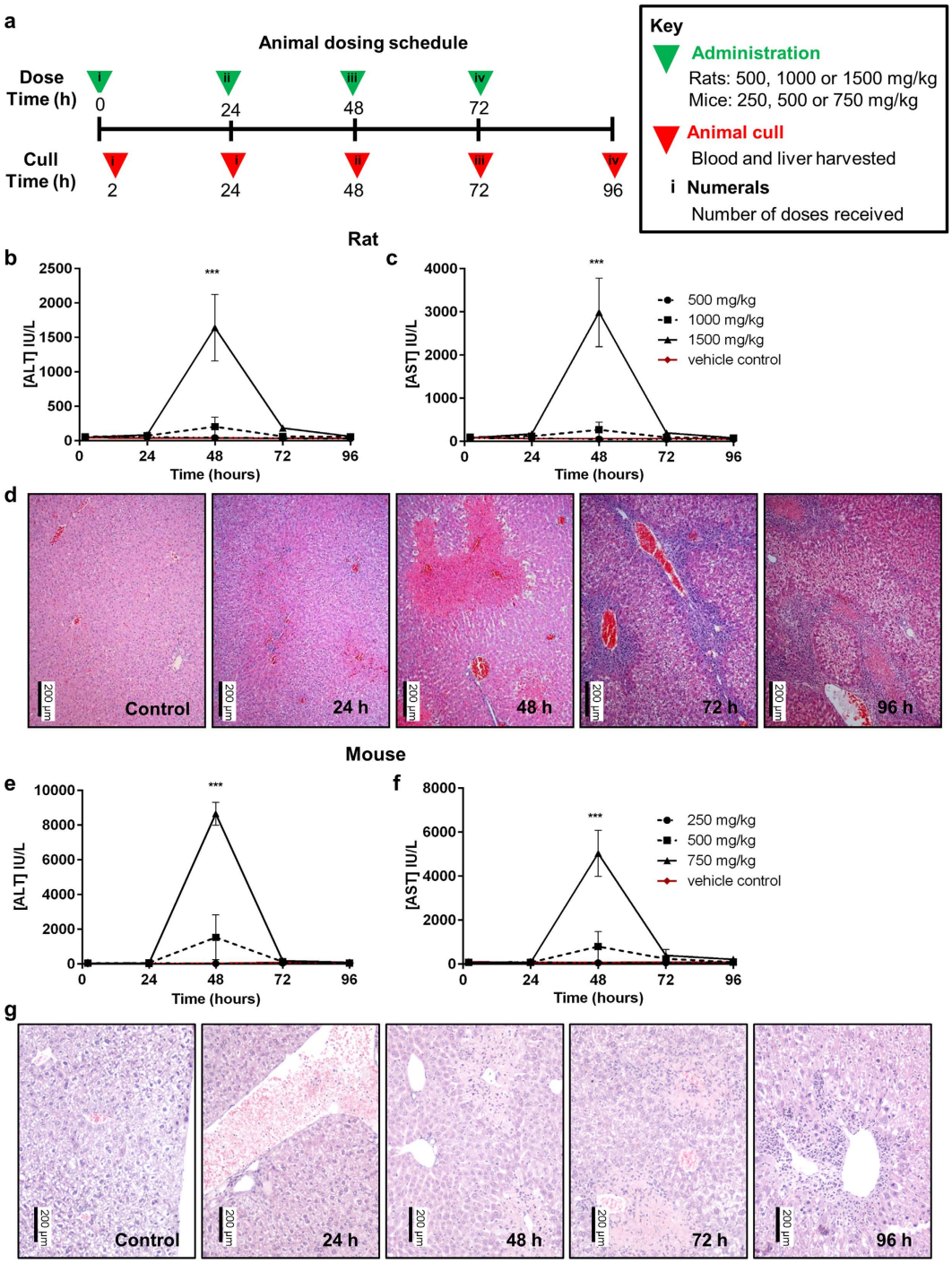

Figure 1. Autoprotection occurs in the rat and the mouse following repeat acetaminophen exposure. (**a**) Dosing protocol used in the study. (**b**) ALT and (**c**) AST were determined in rat serum (n = 6). Both biomarkers were significantly elevated in the 1500 mg/kg dose group alone (ANOVA with Tukey post-test, ***$p < 0.001$; 500 mg/kg circle, 1000 mg/kg square, 1500 mg/kg triangle, vehicle control diamond). (**d**) H&E staining of liver slices for groups of rats at each time-point in 1500 mg/kg group showed progression of injury (n = 4, representative images shown). (**e**) ALT and (**f**) AST were determined in mouse serum (n = 6). Both biomarkers were significantly elevated in the 750 mg/kg dose group alone (ANOVA with Tukey post-test, ***$p < 0.001$; 250 mg/kg circle, 500 mg/kg square, 750 mg/kg triangle, vehicle control diamond). (**g**) H&E staining of liver slices for groups of mice at each time-point in 750 mg/kg group showed progression of injury (n = 4, representative images shown).

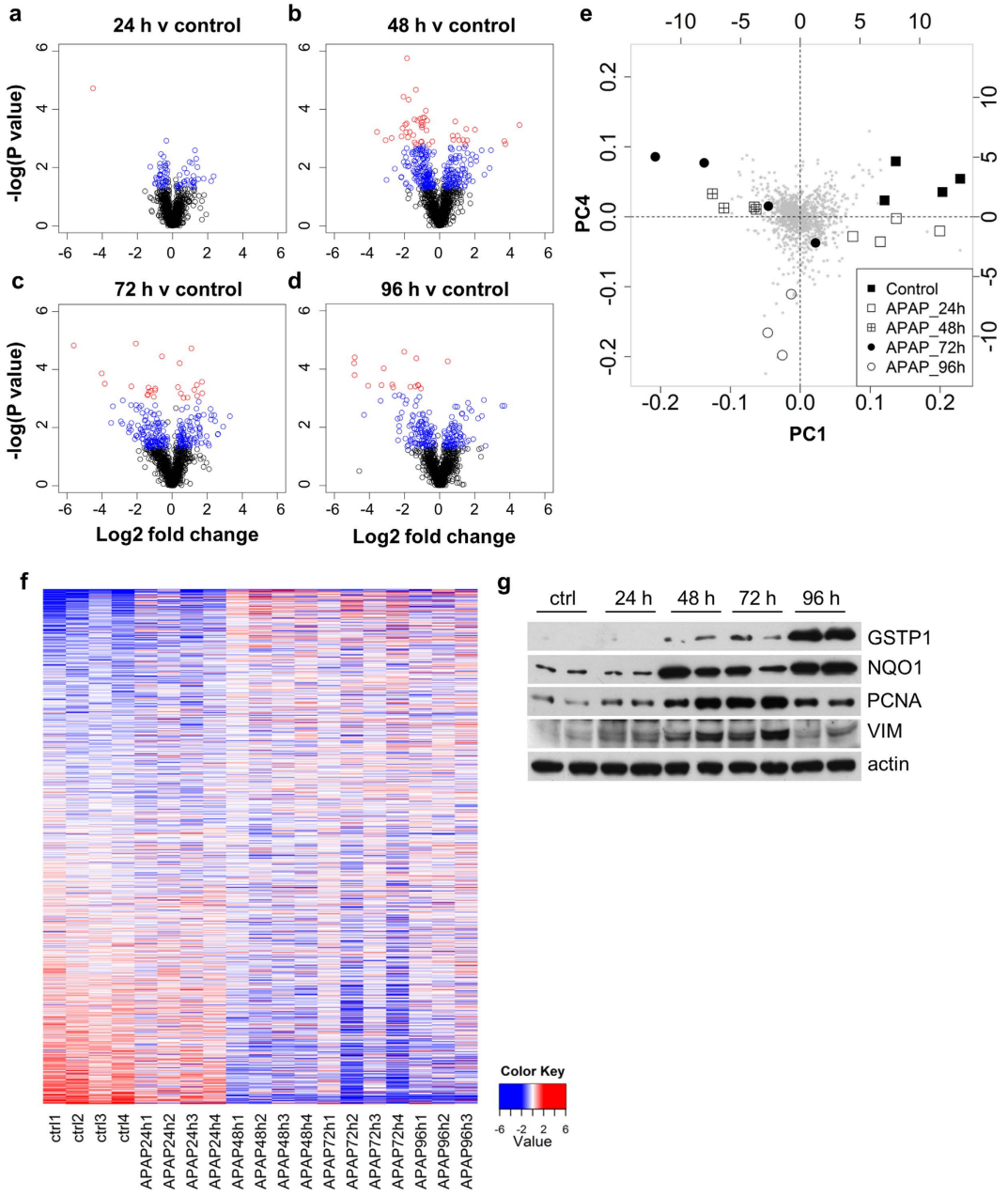

Figure 2. Widespread changes in protein abundance occur in rat liver following repeated acetaminophen exposure. (**a**–**d**) Volcano plots of all common proteins quantified by iTRAQ analysis, at each time-point (**a**) 24 h, (**b**) 48 h, (**c**) 72 h, (**d**) 96 h, relative to vehicle control. A complete list is provided in Supplementary Tables 1a–d. Coloured circles represent differential expression (blue - raw P value, $p < 0.05$; red – FDR, $p \leq 0.05$). (**e**) Principal Components Analysis identified the greatest differences between single and repeat dose samples. (**f**) Heat map representing the 1169 proteins common to all samples and all time-points identified distinct changes in protein abundance in repeat-dosed animals (red indicates increased abundance, blue indicates decreased abundance). (**g**) Western blots for GSTP1, NQO1, PCNA and VIM, performed in order to validate proteomic findings. Representative blots of two rats at each time-point are shown. Actin was used as a loading control.

Ingenuity pathway analysis identified the top twenty-five most perturbed canonical pathways during the process of adaptation to APAP (Fig. 3, a full list of proteins is shown in Supplementary Table 3). The changes highlight alterations in pathways that could be anticipated in our model, e.g. *NFE2L2-mediated oxidative stress response* and *the acute phase response* and others that were unexpected, e.g. *melatonin degradation and dopamine degradation*. This indicates, on a pathway-scale, that autoprotection to APAP involves a range of liver processes that are much more diverse than previously recognised.

Timepoint (h)	Doses administered	Proteins increased abundance ($p < 0.05$)	Proteins decreased abundance ($p < 0.05$)	Total	Percentage of quantifiable proteome
24	1	30	43	73	6.24
48	2	116	199	315	26.95
72	3	111	145	256	21.90
96	4	86	125	211	18.05

Table 1. Relative changes in protein abundance in rat liver in response to repeat acetaminophen exposure. The number of proteins that were increased or decreased in abundance in rat liver at each timepoint compared to control animals is indicated. The total number of changed proteins is expressed as a percentage of the total number of proteins quantified in the analysis (1169).

	(-log)p INCREASED abundance proteins				(-log)p DECREASED abundance proteins				Total Proteins
CANONICAL PATHWAY	24	48	72	96	24	48	72	96	
LPS/IL-1 Mediated Inhibition of RXR Function	0.32	0	0	1.64	3.91	13.59	9.16	10.01	34
Superpathway of Melatonin Degradation	1.86	0.33	0	1.98	1.68	10.78	5.14	5.49	17
Melatonin Degradation I	1.92	0.36	0	2.06	1.73	9.92	5.34	5.7	16
Dopamine Degradation	0	0	0	0.83	2.58	9.14	5.43	7.29	9
NFE2L2-mediated Oxidative Stress Response	1.86	4.26	1.77	9.53	0	3.11	2.33	0.55	27
γ-linolenate Biosynthesis II (Animals)	0	0	0	0.92	4.53	6.69	4.4	6.21	7
Xenobiotic Metabolism Signaling	0.74	1.76	0.7	2.46	0.59	6.89	4.78	3.94	34
Serotonin Degradation	0.82	0.36	0	2.09	1.75	7.61	4.31	3.53	15
Nicotine Degradation II	1.85	0.33	0	2.94	0	7.11	3.06	4.32	16
Fatty Acid β-oxidation I	0	0	0	1.6	2.19	7.29	4.4	3.41	11
EIF2 Signaling	0.45	7.71	3.58	4.95	1.79	0	0	0	19
Estrogen Biosynthesis	0.93	0	0	0.56	0	7.59	3.86	5.32	11
Acute Phase Response Signaling	6.13	6.57	3.73	0.8	0	0	0	0.23	21
Nicotine Degradation III	1.94	0.36	0	3.13	0	6.47	2.36	2.55	18
Bile Acid Biosynthesis, Neutral Pathway	0	0	0	2.15	1.21	5.17	2.99	4.6	7
Fatty Acid Activation	0	0	0	1.07	3.09	4.51	3.5	3.66	5
Thyroid Hormone Metabolism II (via Conj'n &or Degr'n)	1.08	0.59	0	1.71	2.3	3.94	3.44	2.45	8
Mitochondrial L-carnitine Shuttle Pathway	0	0	0	2.15	2.76	3.79	2.99	3.14	6
Aryl Hydrocarbon Receptor Signaling	0.45	2.46	2.79	2.35	0	3.04	2.08	1.15	20
Bupropion Degradation	1.06	0	0	0.69	0	6.27	2.25	3.56	8
Acetone Degradation I (to Methylglyoxal)	1.06	0	0	0.69	0	6.27	2.25	3.56	8
Glutathione-mediated Detoxification	0	0.57	0.63	2.85	0	5.01	3.36	1.38	9
Aldosterone Signaling in Epithelial Cells	0.56	8.06	3.46	1.33	0	0	0	0	13
PXR/RXR Activation	0	0	0	0.36	0	5.3	3.56	3.84	12
Superpathway of Cholesterol Biosynthesis	0	0	0	0	2.22	2.7	0.49	7.57	8

Figure 3. Analysis of the rat liver proteome reveals widespread pathway changes in response to repeat acetaminophen exposure. Ingenuity pathway analysis showing the top twenty-five most perturbed canonical pathways during the process of adaptation to APAP exposure. The left panel shows the significance of increased abundance proteins and the right panel show significance of reduced abundance proteins. The final column denotes the number of unique proteins identified per canonical pathway. Lists are shown in Supplementary Table 3. Values in red are significant with colour intensity proportional to significance.

Changes in the proteins responsible for the disposition of most drugs, the so-called Phase I, II and III proteins, were explored in more depth (Fig. 4a–d). Thirteen out of the twenty-three quantified CYP enzymes, the single most important set of proteins that govern how the liver initially processes a drug, were found to be present at lower abundance at 48 h. This included CYP2E1, which is largely expressed in the centrilobular region of the liver and CYP2C6, which is expressed across all zones of the liver (36% and 30% of control values, respectively), although both of these proteins increased after 96 h (Fig. 4a,b). The majority of detected phase I and II proteins decreased during the process of adaptation to APAP. Notable exceptions to this were NQO1 and GSTP1. Both of these enzymes were more abundant at 48 h (273% and 269% of control values respectively, Fig. 4c), as well as at 96 h (Fig. 4d). The profound changes in the phenotype of the liver shown here after two successive doses of APAP are likely to influence the fate of subsequent APAP exposure. Importantly, there was no evidence from analysis of intrahepatic albumin expression for a global loss of hepatocytes during the process of adaptation to APAP (Fig. 4e).

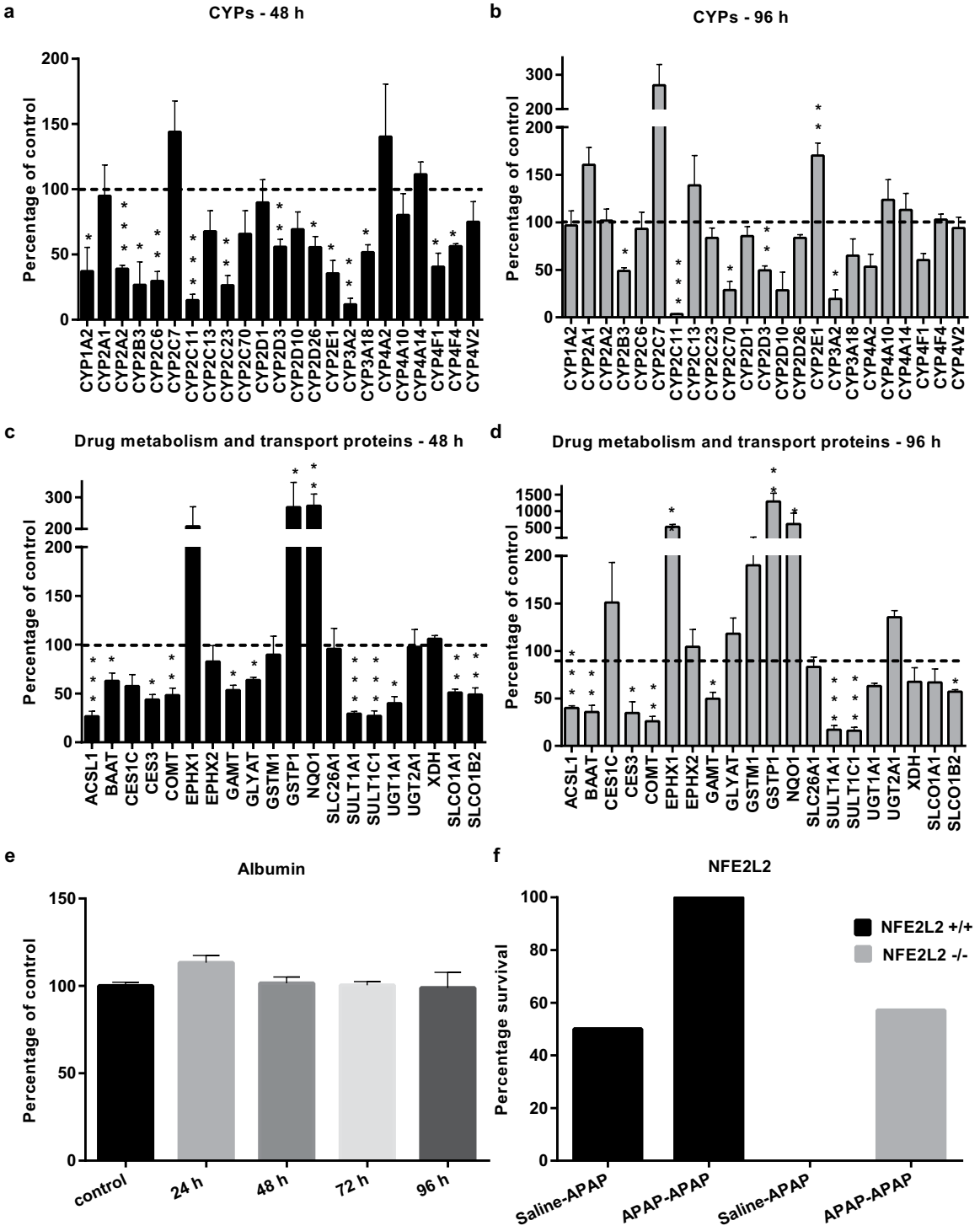

Figure 4. Investigation of key liver pathways identified by proteomic analysis in response to repeat acetaminophen exposure. In rats, while the abundance of phase I (CYP450) proteins at (**a**) 48 h and (**b**) 96 h, and phase II and III proteins at (**c**) 48 h and (**d**) 96 h was altered compared to control, serum albumin (**e**) remained statistically unchanged throughout the timecourse. Bars represent mean protein abundance (n = 3–4; percentage of control +SEM). Dashed lines indicate mean control value. Statistical analysis was performed using a linear model in the R programming environment (ANOVA with Dunnett's post-test, *$p < 0.05$, **$p < 0.01$, ***$p < 0.001$). (**f**) Survival of NFE2L2$^{+/+}$ and NFE2L2$^{-/-}$ mice in APAP adaptation study. Bar chart comparing survival of toxic challenge after APAP or saline (0.9%) pretreatment in NFE2L2$^{+/+}$ or NFE2L2$^{-/-}$ animals. Mice were pretreated with incremental doses of APAP ranging from 150–600 mg/kg i.p. or vehicle control for 8 days followed by a final challenge of 1000 mg/kg APAP or vehicle on day 9.

Together with the ALT and histopathology data (Fig. 1), these observations indicate that although there is evidence of significant injury at 48 h, with key protein changes, albumin, a classical marker of liver function, remains invariant.

To look at the level of redundancy in the process of autoprotection to APAP, we then investigated the role of one of the key processes identified by pathway analysis, as described above, namely the 'NFE2L2-mediated Oxidative Stress Response'. Nuclear factor erythroid 2-related factor 2 (NFE2L2; also known as NRF2) is a transcription factor that has been shown to play a vital role in the cytoprotective response against the type of oxidative and chemical stresses elicited by APAP[15–19]. We therefore employed a genetic strategy to test the hypothesis that interference with such a key pathway would affect the outcome of the adaptive response. The effect of pre-treatment with APAP on the ability of NFE2L2$^{+/+}$ and NFE2L2$^{-/-}$ mice to withstand a toxic challenge was investigated. All NFE2L2$^{+/+}$ mice pre-treated with APAP survived a toxic challenge of APAP, whereas only 50% of NFE2L2$^{+/+}$ mice which were not APAP-pre-treated survived (Fig. 4f). Amongst the NFE2L2$^{-/-}$ mice, whilst none of the animals which were not APAP-pre-treated survived, 50% of animals which were APAP-pre-treated survived, despite NFE2L2 deletion. The effect of APAP pre-treatment on the ability of NFE2L2$^{+/+}$ and NFE2L2$^{-/-}$ mice to withstand a toxic challenge is summarised (Fig. 4f), and shows that in both wild type and NFE2L2$^{-/-}$ mice, APAP pre-treatment increases survival upon toxic challenge, i.e. in the absence of a key liver defence pathway, adaptation still occurs. This clearly demonstrates for the first time that it is unlikely that a single gene or pathway underlies the complexities of the adaptive process to APAP exposure.

In fact, when we looked in greater detail at another of the key changes visualized in our proteomic analysis, we determined that the process of autoprotection is yet more complicated than straightforward changes in the expression of a specific protein. Our proteomic data for CYP2E1 (Fig. 4a,b) looked to be particularly pertinent in the process of adaptation to APAP, as it shows a loss of the pre-eminent metabolising enzyme responsible for formation of the toxic metabolite of APAP (NAPQI). We therefore looked at the metabolism of both APAP (Fig. 5a) and the CYP2E1 probe substrate chlorzoxazone (Fig. 5b) in our rat model. Whilst overall APAP metabolism was significantly increased at 96 h (Fig. 5a), specific CYP2E1 activity was reduced at 48 h and increased at 96 h (Fig. 5b). Relative CYP2E1 activity was 0.78 at 48 h, and 1.43 at 96 h, compared to control (arbitrary value of 1). These findings, which mirrored our proteomic data for CYP2E1, indicated the potential for an increase in the generation of NAPQI *in vivo*, which was difficult to resolve with the observed process of adaptation to repeated exposure.

We therefore employed immunohistochemical techniques to further probe the expression of CYP2E1. In fact, CYP2E1 is shown to undergo a profound change in its distribution within the liver during the process of adaptation to APAP (Fig. 5c). Basally, CYP2E1 is mainly expressed in centrilobular regions. Upon APAP challenge, CYP2E1 staining becomes diffuse and extends into midzonal regions. Two doses produce acute centrilobular necrosis, with markedly reduced CYP2E1 staining in centrilobular regions. At later time-points, staining extends diffusely into periportal regions which are CYP2E1-negative in control animals. This is clear evidence that the process of adaptation to APAP is yet more complex than wide-scale changes in the hepatoproteome, and may also involve a regional reprogramming of gene expression in a key step in APAP metabolism. This would not be detected if protein abundance alone was measured (Fig. 5d), which shows overall loss and re-establishment of liver CYP2E1, as predicted from the proteomic data (Fig. 4a,b). This re-direction of phase I metabolism towards the periportal areas of the liver, where the levels of the reducing buffer GSH are highest, is likely to be hepatoprotective. Critically, when we looked at expression of another protein which is highly abundant in the centrilobular region, glutamine synthetase (GLUL) we did not see the same change (Fig. 5d), showing some degree of selectivity in the restoration of adaptive liver function. This is the first time that a regio-spatial control of expression of a gene, specifically with respect to hepatic APAP autoprotection, and generally as part of a response to a pharmaceutical agent, has been shown. A graphical summary is presented in Fig. 5e and shows the evolution of key aspects of the adaptive process in this model.

Discussion

Drug induced liver injury (DILI) is a major problem both in the clinic and for the pharmaceutical industry. Our relative lack of understanding of the physiological and toxicological mechanisms involved can lead to the loss of potentially effective drugs during development. APAP poisoning is itself also a significant clinical problem[1,2]. Furthermore, APAP is probably the best characterised hepatotoxin in pre-clinical models, and therefore provides a means to interrogate the various processes of adaptation and regeneration in the liver, which are also relevant to man and may be applicable to other drugs associated with DILI.

In our model of APAP autoprotection, significant hepatotoxicity was only observed at a dose of 1500 mg/kg, confirming that the rat is relatively resistant to APAP toxicity as reported earlier[20–22]. While hepatotoxicity was evident at 48 h (35% cell death, $p < 0.001$, data not shown), significantly less or no necrosis was observed at 72 and 96 h, despite repeated exposure to APAP. Liver function was maintained at these points, as assessed by serum transaminases and albumin synthesis. These observations demonstrate an adaptive response in this model, protecting the liver from further injury, and this adaptation involves changes in a very large proportion of the expressed hepatoproteome.

Our data during the early phase of the development of the model, confirms previous studies which have shown that hepatic CYP2E1, the predominant enzyme involved in APAP metabolism and CYP1A2,

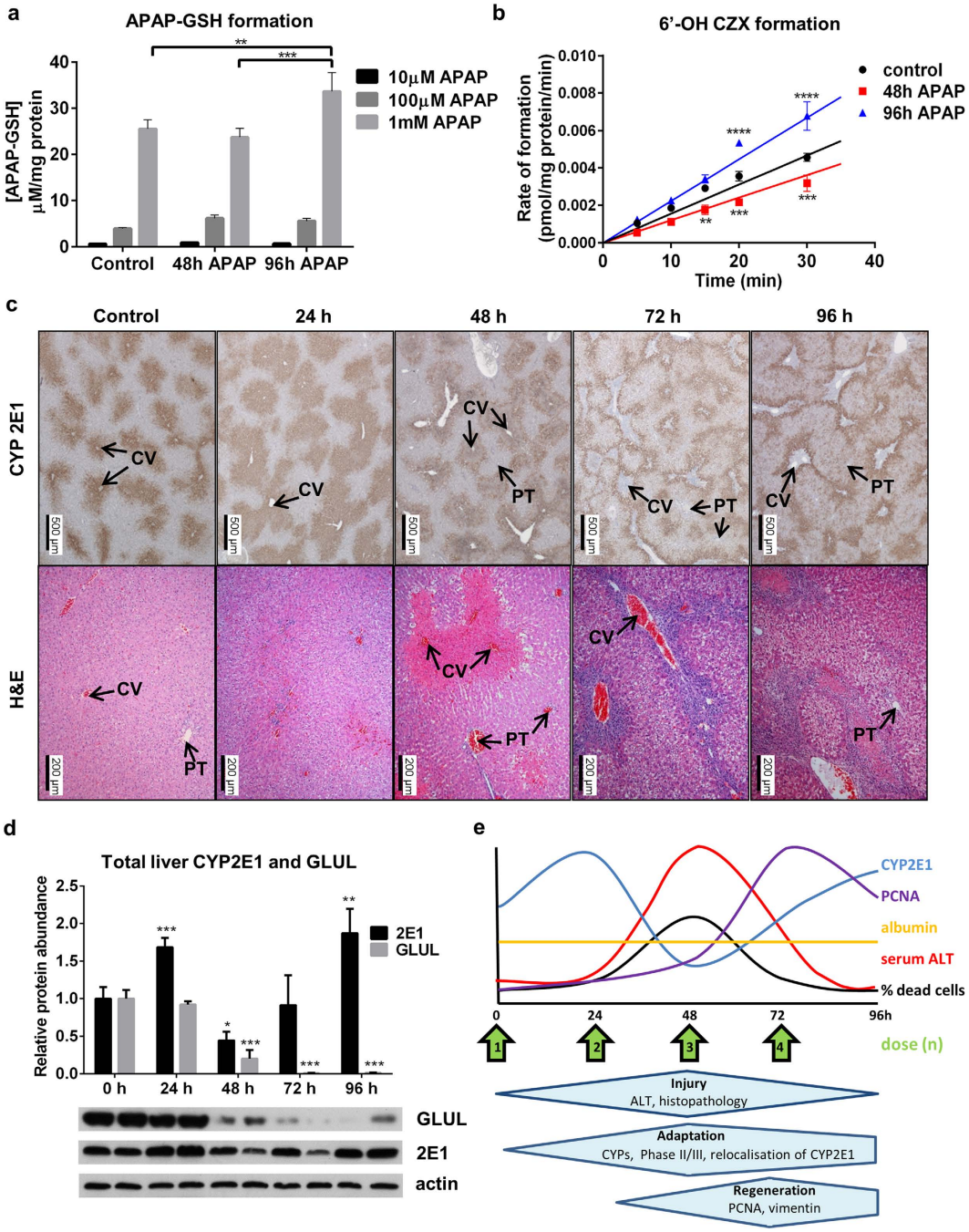

Figure 5. Rat liver CYP2E1 activity and localisation changes in response to repeat acetaminophen exposure. Microsomal formation of (**a**) APAP-GSH and (**b**) 6′-OH chlorzoxazone in animals which were either vehicle control treated, or repeat dosed with or without toxicity. Microsomal CYP2E1 activity is reduced in toxic (48 h treated, red squares) group and increased in non-toxic (96h treated, blue triangles) group compared to control (black circles). APAP metabolism is significantly higher in non-toxic (96h treated) group (**$p < 0.01$, ***$p < 0.001$, ****$p < 0.0001$). Best fit curves for each group (solid lines) were modelled using literature values for K_m and V_{max}. (**c**) Top panel shows representative IHC staining for CYP2E1 across the timecourse; bottom panel shows H&E stain. CV indicates central vein, while PT indicates the portal triad. CYP2E1 redistributes markedly as the timecourse progresses. (**d**) Densitometric analysis of total liver GLUL, CYP2E1 and actin detected by western blot, showing preferential restitution of CYP2E1 abundance over the similarly centrilobular glutamine synthetase (*$p < 0.05$, **$p < 0.01$, ***$p < 0.001$). (**e**) Graphical summary of the model.

which also plays a minor role in APAP metabolism[23,24], are depleted, whilst the rate-limiting enzyme involved in the formation of the protective tripeptide GSH, i.e. glutamate-cysteine ligase regulatory subunit (GCLC)[6,25], is increased, after pre-treatment with APAP. These proteins are likely to contribute to protection from toxicity, by reducing the CYP-catalysed bioactivation of APAP to NAPQI, and by increasing detoxification of NAPQI through enhanced synthesis of GSH. However, in this study, which is the first to formally and quantitatively assess over one thousand liver proteins from an *in vivo* model during adaptation to chemical exposure, we can now see that these changes are only one small part of a greatly altered and dynamic phenotype.

The change in the hepatoproteome may enable an adaptation that prevents toxicity from subsequent doses of APAP and maintains normal liver function despite repeated exposure to a toxic dose. Although Fig. 3, showing the top 25 most perturbed canonical pathways, indicates widespread loss of protein abundance, particularly at the peak of toxicity, a number of pathways showed increased abundance, including '*acute phase response signalling*', '*NFE2L2-mediated oxidative stress response*' and '*glutathione-mediated detoxification*' which are all well-characterised reactions to toxic injury. We therefore employed a conventional reductionist approach to examine in greater detail the role of transcription factor NFE2L2 in the process of adaptation. Whilst NFE2L2$^{-/-}$ mice showed a greater susceptibility to APAP toxicity compared to wild types, after pretreatment with APAP an adaptive response was still evident in the absence of NFE2L2, albeit to a lesser degree. NFE2L2-mediated transcription is therefore not the only mechanism of adaptation to repeated toxic insult in this model, and provides a demonstration that the process of adaptation is more wide-ranging than previously thought.

Beyond confirming existing knowledge that several CYPs relevant to APAP metabolism are down-regulated upon repeat APAP exposure, we have shown that liver tissue from repeat dosed rats shows a significantly reduced abundance of proteins across all phases of drug metabolism (Fig. 4a–d). We hypothesise that this reduction in expression represents a key facet of adaptation, and provides an environment which facilitates compensatory hyperplastic activity, preserving critical function. At the peak of toxicity, the mean of all detected CYPs is reduced to approximately 60% of control values. This change in phenotype is likely to be, at least partly, a consequence of the changing cell population in the liver over time. The initial toxic insult clearly destroys vulnerable hepatocytes at the centre of the lobule. CYP enzymes show predominantly centrilobular expression, and the differential expression of CYPs in intact zones may account for the overall change seen at 48 h. Nevertheless, a number of CYPs are pan-zonally expressed in rat liver[26], and of the ones that are also identified in the present work (1A, 2B, 2C6 and 2C7, a close homologue of the pan-zonal CYPEtOH2 enzyme[27–30]), all are significantly less abundant at 48 h, dropping to around 30% of control (with the exception of 2C7 which is not significantly changed). This suggests an active change in the phenotype of intact cells, as has been previously postulated, indicating a global dedifferentiation resulting in decreased liver-specific protein expression as part of an adaptive response to injury[31,32], rather than a passive destruction of CYP-rich tissue.

To further elucidate the complex mechanism of adaptation, we focused on CYP2E1 activity and localisation in response to repeat APAP exposure. Consistent with proteomic data obtained for CYP2E1 abundance, microsomal activity assays show a loss of activity at 48h when acute injury is seen. Despite continued APAP exposure, however, at 96h a rebound of both expression and activity of CYP2E1 is seen (Fig. 5b,d). This is not consistent with the fall in toxicity observed after 48 h (Fig. 1). We therefore examined the tissue histologically, and identified a diffuse redistribution of CYP2E1 into CYP2E1-negative regions (Fig. 5c). Importantly, the loss and restoration of total liver 2E1 was not observed for another similarly perivenous enzyme, glutamine synthetase (Fig. 5d), suggesting that this process is selective. We hypothesise from these observations that, as a defence mechanism, diffuse expression of CYP2E1 may prevent the intracellular threshold of NAPQI toxicity being reached, thereby avoiding the initiation of further waves of cell death at later timepoints. Furthermore, in the regions where NAPQI is generated after redistribution of CYP2E1 expression, there are known to be higher intracellular concentrations of the reducing buffer GSH[33]. This phenomenon of CYP2E1 redistribution as an adaptive response has only been seen after treatment with carbon tetrachloride[34] and ethanol[35], but has not been detected previously after treatment with any pharmaceutical compound.

Proliferating liver demonstrates enhanced resistance to toxicity[4,25,36], but the precise mechanism by which this occurs is unclear. Consistent with the findings presented here, rats which have been pretreated with APAP show signs of a regenerative hepatocyte response, determined through expression of PCNA, upon a second toxic challenge[25]. It has been shown that these new hepatocytes have a greater capacity for GSH production, allowing regenerating liver to detoxify NAPQI more efficiently[25], but this hypothesis needs to be investigated in our model. Furthermore, a single dose of APAP has been shown to induce the expression of the transporter protein ABCC4 in proliferating hepatocytes, peaking at 48 h after dosing[6]. A number of transporters were detected in the current work, and of those that were changed, all were decreased in abundance at 48 h and onwards. A list of the transporters can be found in Supplementary Table 4. This may demonstrate a change in the liver phenotype away from drug metabolism and towards self-preservation and regeneration. A single dose control experiment was also performed in our study, and this showed a similar profile of toxicity to the repeat dose group (Supplementary Fig. 1). When experimental animals were given subsequent exposures, this toxicity was not exacerbated, indicating that a single exposure is all that is required to initiate liver adaptive processes.

How these observations relate to the likely hepatic changes seen during chronic dosing in humans will be a key next step in this work. The identification of accessible translational biomarkers that can be used in rodents and man[37,38] will be necessary to examine whether this process occurs in man at therapeutic doses of APAP, as well as with other drugs than can cause DILI.

Materials and Methods

Materials. 8-plex iTRAQ protein labelling kit/reagents were from AB Sciex (Framingham, MA). Sequencing grade trypsin was from Promega UK (Southampton, UK). PCNA, GLUL and NQO1 antibodies were from Abcam (Cambridge, UK; cat. no. ab29, ab49873 and ab2346 respectively). VIM antibody was from Sigma (St. Louis, MO; cat. no. V6389). GSTP1 antibody was from Enzo Life Sciences (Farmingdale, NY; msa-102). CYP2E1 antibody was kindly provided by Magnus Ingelman-Sundberg, Karolinska Institute, Sweden. Parent drugs for LC-MS analysis were obtained from Sigma-Aldrich (Gillingham, UK), internal standards from Toronto Research Chemicals (Toronto, Canada) and Alsachim (Illkirch-Graffenstaden, France). Metabolites were obtained from the same sources. All other reagents were of analytical grade and quality and purchased from Sigma (St. Louis, MO).

Animals. Male Crl:WI (Han) rats and Crl:CD1 (ICR) mice (6–8 weeks) from Charles River Laboratories (Lyon, France) were acclimatised for 1 week. Six animals were housed per cage, on a 12 h light/dark cycle, at constant temperature (22 ± 2 °C). Standard food and tap water were provided *ad libitum*. Care of animals was undertaken in compliance with the European Community Directive 86/609/CEE for the use of laboratory animals and with the Autonomous Catalan law (Decret 214/1997). All experimental procedures were approved by the Almirall Ethics Committee.

Study design. APAP was dissolved in vehicle (0.5% methylcellulose and 0.1% Tween 80 in distilled water, 10 ml/kg) and administered by oral (po) gavage without prior fasting. Formulations were prepared daily. Some animals (n = 6) received a single dose of APAP or vehicle at 0 h (for 2 or 24 h). Other animals (n = 6) received subsequent administrations every 24 h of APAP or vehicle for 24, 48 or 72 h and were sacrificed 24 h after last administration. Mice received 250, 500 or 750 mg/kg of APAP; rats received 500, 1000 or 1500 mg/kg of APAP. Based on clinical chemistry and histopathology analysis of liver injury, the rat 1500 mg/kg group was taken forward for further analysis. Terminal blood samples without previous fasting were collected from the retroorbital plexus under isoflurane anaesthesia (4% induction, 1.5–3% maintenance). Blood samples were centrifuged for 10 min at 3000 rpm, serum collected and stored at −80 °C. Immediately after blood collection, animals were exsanguinated by cutting the abdominal aorta under isoflurane anaesthesia.

Toxicological assessment. A Synchron Clinical System cx7® (Beckman, Brea, CA) was used to determine ALT (IU/L) and AST (IU/L). Samples of liver were frozen in liquid nitrogen before storage at −80 °C. The hepatic median lobe was formalin-fixed and embedded in paraffin, sectioned and stained with haematoxylin and eosin (H&E) for histological blind examination under light microscopy. Percentage of live cells was assessed in a complete section from each animal, and data expressed as mean ± standard error of mean (SEM).

NFE2L2$^{(-/-)}$ study. All experiments were undertaken in accordance with criteria outlined in a licence granted under the Animals (Scientific Procedures) Act 1986, and approved by the Animal Ethics Committee of the University of Liverpool. Generation of the NFE2L2 knockout mouse and genotyping of progeny have been described elsewhere[15,16]. Non-fasted male littermate NFE2L2$^{(+/+)}$ and NFE2L2$^{(-/-)}$ mice (C57BL6J background, 10–12 weeks of age) were used throughout the study. Mice were housed between 19 °C–23 °C, on a 12 h light/dark cycle, and given access to food and water *ad libitum*. Dosing began at 10 am each day and APAP was freshly prepared in warmed saline (0.9%). Pilot dose ranging studies confirmed the dose dependent nature of APAP-induced hepatotoxicity. In order to explore both the changes occurring during the pre-treatment phase and the effects of pre-treatment on susceptibility to a toxic challenge, two independent groups of mice were used:

NFE2L2$^{(+/+)}$ and NFE2L2$^{(-/-)}$ mice received increasing daily doses of APAP (2 × 150 mg/kg, 2 × 300 mg/kg, 2 × 450 mg/kg, 2 × 600 mg/kg, *i.p.*) over 8 days, or vehicle control ($n = 4$). On day 9 mice were challenged with 1000 mg/kg APAP (*i.p.)* or vehicle ($n = 4$–8). Mice were culled 5 h after the final dose by exposure to a rising concentration of CO_2 followed by cervical dislocation.

iTRAQ labelling and mass spectrometric analysis of liver homogenates. Rat liver samples (n = 4 animals per time-point, 1500 mg/kg group, ~100 mg wet weight) were homogenised in 0.5 M triethylammonium bicarbonate/0.1% SDS using a Mixer Mill 220 (Retsch, Haan, Germany), and centrifuged at 14000 g for 10 min. iTRAQ tagging and analysis was performed as described previously[39].

iTRAQ protein identification and statistical analyses. Liver samples from rats treated with APAP or vehicle control were analysed across four iTRAQ runs. Data analysis was performed using ProteinPilot (Version 3, Life Technologies, Paisley, UK). The SwissProt database was searched with a confidence interval of 95%, and screened in reverse to facilitate false discovery rate analysis. Proteins identified from

peptides with >95% confidence and global false discovery rate of <1% were included in the statistical analysis (1169 proteins).

Mean fold changes were calculated using the limma package within the R programming environment (Team, 2005) and analysis conducted on the logged fold-change values. Unadjusted (raw) p values and p values following FDR correction for multiple testing were determined.

Ontology and pathway analysis. Pathway analysis was performed using Ingenuity Pathway Analysis (Qiagen, Venlo, Netherlands). Ingenuity successfully mapped 1163/1169 proteins to pathways. At each timepoint, a 'Core Analysis' was performed on all proteins that were differentially expressed compared to control animals (raw $p < 0.05$) using the 'Ingenuity Knowledge Base (Gene Only) Background'. The canonical pathways that were statistically significantly altered at each timepoint were compared using the 'Comparison Analysis' function.

Western immunoblotting. Buffered homogenates of standardised protein concentration ($n = 4$) were run on polyacrylamide gel, transferred onto nitrocellulose membrane (GE Healthcare, Little Chalfont, UK) and visualised using Western Lightning Plus ECL (Perkin Elmer, Waltham, MA). Proteins were normalised to actin. For GLUL, equal protein loading was confirmed using a Ponceau S stain.

Enzyme activity. Microsomes were prepared from livers of animals assigned to 2 h vehicle control, 48 h APAP (repeat exposure with toxicity) or 96 h APAP (repeat exposure, no toxicity) groups by homogenisation and ultracentrifugation, quantified using the Lowry method[40], snap frozen and stored at −80 °C until required. Microsomes from individual animals were incubated with either APAP (1 mM, 100 uM or 10 uM for up to 4 h) or the CYP2E1 probe chlorzoxazone (1 uM for up to 90 mins) at 37 °C in a shaking water bath. Reactions were stopped with the addition of equal volumes of ice cold acetonitrile containing evaporation standard fluconazole and stored at −80 °C until analysis by HPLC-MS.

Analysis by HPLC-MS/MS. Test samples were treated with acetonitrile, to remove matrix-based interferences. They were diluted with water prior to analysis by LC-MS/MS on a Sciex API 4000 (Warrington, UK) equipped with a Turbo V™ electrospray source (ESI). The gradients were based on mobile phases containing 0.1% v/v formic acid in both water (A) and acetonitrile (B).

Measurement of chlorzoxazone and its putative major metabolite, 6-hydroxy chlorzoxazone. The separation was performed on a 2.7 μM Halo® C18 column (50 × 2.1 mm ID) obtained from HiChrom (Reading, UK), and at a temperature of 40 °C and a flow-rate of 0.6 mL min^{-1}. The following gradient was used: 0 min 5% B, 0.5 min 5% B, 1.5 min 95% B, 2 min 95% B, 2.1 min 5% B and 2.6 min 5% B. D^4-diclofenac was employed as the internal standard. The MS was operated in negative ion mode.

Measurement of APAP and its major metabolites. Separations were performed on a 2.6 μm Kinetex® XB-C18 column (50 × 2.1 mm ID) obtained from Phenomenex (Macclesfield, UK), at a temperature of 40 °C and a flow-rate of 0.5 mL min^{-1}. The following gradient was used: 0 min 0% B, 0.3 min 0% B then 2.3 min 50% B. The column was flushed with 100% B, and then returned to 0% B using a flow-rate of 0.7 mL min^{-1}, giving a programmed cycle time of 4.2 minutes. A panel of deuterated internal standards was employed. The MS was operated in negative ion mode for measuring all but one of the putative major metabolites and high concentrations of APAP. It was operated in positive ion mode for measuring the remaining metabolite and low concentrations of APAP.

CYP2E1 localisation via immunohistochemistry. Immunohistochemical staining for CYP2E1 was performed on formalin-fixed, paraffin-embedded liver sections of 3 μm. Sections were mounted on poly-L-lysine coated slides, air-dried, deparaffinized and rehydrated. Slides were incubated with rabbit anti CYP2E1 antibody in 20% NGS/TBS-T. Secondary antibody was SignalStain® Boost IHC Detection Reagent (HRP, rabbit; Cell Signalling Technology, Beverly, MA, USA). The reaction was developed using 3′,3′-diaminobenzidine tetrahydrochloride. Sections were counterstained with Harris haematoxylin.

Data evaluation and statistical analysis. Clinical chemistry data are expressed as mean ± SEM ($n = 6$). Serum ALT and AST data for vehicle- and APAP-treated animals were compared to time-matched controls by one-way ANOVA with Tukey's post-hoc test using GraphPad PRISM (version 6.03 for Windows, GraphPad Software, San Diego, CA). Western immunoblotting data were analysed using a one-way ANOVA with Dunnetts post-hoc test. Microsomal data were analysed using an ordinary two-way ANOVA with Dunnett's post-hoc test.

Literature estimates for K_m are reported to be 30–300 times larger[41,42] than the CZX concentration considered (1 uM) so we were able to adopt linear kinetics for CYP2E1 activity (enzyme velocity $= \alpha[S]$, where $[S] =$ CZX concentration and $\alpha = V_{max}/K_m$) instead of the full nonlinear Michaelis-Menten form. Solving the resulting first order ordinary differential equation then yields the following expression for 6′-OH CZX formation versus time (using notation $[P](t)$ to denote concentration at time t (min)): $[P](t) = [S](0)(1 - \exp(-\alpha t/V))$, where $[S](0) =$ initial CZX concentration (1 uM) and V is the sample volume (0.02 ml). We used a Levenberg Marquardt (non-linear regression) algorithm to then find best

fit values for $\alpha = V_{max}/K_m$ for the control, 48 and 96 hour cases. Note that, in each case, our estimates for $\alpha = V_{max}/K_m$ were found to lie within acceptable literature ranges. Under the assumption that enzyme-substrate binding affinity ($1/K_m$) is unaffected by microsomal conditions, ratios of α estimates were then used to compare relative enzyme activities.

References

1. Ryder, S. D. & Beckingham, I. J. ABC of diseases of liver, pancreas, and biliary system. Other causes of parenchymal liver disease. *Bmj* **322,** 290–292 (2001).
2. Larson, A. M. *et al.* Acetaminophen-induced acute liver failure: results of a United States multicenter, prospective study. *Hepatology* **42,** 1364–1372, doi: 10.1002/hep.20948 (2005).
3. Dart, R. C. *et al.* Acetaminophen poisoning: an evidence-based consensus guideline for out-of-hospital management. *Clin Toxicol (Phila)* **44,** 1–18 (2006).
4. Shayiq, R. M. *et al.* Repeat exposure to incremental doses of acetaminophen provides protection against acetaminophen-induced lethality in mice: an explanation for high acetaminophen dosage in humans without hepatic injury. *Hepatology* **29,** 451–463, doi: 10.1002/hep.510290241 (1999).
5. Borlak, J., Chatterji, B., Londhe, K. B. & Watkins, P. B. Serum acute phase reactants hallmark healthy individuals at risk for acetaminophen-induced liver injury. *Genome Med* **5,** 86, doi: 10.1186/gm493 (2013).
6. Aleksunes, L. M., Campion, S. N., Goedken, M. J. & Manautou, J. E. Acquired resistance to acetaminophen hepatotoxicity is associated with induction of multidrug rsistance-associated protein 4 (Mrp4) in proliferating hepatocytes. *Toxicol Sci* **104,** 261–273, doi: 10.1093/toxsci/kfn093 (2008).
7. O'Connor, M. A. *et al.* Analysis of changes in hepatic gene expression in a murine model of tolerance to acetaminophen hepatotoxicity (autoprotection). *Toxicol Appl Pharmacol* **274,** 156–167, doi: 10.1016/j.taap.2013.09.025 (2014).
8. Rudraiah, S. *et al.* Tolerance to acetaminophen hepatotoxicity in the mouse model of autoprotection is associated with induction of flavin-containing monooxygenase-3 (FMO3) in hepatocytes. *Toxicol Sci* **141,** 263–277, doi: 10.1093/toxsci/kfu124 (2014).
9. Bushel, P. R. *et al.* Blood gene expression signatures predict exposure levels. *Proc Natl Acad Sci USA* **104,** 18211–18216, doi: 10.1073/pnas.0706987104 (2007).
10. Hadi, M. *et al.* AMAP, the alleged non-toxic isomer of acetaminophen, is toxic in rat and human liver. *Arch Toxicol* **87,** 155–165, doi: 10.1007/s00204-012-0924-1 (2013).
11. Kienhuis, A. S. *et al.* Parallelogram approach using rat-human *in vitro* and rat *in vivo* toxicogenomics predicts acetaminophen-induced hepatotoxicity in humans. *Toxicol Sci* **107,** 544–552, doi: 10.1093/toxsci/kfn237 (2009).
12. Galand, P. & Degraef, C. Cyclin/PCNA immunostaining as an alternative to tritiated thymidine pulse labelling for marking S phase cells in paraffin sections from animal and human tissues. *Cell Tissue Kinet* **22,** 383–392 (1989).
13. Eckes, B. *et al.* Impaired wound healing in embryonic and adult mice lacking vimentin. *J Cell Sci* **113** (Pt 13), 2455–2462 (2000).
14. Zeisberg, M. *et al.* Fibroblasts derive from hepatocytes in liver fibrosis via epithelial to mesenchymal transition. *J Biol Chem* **282,** 23337–23347, doi: 10.1074/jbc.M700194200 (2007).
15. Itoh, K. *et al.* An Nrf2/small Maf heterodimer mediates the induction of phase II detoxifying enzyme genes through antioxidant response elements. *Biochem Biophys Res Commun* **236,** 313–322 (1997).
16. McMahon, M. *et al.* The Cap'n'Collar basic leucine zipper transcription factor Nrf2 (NF-E2 p45-related factor 2) controls both constitutive and inducible expression of intestinal detoxification and glutathione biosynthetic enzymes. *Cancer Res* **61,** 3299–3307 (2001).
17. Chan, K., Han, X. D. & Kan, Y. W. An important function of Nrf2 in combating oxidative stress: detoxification of acetaminophen. *Proc Natl Acad Sci USA* **98,** 4611–4616, doi: 10.1073/pnas.081082098 (2001).
18. Enomoto, A. *et al.* High sensitivity of Nrf2 knockout mice to acetaminophen hepatotoxicity associated with decreased expression of ARE-regulated drug metabolizing enzymes and antioxidant genes. *Toxicol Sci* **59,** 169–177 (2001).
19. Goldring, C. E. *et al.* Activation of hepatic Nrf2 *in vivo* by acetaminophen in CD-1 mice. *Hepatology* **39,** 1267–1276, doi: 10.1002/hep.20183 (2004).
20. Buttar, H. S., Nera, E. A. & Downie, R. H. Serum enzyme activities and hepatic triglyceride levels in acute and subacute acetaminophen-treated rats. *Toxicology* **6,** 9–20 (1976).
21. Strubelt, O., Siegers, C. P., Volpel, M. & Younes, M. Studies on the mechanism of paracetamol-induced protection against paracetamol hepatotoxicity. *Toxicology* **12,** 121–133 (1979).
22. Poulsen, H. E. & Thomsen, P. Long-term administration of toxic doses of paracetamol (acetaminophen) to rats. *Liver* **8,** 151–156 (1988).
23. Manyike, P. T., Kharasch, E. D., Kalhorn, T. F. & Slattery, J. T. Contribution of CYP2E1 and CYP3A to acetaminophen reactive metabolite formation. *Clin Pharmacol Ther* **67,** 275–282, doi: 10.1067/mcp.2000.104736 (2000).
24. Patten, C. J. *et al.* Cytochrome P450 enzymes involved in acetaminophen activation by rat and human liver microsomes and their kinetics. *Chem Res Toxicol* **6,** 511–518 (1993).
25. Dalhoff, K. *et al.* Autoprotection in acetaminophen intoxication in rats: the role of liver regeneration. *Pharmacol Toxicol* **88,** 135–141 (2001).
26. Oinonen, T. & Lindros, K. O. Zonation of hepatic cytochrome P-450 expression and regulation. *Biochem J* **329** (Pt 1), 17–35 (1998).
27. Foster, J. R. *et al.* Immunocytochemical localization of cytochrome P-450 in hepatic and extra-hepatic tissues of the rat with a monoclonal antibody against cytochrome P-450 c. *Biochem Pharmacol* **35,** 4543–4554 (1986).
28. Wojcik, E. *et al.* Demonstration by *in situ* hybridization of the zonal modulation of rat liver cytochrome P-450b and P-450e gene expression after phenobarbital. *J Clin Invest* **82,** 658–666, doi: 10.1172/jci113645 (1988).
29. Omiecinski, C. J., Hassett, C. & Costa, P. Developmental expression and *in situ* localization of the phenobarbital-inducible rat hepatic mRNAs for cytochromes CYP2B1, CYP2B2, CYP2C6, and CYP3A1. *Mol Pharmacol* **38,** 462–470 (1990).
30. Buhler, R., Lindros, K. O., Nordling, A., Johansson, I. & Ingelman-Sundberg, M. Zonation of cytochrome P450 isozyme expression and induction in rat liver. *Eur J Biochem* **204,** 407–412 (1992).
31. Ito, Y. *et al.* Depression of liver-specific gene expression in regenerating rat liver: a putative cause for liver dysfunction after hepatectomy. *J Surg Res* **51,** 143–147 (1991).
32. Kurumiya, Y. *et al.* Differential suppression of liver-specific genes in regenerating rat liver induced by extended hepatectomy. *J Hepatol* **32,** 636–644 (2000).
33. Sastre, J. *et al.* Effect of aging on metabolic zonation in rat liver: acinar distribution of GSH metabolism. *Mech Ageing Dev* **62,** 181–190 (1992).
34. Irie, H. *et al.* Striking LD50 variation associated with fluctuations of CYP2E1-positive cells in hepatic lobule during chronic CCl4 exposure in mice. *Virchows Arch* **456,** 423–431, doi: 10.1007/s00428-009-0872-1 (2010).
35. Bertola, A., Mathews, S., Ki, S. H., Wang, H. & Gao, B. Mouse model of chronic and binge ethanol feeding (the NIAAA model). *Nat Protoc* **8,** 627–637, doi: 10.1038/nprot.2013.032 (2013).

36. Chanda, S., Mangipudy, R. S., Warbritton, A., Bucci, T. J. & Mehendale, H. M. Stimulated hepatic tissue repair underlies heteroprotection by thioacetamide against acetaminophen-induced lethality. *Hepatology* **21,** 477–486 (1995).
37. Antoine, D. J. *et al.* Molecular forms of HMGB1 and keratin-18 as mechanistic biomarkers for mode of cell death and prognosis during clinical acetaminophen hepatotoxicity. *J Hepatol* **56,** 1070–1079, doi: 10.1016/j.jhep.2011.12.019 (2012).
38. Antoine, D. J. *et al.* Mechanistic biomarkers provide early and sensitive detection of acetaminophen-induced acute liver injury at first presentation to hospital. *Hepatology* **58,** 777–787, doi: 10.1002/hep.26294 (2013).
39. Walsh, J. *et al.* Identification and quantification of the basal and inducible Nrf2-dependent proteomes in mouse liver: Biochemical, pharmacological and toxicological implications. *J Proteomics*, doi: 10.1016/j.jprot.2014.05.007 (2014).
40. Lowry, O. H., Rosebrough, N. J., Farr, A. L. & Randall, R. J. Protein measurement with the Folin phenol reagent. *J Biol Chem* **193,** 265–275 (1951).
41. Muzeeb, S., Pasha, M. K., Basha, S. J., Mullangi, R. & Srinivas, N. R. Effect of 1-aminobenzotriazole on the *in vitro* metabolism and single-dose pharmacokinetics of chlorzoxazone, a selective CYP2E1 substrate in Wistar rats. *Xenobiotica* **35,** 825–838, doi: 10.1080/00498250500307301 (2005).
42. Guo, S. *et al.* Effects of eleutheroside B and eleutheroside E on activity of cytochrome P450 in rat liver microsomes. *BMC Complement Altern Med* **14,** 1, doi: 10.1186/1472-6882-14-1 (2014).

Acknowledgements

This work was supported by the SAFE-T programme, a European Community project under the Innovative Medicines Initiative Programme [grant agreement number 115003]. Additional support was provided by the Medical Research Council Centre for Drug Safety Science [grant number G0700654]. The authors thank Magnus Ingelman-Sundberg for his generous gift of the anti-CYP2E1 antibody. The authors thank Antanas Sleckus for help with the immunoblot analyses.

Author Contributions

Study concept and design: R.E., L.R., I.S.K., N.P., M.A., N.K. and C.G. Acquisition of data: R.E., J.W., L.R., R.J., I.S.K., N.P., M.A. and M.B. Analysis and interpretation of data: R.E., J.W., L.R., R.J., C.R., P.S.L., O.V., M.B., S.W., N.K. and C.G. Statistical analysis: R.E., J.W., L.R., C.R., O.V., S.W. and N.K. Drafting of manuscript: R.E., J.W., P.S.L. and C.G. Critical revision of manuscript: R.E., J.W., I.S.K., P.S.L., N.P., M.A., J.R., N.K., C.G. and B.K.P. Study supervision: I.S.K., N.P., M.A., N.K., C.G. and B.K.P. Obtained funding: I.S.K. and B.K.P

Additional Information

Supplementary information accompanies this paper at http://www.nature.com/srep

Competing financial interests: The authors declare no competing financial interests.

How to cite this article: Eakins, R. *et al.* Adaptation to acetaminophen exposure elicits major changes in expression and distribution of the hepatic proteome. *Sci. Rep.* **5**, 16423; doi: 10.1038/srep16423 (2015).

This work is licensed under a Creative Commons Attribution 4.0 International License. The images or other third party material in this article are included in the article's Creative Commons license, unless indicated otherwise in the credit line; if the material is not included under the Creative Commons license, users will need to obtain permission from the license holder to reproduce the material. To view a copy of this license, visit http://creativecommons.org/licenses/by/4.0/